Mathematisches Institut
Justus-Liebig-Universität Giessen

New Classes of Radial Basis Functions for Quasi-Interpolation

Dissertation

zur Erlangung des Doktorgrades
der Naturwissenschaftlichen Fachbereiche der
Justus-Liebig-Universität Gießen

Autor:
Mathis Ortmann

Betreuer:
Prof. Dr. Martin D. Buhmann

August 4, 2025

Kurzfassung:

Radiale Basisfunktionen (RBFs) sind ein wichtiges Werkzeug der numerischen Mathematik zur Approximation von Funktionen anhand gestreuter Daten. Oft werden diese als Interpolationsmethode verwendet. Dabei muss ein lineares Gleichungssystem gelöst werden. Die Größe des linearen Gleichungssystems hängt von der Anzahl der Interpolationspunkte ab. Mit steigender Anzahl von Interpolationspunkten neigt die Lösung zu numerischer Instabilität, wodurch die Approximation der Funktion anhand der gestreuten Daten fehlerhaft wird. Ein möglicher Ansatz, um dieses Problem zu umgehen, ist die Quasi-Interpolation mittels RBFs. Die Quasi-Interpolation bietet eine effiziente Approximationsmethode, ohne dass ein lineares Gleichungssystem gelöst werden muss. Genau wie die Interpolation mit RBFs ist die Quasi-Interpolation in beliebigen Dimensionen anwendbar. Da viele Aufgaben aus Industrie und Wissenschaft auf die Approximation gestreuter Daten zurückzuführen sind, kommt der Erforschung effizienter Approximationsmethoden eine zentrale Rolle zu. Mit der stark steigenden Anzahl verfügbarer Daten gewinnt die Quasi-Interpolation im Vergleich zur klassischen Interpolation zunehmend an Bedeutung.

Zur Berechnung der Quasi-Interpolation muss vorab eine RBF bestimmt werden. Die Wahl der RBF beeinflusst die Güte der Approximation. Die optimale RBF für ein gegebenes Approximationsproblem zu wählen ist ein offenes Forschungsgebiet.

In dieser Arbeit werden zwei neue Klassen von RBFs vorgestellt, die die Approximation mittels Quasi-Interpolation verbessern. Die Güte einer Approximation wird durch die Approximationsordnung bestimmt. Eine Aussage über die Approximationsordnung liefern die Strang- und Fix-Bedingungen. Für deren Anwendung wird das asymptotische Verhalten der distributionellen Fourier-Transformation der RBF benötigt. Neben den zwei neuen Klassen von RBFs wird zudem eine neue Klasse von nicht-RBFs für die Verwendung in der Quasi-Interpolation eingeführt. Die Analyse der Approximationsordnungen zwischen RBFs und nicht-RBFs unterscheidet sich fundamental und eröffnet neue Ansatzpunkte für weitere nicht-RBFs in der Quasi-Interpolation. Die Ergebnisse zeigen ausgezeichnete Konvergenzeigenschaften bei geringem Rechenaufwand. Die vorgestellten theoretischen Ergebnisse werden durch numerische Beispiele verifiziert.

Abstract:

Radial basis functions (RBFs) are considered an important tool in numerical mathematics for approximating functions based on scattered data. They are often used as an interpolation method. In this process, a system of linear equations has to be solved. The size of the linear system is determined by the number of interpolation points. As the number of interpolation points increases, the solution tends to become numerically unstable, which results in the approximation of the function based on the scattered data becoming inaccurate. One possible approach to avoid this problem is provided by quasi-interpolation using RBFs. Quasi-interpolation is an efficient approximation method that does not require a system of linear equations to be solved. Just like interpolation with RBFs, quasi-interpolation is applied in arbitrary dimensions. Since many problems in industry and science are based on the approximation of scattered data, efficient approximation is regarded as a central task. With a rapidly increasing amount of available data, quasi-interpolation is gaining importance compared to classical interpolation.

To compute the quasi-interpolation, a RBF has to be selected in advance. The approximation quality is affected by the selected RBF. The determination of an optimal RBF for a given approximation problem is considered an open research challenge.

In this work, two new classes of RBFs are presented that are used to improve approximation by quasi-interpolation. The quality of an approximation is determined by the approximation order. A statement about the approximation order is provided by the Strang and Fix conditions. For their application, the asymptotic behavior of the distributional Fourier transform of the RBF is required. In addition to the two new classes of RBFs, a new class of non-RBFs is also introduced for use in quasi-interpolation. The analysis of approximation orders between RBFs and non-RBFs is fundamentally distinguished, and new approaches for further non-RBFs in quasi-interpolation are opened up. The results are shown to yield excellent convergence properties with low computational effort. The theoretical results presented are verified by numerical examples.

'It is not knowledge, but the act of learning, not possession but the act of getting there, which grants the greatest enjoyment.'

— Carl Friedrich Gauss
(Gauss to Bolyai 1808)

Acknowledgement:

I would like to begin by expressing my gratitude to my advisor, Prof. Martin Buhmann, for his invaluable support and guidance throughout my doctoral studies. His insights have consistently encouraged me to explore new avenues of thought and action. Despite his numerous commitments to various committees, he always found time to engage in discussions about new results and challenges.

I extend my thanks to Prof. Oleg Davydov, Dr. Janin Jäger, and the entire numerical analysis group for making my four years of Ph.D. study a rewarding and enlightening experience.

Additionally, I would like to thank the remaining members of the examination committee, Prof. Christian Rieger, Prof. Lorenz von Smekal, and Prof. Bernhard Lani-Wayda, for their valuable time and effort.

Besonderer Dank gebührt meiner Familie, die mich immer unterstützt und an mich geglaubt hat. Speziell danke ich meinen Brüdern Jan und Till für ihre wertvollen Erkenntnisse und Hinweise aus den Bereichen der Elektro- und Informationstechnik sowie der Chemie. Meinen Eltern Heike und Thomas danke ich für den Rückhalt, der für diese Arbeit essentiell war. Außerdem danke ich meiner Freundin Leona, die mich während der Entstehung dieser Arbeit mit viel Verständnis begleitet hat.

Contents

Chapter 1

Introduction

Multivariate approximation theory is a branch of mathematical analysis that deals with approximating multivariate functions. This field has numerous applications across scientific and engineering disciplines, including numerical analysis, machine learning, and data fitting. The primary objective is to develop methods to approximate a given multivariate function $f : \mathbb{R}^n \to \mathbb{R}$ using compositions of more tractable functions.

In machine learning, for example, radial basis functions (RBFs) are used in regression and classification problems to predict outcomes based on input features [48]. In computer graphics, surface reconstruction and modeling require approximation techniques to generate smooth surfaces from discrete data points [36], [47]. Geostatistics utilizes kriging, a method for spatial interpolation, which relies on approximating spatial data to predict values at unobserved locations [7]. Engineering applications often involve approximating stress and strain distributions to aid in the design and analysis of structures [54]. In the domain of robotics, this methodology is also employed for the purpose of predictive maintenance [41]. RBFs have also great impact on the solution of partial differential equations [18].

Several methods are employed for multivariate approximation. Polynomial interpolation extends the concept of univariate polynomial interpolation to multivariate functions. However, there are limitations to this approach, particularly with regard to the construction of an adequate polynomial space that can guarantee the unisolvence of the interpolation problem [25]. Spline interpolation uses piecewise polynomials to approximate functions, with B-splines and NURBS (non-uniform rational B-Splines) being commonly used in computer graphics and CAD (computer-aided design) [45]. Wavelet transforms offer a multi-resolution approach to approximating functions and are useful in signal processing and image compression [38]. RBFs, which use radially symmetric basis functions

for interpolation and approximation, have gained popularity due to their flexibility and ability to handle scattered data efficiently [52]. The contents of this thesis are mainly based on the approximation with RBFs.

1.1 Radial Basis Functions

RBFs are a powerful tool for multivariate interpolation and approximation, particularly useful for scattered data in higher dimensions [3].

A RBF is a real-valued function $\phi : \mathbb{R}^n \to \mathbb{R}$ that depends only on the radial part of the argument, and can therefore be expressed as

$$\phi(x) = \varphi(\|x\|),$$

where $\|\cdot\|$ denotes the Euclidean norm and $\varphi : \mathbb{R} \to \mathbb{R}$ is the associated univariate RBF. Commonly used RBFs are listed in table 1.1. Most of the examples listed provide the so-called shape parameter $c > 0$, which can be chosen arbitrarily.

Name	Multivariate RBF	Univariate RBF
Gaussian	$\phi(x) = \mathrm{e}^{-c^2\|\|x\|\|^2}$	$\varphi(r) = \mathrm{e}^{-(cr)^2}$
Multiquadric	$\phi(x) = \sqrt{\|\|x\|\|^2 + c^2}$	$\varphi(r) = \sqrt{r^2 + c^2}$
Thin plate spline	$\phi(x) = \|\|x\|\|^2 \log(\|\|x\|\|)$	$\varphi(r) = r^2 \log(r)$
Inverse multiquadric	$\phi(x) = \frac{1}{\sqrt{\|\|x\|\|^2+c^2}}$	$\varphi(r) = \frac{1}{\sqrt{r^2+c^2}}$

Table 1.1: List of commonly used RBFs [12, p. 4].

Given a finite set of data points $\{(x_i, f_i)\}_{i=1}^N$, where $N \in \mathbb{N}$, $x_i \in \mathbb{R}^n$, and $f_i \in \mathbb{R}$, the RBF interpolation problem seeks to find a function $s(\mathbf{x})$ of the form:

$$s(x) = \sum_{i=1}^{N} \lambda_i \phi(x - x_i)$$

with the condition

$$s(x_i) = f(x_i), \qquad \forall i \in \{1, 2, \ldots, N\}.$$

The set of coefficients $\{\lambda_i\}$ is determined by solving the linear system of equations [41]

$$\underbrace{\begin{bmatrix} \phi(x_1 - x_1) & \phi(x_1 - x_2) & \dots & \phi(x_1 - x_N) \\ \phi(x_2 - x_1) & \phi(x_2 - x_2) & \dots & \phi(x_2 - x_N) \\ \vdots & \vdots & \ddots & \vdots \\ \phi(x_N - x_1) & \phi(x_N - x_2) & \dots & \phi(x_N - x_N) \end{bmatrix}}_{\mathbf{A}} \underbrace{\begin{bmatrix} \lambda_1 \\ \lambda_2 \\ \vdots \\ \lambda_N \end{bmatrix}}_{\boldsymbol{\lambda}} = \underbrace{\begin{bmatrix} f(x_1) \\ f(x_2) \\ \vdots \\ f(x_N) \end{bmatrix}}_{\mathbf{f}}.$$

The form of the interpolant can also be interpreted as a fully connected, single-layer neural network [6]. Consequently, there exists a close resemblance to adaptive network theory [8]. In this interpretation, $s(x)$ is called a RBF-network [50]. However, this particular interpretation will not be the focus of the discussion. Instead, a conventional perspective on the issue of interpolation will be adopted. The interpolation condition can only be satisfied if the system of linear equations has a unique solution. The RBFs listed in table 1.1 ensure that the aforementioned linear system of equations has a unique solution. This is primarily demonstrated through the property of positive definiteness. This property is addressed in the following section.

1.1.1 Positive Definiteness and Solvability

The key property of many RBFs is positive definiteness. A function ϕ is said to be positive definite if for any set of distinct points $\{x_i\}_{i=1}^N$, the matrix $\mathbf{A}$ with entries $\mathbf{A}_{ij} = \phi(x_i - x_j)$ is positive definite. This implies that for any non-zero vector $\mathbf{v}$,

$$\mathbf{v}^T \mathbf{A} \mathbf{v} > 0.$$

Positive definiteness guarantees that the interpolation matrix $\mathbf{A}$ is invertible, ensuring that the linear system $\mathbf{A}\boldsymbol{\lambda} = \mathbf{f}$ has a unique solution [52]. For example, the Gaussian RBF is positive definite, which can be proven using the Bochner theorem, that states a function $\phi(x)$ is positive definite if and only if it is the Fourier transform of a non-negative measure [33]. The Fourier transform of a Gaussian is again a Gaussian [49, p. 309]

$$\phi(x) = \mathrm{e}^{-c^2||x||^2}, \qquad \hat{\phi}(y) = \pi^{n/2} c^{-n} \mathrm{e}^{-\frac{||y||^2}{4c^2}},$$

which is always non-negative, thus proving its positive definiteness. In this thesis, the n-dimensional Fourier transform is defined as $\hat{f}(y) = \int_{\mathbb{R}^n} \mathrm{e}^{-ix\cdot y} f(x)\,\mathrm{d}x$. In theory, the parameter $c > 0$ does not influence the problem's structure, or its solvability. However,

in practical applications, it has been demonstrated that the shape parameter exerts a significant influence on the function's behavior between two interpolation points. A vast variety of literature has been published on the subject of selecting an appropriate shape parameter for a given set of data points [17], [40].

1.1.2 Advantages of RBFs

RBFs offer several advantages. They are mesh-free, so they do not require a grid or mesh, making them a promising candidate for the approximation of scattered data. Interpolating with RBFs does not depend on the dimensionality of the data, making them suitable for high-dimensional problems. Different RBFs can be selected based on the specific requirements of the problem, offering flexibility in approximation. Additionally, the positive definiteness of certain RBFs ensures that the linear system of equations is always solvable, which is a significant benefit in real-world applications.

1.1.3 Disadvantages of RBFs

RBF-interpolation suffers from some disadvantages. Solving the linear system of equations has a computational cost of $\mathcal{O}(N^3)$ for direct methods [53]. This turns out to be prohibitively expensive for large datasets. The interpolation matrix can become ill-conditioned, especially for certain choices of the shape parameter or when the data points are clustered. This leads to numerical instability and inaccuracies in the solution. The condition number also depends on the choice of the shape parameter. Finding the optimal shape parameter is often non-trivial and may require costly cross-validation or other optimization techniques. Many researchers are looking for the best algorithms to determine the shape parameter for specific problems [23], [17], [28]. Lastly, the choice of the RBF itself can significantly impact the interpolation quality. There is no universally optimal RBF, and the optimal choice may depend on the specific problem and dataset characteristics.

Some of these disadvantages can be compensated by going from interpolation to quasi-interpolation.

1.2 Quasi-Interpolation

Quasi-interpolation is an alternative to interpolation that provides a way to approximate a function without necessarily passing through all given data points. Quasi-interpolation

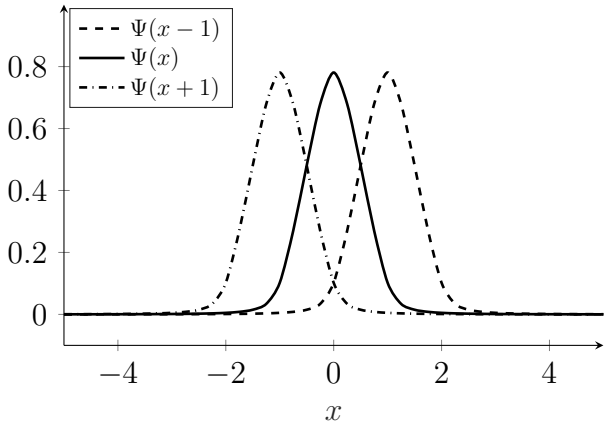

Figure 1.1: Visualization of a quasi-Lagrange function in one dimension. The used function is $\Psi(x) = \frac{1}{2}\phi(x-1) - \phi(x) + \frac{1}{2}\phi(x+1)$. The function $\phi(x) = \sqrt{0.25^2 + ||x||^2}$ is also visualized in figure 1.2.

constructs an approximant $Q[f]$ that approximates the function f based on a set of points, but softens the requirement that $Q[f](x_i) = f(x_i)$ for all i. This approach leads to a reduction of complexity and numerically stable computations [15].

In the context of quasi-interpolation, the conventional condition of interpolation is substituted by the condition of polynomial reproduction. This substitution ensures the exact approximation of polynomials up to a certain degree. For many functions f, the Taylor series can be employed to approximate the function locally as a polynomial. The first terms of the Taylor series can be reproduced exactly, leading to accurate local approximations. Quasi-interpolation using RBFs involves constructing a quasi-Lagrange operator of the form

$$Q_h[f](x) = \sum_{j \in \mathbb{Z}^n} f(jh)\Psi(x/h - j), \qquad h \in \mathbb{R}, x \in \mathbb{R}^n,$$

where h is some grid spacing and Ψ is the quasi-Lagrange function, which is not required to perform exact interpolation. The quasi-Lagrange operator is a linear operator that maps a function or a set of data points to an approximating function. To give an intuition of how the quasi-Lagrange functions look like, an example is shown in figure 1.1. In the sum of the quasi-Lagrange operator, the quasi-Lagrange function serves as a weighting function for each given data point. This can alternatively be interpreted as a smoothing technique for the data points. This thesis deals with the question of how quasi-Lagrange functions can be constructed to improve the approximation properties. To do so, the

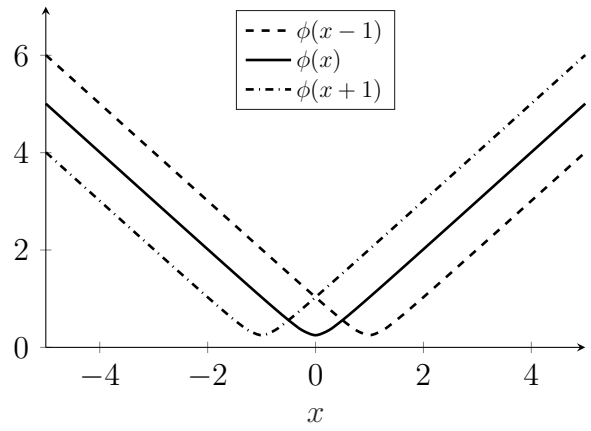

Figure 1.2: Visualization of the shifted RBF $\phi(x) = \sqrt{0.25^2 + ||x||^2}$.

following approach for the quasi-Lagrange function is chosen

$$\Psi(x) = \sum_{k \in \mathbb{Z}^n} \mu_k \phi(x - k), \qquad x \in \mathbb{R}^n. \tag{1.1}$$

In other words, the quasi-Lagrange function is a linear combination of shifted RBFs. An example of a shifted RBF is shown in figure 1.2. This example explicitly demonstrates that the RBFs used in this thesis grow for large values of x, whereas the linear combination (the quasi-Lagrange function) decays for large arguments, see figure 1.1. An explicit example is provided in subsection 1.2.2. To achieve this behaviour, the growing parts of the asymptotic series of the RBF have to be canceled out. Therefore, the choice of the RBF and the coefficients μ_k are important for the accuracy of the quasi-interpolation. In classical quasi-interpolation, the coefficients μ_k are compactly supported, meaning that the sum is finite, thus avoiding issues with convergence. This concept can be extended to non-compactly supported coefficients, but it is no longer referred as classical quasi-interpolation [16].

In the following, we will first focus on the quasi-Lagrange function and determine the properties that need to be satisfied. Subsequently, we will construct a quasi-Lagrange function that fulfills these properties. The construction will be achieved by determining the weights μ_k for a given choice of RBF. As mentioned previously, the objective is to achieve some form of polynomial reproduction.

1.2.1 Polynomial Reproduction

Polynomial reproduction is a desirable property of quasi-interpolants, where the quasi-interpolation operator $Q_h[f]$ exactly reproduces polynomials up to a certain degree. This property ensures that the quasi-interpolant is accurate for analytic functions and can provide high-quality approximations.

Polynomial reproduction by the quasi-Lagrange operator $Q_h[f]$ can be described mathematically as

$$Q_h[p](x) = p(x) \quad \text{for all polynomials } p \text{ with } \deg(p) \leq m. \tag{1.2}$$

For the quasi-Lagrange function to satisfy this condition, sufficient rapid decay is required to ensure the quasi-Lagrange operator is absolutely convergent. Further conditions will be derived using the Poisson summation formula, which will result in conditions not directly related to the quasi-Lagrange function but to the corresponding Fourier transform. For clarity, a short yet representative example in one dimension is presented, using a grid with a grid spacing of $h = 1$. The goal is to find $\Psi(x)$ such that the quasi-Lagrange operator reproduces polynomials of degree one. To do so, we first assume that $\Psi(x)$ decays fast enough so that the quasi-Lagrange operator is absolutely convergent. The Poisson summation formula states that [21]

$$\sum_{j\in\mathbb{Z}} \Psi(j) = \sum_{k\in\mathbb{Z}} \hat{\Psi}(2\pi k).$$

We begin with the reproduction of constants, i. e., $p(x) = C$. In this case, the condition (1.2) translates to

$$C \overset{!}{=} Q_1[p](x) = \sum_{j=-\infty}^{\infty} p(j)\Psi(x-j) = C \sum_{j=-\infty}^{\infty} \Psi(x-j).$$

Due to the linearity, the specific constant C does not affect the result. So the condition to the quasi-Lagrange function is

$$1 \overset{!}{=} \sum_{j=-\infty}^{\infty} \Psi(x-j).$$

The utilization of the Poisson summation formula with the incorporated shift of x results

in the following equation

$$1 \stackrel{!}{=} \sum_{j=-\infty}^{\infty} \Psi(x-j) = \sum_{k=-\infty}^{\infty} \hat{\Psi}(2\pi(k+x)) = \sum_{k=-\infty}^{\infty} \mathrm{e}^{2\pi \mathrm{i} k x} \hat{\Psi}(2\pi k).$$

The equation has to hold for all $x \in \mathbb{R}$, and since the exponential functions are linear independent, all terms except of the zeroth have to vanish. Hence, in order to reproduce constants, the Fourier transform of the quasi-Lagrange function has to satisfy

$$\hat{\Psi}(2\pi k) = \delta_{0,k}, \qquad \forall k \in \mathbb{Z}, \tag{1.3}$$

where $\delta_{0,k}$ denotes the Kronecker delta function. As an example the $\mathrm{sinc}(x) = \frac{\sin(x)}{x}$ function satisfies the condition.

In the next step we extend the aforementioned condition by reproducing linear polynomials, say $p(x) = ax + C$ with $C, a, x \in \mathbb{R}$. The condition of polynomial reproduction is then

$$\begin{aligned} ax + C \stackrel{!}{=} Q_1[p](x) &= \sum_{j=-\infty}^{\infty} p(j)\Psi(x-j) = \sum_{j=-\infty}^{\infty} (aj + C)\Psi(x-j) \\ &= C \sum_{j=-\infty}^{\infty} \Psi(x-j) + a \sum_{j=-\infty}^{\infty} j\Psi(x-j). \end{aligned}$$

Using the conditions for the reproduction of constants and the linearity of the quasi-Lagrange operator, the following observation can be made

$$\begin{aligned} x \stackrel{!}{=} \sum_{j=-\infty}^{\infty} j\Psi(x-j) &= \sum_{k=-\infty}^{\infty} \left(\int_{\mathbb{R}} t\Psi(x-t)\mathrm{e}^{-\mathrm{i}ty} \mathrm{d}t \Big|_{y=2\pi k} \right) \\ &= \sum_{k=-\infty}^{\infty} \left(\mathrm{i}\frac{\mathrm{d}}{\mathrm{d}y} \int_{\mathbb{R}} \Psi(x-t)\mathrm{e}^{-\mathrm{i}ty} \mathrm{d}t \Big|_{y=2\pi k} \right) \\ &= \sum_{k=-\infty}^{\infty} \left(\mathrm{i}\frac{\mathrm{d}}{\mathrm{d}y} \int_{\mathbb{R}} \Psi(\tilde{t})\mathrm{e}^{-\mathrm{i}(x-\tilde{t})y} \mathrm{d}\tilde{t} \Big|_{y=2\pi k} \right) \\ &= \sum_{k=-\infty}^{\infty} \mathrm{i} \left(\frac{\mathrm{d}}{\mathrm{d}y} \mathrm{e}^{-\mathrm{i}xy} \hat{\Psi}(-y) \right) \Big|_{y=2\pi k} \\ &= x + \mathrm{i} \sum_{k=-\infty}^{\infty} \mathrm{e}^{-i2\pi kx} \frac{\mathrm{d}}{\mathrm{d}y} \hat{\Psi}(-y) \Big|_{y=2\pi k}. \end{aligned}$$

In the last line, the derivative is evaluated and the condition for the reproduction of

constants is used. The remaining sum has to be identically zero for all $x \in \mathbb{R}$, and since the exponential functions are linearly independent, the derivative of the Fourier transform of the quasi-Lagrange function must vanish at all lattice points. To reproduce linear polynomials, $\hat{\Psi}$ has to satisfy the additional condition

$$\frac{\mathrm{d}}{\mathrm{d}y}\hat{\Psi}(y)\bigg|_{y=2\pi k} = 0, \qquad \forall k \in \mathbb{Z}.$$

For this example we have now derived all the conditions the quasi-Lagrange function has to satisfy. In a similar way, higher-order polynomial reproduction can be demonstrated to lead to additional conditions for higher derivatives of $\hat{\Psi}$.

So far, we have identified the conditions that the quasi-Lagrange function has to satisfy. The next subsection deals with the construction of a quasi-Lagrange function that meets these properties.

1.2.2 Determining the Coefficients

While the required properties of the quasi-Lagrange functions are known, the construction of a function that precisely satisfies these properties remains open. Upon examining the conditions, the necessity of the Fourier transform as an essential component becomes clear. We recall the approach of the quasi-Lagrange function from equ. (1.1)

$$\Psi(x) = \sum_{k\in\mathbb{Z}^n} \mu_k \phi(x-k), \qquad x \in \mathbb{R}^n.$$

The Fourier transform of the approach results in

$$\begin{aligned}\hat{\Psi}(y) &= \sum_{k\in\mathbb{Z}} \mu_k \mathrm{e}^{-iky}\hat{\phi}(y), \qquad y \in \mathbb{R}^n \\ &= \hat{\phi}(y)\sum_{k\in\mathbb{Z}} \mu_k \mathrm{e}^{-iky} = \hat{\phi}(y)P(y).\end{aligned}$$

The Fourier transform of the quasi-Lagrange function is the product between the Fourier transform of a given RBF and a 2π-periodic function $P(y)$. The function $P(y)$ is called the trigonometric polynomial. We begin by addressing the reproduction of constants and, to that end, recall the conditions from equ. (1.3)

$$\hat{\Psi}(2\pi k) = \delta_{0,k}, \qquad \forall k \in \mathbb{Z}. \tag{1.4}$$

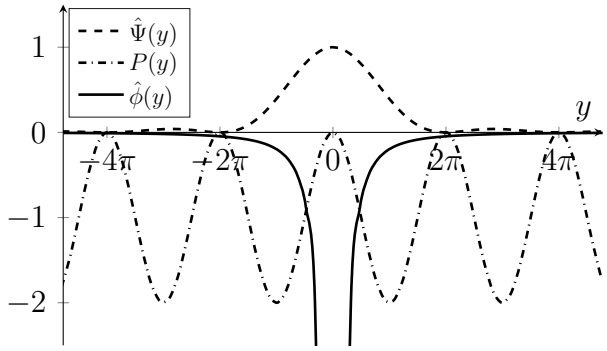

Figure 1.3: Visualization of the components of the Fourier transform of the quasi-Lagrange function with the explicit functions $P(y) = \cos(y) - 1$, $\hat{\phi}(y) = -\frac{1}{10|y|} K_1\left(\frac{|y|}{20}\right)$ and $\hat{\Psi} = \hat{\phi}(y)P(y)$. Here, K_1 denotes the modified Bessel function of the second kind.

In general, the Fourier transform of the RBF will not vanish at the desired positions. However, the trigonometric polynomial can be enforced to vanish at the origin, and through the 2π-periodicity, we can ensure that $P(y)$ vanishes at all required lattice points. If we do so, $\hat{\Psi}$ satisfies the conditions (1.4) everywhere except at the origin. At this point, the RBF comes into consideration. To achieve $\hat{\Psi}(0) = 1$, the Fourier transform of the RBF has to be singular at the origin and the zero of $P(y)$ has to be of the same order as the singularity. It becomes evident that we cannot rely on classical Fourier transforms, as they would not exhibit singularities. For instance, the commonly used Gaussian RBF fails to reproduce constants, as the corresponding Fourier transform is also Gaussian and lacks a singularity at the origin. If we choose an RBF that grows at least at a polynomial rate for large arguments, the generalized (or distributional) Fourier transform will exhibit a singularity at the origin. This is precisely the approach employed in this thesis. We will compute the generalized Fourier transforms of new RBFs, analyze the singularity at the origin, and construct $P(y)$ such that the conditions for $\hat{\Psi}(y)$ are satisfied. Figure 1.3 visualizes the Fourier transform of the quasi-Lagrange function by separately showing an example of the generalized Fourier transform of the RBF $\hat{\phi}(y)$, the trigonometric polynomial $P(y)$ and the Fourier transform of the quasi-Lagrange function as the product of the two aforementioned components, $\hat{\Psi}(y) = \hat{\phi}(y)P(y)$.

For further illustration, let us examine a short example. We choose our RBF to be $\phi(x) = \sqrt{c^2 + ||x||^2}, x \in \mathbb{R}, c > 0$. This is the well-known multiquadric and has the generalized Fourier transform

$$\hat{\phi}(y) = -2(c/|y|)K_1(c|y|), \qquad y \in \mathbb{R},$$

where K_1 is the modified Bessel function of the second kind [15, p. 154]. The function K_1 is smooth, decays exponentially for large arguments and is singular at zero. This is also visualized in figure 1.3. More precisely, for small arguments the Bessel function behaves as

$$K_1(c|y|) = \frac{1}{c|y|} - \frac{c|y|}{4} + \frac{c|y|\gamma}{2} + \frac{c|y|}{2}\log\left(\frac{c|y|}{2}\right) + \mathcal{O}(|y|^2),$$

where γ denotes the Euler-Mascheroni-constant. In total we have

$$\hat{\phi}(y) = -\frac{2}{y^2} + \left(\frac{1}{2} - \gamma\right)c^2 - c^2\log\left(\frac{c|y|}{2}\right) + \mathcal{O}(|y|).$$

Knowing the behaviour of the generalized Fourier transform of the RBF, we can now construct the trigonometric polynomial such that the product of $\hat{\phi}(0)$ and $P(0)$ is one. To do so, we expand the exponential function in the well-known series representation

$$\begin{aligned} P(y) &= \sum_{k\in\mathbb{Z}} \mu_k \mathrm{e}^{-iky} = \sum_{k\in\mathbb{Z}} \mu_k \left(1 - iyk - \frac{y^2}{2}k^2 + \mathcal{O}(y^3)\right) \\ &= \sum_{k\in\mathbb{Z}} \mu_k - iy\sum_{k\in\mathbb{Z}} \mu_k k - \frac{y^2}{2}\sum_{k\in\mathbb{Z}} \mu_k k^2 + \mathcal{O}(y^3) \overset{!}{=} -\frac{y^2}{2} + \mathcal{O}(y^3). \end{aligned}$$

Equating the coefficients we get three equations

$$\begin{aligned} \sum_{k\in\mathbb{Z}} \mu_k &= 0, \\ \sum_{k\in\mathbb{Z}} \mu_k k &= 0, \\ \sum_{k\in\mathbb{Z}} \mu_k k^2 &= 1, \end{aligned}$$

called the moment conditions. Since we have potentially infinitely many coefficients to determine, there is no unique solution to these three equations. One of the most common solution is given by

$$\begin{aligned} \mu_{-1} = \frac{1}{2}, \quad \mu_0 = -1, \quad \mu_1 = \frac{1}{2}, \\ \mu_k = 0 \quad \forall k \in \mathbb{Z}\backslash\{-1, 0, 1\}. \end{aligned}$$

With this choice, the trigonometric polynomial simplifies to $P(y) = \cos(y) - 1$, which is visualized in figure 1.3. Furthermore, the coefficients are compactly supported, ensuring

that the quasi-Lagrange function in equ. (1.1) remains well-defined and finite. A finite selection of coefficients is always possible if the highest-order term has an even power, which is consistently the case in classical quasi-interpolation. Otherwise, an infinite solution may be applicable. In this case, one must verify that the sum is convergent. This thesis adopts classical quasi-interpolation throughout, and references to alternative approaches if this condition does not hold.

Continuing with the example we end up with

$$\begin{aligned}\hat{\Psi}(y) &= \hat{\phi}(y)P(y) \\ &= \left(-\frac{2}{y^2} + \left(\frac{1}{2} - \gamma\right)c^2 - c^2 \log\left(\frac{c|y|}{2}\right) + \mathcal{O}(y)\right)\left(-\frac{y^2}{2} + \mathcal{O}(y^3)\right) \\ &= 1 + \mathcal{O}(y).\end{aligned}$$

So far we have coefficients for a given RBF such that $\hat{\Psi}(0) = 1$ and $\hat{\Psi}(2\pi k) = 0 \ \forall k \in \mathbb{Z}\backslash\{0\}$. In other words, we have constructed an explicit quasi-Lagrange function that reproduces constants. Explicitly, we constructed

$$\begin{aligned}\Psi(x) &= \sum_{k\in\mathbb{Z}} \mu_k \phi(x-k), \qquad x \in \mathbb{R} \\ &= \frac{1}{2}\phi(x-1) - \phi(x) + \frac{1}{2}\phi(x-1) \\ &= \frac{1}{2}\sqrt{c^2 + ||x-1||^2} - \sqrt{c^2 + ||x||^2} + \frac{1}{2}\sqrt{c^2 + ||x+1||^2},\end{aligned}$$

which is the exactly example visualized in figure 1.1.

The next step is to check if linear polynomials can also be reproduced. We recall the condition for reproducing linear polynomials

$$\frac{\mathrm{d}}{\mathrm{d}y}\hat{\Psi}(y)\bigg|_{y=2\pi k} = 0, \qquad \forall k \in \mathbb{Z}.$$

First, we have a look on every point $k \in \mathbb{Z}\backslash\{0\}$. The derivative can be written as

$$\begin{aligned}\frac{\mathrm{d}}{\mathrm{d}y}\hat{\Psi}(y) &= \frac{\mathrm{d}}{\mathrm{d}y}\left(\hat{\phi}(y)P(y)\right) \\ &= \left(\frac{\mathrm{d}}{\mathrm{d}y}\hat{\phi}(y)\right)P(y) + \hat{\phi}(y)\frac{\mathrm{d}}{\mathrm{d}y}P(y)\bigg|_{y=2\pi k}.\end{aligned}$$

We already know that $P(2\pi k) = 0 \quad \forall k \in \mathbb{Z}$, so the first term vanishes.

Since $P(y) = -\frac{y^2}{2} + \mathcal{O}(y^3)$, we know that

$$\frac{\mathrm{d}}{\mathrm{d}y} P(y) = -y + \mathcal{O}(y^2)$$

and conclude

$$\frac{\mathrm{d}}{\mathrm{d}y} P(y)\bigg|_{y=0} = 0.$$

Due to the periodicity of $P(y)$, the second term is also zero for all $k \in \mathbb{Z}\backslash\{0\}$. Therefore, these conditions are already satisfied. Finally, we need to check if this holds true for $k = 0$. For $k = 0$, we have to figure out the next order behaviour of $\Psi(y)$ for small arguments. To do so, we have to expand $P(y)$ to further orders and obtain

$$P(y) = -\frac{y^2}{2} + \frac{\mathrm{i}}{6} y^3 \sum_{k\in\mathbb{Z}} \mu_k k^3 + \mathcal{O}(y^4).$$

Since $\sum_{k\in\mathbb{Z}} \mu_k k^3 = 0$ is already satisfied with the given coefficients, we have $P(y) = -\frac{y^2}{2} + \mathcal{O}(y^4)$. Multiplying the result with the expansion of the RBF at the origin results in

$$\begin{aligned}
\hat{\Psi}(y) &= \hat{\Phi}(y) P(y) \\
&= \left(-\frac{2}{y^2} + \left(\frac{1}{2} - \gamma\right) c^2 - c^2 \log\left(\frac{c|y|}{2}\right) + \mathcal{O}(y)\right)\left(-\frac{y^2}{2} + \mathcal{O}(y^4)\right) \\
&= 1 + \frac{c^2 y^2}{2} \log\left(\frac{c|y|}{2}\right) + \mathcal{O}(y^2).
\end{aligned}$$

The derivative of the Fourier transform of the quasi-Lagrange function near the origin is given by

$$\frac{\mathrm{d}}{\mathrm{d}y} \hat{\Psi}(y) = \frac{1}{2} c^2 y \left(2 \log\left(\frac{c|y|}{2}\right) + 1\right) + \mathcal{O}(y).$$

In this form, we can observe that $\lim_{y\to 0} \frac{\mathrm{d}}{\mathrm{d}y} \hat{\Psi}(y) = 0$, since $\lim_{y\to 0} y \log(|y|) = 0$. In fact, the conditions for linear polynomial reproduction are already satisfied with the given coefficients. Thus, we have constructed a quasi-Lagrange function that reproduces polynomials of degree one. The most important aspect is the expansion of $\hat{\Psi}$ near the origin. To achieve this, we have to multiply the expansion of the Fourier transform of the RBF with the trigonometric polynomial near the origin. From this, the conditions on

the coefficients μ_k emerge. Note that this always results in a linear system of equations, which can thus be solved systematically.

Polynomial reproduction of order higher than one cannot be achieved because the second derivative of $P(y)$ will not be zero at the lattice points anymore. For the given RBF, the coefficients obtained are optimal. Other RBFs may achieve higher polynomial reproduction and approximation orders. The main focus of this thesis is the investigation of new RBFs and their applications in quasi-interpolation. The following subsection will address the approximation order, which is a criterion for the quality of a RBF used in quasi-interpolation.

1.2.3 Approximation Order

The approximation order of a quasi-interpolation scheme refers to the rate at which the approximation error decreases as the density of the data points increases. We continue with the previous example and outline how to derive the approximation order of the quasi-Lagrange operator. To do so, we define a linear polynomial for some function f to be approximated

$$p(y) = f(x) + (x - y)f'(x).$$

The polynomial is of degree one, and consequently, the quasi-Lagrange operator will exactly reproduce it. Furthermore, the polynomial has the special value $p(x) = f(x)$. In other words, $Q_h[p](y) = p(y)$, and in particular, $Q_h[p](x) = p(x) = f(x)$. For the proof of the approximation order, we explicitly require the decay rate of the quasi-Lagrange function. One method is to expand asymptotic series of the RBF for large arguments and determine the decay rate with the previously calculated coefficients μ_k. In chapter 4 we will show an easier method to determine the decay rate. For now, we assume that $\Psi(x) = \mathcal{O}\left((1+x)^{-4}\right)$ as $x \to \pm\infty$. The approximation order is then derived by the following steps

$$\begin{aligned}
|f(x) - Q_h[f](x)| &= |Q_h[p](x) - Q_h[f](x)| \\
&= |Q_h[p - f](x)| \\
&= \left| \sum_{j=-\infty}^{\infty} (p(jh) - f(jh))\Psi(x/h - j) \right| \\
&\leq \sum_{j=-\infty}^{\infty} |p(jh) - f(jh)||\Psi(x/h - j)|
\end{aligned}$$

$$
\begin{aligned}
&\leq C_1 \frac{||f''||_\infty}{2} \left(\sum_{|x-jh|<h} (x-jh)^2 \Psi\left(\frac{x-jh}{h}\right) + \sum_{|x-jh|\geq h} (x-jh)^2 \frac{h^4}{(x-jh)^4} \right) \\
&\leq C_2 \frac{||f''||_\infty}{2} \left(h^2 + h^3 \int_h^\infty \frac{1}{y^2} \mathrm{d}y \right) \\
&\leq C_3 \frac{||f''||_\infty}{2} h^2,
\end{aligned}
$$

where C_1, C_2 and C_3 are some constants. In line five we used that $p - f$ can be estimated using the Taylor error bound. This holds if the function f is two times continuously differentiable and the second derivative is bounded. In line seven, we used the fact that $\Psi(x)$ is nearly one (or finite) for small arguments, and for large arguments, it decays like x^{-4}. We also estimated the sum by the integral. The example demonstrates an approximation order of two. In this thesis, we introduce novel classes of RBFs, whose primary objective is to determine the approximation order for each class. The provided example illustrates the methodological steps required to achieve this goal.

The concepts underlying the proof can be extended to higher dimensions, an achievement attributed to Strang and Fix. The polynomial reproduction property and the approximation order in full detail are established by the famous theorem of Strang and Fix.

1.2.4 Strang and Fix Conditions

Let $\Psi : \mathbb{R}^n \to \mathbb{R}$ be a continuous function such that

1. there exists a positive ℓ such that for some nonnegative integer m, when $\|x\| \to \infty$, $|\Psi(x)| = \mathcal{O}(\|x\|^{-n-m-\ell})$, which immediately implies m-fold differentiability of the Fourier transform,

2. $D^\alpha \hat{\Psi}(0) = 0$, $\forall \alpha \in \mathbb{Z}_+^n$, $1 \leq |\alpha| \leq m$, and $\hat{\Psi}(0) = 1$,

3. $D^\alpha \hat{\Psi}(2\pi j) = 0$, $\forall j \in \mathbb{Z}^n \setminus \{0\}$ and $\forall \alpha \in \mathbb{Z}_+^n$ with $|\alpha| \leq m$.

Then the quasi-interpolant

$$
Q_h[f](x) = \sum_{j \in \mathbb{Z}^n} f(jh) \Psi(x/h - j), \qquad x \in \mathbb{R}^n,
$$

is well-defined and exact on the space of polynomials of degree m and the approximation

error can be estimated by

$$\|Q_h[f] - f\|_\infty = \begin{cases} \mathcal{O}(h^{m+\ell}), & \text{when } 0 < \ell < 1, \\ \mathcal{O}(h^{m+1}\log(1/h)), & \text{when } \ell = 1, \\ \mathcal{O}(h^{m+1}), & \text{when } \ell > 1, \end{cases}$$

for $h \to 0$ and a bounded function $f \in C^{m+1}(\mathbb{R}^n)$ with bounded derivatives [16].

The Strang and Fix conditions play a central role in this thesis. They are employed to determine the approximation order of the quasi-interpolants. The steps outlined in the following chapters are necessary to establish the requirements for applying the Strang and Fix conditions. Thus, the overarching goal throughout this thesis is to apply this theorem.

1.2.5 Choice of RBF

The assumption that the Fourier transform has a singularity at the origin is only valid if the RBF does not have a classical Fourier transform. The order of the singularity also limits the polynomial reproduction rate and, consequently, the approximation order. The selection of the RBF has a significant influence. However, the order of the singularity of the Fourier transform is dependent on the spatial dimension n. Consequently, an even order is only attainable in certain dimensions. This phenomenon is referred to as the curse of dimensionality. Classical quasi-interpolation often uses the multiquadric function in odd dimensions and the shifted thin plate spline $\varphi(r) = (c^2 + r^2)\log(c^2 + r^2)$ is used in even dimensions. But as previously mentioned, this limitation can be overcome by using non-compactly supported coefficients μ_k [16].

A universal method for determining the optimal RBF does not exist. Consequently, the investigation of novel RBFs, that are more effective than traditional approaches, is a highly relevant area of research. This thesis presents a comprehensive generalization of existing and commonly used RBFs, demonstrating the potential of these novel RBF classes to enhance the approximation achieved through quasi-interpolation.

1.3 Concluding Remarks

In order to analyze the approximation order and to illustrate the concepts with short examples, we will use gridded data. For the sake of simplicity, every formula is presented for gridded data. However, it should be noted that quasi-interpolation is a mesh-free

multivariate approximation method. For scattered data, the formulas undergo only slight modifications. Let $\Xi \subset \mathbb{R}^n$ be a set of scattered data points. The quasi-Lagrange function is then given by

$$\Psi_\zeta(x) = \sum_{\xi \in \Xi} \mu_{\zeta,\xi} \phi(x - \xi), \qquad \zeta \in \Xi, x \in \mathbb{R}^n.$$

Accordingly, the quasi-Lagrange operator is given by

$$Q[f](x) = \sum_{\zeta \in \Xi} f(\zeta) \Psi_\zeta(x).$$

The conceptual framework and the method for determining the coefficients remain unchanged.

This thesis is structured such that we will derive all relevant properties of our new classes of RBF for the use of the Strang and Fix conditions 1.2.4. First, we derive a general result of the Fourier transform for a broad class of RBFs and then explicitly calculate the Fourier transform for our purposes. In section 3 we will see how to extract the asymptotic behaviour for small and large arguments in general and explicitly expand the functions of our interest. In chapter 4 we will apply the Strang and Fix condition to the RBFs of interest using the results from the previous chapters. Furthermore, we abandon the RBF approach and derive some new non-RBF functions which can be used in quasi-interpolation. This gives new insight in the method itself and rise to new proof and practical use strategies. In chapter 5 we present some numerical examples with the RBFs derived in previous sections. Finally, we provide a summary of the results and an outlook in chapter 6.

Chapter 2

Fourier Transform

To apply the Strang and Fix conditions, the Fourier transform of the quasi-Lagrange function is required. Since the quasi-Lagrange function is a linear combination of RBFs, the Fourier transform of the quasi-Lagrange function can be expressed in terms of the Fourier transform of the RBFs. This chapter begins with the derivation of a general expression for the Fourier transform of a large class of RBFs. These results are subsequently applied to a newly generalized version of the multiquadric and a newly generalized version of the thin plate spline, both of which serve as RBFs of particular interest in quasi-interpolation applications. For each class of RBFs, a connection between the general form of their Fourier transforms and certain special cases where the Fourier transform is already known is established. The Fourier transform is calculated using special function representations that involve contour integrals. Finally, the general results are validated with respect to powers of logarithms, which cannot be represented as special functions.

2.1 Preface

Prior to addressing the calculation of the Fourier transform, we revise some special functions that are useful in this section. The first one is the Gamma function, which is defined as

$$\Gamma(z) = \int_0^\infty t^{z-1} \mathrm{e}^{-t} \mathrm{d}t, \qquad \mathrm{Re}(z) > 0.$$

The Gamma function is a continuation of the factorial function in such a way that

$$\Gamma(m) = (m-1)!, \qquad m \in \mathbb{N}.$$

Furthermore, the Gamma function can be evaluated for arguments with negative real part by the property

$$\Gamma(z+1) = z\Gamma(z), \qquad z \in \mathbb{C}.$$

From this property, we can deduce that there are poles for all negative integers including zero, for example

$$\begin{aligned}\lim_{\varepsilon\to 0_+} \Gamma(-1+\varepsilon) &= \lim_{\varepsilon\to 0_+} \frac{\Gamma(\varepsilon)}{-1+\varepsilon} = \lim_{\varepsilon\to 0_+} \frac{\Gamma(1+\varepsilon)}{(-1+\varepsilon)\varepsilon} = \lim_{\varepsilon\to 0_+} \frac{\Gamma(1)}{(-1+\varepsilon)\varepsilon} = \lim_{\varepsilon\to 0_+} \frac{1}{(-1+\varepsilon)\varepsilon} \\ &= -\infty.\end{aligned}$$

These are important properties we will employ in the following subsections. Further introduction to the Gamma functions can be found in [22], [2]. The Gamma function is often part of Mellin-Barnes type integrals. Two prominent representatives of Mellin-Barnes type integrals are the Meijer G-function and the Fox H-function. These functions are highly versatile, with the capacity to express a multitude of functions. The Meijer G-function is defined by the Mellin-Barnes integral

$$G_{p,q}^{m,n}\left(\begin{matrix} a_1,\dots,a_p \\ b_1,\dots,b_q \end{matrix}\,\middle|\, z\right) = \frac{1}{2\pi \mathrm{i}} \int_L \frac{\prod_{j=1}^{m}\Gamma(b_j-t)\prod_{j=1}^{n}\Gamma(1-a_j+t)}{\prod_{j=m+1}^{q}\Gamma(1-b_j+t)\prod_{j=n+1}^{p}\Gamma(a_j-t)}\, z^t \,\mathrm{d}t,$$

where the integration path L separates the poles of the factors $\Gamma(b_j - t)$ from those of the factors $\Gamma(1 - a_j + t)$ [1]. There are three possible choices for L

1. L goes from $-\mathrm{i}\infty$ to $\mathrm{i}\infty$. The integral converges if $p+q < 2(m+n)$ and $|\arg z| < (m+n-\frac{1}{2}(p+q))\pi$.

2. L is a loop that starts at infinity on a line parallel to the positive real axis, encircles the poles of the $\Gamma(b_j - t)$ once in the negative sense and returns to infinity on another line parallel to the positive real axis. The integral converges for all $z (z \neq 0)$ if $p < q$, and for $0 < |z| < 1$ if $p = q \geq 1$.

3. L is a loop that starts at infinity on a line parallel to the negative real axis, encircles the poles of the $\Gamma(1 - a_j + t)$ once in the positive sense and returns to infinity on another line parallel to the negative real axis. The integral converges for all z if $p > q$, and for $|z| > 1$ if $p = q \geq 1$.

If multiple paths are applicable, they yield the same value for the Meijer G-function. Figure 2.1 visualizes the three different cases for the path L.

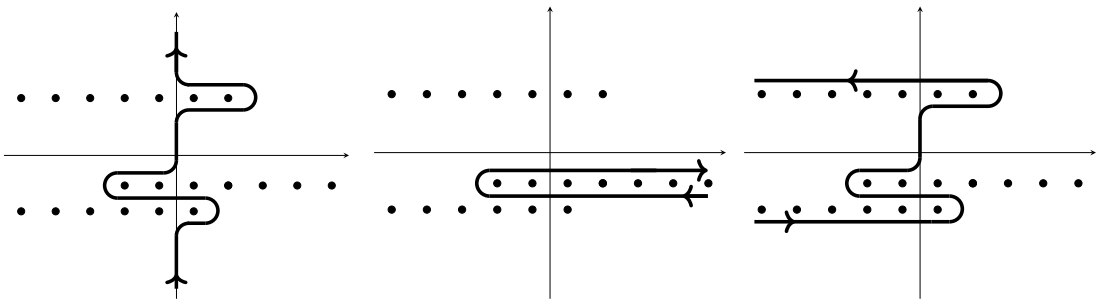

First case. Second case. Third case.

Figure 2.1: Visualization of the possible paths L for the Meijer G-function. The dots visualize the poles of the Gamma functions of $\Gamma(b_j - t)$ and $\Gamma(1 - a_j + t)$, respectively.

The Meijer G-function has two important properties that are particularly useful in this context. These properties are

$$z^{\rho}\, G_{p,q}^{m,n}\left(\begin{matrix}\mathbf{a_p}\\ \mathbf{b_q}\end{matrix}\,\middle|\, z\right) = G_{p,q}^{m,n}\left(\begin{matrix}\mathbf{a_p}+\rho\\ \mathbf{b_q}+\rho\end{matrix}\,\middle|\, z\right) \tag{2.1}$$

and

$$G_{p,q}^{m,n}\left(\begin{matrix}\mathbf{a_p}\\ \mathbf{b_q}\end{matrix}\,\middle|\, z\right) = G_{q,p}^{n,m}\left(\begin{matrix}1-\mathbf{b_q}\\ 1-\mathbf{a_p}\end{matrix}\,\middle|\, z^{-1}\right), \tag{2.2}$$

where $\mathbf{a_p} = [a_1, \ldots, a_p]$ and $\mathbf{b_q} = [b_1, \ldots, b_q]$ are the parameter vectors. The Fox H-function is a further generalization of the Meijer G-function and is defined as

$$H_{p,q}^{m,n}\left(\begin{matrix}(a_1, A_1), \ldots, (a_p, A_p)\\ (b_1, B_1), \ldots, (b_q, B_q)\end{matrix}\,\middle|\, z\right) = \frac{1}{2\pi \mathrm{i}} \int_L \frac{\prod_{j=1}^{m} \Gamma(b_j - B_j t) \prod_{j=1}^{n} \Gamma(1 - a_j + A_j t)}{\prod_{j=m+1}^{q} \Gamma(1 - b_j + B_j t) \prod_{j=n+1}^{p} \Gamma(a_j - A_j t)} z^t \,\mathrm{d}t,$$

where $A_1, \ldots, A_p$ and $B_1, \ldots, B_q$ are positive real numbers. The path L is one of three possible choices, analogous to the case of the Meijer G-function. The convergence properties are more challenging to determine and can be found in [10]. The utilization of these functions forms a framework of highly generalized integral formulas for the calculation of the Fourier transform.

In the following, we assume that the RBF of interest can be represented as a Mellin-Barnes integral. The Meijer G-function and the Fox H-function are notable examples demonstrating that this assumption holds for a wide class of functions. If a function is

not initially given as a Mellin-Barnes integral, the Mellin transform

$$\mathcal{M}(f)(s) = f^*(s) = \int_0^\infty f(r) r^{s-1} \mathrm{d}r$$

can be applied, where $C_1 < \mathrm{Re}(s) < C_2$ for some constants C_1 and C_2, such that the integral is well defined. Furthermore, the inverse Mellin transform is given by

$$\mathcal{M}^{-1}(f^*)(r) = f(r) = \int_{C-\mathrm{i}\infty}^{C+\mathrm{i}\infty} f^*(s) r^{-s} \mathrm{d}s,$$

where $r > 0$ and $C_1 < C < C_2$ [29, p. 417].

2.2 General Calculation of the Fourier Transform

In this chapter, we explicitly calculate the n-dimensional generalized Fourier transform of a function $\phi : \mathbb{R}^n \to \mathbb{R}$ with the following properties:

- ϕ is non-singular for $\forall x \in \mathbb{R}^n \backslash \{0\}$,
- $\phi(x) \in \mathcal{O}(||x||^m)$ as $||x|| \to \infty$ for some $m \in \mathbb{N}$,
- $\phi(x) = \frac{1}{2\pi \mathrm{i}} \int_L f(t) \left(\frac{||x||}{c}\right)^{at} \mathrm{d}t$,

where $a \in \mathbb{R}$, $c \in \mathbb{R}_+$ and L is some path in the complex plane and the function $f(t)$ ensures that the integral along the path is absolutely convergent for all parameters a, c and for all $x \in \mathbb{R}^n$. The function typically consists of Gamma or trigonometric functions containing poles or branch cuts [44, p. 179]. For many cases, the function f is the Mellin transform of the RBF. Note that this includes any function that can be expressed as a Mellin-Barnes integral, such as Meijer G-functions and Fox H-functions. At the end of the section, we explicitly show the Fourier transform of the new types of RBFs that we propose and analyze for use in quasi-interpolation.

For an integrable function f, we recall the Fourier transform as

$$\hat{f}(y) = \int_{\mathbb{R}^n} f(x) \mathrm{e}^{-ix \cdot y} \mathrm{d}x, \qquad y \in \mathbb{R}^n.$$

For every radially symmetric function, the Fourier transform is also radially symmetric [30]. We can use this to work with the univariate function $\varphi(||x||) = \phi(x)$ instead of the multivariate one. Furthermore, we introduce the shorthand notation $||x|| = r$. As mentioned in the introduction, we have to deal with generalized Fourier transforms, since

we assume that the Fourier transform of the RBF is singular at the origin. To calculate the generalized Fourier transform, we have to introduce some regularization [30], [27]. This is done by introducing a Gaussian function, resulting in

$$\hat{\phi}(y) = \lim_{\varepsilon \to 0_+} \int_{\mathbb{R}^n} \phi(x) \mathrm{e}^{-ix \cdot y} \mathrm{e}^{-\varepsilon ||x||^2} \mathrm{d}x, \qquad y \in \mathbb{R}^n.$$

A considerable amount of literature discusses Fourier transforms of tempered distributions [34], [19], [51]. The fact that the Fourier transform of an RBF is also an RBF allows us to rewrite the Fourier transform as a Hankel or Mellin transform

$$\hat{\varphi}(s) = \lim_{\varepsilon \to 0_+} \frac{(2\pi)^{\frac{n}{2}}}{s^{\frac{n}{2}-1}} \int_0^\infty r^{\frac{n}{2}} \varphi(r) J_{\frac{n}{2}-1}(sr) \mathrm{e}^{-\varepsilon r^2} \, \mathrm{d}r, \qquad s = ||y||,$$

where $J_{\frac{n}{2}-1}(sr)$ denotes the Bessel function of the first kind. Next, we use the integral representation of the RBF $\varphi(r)$, yielding

$$\hat{\varphi}(s) = \lim_{\varepsilon \to 0_+} \frac{(2\pi)^{\frac{n}{2}}}{s^{\frac{n}{2}-1}} \int_0^\infty r^{\frac{n}{2}} \frac{1}{2\pi \mathrm{i}} \int_L f(t) \left(\frac{r}{c}\right)^{at} \mathrm{d}t J_{\frac{n}{2}-1}(sr) \mathrm{e}^{-\varepsilon r^2} \, \mathrm{d}r, \qquad s = ||y||.$$

The change of the integration is valid through the theorem of Fubini-Tonelli. Thus, we can write

$$\hat{\varphi}(s) = \lim_{\varepsilon \to 0_+} \frac{(2\pi)^{\frac{n}{2}}}{s^{\frac{n}{2}-1}} \frac{1}{2\pi \mathrm{i}} \int_L \frac{f(t)}{c^{at}} \int_0^\infty r^{\frac{n}{2}+at} J_{\frac{n}{2}-1}(sr) \mathrm{e}^{-\varepsilon r^2} \, \mathrm{d}r \, \mathrm{d}t.$$

Next, we express the Bessel function as a Meijer G-function [37, p. 307]

$$J_{\frac{n}{2}-1}(sr) = G_{0,2}^{1,0}\left(\begin{matrix} - \\ \frac{n-2}{4}, -\frac{n-2}{4} \end{matrix} \middle| \frac{(sr)^2}{4} \right)$$

and get

$$\hat{\varphi}(s) = \lim_{\varepsilon \to 0_+} \frac{(2\pi)^{\frac{n}{2}}}{s^{\frac{n}{2}-1}} \frac{1}{2\pi \mathrm{i}} \int_L \frac{f(t)}{c^{at}} \int_0^\infty r^{\frac{n}{2}+at} G_{0,2}^{1,0}\left(\begin{matrix} - \\ \frac{n-2}{4}, -\frac{n-2}{4} \end{matrix} \middle| \frac{(sr)^2}{4} \right) \mathrm{e}^{-\varepsilon r^2} \, \mathrm{d}r \, \mathrm{d}t.$$

After the substitution $\tilde{r} = r^2$, we obtain

$$\hat{\varphi}(s) = \lim_{\varepsilon \to 0_+} \frac{(2\pi)^{\frac{n}{2}}}{2s^{\frac{n}{2}-1}} \frac{1}{2\pi \mathrm{i}} \int_L \frac{f(t)}{c^{at}} \int_0^\infty \tilde{r}^{\frac{n-2}{4}+\frac{at}{2}} G_{0,2}^{1,0}\left(\begin{matrix} - \\ \frac{n-2}{4}, -\frac{n-2}{4} \end{matrix} \middle| \frac{s^2 \tilde{r}}{4} \right) \mathrm{e}^{-\varepsilon \tilde{r}} \, \mathrm{d}\tilde{r} \, \mathrm{d}t.$$

Using the property from equ. (2.1) with $\rho = \frac{n-2}{4}$ we get

$$\hat{\varphi}(s) = \lim_{\varepsilon \to 0_+} \frac{2^n \pi^{\frac{n}{2}}}{4 s^{n-2}} \frac{1}{2\pi \mathrm{i}} \int_L \frac{f(t)}{c^{at}} \int_0^\infty \tilde{r}^{\frac{at}{2}} G_{0,2}^{1,0}\left(\begin{matrix} - \\ \frac{n}{2} - 1, 0 \end{matrix} \middle| \frac{s^2 \tilde{r}}{4} \right) \mathrm{e}^{-\varepsilon \tilde{r}} \, \mathrm{d}\tilde{r} \, \mathrm{d}t.$$

In this form, the solution of the inner integral is shown in [10, p. 350] and provides

$$\hat{\varphi}(s) = \lim_{\varepsilon \to 0_+} \frac{2^n \pi^{\frac{n}{2}}}{4 s^{n-2}} \frac{1}{2\pi \mathrm{i}} \int_L \frac{f(t)}{c^{at}} \varepsilon^{-1-\frac{at}{2}} G_{1,2}^{1,1}\left(\begin{matrix} -\frac{at}{2} \\ \frac{n}{2} - 1, 0 \end{matrix} \middle| \frac{s^2}{4\varepsilon} \right) \mathrm{d}t.$$

The resulting Meijer G-function can be expressed in the form

$$\begin{aligned} \varepsilon^{-1-\frac{at}{2}} G_{1,2}^{1,1}\left(\begin{matrix} -\frac{at}{2} \\ \frac{n}{2} - 1, 0 \end{matrix} \middle| \frac{s^2}{4\varepsilon} \right) &= \varepsilon^{-1-\frac{at}{2}} \frac{\Gamma\left(\frac{n+at}{2}\right)}{\Gamma\left(-\frac{at}{2}\right)} \left(\frac{s^2}{4\varepsilon}\right)^{-1-\frac{at}{2}} + R(s,t,\varepsilon,n,a) \\ &= \frac{\Gamma\left(\frac{n+at}{2}\right)}{\Gamma\left(-\frac{at}{2}\right)} \left(\frac{s^2}{4}\right)^{-1-\frac{at}{2}} + R(s,t,\varepsilon,n,a), \end{aligned} \tag{2.3}$$

where the remainder $R(s,t,\varepsilon,n,a)$ can be upper bounded by

$$|R(s,t,\varepsilon,n,a)| \leq \varepsilon^{\frac{1}{2}} C(n,a,t) \left(\frac{s^2}{4}\right)^{-\frac{3}{2}-\frac{at}{2}},$$

where $C(n,a,t)$ is some function no longer depending on s and ε. These results are obtained by analyzing the asymptotic behavior of the Meijer G-function for large arguments. The derivation of this approach is presented in detail in chapter 3.1. Using equ. (2.3), we get

$$\hat{\varphi}(s) = \lim_{\varepsilon \to 0_+} \frac{2^n \pi^{\frac{n}{2}}}{4 s^{n-2}} \frac{1}{2\pi \mathrm{i}} \left(\int_L \frac{f(t)}{c^{at}} \left(\frac{\Gamma\left(\frac{n+at}{2}\right)}{\Gamma\left(-\frac{at}{2}\right)} \left(\frac{s^2}{4}\right)^{-1-\frac{at}{2}} + R(s,t,\varepsilon,n,a) \right) \mathrm{d}t \right),$$

where the first part does not depend on ε anymore, and the remaining part can be estimated by an upper bound

$$\begin{aligned} &\lim_{\varepsilon \to 0_+} \left| \frac{2^n \pi^{\frac{n}{2}}}{4 s^{n-2}} \frac{1}{2\pi \mathrm{i}} \int_L \frac{f(t)}{c^{at}} R(s,t,\varepsilon,n,a) \, \mathrm{d}t \right| \\ &\leq \lim_{\varepsilon \to 0_+} \frac{2^n \pi^{\frac{n}{2}}}{4 s^{n-2}} \frac{1}{2\pi} \int_L \left| \frac{f(t)}{c^{at}} R(s,t,\varepsilon,n,a) \right| \mathrm{d}t \end{aligned}$$

$$\leq \underbrace{\lim_{\varepsilon\to 0_+} \varepsilon^{\frac{1}{2}}}_{=0} \underbrace{\frac{2^n\pi^{\frac{n}{2}}}{4s^{n-2}}\frac{1}{2\pi}\int_L \left|\frac{f(t)}{c^{at}}C(n,a,t)\left(\frac{s^2}{4}\right)^{-\frac{3}{2}-\frac{at}{2}}\right| \mathrm{d}t}_{<\infty} = 0.$$

The remaining part vanishes in the limit $\varepsilon \to 0_+$. The integral in the last step is absolute convergent. This is also demonstrated in chapter 3.1, where we explicitly show the form of the function $C(n, a, t)$.

In summary, we end up with the final integral representation of the Fourier transform of the RBF,

$$\hat{\varphi}(s) = \frac{2^n\pi^{\frac{n}{2}}}{s^n}\frac{1}{2\pi\mathrm{i}}\int_L f(t)\frac{\Gamma\left(\frac{n+at}{2}\right)}{\Gamma\left(-\frac{at}{2}\right)}\left(\frac{2}{cs}\right)^{at}\mathrm{d}t. \tag{2.4}$$

This is a very general result, which is useful for determining the asymptotic behaviour without solving the integral explicitly. We will use this in the following section. However, in many special cases, the integral can be evaluated.

2.3 New Radial Basis Functions

In this section, we will use the derived integral representation and apply it to new classes of RBFs. We calculate the Fourier transform of new classes of **generalized multiquadrics**

$$\varphi(r) = \left(c^\lambda + r^\lambda\right)^\beta, \qquad \lambda \in \mathbb{R},\ \beta \in \mathbb{R}\backslash\mathbb{N},\ r = ||x||,\ x \in \mathbb{R}^n$$

and **generalized thin plate splines**

$$\varphi(r) = (c^\lambda + r^\lambda)\log(c^\beta + r^\beta), \qquad \lambda, \beta \in \mathbb{R},\ r = ||x||,\ x \in \mathbb{R}^n.$$

Furthermore, we calculate the Fourier transform of **powers of logarithms**

$$\varphi(r) = r^\lambda \log^k(r), \qquad k \in \mathbb{N},\ \lambda \in \mathbb{R},\ r = ||x||,\ x \in \mathbb{R}^n,$$

to demonstrate the wide range of applications where this approach can be employed. We always relate the result to known special cases where the Fourier transform has been established in the literature.

Prior to advancing with the first generalization, we first revisit the residue theorem, which is a useful tool to evaluate certain integrals and will be utilized extensively in the

subsequent chapter. The residue theorem states that if f is an analytic function in the complex plane $\mathbb{C}$ except for a countable set of isolated singularities at points $a_1, a_2, \ldots$, and L is a closed contour in $\mathbb{C}$ such that for all $j \in \mathbb{N}$, the singularity a_j does not lie on the contour L, then the contour integral of f around L is given by the following expression

$$\frac{1}{2\pi \mathrm{i}} \int_L f(z) \mathrm{d}z = \sum_j \operatorname{Ind}(L, a_j) \operatorname{Res}_{a_j} f,$$

where the function $\operatorname{Ind}(L, a_j)$ counts how many times the path L encircles the singularity a_j in a positive mathematical sense [39, p. 141]. If the singularity of the function f at a_j is a pole of order m, then the residue can be calculated by the formula

$$\operatorname{Res}_{a_j} f = \frac{1}{(m-1)!} \lim_{z \to a_j} \frac{\mathrm{d}^{m-1}}{\mathrm{d}z^{m-1}} \left((z - a_j)^m f(z) \right).$$

There is a large body of literature introducing the topic of complex analysis [35, p. 106], [9, p. 219], and [31, p. 86]. A special case that will be frequently used is the residue of the Gamma function. The Gamma function has countably many simple poles at the negative integers, including zero. The residues of the Gamma function evaluated at these poles are given by [4, p. 16]

$$\begin{aligned} \operatorname{Res}_{-k} \Gamma(z) &= \frac{(-1)^k}{k!}, && k \in \mathbb{N}, \\ \operatorname{Res}_{k} \Gamma(-z) &= \frac{(-1)^{k+1}}{k!}, && k \in \mathbb{N}. \end{aligned} \tag{2.5}$$

We now present a brief example to illustrate how the residue theorem can be applied to evaluate a Meijer G-function. As an example, we use the function

$$G_{1,0}^{0,1}\left(\begin{matrix} - \\ 0 \end{matrix} \middle| z^2 \right) = \frac{1}{2\pi \mathrm{i}} \int_L \Gamma(-t) z^{2t} \mathrm{d}t. \tag{2.6}$$

The poles and the path L are shown in figure 2.2. The path L is a loop that contains countably many poles of the Gamma function. Hence, the integral is equal to the sum of infinitely many residues of the Gamma function. The residues for the poles are given by

$$\begin{aligned} \operatorname{Res}_0 \Gamma(-t)(-z)^{2t} &= -1 \\ \operatorname{Res}_1 \Gamma(-t)(-z)^{2t} &= z^2 \\ \operatorname{Res}_2 \Gamma(-t)(-z)^{2t} &= -\frac{z^4}{2} \end{aligned}$$

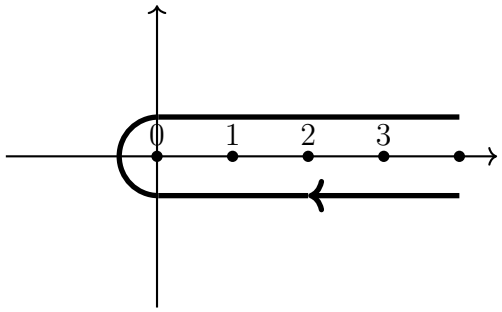

Figure 2.2: Visualization of the poles of $\Gamma(-s)$ and the path L in the complex plane for the Meijer G-function $G_{1,0}^{0,1}\left(\begin{matrix}-\\0\end{matrix}\middle|\, z^2\right)$.

$$\vdots$$

$$\operatorname{Res}_k \Gamma(-t)(-z)^{2t} = -\frac{(-1)^k z^{2k}}{k!}.$$

Every pole is encircled in the mathematical negative sense. Hence, a minus sign has to be included. Summing up all residues, we end up with

$$G_{1,0}^{0,1}\left(\begin{matrix}-\\0\end{matrix}\middle|\, z^2\right) = \frac{1}{2\pi \mathrm{i}} \int_L \Gamma(-s) z^{2t} \mathrm{d}t = \sum_{k=0}^{\infty} \frac{(-1)^k z^{2k}}{k!} = \mathrm{e}^{-z^2}. \tag{2.7}$$

The series representation of the Meijer G-function is equal to the series representation of the exponential function e^{-z^2}. Additionally, the example showed how to evaluate a Meijer G-function, and we found the Meijer G-function representation of the exponential function.

After providing these insights into the evaluation of a Mellin-Barnes type integral, we now proceed with the Fourier transforms of the new classes of RBFs and their known special cases.

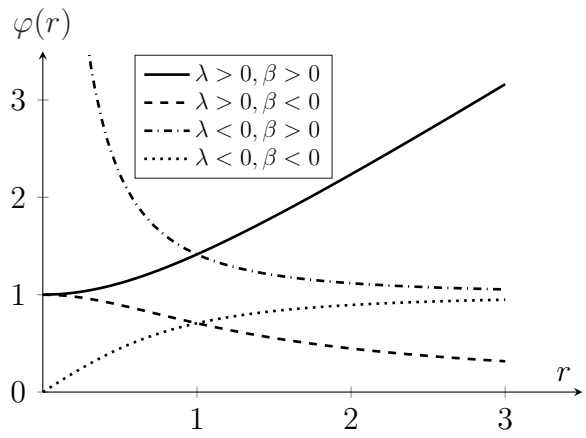

Figure 2.3: Visualization of the generalized multiquadric $\varphi(r) = \left(c^\lambda + r^\lambda\right)^\beta$ for different signs of the parameters λ and β. The visualization is generated using the parameters $|\lambda| = 2$, $|\beta| = \frac{1}{2}$, and $c = 1$.

2.3.1 Generalized Multiquadric

The first new RBF is the generalized multiquadric

$$\begin{aligned}\varphi(r) = \left(c^\lambda + r^\lambda\right)^\beta &= \frac{c^{\lambda\beta}}{\Gamma(-\beta)} G_{1,1}^{1,1}\left(\begin{matrix} 1+\beta \\ 0 \end{matrix}\,\middle|\, \left(\frac{r}{c}\right)^\lambda\right) \\ &= \frac{c^{\lambda\beta}}{\Gamma(-\beta)} \frac{1}{2\pi\mathrm{i}} \int_L \Gamma(-t)\Gamma(-\beta+t) \left(\frac{r}{c}\right)^{\lambda t} \mathrm{d}t.\end{aligned}$$

The RBF is visualized in figure 2.3. Note that the qualitative behaviour of the function is intrinsically dependent on the signs of the parameters λ and β. As stated in the introducing example, the Meijer G-function representation can be verified by the series representation. Comparing the integral representation with the assumed form of the RBF $\varphi(r) = \frac{1}{2\pi\mathrm{i}} \int_L f(t) \left(\frac{r}{c}\right)^{at} \mathrm{d}t$, we obtain

$$f(t) = \frac{c^{\lambda\beta}}{\Gamma(-\beta)} \Gamma(-t)\Gamma(-\beta+t).$$

Using equ. (2.4), the Fourier transform of the generalized multiquadric is given by

$$\hat{\varphi}(s) = \frac{2^n \pi^{\frac{n}{2}} c^{\lambda\beta}}{\Gamma(-\beta) s^n} \frac{1}{2\pi\mathrm{i}} \int_L \frac{\Gamma(-t)\Gamma(-\beta+t)\Gamma\left(\frac{n+\lambda t}{2}\right)}{\Gamma\left(-\frac{\lambda t}{2}\right)} \left(\frac{2}{cs}\right)^{\lambda t} \mathrm{d}t, \tag{2.8}$$

where L is a path from $-\mathrm{i}\infty$ to $\mathrm{i}\infty$, separating the poles of the Gamma functions in the numerator. The direction in which the path L can be closed at infinity depends on the

signs of the parameters λ and β. The parameters λ and β are pivotal in determining which poles have to be taken into account to employ the residue theorem. For the special case $\lambda = 2d, \beta = \frac{1}{2}, d \in \mathbb{N}$, this result was first discovered by [42]. The formula presented here is valid for $\lambda \in \mathbb{R}$ and $\beta \in \mathbb{R}\backslash\mathbb{N}$ and therefore more general.

2.3.1.1 Special Cases

In order to determine the residues of the relevant poles, the locations of poles in the complex plane that are encircled by the path of integration must be known. For the generalized multiquadric this is illustrated in figures 3.2, 3.3, 3.4, and 3.5.

1. The first special case is given for $\lambda = 2$ and $\beta \notin \mathbb{N}$. The Fourier transform from equ. (2.8) simplifies to

$$\begin{aligned}\hat{\varphi}(s) &= \frac{2^n \pi^{\frac{n}{2}} c^{2\beta}}{\Gamma(-\beta) s^n} \frac{1}{2\pi \mathrm{i}} \int_L \Gamma(-\beta + t) \Gamma\left(\frac{n}{2} + t\right) \left(\frac{2}{cs}\right)^{2t} \mathrm{d}t \\ &= \frac{2^n \pi^{\frac{n}{2}} c^{2\beta}}{\Gamma(-\beta) s^n} G_{2,0}^{0,2}\left(\begin{matrix} 1+\beta, 1-\frac{n}{2} \\ - \end{matrix} \middle| \left(\frac{2}{cs}\right)^2\right),\end{aligned}$$

   using property (2.2), we obtain

$$= \frac{2^n \pi^{\frac{n}{2}} c^{2\beta}}{\Gamma(-\beta) s^n} G_{0,2}^{2,0}\left(\begin{matrix} - \\ -\beta, \frac{n}{2} \end{matrix} \middle| \left(\frac{cs}{2}\right)^2\right).$$

   This Meijer G-function can be simplified to the modified Bessel function of the second kind [37, p. 307]

$$G_{0,2}^{2,0}\left(\begin{matrix} - \\ a, b \end{matrix} \middle| z^2\right) = 2 z^{a+b} K_{a-b}(2z), \qquad a, b, z \in \mathbb{R}.$$

   With this representation, we proceed with the calculation of the Fourier transform

$$\begin{aligned}\hat{\varphi}(s) &= \frac{2^n \pi^{\frac{n}{2}} c^{2\beta}}{\Gamma(-\beta) s^n} 2 \left(\frac{cs}{2}\right)^{\frac{n}{2}-\beta} K_{\frac{n}{2}+\beta}(cs) \\ &= \frac{2^{\frac{n}{2}+1+\beta} \pi^{\frac{n}{2}} c^{\frac{n}{2}+\beta}}{\Gamma(-\beta) s^{\frac{n}{2}+\beta}} K_{\frac{n}{2}+\beta}(cs) \\ &= \frac{2\pi^{\frac{n}{2}}}{\Gamma(-\beta)} \left(\frac{2c}{s}\right)^{\frac{n}{2}+\beta} K_{\frac{n}{2}+\beta}(cs).\end{aligned}$$

For this special case, the abstract contour integral simplifies to well-known functions.

2. A further specialization is the most famous and widely used RBF, Hardy's multiquadric ($\lambda = 2$, $\beta = \frac{1}{2}$). In this case, the Fourier transform further simplifies to

$$\begin{aligned}\hat{\varphi}(s) &= \frac{2\pi^{\frac{n}{2}}}{\Gamma(-\frac{1}{2})}\left(\frac{2c}{s}\right)^{\frac{n}{2}+\frac{1}{2}} K_{\frac{n}{2}+\frac{1}{2}}(cs) \\ &= -\pi^{-1}\left(\frac{2\pi c}{s}\right)^{\frac{n+1}{2}} K_{\frac{n+1}{2}}(cs),\end{aligned}$$

where we used that $\Gamma\left(-\frac{1}{2}\right) = -2\sqrt{\pi}$. This result is also stated in [15, p. 154] and [11, p. 108].

3. The next special case is the inverse multiquadric ($\lambda = 2, \beta = -\frac{1}{2}$). The Fourier transform evaluates to

$$\hat{\varphi}(s) = \frac{2\pi^{\frac{n}{2}}}{\Gamma(\frac{1}{2})}\left(\frac{2c}{s}\right)^{\frac{n}{2}-\frac{1}{2}} K_{\frac{n}{2}-\frac{1}{2}}(cs).$$

Using $\Gamma\left(\frac{1}{2}\right) = \sqrt{\pi}$, we get

$$= 2\left(\frac{2\pi c}{s}\right)^{\frac{n-1}{2}} K_{\frac{n-1}{2}}(cs).$$

This result is also presented in [15, p. 156].

4. The last special case of the generalized multiquadric is the limit $c \to 0_+$. Without loss of generality, we set $\lambda = 2$. There are three different scenarios to consider. The first is for $\beta \in \mathbb{N}$. In this case the RBF is a polynomial, and the generalized Fourier transform is given by derivatives of the Delta distribution, denoted by $\delta(s)$

$$\hat{\varphi}(s) = (2\pi)^n(-1)^\beta\left(\partial_1^2 + \cdots + \partial_n^2\right)^\beta \delta(s), \qquad \beta \in \mathbb{N}.$$

This case is well known and can be looked up, for example in [27, p. 359].

The second scenario is for $\beta \notin \mathbb{N}$ and $\beta \notin -\mathbb{N} - \frac{n}{2}$. This limit can be evaluated using the residue theorem. The only non-vanishing term is induced by the simple

pole at $t = \beta$. Using the identity (2.5), the Fourier transform simplifies to

$$\begin{aligned}\hat{\varphi}(s) &= \lim_{c\to 0} \frac{2^n \pi^{\frac{n}{2}} c^{2\beta}}{\Gamma(-\beta) s^n} \frac{1}{2\pi \mathrm{i}} \int_L \Gamma(-\beta + t)\Gamma\left(\frac{n}{2} + t\right) \left(\frac{2}{cs}\right)^{2t} \mathrm{d}t \\ &= 2^{n+2\beta} \pi^{\frac{n}{2}} \frac{\Gamma\left(\frac{n}{2} + \beta\right)}{\Gamma\left(-\beta\right)} s^{-n-2\beta}, \qquad \beta \notin \mathbb{N} \text{ and } \beta \notin -\frac{n}{2} - \mathbb{N}.\end{aligned}$$

This result is also stated in the literature [34] and [27].

The third scenario is for $\beta = -k - \frac{n}{2}, k \in \mathbb{N}$. The first non-vanishing term is induced by the double pole at $t = \beta$. Evaluating the residue at $t = \beta$ leads to

$$\mathrm{Res}_\beta \, \Gamma(-\beta + t)\Gamma\left(-k - \beta + t\right) \left(\frac{2}{cs}\right)^{2t} = \frac{(-1)^k \left(\frac{2}{cs}\right)^{2\beta} \left(2 \log\left(\frac{2}{cs}\right) + \psi^{(0)}(k+1) - \gamma\right)}{k!},$$

where $\psi^{(0)}(k+1) = \dfrac{\mathrm{d}}{\mathrm{d}z} \log\left(\Gamma(z)\right)|_{z=k+1}$ is the Digamma function [20, p. 89]. In summary, we derive

$$\begin{aligned}\hat{\varphi}(s) &= \lim_{c\to 0_+} \frac{(-1)^k \pi^{n/2} s^{2k} \left(\log\left(\frac{2}{cs}\right) + \frac{\psi^{(0)}(k+1)}{2} - \frac{\gamma}{2}\right)}{2^{2k-1} k! \Gamma\left(k + \frac{n}{2}\right)} \\ &= \frac{(-1)^k \pi^{n/2} s^{2k}}{2^{2k-1} k! \Gamma\left(k + \frac{n}{2}\right)} \left(\log\left(\frac{2}{s}\right) + \frac{\psi^{(0)}(k+1)}{2} - \frac{\gamma}{2} - \lim_{c\to 0_+} \log(c)\right) = \infty.\end{aligned}$$

In the limit $c \to 0_+$, we see that the Fourier transform divergences. Consequently, this particular case will be excluded from further studies. The finite part of the expression corresponds precisely to what Jones asserted as the Fourier transform [34]. Our position is that Jones' assertion is erroneous, and the Fourier transform for this case cannot be properly calculated. This viewpoint is also supported by [27].

With these special cases, the calculation of the generalized Fourier transform of the generalized multiquadric is completed. We calculated the Fourier transform in general and demonstrated for special cases that it is consistent with those reported in the existing literature. In the next subsection, the generalized Fourier transform for the generalized thin plate spline is presented.

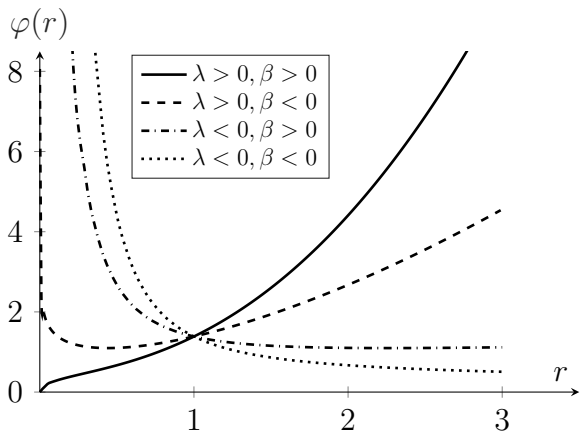

Figure 2.4: Visualization of the generalized thin plate spline $\varphi(r) = (c^\lambda + r^\lambda)\log(c^\beta + r^\beta)$ for different signs of the parameters λ and β. The visualization is generated using the parameters $|\lambda| = 2$, $|\beta| = \frac{1}{2}$ and $c = 1$.

2.3.2 Generalized Thin Plate Spline

In this section, we calculate the Fourier transform of a generalized version of the shifted thin plate spline

$$\varphi(r) = (c^\lambda + r^\lambda)\log(c^\beta + r^\beta), \qquad ||x|| = r \in \mathbb{R}_{>0}, x \in \mathbb{R}^n.$$

The function is visualized in figure 2.4. Furthermore, we derive some known expressions for special cases. Ortmann and Buhmann showed the calculation in the case that $\lambda = \beta$ are even positive numbers [43]. In order to achieve this, the function is decomposed into four distinct parts. Subsequently, each part is transformed individually. These four parts are:

$$\begin{aligned}
\varphi(r) &= \varphi_1(r) + \varphi_2(r) + \varphi_3(r) + \varphi_4(r),\\
\varphi_1(r) &= c^\lambda \log(c^\beta),\\
\varphi_2(r) &= r^\lambda \log(c^\beta),\\
\varphi_3(r) &= c^\lambda \log\left(1 + \left(\frac{r}{c}\right)^\beta\right),\\
\varphi_4(r) &= r^\lambda \log\left(1 + \left(\frac{r}{c}\right)^\beta\right).
\end{aligned}$$

The generalized Fourier transforms of $\varphi_1(r)$ and $\varphi_2(r)$ are well documented [34]. The function $\varphi_1(r)$ is a constant and hence the generalized Fourier transform is given by $\hat{\varphi}_1(s) = (2\pi)^n c^\lambda \log\left(c^\beta\right)\delta(s)$. Since we are interested in $\varphi(s)$ for $s > 0$, this term has

no further relevance in the subsequent analysis. Later it can be shown that the sum $\sum_{k\in\mathbb{Z}^n}\mu_k\varphi_1\left(||x-k||\right)=0$ vanishes identically. The Fourier transform of $\varphi_2(r)$ is shown in section 2.3.1 in the limit for $c\to 0_+$ and is also presented in [34]. It is given by

$$\hat{\varphi}_2(s)=\begin{cases}\beta\log(c)\frac{\Gamma\left(\frac{n+\lambda}{2}\right)}{\Gamma(-\frac{\lambda}{2})}2^{\lambda+n}\pi^{n/2}s^{-n-\lambda}, & \frac{\lambda}{2}\notin\mathbb{N}\wedge\frac{\lambda}{2}\notin-\mathbb{N}-\frac{n}{2}\\ \beta\log(c)\left(2\pi\right)^n\left(-1\right)^{\frac{\lambda}{2}}\left(\partial_1^2+\cdots+\partial_n^2\right)^{\frac{\lambda}{2}}\delta(s), & \frac{\lambda}{2}\in\mathbb{N}.\end{cases}$$

In the next step, we explicitly present the calculation of $\varphi_4(r)$. The calculation of the Fourier transform of $\varphi_3(r)$ follows the same approach. The Meijer G-function representation of the logarithm is given by [29, p. 478]

$$\log\left(1+\left(\frac{r}{c}\right)^\beta\right)=G_{2,2}^{1,2}\left(\begin{matrix}1,1\\1,0\end{matrix}\middle|\,\left(\frac{r}{c}\right)^\beta\right).$$

Hence, $\varphi_4(r)$ can be written as

$$\begin{aligned}\varphi_4(r)&=r^\lambda G_{2,2}^{1,2}\left(\begin{matrix}1,1\\1,0\end{matrix}\middle|\,\left(\frac{r}{c}\right)^\beta\right)\\&=c^\lambda\left(\left(\frac{r}{c}\right)^\beta\right)^{\frac{\lambda}{\beta}}G_{2,2}^{1,2}\left(\begin{matrix}1,1\\1,0\end{matrix}\middle|\,\left(\frac{r}{c}\right)^\beta\right)\\&=c^\lambda G_{2,2}^{1,2}\left(\begin{matrix}\frac{\beta+\lambda}{\beta},\frac{\beta+\lambda}{\beta}\\\frac{\beta+\lambda}{\beta},\frac{\lambda}{\beta}\end{matrix}\middle|\,\left(\frac{r}{c}\right)^\beta\right)\\&=c^\lambda\frac{1}{2\pi\mathrm{i}}\int_L\frac{\Gamma\left(1+\frac{\lambda}{\beta}-t\right)\Gamma\left(-\frac{\lambda}{\beta}+t\right)^2}{\Gamma\left(1-\frac{\lambda}{\beta}+t\right)}\left(\frac{r}{c}\right)^{\beta t}\mathrm{d}t.\end{aligned}$$

Comparing this with the general Fourier transform in equ. (2.4), we conclude that $f(t)=c^\lambda\frac{\Gamma\left(1+\frac{\lambda}{\beta}-t\right)\Gamma\left(-\frac{\lambda}{\beta}+t\right)^2}{\Gamma\left(1-\frac{\lambda}{\beta}+t\right)}$. The Fourier transform is expressed as

$$\hat{\varphi}_4(s)=\frac{2^n\pi^{\frac{n}{2}}c^\lambda}{s^n}\frac{1}{2\pi\mathrm{i}}\int_L\frac{\Gamma\left(1+\frac{\lambda}{\beta}-t\right)\Gamma\left(-\frac{\lambda}{\beta}+t\right)^2\Gamma\left(\frac{n+\beta t}{2}\right)}{\Gamma\left(1-\frac{\lambda}{\beta}+t\right)\Gamma\left(-\frac{\beta t}{2}\right)}\left(\frac{2}{cs}\right)^{\beta t}\mathrm{d}t$$

and analog

$$\hat{\varphi}_3(s)=\frac{2^n\pi^{\frac{n}{2}}c^\lambda}{s^n}\frac{1}{2\pi\mathrm{i}}\int_L\frac{\Gamma\left(1-t\right)\Gamma\left(t\right)^2\Gamma\left(\frac{n+\beta t}{2}\right)}{\Gamma\left(1+t\right)\Gamma\left(-\frac{\beta t}{2}\right)}\left(\frac{2}{cs}\right)^{\beta t}\mathrm{d}t.$$

Note that $\hat{\varphi}_3(s) = c^\lambda \left(\hat{\varphi}_4(s) \Big|_{\lambda=0} \right)$. If $\frac{\lambda}{\beta} < 1$, then the path L for $\hat{\varphi}_3(s)$ and $\hat{\varphi}_4(s)$ can be chosen identically, and therefore the integrands can be added. The addition of the integrands is also valid if $\beta \in 2\mathbb{N}$ and $\frac{\lambda}{\beta} \in \mathbb{N}$. In this case, all poles of the integrands $\hat{\varphi}_3(s)$ and $\hat{\varphi}_4(s)$ tending to plus infinity cancel out. In this case, we obtain

$$\hat{\varphi}_3(s) + \hat{\varphi}_4(s) = \frac{2^n \pi^{\frac{n}{2}} c^\lambda}{s^n} \frac{1}{2\pi \mathrm{i}} \int_L \frac{\Gamma\left(\frac{n+\beta t}{2}\right)}{\Gamma\left(-\frac{\beta t}{2}\right)} \left(\frac{\Gamma(1-t)\,\Gamma(t)^2}{\Gamma(1+t)} + \right. \\ \left. + \frac{\Gamma\left(1+\frac{\lambda}{\beta}-t\right)\Gamma\left(-\frac{\lambda}{\beta}+t\right)^2}{\Gamma\left(1-\frac{\lambda}{\beta}+t\right)} \right) \left(\frac{2}{cs}\right)^{\beta t} \mathrm{d}t.$$

If this is not the case, the functions have to be analyzed individually.

2.3.2.1 Special cases

In general, visualizing the location of the poles in the complex plane and the path of integration is advisable. For the generalized thin plate spline, this is done in the figures 3.6, 3.7, 3.8, and 3.9 for different signs of λ and β.

1. The first special case is given for $\lambda = \beta \in 2\mathbb{N}$, where $2\mathbb{N}$ denotes the set of all positive even integers. Hence, the Fourier transform simplifies to

$$\hat{\varphi}_3(s) + \hat{\varphi}_4(s) = \frac{2^n \pi^{\frac{n}{2}} c^\lambda}{s^n} \frac{1}{2\pi \mathrm{i}} \int_L \frac{\Gamma\left(\frac{n+\lambda t}{2}\right)}{\Gamma\left(-\frac{\lambda t}{2}\right)} \left(\frac{\Gamma(1-t)\,\Gamma(t)^2}{\Gamma(1+t)} + \right. \\ \left. + \frac{\Gamma(2-t)\,\Gamma(-1+t)^2}{\Gamma(t)} \right) \left(\frac{2}{cs}\right)^{\lambda t} \mathrm{d}t. \tag{2.9}$$

   Using the identity $z\Gamma(z) = \Gamma(z+1), \forall z \in \mathbb{C}$, the sum can be simplified to

$$\frac{\Gamma(2-t)\,\Gamma(t-1)^2}{\Gamma(t)} = -\frac{\Gamma(2-t)\,\Gamma(t-1)}{1-t} = -\Gamma(1-t)\,\Gamma(t-1) \\ = \Gamma(-t)\,\Gamma(t)\,\frac{t}{t-1}$$

   and analog

$$\frac{\Gamma(1-t)\,\Gamma(t)^2}{\Gamma(1+t)} = -\Gamma(-t)\,\Gamma(t)\,.$$

Summing both expressions leads to

$$\frac{\Gamma(2-t)\,\Gamma(t-1)^2}{\Gamma(t)} + \frac{\Gamma(1-t)\,\Gamma(t)^2}{\Gamma(1+t)} = \Gamma(-t)\,\Gamma(t)\,\frac{1}{t-1} = \Gamma(-t)\,\Gamma(t-1)\,.$$

Using this in equ. (2.9) results in

$$\hat{\varphi}_3(s) + \hat{\varphi}_4(s) = \frac{2^n \pi^{\frac{n}{2}} c^\lambda}{s^n} \frac{1}{2\pi \mathrm{i}} \int_L \frac{\Gamma(-t)\,\Gamma(t-1)\,\Gamma\left(\frac{n+\lambda t}{2}\right)}{\Gamma\left(-\frac{\lambda t}{2}\right)} \left(\frac{2}{cs}\right)^{\lambda t} \mathrm{d}t. \tag{2.10}$$

This result is also shown in [43]. Note that $\hat{\varphi}_1(s)$ and $\hat{\varphi}_2(s)$ also have to be taken into account for the initial Fourier transform of the generalized thin plate spline. However, these are merely Delta distributions and, as such, are not further considered. This is caused by the fact that in this special case the sums $\sum_{k\in\mathbb{Z}^n} \mu_k \varphi_1(||x-k||) = 0$ and $\sum_{k\in\mathbb{Z}^n} \mu_k \varphi_2(||x-k||) = 0$ will vanish identically.

2. The next case is the well-known thin plate spline ($\lambda = \beta = 2$). With these parameters, the Fourier transform simplifies to

$$\begin{aligned}
\hat{\varphi}_3(s) + \hat{\varphi}_4(s) &= \frac{2^n \pi^{\frac{n}{2}} c^2}{s^n} \frac{1}{2\pi \mathrm{i}} \int_L \Gamma(t-1)\,\Gamma\left(\frac{n}{2}+t\right) \left(\frac{2}{cs}\right)^{2t} \mathrm{d}t \\
&= \frac{2^n \pi^{\frac{n}{2}} c^2}{s^n} G_{2,0}^{0,2}\left(\begin{matrix} 1-\frac{n}{2}, 2 \\ - \end{matrix} \,\middle|\, \left(\frac{2}{cs}\right)^2\right) \\
&= \frac{2^n \pi^{\frac{n}{2}} c^2}{s^n} G_{2,0}^{0,2}\left(\begin{matrix} - \\ \frac{n}{2}, -1 \end{matrix} \,\middle|\, \left(\frac{cs}{2}\right)^2\right) \\
&= \frac{2^n \pi^{\frac{n}{2}} c^2}{s^n} \left(\frac{cs}{2}\right)^{\frac{n-2}{2}} G_{2,0}^{0,2}\left(\begin{matrix} - \\ \frac{n+2}{4}, -\frac{n+2}{4} \end{matrix} \,\middle|\, \left(\frac{cs}{2}\right)^2\right) \\
&= 4\,(2\pi)^{\frac{n}{2}} \left(\frac{c}{s}\right)^{\frac{n}{2}+1} K_{\frac{n}{2}+1}(cs).
\end{aligned}$$

The result is also stated in the literature [15, p. 156]. As before, $\hat{\varphi}_1(s)$ and $\hat{\varphi}_2(s)$ are Delta distributions and are therefore not further considered.

3. The last special case is the limit $c^\lambda \to 0_+$. Without loss of generality, we can use $\lambda = \beta$. Again, there are some cases to distinguish. First let $\lambda = 2k, k \in \mathbb{N}$. Then we can make use of equ. (2.10). The first non-vanishing pole is of first order. Evaluating the residue at $t = 1$ leads to

$$\hat{\varphi}_3(s) + \hat{\varphi}_4(s) = (-1)^{k+1} \frac{2^{n+2k} \pi^{\frac{n}{2}}}{s^{n+2k}} k k! \Gamma\left(k + \frac{n}{2}\right).$$

Up to some Delta distribution, this result matches the result given in [34, p. 530] and [27, p. 364].

If $\lambda \notin 2\mathbb{N}$, then the functions have to be analyzed separately. For $\hat{\varphi}_3(s)$, the first non-vanishing pole is located at $t = 0$. Evaluating the residue at $t = 0$ leads to

$$\begin{aligned}\left|\lim_{c\to 0} \hat{\varphi}_3(s)\right| &= \lim_{c^\lambda \to 0} \left| \frac{2^n \pi^{\frac{n}{2}} c^\lambda}{s^n} \frac{1}{2\pi \mathrm{i}} \int_L \frac{\Gamma(1-t)\,\Gamma(t)^2\,\Gamma\left(\frac{n+\lambda t}{2}\right)}{\Gamma(1+t)\,\Gamma\left(-\frac{\lambda t}{2}\right)} \left(\frac{2}{cs}\right)^{\lambda t} \mathrm{d}t \right| \\ &\leq \lim_{c^\lambda \to 0} \left| C c^\lambda \right| = 0.\end{aligned}$$

The residues of the following poles vanish even faster than the evaluated pole. For $\hat{\varphi}_4(s)$, the first non-vanishing pole is located at $t = 1$. The pole is of second order, and evaluating the residue leads to

$$\hat{\varphi}_4(s) = \lim_{c^\lambda \to 0} \frac{\pi^{n/2} 2^{\lambda+n-1} \Gamma\left(\frac{n+\lambda}{2}\right) s^{-\lambda-n} \lambda \left(2\log\left(\frac{2}{cs}\right) + \psi^{(0)}\left(-\frac{\lambda}{2}\right) + \psi^{(0)}\left(\frac{n+\lambda}{2}\right)\right)}{\Gamma\left(-\frac{\lambda}{2}\right)}.$$

Note that in the limit, the expression is singular but the logarithmic singularity is exactly canceled by

$$\hat{\varphi}_2(s) = \lambda \log(c) \frac{\Gamma\left(\frac{n+\lambda}{2}\right)}{\Gamma(-\frac{\lambda}{2})} 2^{\lambda+n} \pi^{n/2} s^{-n-\lambda}.$$

In summary, we obtain

$$\hat{\varphi}(s) = \frac{\lambda \pi^{n/2} 2^{\lambda+n} \Gamma\left(\frac{n+\lambda}{2}\right) s^{-\lambda-n}}{\Gamma\left(-\frac{\lambda}{2}\right)} \left(\log\left(\frac{2}{s}\right) + \frac{1}{2}\psi^{(0)}\left(-\frac{\lambda}{2}\right) + \frac{1}{2}\psi^{(0)}\left(\frac{n+\lambda}{2}\right)\right).$$

Note that in the limit, $\hat{\varphi}_1(s)$ is also zero. This finding also agrees with the results reported in the literature [34, p. 530] and [27, p. 364] .

2.3.3 Powers of Logarithms

In this subsection, we focus on the RBF

$$\varphi(r) = r^\lambda \log^k(r), \qquad k \in \mathbb{N},\ \lambda \in \mathbb{R}.$$

The function is visualized in figure 2.5. Powers of logarithms can be covered by the

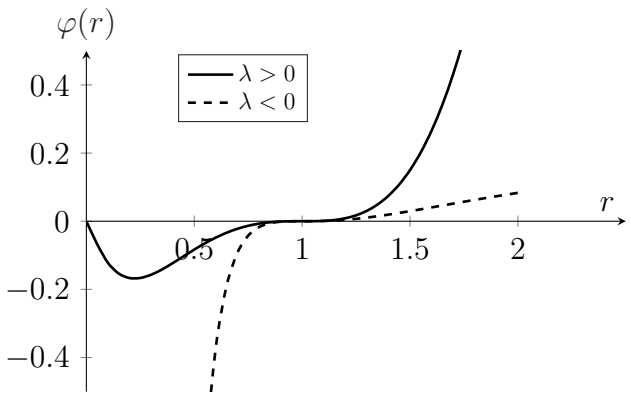

Figure 2.5: Visualization of powers of logarithms $\varphi(r) = r^\lambda \log^k(r)$ for different signs of the parameter λ. The visualization is made with the parameters $|\lambda| = 2$ and $k = 3$.

following contour integral

$$\log^k(r) = \frac{\Gamma(k+1)}{2\pi\mathrm{i}} \oint_L \frac{r^t}{t^{k+1}} \mathrm{d}t,$$

where L is a circle centered at the origin. Note that in this case we use the abstract contour integral representation, which is explicitly not a Meijer G- or Fox H-function representation. This equation can be verified using the residue theorem. Hence,

$$r^\lambda \log^k(r) = \frac{\Gamma(k+1)}{2\pi\mathrm{i}} \oint_L \frac{r^t}{(t-\lambda)^{k+1}} \mathrm{d}t,$$

where L is a circle centered at λ. This result is valid for $k \in \mathbb{N}$. Note that the generalization to $k \in \mathbb{R}$ is complicated because the contour L then depends on the argument r. This is due to the fact that the integrand has no isolated singularities anymore, but a branch cut. For $0 < r < 1$, the path L encircles the branch cut of the negative real line, while for $r > 1$ the path L encircles the positive real axis. This is why we stick to the special case $k \in \mathbb{N}$ and find $f(t) = \Gamma(k+1)(t-\lambda)^{-k-1}$. The Fourier transform is therefore given by

$$\hat{\varphi}(s) = \frac{2^n \pi^{\frac{n}{2}}}{s^n} \frac{1}{2\pi\mathrm{i}} \int_L \frac{\Gamma(k+1)}{(t-\lambda)^{k+1}} \frac{\Gamma\left(\frac{n+t}{2}\right)}{\Gamma\left(-\frac{t}{2}\right)} \left(\frac{2}{s}\right)^t \mathrm{d}t.$$

While the only contributing pole is at $t = \lambda$, we can explicitly use the residue theorem and obtain

$$\hat{\varphi}(s) = \frac{2^n \pi^{\frac{n}{2}}}{s^n} \lim_{t\to\lambda} \left(\frac{\mathrm{d}}{\mathrm{d}t}\right)^k \frac{\Gamma\left(\frac{n+t}{2}\right)}{\Gamma\left(-\frac{t}{2}\right)} \left(\frac{2}{s}\right)^t.$$

For the special cases $k = 1$ and $k = 2$, this result matches with the results presented in [26, p. 350].

This result further demonstrates the universality of the derived formula. However, this particular case will not be pursued further, as the focus will shift towards classical quasi-interpolation, which requires the highest singularity to be algebraic.

2.4 Summary

In this chapter, we derived an expression for the generalized Fourier transform applicable to a wide class of RBFs. For an RBF satisfying the properties

- ϕ is non-singular for $\forall x \in \mathbb{R}^n \backslash \{0\}$,
- $\phi(x) \in \mathcal{O}(||x||^m)$ as $||x|| \to \infty$ for some $m \in \mathbb{N}$,
- $\phi(x) = \frac{1}{2\pi \mathrm{i}} \int_L f(t) \left(\frac{||x||}{c}\right)^{at} \mathrm{d}t$,

the generalized Fourier transform is given by

$$\hat{\varphi}(s) = \frac{2^n \pi^{\frac{n}{2}}}{s^n} \frac{1}{2\pi \mathrm{i}} \int_L f(t) \frac{\Gamma\left(\frac{n+at}{2}\right)}{\Gamma\left(-\frac{at}{2}\right)} \left(\frac{2}{cs}\right)^{at} \mathrm{d}t.$$

Furthermore, we verified these result through several special cases and compared them to those reported in the literature. In the next section, we will use this representation of the Fourier transform to analyze the asymptotic behavior for large and small arguments.

Chapter 3

Asymptotic Behaviour of the Fourier Transform

The goal of this chapter is to determine the asymptotic behaviour of the Fourier transform of the RBF for small and large arguments, in order to apply the Strang and Fix conditions (1.2.4). Remember that the Fourier transform of the quasi-Lagrange function is given by

$$\hat{\Psi}(y) = \sum_{k\in\mathbb{Z}^n} \mu_k \mathrm{e}^{-ik\cdot y}\hat{\varphi}(||y||) = P(y)\hat{\varphi}(||y||), \qquad y \in \mathbb{R}^n,$$

where $P(y) = \sum_{k\in\mathbb{Z}^n} \mu_k \mathrm{e}^{-ik\cdot y}$ is the trigonometric polynomial, and $\hat{\varphi}(||y||)$ is the Fourier transform of our RBF calculated in the previous chapter. To apply the Strang and Fix conditions, the minimum requirements are

$$\hat{\Psi}(0) = 1 \quad \text{and} \quad \hat{\Psi}(2\pi j) = 0, \quad \forall j \in \mathbb{Z}^n\backslash\{0\}. \tag{3.1}$$

The trigonometric polynomial is 2π- periodic and if we choose the coefficients μ_k such that $P(0) = 0$, then the second condition in equ. (3.1) is satisfied under the constraint that $\hat{\varphi}(s)$ is finite on these points. This chapter will demonstrate that some of the previously calculated Fourier transforms are singular at the origin. This is exactly what is required to fulfill the first condition in equ. (3.1). One can select the order of the zeros of $P(y)$ in such a manner that the singularity of the RBF at the origin cancel out each other, and therefore $\hat{\Psi}(0) = P(0)\hat{\varphi}(0) = 1$. For all other values, the Fourier transforms of the RBFs are finite and so the first order conditions of Strang and Fix are satisfied. Note that the singularity of the Fourier transform of the RBF determines the order of the zeros of $P(y)$, which in turn constrains the order of the Strang and Fix conditions

that can be satisfied. This relationship highlights the influence of the RBF on the quasi-interpolation method, underscoring the significance of selecting an appropriate RBF. To determine the trigonometric polynomial, we need to know how the Fourier transform of the RBF behaves near the origin. The decay rate for large arguments for the function and its derivatives is needed to determine the decay behaviour of the quasi-Lagrange function.

The starting point of the analysis is the general form of the Fourier transform of the RBF

$$\hat{\varphi}(s) = \frac{2^n \pi^{\frac{n}{2}}}{s^n} \frac{1}{2\pi \mathrm{i}} \int_L f(t) \frac{\Gamma\left(\frac{n+at}{2}\right)}{\Gamma\left(-\frac{at}{2}\right)} \left(\frac{2}{cs}\right)^{at} \mathrm{d}t,$$

see chapter 2. This representation of the Fourier transform allows us to determine the asymptotic behaviour in a very elegant way.

3.1 Asymptotic Behaviour of General Integral Representations

In this section, we adapt the notation presented in [5] and define the asymptotic relation "$\sim$" for some continuous functions f and g as an equivalence relation

$$f(x) \sim g(x) \text{ as } x \to x_0 \quad \Leftrightarrow \quad \lim_{x \to x_0} \frac{f(x)}{g(x)} = 1.$$

Note that the value of x_0 may also be infinite. The asymptotic relation provides more information compared to the Landau big-$\mathcal{O}$ notation and both will be used depending on whether the precise behaviour is required.

The asymptotic behaviour of $\hat{\varphi}(s)$ is determined by the poles of the integrand and the path of integration. We also used this in the last chapter 2.3.1.1 for the special case 4, where we calculated the Fourier transform in the limit $c \to 0_+$. When the poles and the path of integration are known, the limit for small arguments is determined by the first non-vanishing pole inside the contour. The term "first" denotes the ordering of the poles according to the values of their real parts, arranged in either ascending or descending order, contingent upon the direction of the path of integration. Evaluating the residue leads to the asymptotic behaviour. Evaluating all other poles inside the integration contour determines the full series representation of the function. This is exactly what we did in the example of the residue theorem in the previous chapter. If the integrand

is analytic and there is no singularity or branch cut inside the contour, then the value of the integral vanishes. Using the example from the previous chapter, see equ. (2.7), we have

$$G_{1,0}^{0,1}\left(\begin{matrix}-\\0\end{matrix}\,\middle|\,-z\right) = \frac{1}{2\pi\mathrm{i}}\int_L \Gamma(-s)(-z)^t \mathrm{d}t$$
$$\sim -\operatorname{Res}_0 \Gamma(-t)(-z)^t = 1 \qquad \text{as } z \to 0.$$

To ascertain the higher-order asymptotic behaviour, additional poles have to be taken into account, leading to an asymptotic series

$$G_{1,0}^{0,1}\left(\begin{matrix}-\\0\end{matrix}\,\middle|\,-z\right) \sim \sum_{k=0}^{N} \frac{z^k}{k!} \qquad \text{as } z \to 0,$$

for some $N \in \mathbb{N}$.

For large values of the argument, determining the asymptotic behaviour becomes more complex. Two scenarios are particularly noteworthy: The first one arises when poles lie outside the contour, which restricts the ability to displace the contour towards infinity. This can be seen in figure 3.1. The second scenario occurs when no singularities exist outside the contour, allowing the path to be displaced towards positive or negative infinity. This is visualized in figure 2.2. We start with the first case, as utilized in equ. (2.3), where we determined the limit $\varepsilon \to 0$ of a Meijer G-function for large arguments. As an illustrative example and to justify the presented calculations in the previous chapter, we now determine the asymptotic behaviour for $\varepsilon \to 0$ of

$$\varepsilon^{-1-\frac{at}{2}} G_{1,2}^{1,1}\left(\begin{matrix}-\frac{at}{2}\\ \frac{n}{2}-1, 0\end{matrix}\,\middle|\,\frac{s^2}{4\varepsilon}\right) = \frac{\varepsilon^{-1-\frac{at}{2}}}{2\pi\mathrm{i}}\int_L \frac{\Gamma\left(\frac{n}{2}-1-v\right)\Gamma\left(1+\frac{at}{2}+v\right)}{\Gamma(1+v)}\left(\frac{s^2}{4\varepsilon}\right)^v \mathrm{d}v.$$

The basic idea is to shift the path of integration over the first pole that does not contribute to the original integral. The residue of this pole is the leading order term for large arguments. The error introduced by considering only the leading pole is determined by the integral over the displaced contour. Figure 3.1 visualizes the method, the poles, and the path of integration L for the given Meijer G-function. The leading order term can be computed using the residue theorem. The result is given by

$$\varepsilon^{-1-\frac{at}{2}} G_{1,2}^{1,1}\left(\begin{matrix}-\frac{at}{2}\\ \frac{n}{2}-1, 0\end{matrix}\,\middle|\,\frac{s^2}{4\varepsilon}\right) = \varepsilon^{-1-\frac{at}{2}} \frac{\Gamma\left(\frac{n+at}{2}\right)}{\Gamma\left(-\frac{at}{2}\right)}\left(\frac{s^2}{4\varepsilon}\right)^{-1-\frac{at}{2}} + R(s,t,\varepsilon,n,a)$$

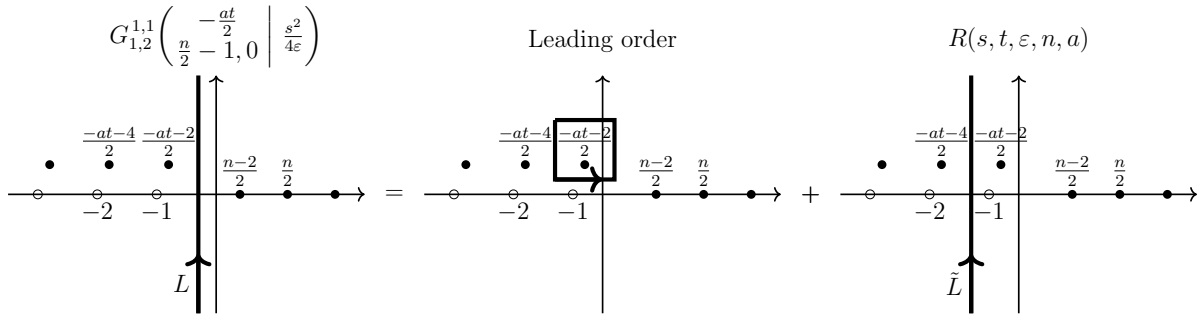

Figure 3.1: Visualization of the method for the determination of the asymptotic behaviour for large arguments. The dots denote the poles of the Gamma function $\Gamma\left(\frac{n}{2}-1-v\right)$ and $\Gamma\left(1+\frac{at}{2}+v\right)$, respectively. The circles represent the poles of the Gamma function $\Gamma(1+v)$.

$$= \frac{\Gamma\left(\frac{n+at}{2}\right)}{\Gamma\left(-\frac{at}{2}\right)}\left(\frac{s}{2}\right)^{-2-at} + R(s,t,\varepsilon,n,a),$$

where $R(s,t,\varepsilon,n,a)$ is the integral over the displaced path $\tilde{L}$. What we need to show next is that the remaining part $R(s,t,\varepsilon,n,a)$ does not grow faster than the leading term as $\varepsilon \to 0$. This can be shown by setting up an upper bound for the remaining part as follows

$$R(s,t,\varepsilon,n,a) = \frac{\varepsilon^{-1-\frac{at}{2}}}{2\pi\mathrm{i}}\int_{\tilde{L}} \frac{\Gamma\left(\frac{n}{2}-1-v\right)\Gamma\left(1+\frac{at}{2}+v\right)}{\Gamma(1+v)}\left(\frac{s^2}{4\varepsilon}\right)^{v}\mathrm{d}v.$$

With the parametrization $v = \mathrm{i}T - \frac{3}{2} - \frac{at}{2}$, we get

$$\begin{aligned}
&= \frac{\varepsilon^{-1-\frac{at}{2}}}{2\pi}\int_{-\infty}^{\infty} \frac{\Gamma\left(\frac{n+1+at}{2}-\mathrm{i}T\right)\Gamma\left(-\frac{1}{2}+\mathrm{i}T\right)}{\Gamma(-\frac{1}{2}-\frac{at}{2}+\mathrm{i}T)}\left(\frac{s^2}{4\varepsilon}\right)^{\mathrm{i}T-\frac{3}{2}-\frac{at}{2}}\mathrm{d}T\\
&\leq \frac{\varepsilon^{-1-\frac{at}{2}}}{2\pi}\left(\frac{s^2}{4\varepsilon}\right)^{-\frac{3}{2}-\frac{at}{2}}\int_{-\infty}^{\infty}\left|\frac{\Gamma\left(\frac{n+1+at}{2}-\mathrm{i}T\right)\Gamma\left(-\frac{1}{2}+\mathrm{i}T\right)}{\Gamma(-\frac{1}{2}-\frac{at}{2}+\mathrm{i}T)}\right|\mathrm{d}T\\
&= \frac{\varepsilon^{\frac{1}{2}}}{2\pi}\left(\frac{s}{2}\right)^{-3-at}\int_{-\infty}^{\infty}\left|\frac{\Gamma\left(\frac{n+1+at}{2}-\mathrm{i}T\right)\Gamma\left(-\frac{1}{2}+\mathrm{i}T\right)}{\Gamma(-\frac{1}{2}-\frac{at}{2}+\mathrm{i}T)}\right|\mathrm{d}T\\
&= \varepsilon^{\frac{1}{2}}\left(\frac{s}{2}\right)^{-3-at}C(n,a,t).
\end{aligned}$$

The function $C(n,a,t)$ is independent of the variables s and ε. The subsequent step is to demonstrate that $C(n,a,t)$ remains finite for all arguments. Following this, we proceed by comparing the remaining terms to show that they are subdominant relative to the leading order. $C(n,a,t)$ is finite if the integrand decays sufficiently fast for all possible

values of the parameters n, a and t. To demonstrate this, we employ the asymptotic behaviour of the absolute value of the Gamma function [1]

$$|\Gamma(x+iy)| \sim \sqrt{2\pi}\,|y|^{x-\frac{1}{2}}\,\mathrm{e}^{-\pi|y|/2} \qquad \text{as } y \to \pm\infty \qquad x, y \in \mathbb{R}.$$

Using the identity, we get

$$\left|\frac{\Gamma\left(\frac{n+1+at}{2} - \mathrm{i}T\right)}{\Gamma(-\frac{1}{2} - \frac{at}{2} + \mathrm{i}T)}\right| \sim \frac{\sqrt{2\pi}|T|^{\frac{n+at}{2}}\mathrm{e}^{-\pi|T|/2}}{\sqrt{2\pi}|T|^{-1-\frac{at}{2}}\mathrm{e}^{-\pi|T|/2}} = |T|^{\frac{n}{2}+1+at} \qquad \text{as } T \to \pm\infty$$

and

$$\left|\Gamma\left(-\frac{1}{2} + \mathrm{i}T\right)\right| \sim \sqrt{2\pi}|T|^{-1}\mathrm{e}^{-\pi|T|/2} \qquad \text{as } T \to \pm\infty.$$

The integrand decays exponentially, and therefore, the function $C(n, a, t)$ is finite. We clearly see that in the limit $\varepsilon \to 0$ the remainder term vanishes while the leading order term stays constant. Hence, the asymptotic behaviour and the limit $\varepsilon \to 0$ is determined, thereby validating the calculations presented in the previous chapter. Higher-order terms can be computed by displacing the contour path over the second pole, third pole, and so on [44]. This example also illustrates the method for determining the asymptotic behaviour of Mellin-Barnes integrals for large arguments.

So far, we discussed how to determine the asymptotic behaviour for large arguments when there are poles outside the contour. The second important case arises when there are no poles outside the contour, allowing the path to be displaced arbitrarily towards positive or negative infinity. In this case, the path can be chosen such that the arguments of all functions are large, and the integrand can be replaced by its asymptotic form. For example, every Gamma function can be replaced by Stirling's formula

$$\Gamma(z) \sim \mathrm{e}^{-z}z^{z}\left(\frac{2\pi}{z}\right)^{\frac{1}{2}} \qquad \text{as } |z| \to \infty, \quad \arg(z) < \pi.$$

With this in mind, the saddle point method can be used to determine the asymptotic behaviour of the Mellin-Barnes integral [44, p. 197]. Using this approach, one can also rigorously identify whether the asymptotic behaviour exhibits exponential decay or oscillatory characteristics. The saddle point method is not employed in the context of this thesis. Instead, we utilize the following result.

If the Mellin-Barnes integral can be parametrized such that the endpoints are at $\pm\mathrm{i}\infty$

and there are no poles outside of the contour then the Mellin-Barnes integral decays more rapidly than any polynomial can grow. We illustrate this with the same example presented in the previous chapter

$$G_{1,0}^{0,1}\left(\begin{matrix}-\\0\end{matrix}\,\middle|\, z^2\right) = \frac{1}{2\pi \mathrm{i}} \int_L \Gamma(-t) z^{2t} \mathrm{d}t, \qquad z \in \mathbb{R},$$

see equ. (2.6) and figure 2.2. From the properties of Meijer G-functions (see section 2.1), we know that the path can also be parameterized by $L = -R + \mathrm{i}T$, where $R > 0$, and T is the integration variable ranging from negative infinity to positive infinity. With this parametrization we get

$$\begin{aligned} G_{1,0}^{0,1}\left(\begin{matrix}-\\0\end{matrix}\,\middle|\, z^2\right) &= \frac{1}{2\pi \mathrm{i}} \int_L \Gamma(-t) z^{2t} \mathrm{d}t \\ &= \frac{1}{2\pi} \int_{-\infty}^{\infty} \Gamma(R - \mathrm{i}T) z^{-2R+2\mathrm{i}T} \mathrm{d}T \\ &\leq \frac{z^{-2R}}{2\pi} \int_{-\infty}^{\infty} |\Gamma(R - \mathrm{i}T)| \, \mathrm{d}T. \end{aligned}$$

Using the asymptotic relation

$$|\Gamma(R - \mathrm{i}T)| \sim \sqrt{2\pi} |T|^{R-\frac{1}{2}} \mathrm{e}^{-\pi|T|/2} \qquad \text{as } T \to \pm\infty,$$

we can deduce that the integral is absolutely convergent for all $R > 0$. Moreover, since R can be chosen arbitrarily large, the Meijer G-function decays faster than any polynomial can grow.

In the following, these two methods are employed to determine the asymptotic behaviour of the newly introduced classes of RBFs, in order to analyze their behaviour for small and large arguments. The behaviour for small arguments is necessary for the construction of the trigonometric polynomial, ensuring that the Fourier transform of the quasi-Lagrange function satisfies the Strang and Fix conditions of a certain order. The behaviour for large arguments will be essential in the next chapter to determine the decay rate of the quasi-Lagrange function.

3.2 New Radial Basis Functions

In this subsection we analyze the asymptotic behaviour of the new classes of RBF. We will see that there are many cases to distinguish and not all of them are suitable for quasi-interpolation. We will restrict the analysis to the cases where classical quasi-interpolation can be applied. This means that the RBF has a singularity of even order at the origin such that we can use finitely many coefficients for the trigonometric polynomial. All cases are analyzed with respect to their asymptotic behaviour for small arguments, but will not be further considered if classical quasi-interpolation is not applicable.

3.2.1 Generalized Multiquadric

As a reminder, we found that for $\varphi(r) = \left(c^\lambda + r^\lambda\right)^\beta$, with the parameters $\lambda \in \mathbb{R}$ and $\beta \in \mathbb{R}\backslash\mathbb{N}$, the Fourier transform is

$$\hat{\varphi}(s) = \frac{2^n \pi^{\frac{n}{2}} c^{\lambda\beta}}{\Gamma(-\beta) s^n} \frac{1}{2\pi \mathrm{i}} \int_L \frac{\Gamma(-t)\Gamma(-\beta+t)\Gamma\left(\frac{n+\lambda t}{2}\right)}{\Gamma\left(-\frac{\lambda t}{2}\right)} \left(\frac{2}{cs}\right)^{\lambda t} \mathrm{d}t, \tag{3.2}$$

where L is a path from $-\mathrm{i}\infty$ to $\mathrm{i}\infty$ separating the poles of the Gamma functions in the numerator. The contour can be deformed according to Cauchy's integral theorem, such that other paths of integration are applicable.

In figure 2.3 we showed that the generalized multiquadric behaves fundamentally different for different signs of the parameters λ and β. The same applies to their Fourier transforms. Therefore, we have to analyze the four cases individually. We start with the case $\lambda > 0$ and $\beta > 0$. For clarity and better insight, each case is introduced with a brief visualization (see table 3.1) of the RBF and the associated contour integral of the Fourier transform.

3.2.1.1 Case 1: $\lambda > 0, \beta > 0$

Parameter configuration	RBF $\varphi(r) = \left(c^\lambda + r^\lambda\right)^\beta$	Contour integral of the Fourier transform $\hat{\varphi}(s)$
$\lambda > 0, \beta > 0$	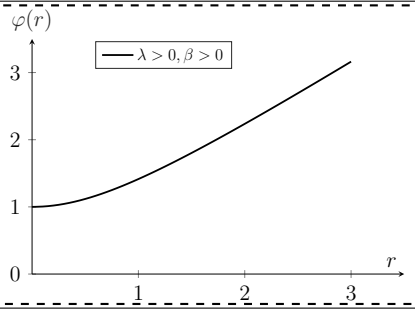	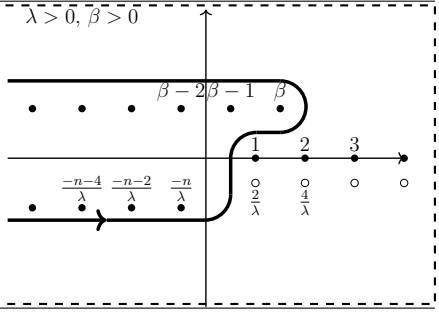
$\lambda > 0, \beta < 0$	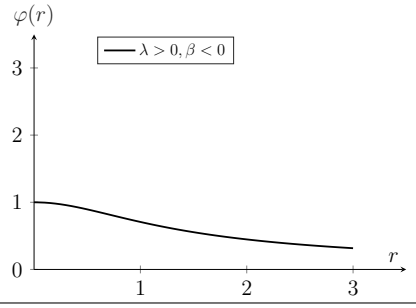	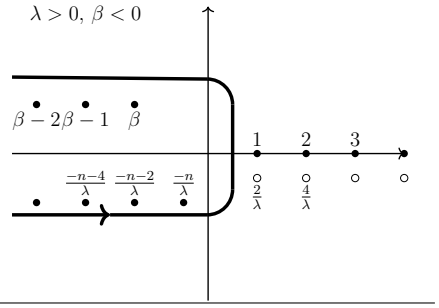
$\lambda < 0, \beta > 0$	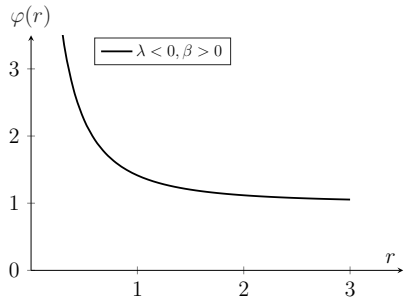	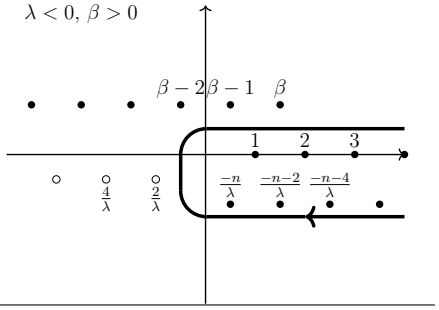
$\lambda < 0, \beta < 0$	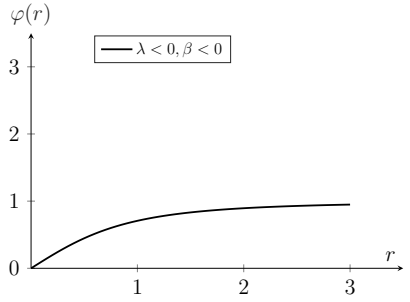	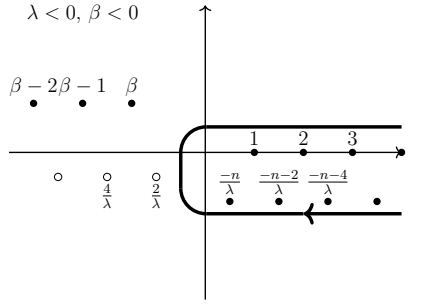

Table 3.1: Overview of the cases considered for the generalized multiquadric. The focus is on the framed case.

We start by analyzing the asymptotic behaviour for small arguments. The poles of the Gamma functions and the path of integration are visualized in figure 3.2. The asymptotic behaviour for $\lambda, \beta > 0$ is contingent upon the specific values of λ and β,

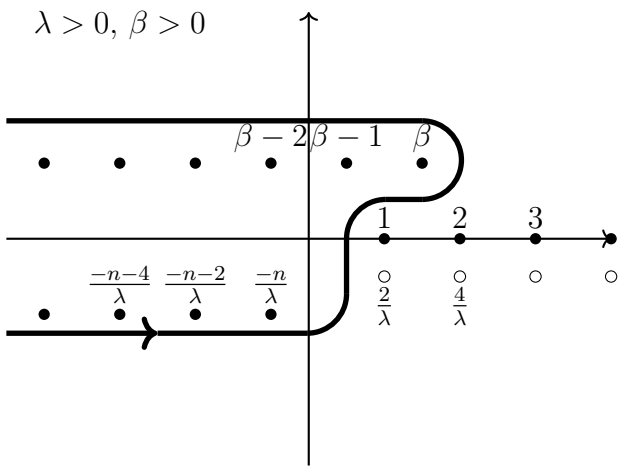

Figure 3.2: Visualization of the poles from equ. (3.2) for $\lambda > 0, \beta > 0$. The singularities of the Gamma functions in the numerator are depicted as dots, whereas the singularities of the Gamma function in the denominator are represented by circles, which may cancel poles. For the purpose of enhanced visualization, the poles have been represented as if they had an imaginary component, although this is not the case. Every pole lies on the real axis. Additionally, the path of integration is depicted and indicates which poles have to be included. The example is provided for $|\lambda| = 2, |\beta| = \frac{3}{2}, n = 1$.

requiring a further distinction of certain cases. The leading-order term is induced by a pole of order one or order two. First, we assume that the leading order term is induced by a pole of order one. Let $a \in \{0, 1, 2, \ldots, \lfloor \beta \rfloor\}$ and therefore $\beta - a \geq 0$. If there is a pole with positive real part that is not cancelled, this pole determines the asymptotic behaviour of $\hat{\varphi}(s)$ for small arguments. Consequently, the following holds

$$\hat{\varphi}(s) \sim \sum_{a=0}^{\lfloor \beta \rfloor} \frac{(-1)^a}{a!} \frac{2^{n+\lambda(\beta-a)} c^{\lambda a} \pi^{\frac{n}{2}}}{s^{n+\lambda(\beta-a)}} \frac{\Gamma(-\beta+a)}{\Gamma(-\beta)} \frac{\Gamma\left(\frac{n+\lambda(\beta-a)}{2}\right)}{\Gamma\left(-\frac{\lambda(\beta-a)}{2}\right)}, \qquad \text{as } s \to 0_+. \tag{3.3}$$

If there is at least one nonzero summand, this expression holds, and the asymptotic behaviour for $s \to 0_+$ is determined. Otherwise, all poles with a positive real part are canceled, and the subsequent poles with negative real parts have to be considered, as, for instance, in the case of $\lambda = 4$ and $\beta = \frac{3}{2}$. These poles may be either of order one or order two. Finally, if $\beta - \lceil \beta \rceil > -\frac{n}{\lambda}$, then the first pole with negative real part is of order one and located at $t = \beta - \lceil \beta \rceil$ and the asymptotic behaviour is then given by

$$\hat{\varphi}(s) \sim \frac{2^{n+\lambda(\beta-\lceil\beta\rceil)} \pi^{\frac{n}{2}} c^{\lambda\lceil\beta\rceil}}{\Gamma(-\beta) s^{n+\lambda(\beta-\lceil\beta\rceil)}} \frac{(-1)^{\lceil\beta\rceil}}{\Gamma(\lceil\beta\rceil+1)} \frac{\Gamma(-\beta+\lceil\beta\rceil)\Gamma\left(\frac{n+\lambda(\beta-\lceil\beta\rceil)}{2}\right)}{\Gamma\left(-\frac{\lambda(\beta-\lceil\beta\rceil)}{2}\right)}, \qquad \text{as } s \to 0_+.$$

On the other hand, if $\beta - \lceil\beta\rceil < -\frac{n}{\lambda}$, then the first pole with negative real part is located at $t = -\frac{n}{\lambda}$. The asymptotic behaviour is given by

$$\hat{\varphi}(s) \sim \frac{\pi^{\frac{n}{2}} c^{\lambda\beta+n}}{\Gamma(-\beta)} \frac{\Gamma(\frac{n}{\lambda})\Gamma(-\beta-\frac{n}{\lambda})}{\Gamma\left(\frac{n}{2}\right)}, \qquad \text{as } s \to 0_+.$$

Finally, if $\beta - \lceil\beta\rceil = -\frac{n}{\lambda}$, then the pole is of order two and we have to evaluate

$$\begin{aligned}\hat{\varphi}(s) &\sim \frac{2^n \pi^{\frac{n}{2}} c^{\lambda\beta}}{\Gamma(-\beta) s^n} \lim_{t\to-\frac{n}{\lambda}} \frac{\partial}{\partial t}\left(t+\frac{n}{\lambda}\right)^2 \frac{\Gamma(-t)\Gamma(-\beta+t)\Gamma\left(\frac{n+\lambda t}{2}\right)}{\Gamma\left(-\frac{\lambda t}{2}\right)} \left(\frac{2}{cs}\right)^{\lambda t}, \qquad \text{as } s \to 0_+ \\ &= \frac{(-1)^{\lceil\beta\rceil+1}\pi^{n/2}\Gamma\left(\frac{n}{\lambda}\right) c^{\beta\lambda+n}}{\lambda\Gamma(-\beta)\Gamma\left(\frac{n}{2}\right)\Gamma(\lceil\beta\rceil+1)} \left(2\lambda\log\left(\frac{cs}{2}\right) - 2H_{\lceil\beta\rceil} + \gamma(\lambda+2) - \lambda\psi^{(0)}\left(\frac{n}{2}\right) + 2\psi^{(0)}\left(\frac{n}{\lambda}\right)\right),\end{aligned}$$

where $H_{\lceil\beta\rceil}$ is the harmonic number, γ is the Euler-Mascheroni constant, and $\psi^{(0)}$ is the Digamma function. These cases represent all possible scenarios for the asymptotic behaviour for small arguments.

By understanding the leading asymptotic behaviour of the Fourier transform of the RBF, we identify the most practical cases for quasi-interpolation. For these cases, we also determine higher order terms of the asymptotic expansion. This is essential for constructing the trigonometric polynomial in such a manner that the Strang and Fix conditions are fulfilled at the origin. In classical quasi-interpolation, the singularity of the RBF has to be an even power of s. Then the trigonometric polynomial can be constructed with a finite number of coefficients μ_k. The first power of s in the asymptotic expansion that is not even (whether it is odd, some other real number, or logarithmic) should appear as late as possible in the asymptotic expansion [42].

With this criterion, we achieve the highest order singularity for $a = 0$ and $\lambda\beta \notin 2\mathbb{N}$. Since we would like to get a singularity of even order, it follows that this is only achievable in odd dimensions n with $\lambda\beta \in 2\mathbb{N} - 1$. To maximize the number of even powers of s in the asymptotic series until a non-even power of s appears, we continue with the condition $\lambda a \in 2\mathbb{N}, \forall a \in \{0, 1, 2, \ldots, \lfloor\beta\rfloor\}$. Thus, λ should also be an even integer. Hence, $\beta \in \mathbb{N} + \frac{1}{2}$.

In summary, the best way to achieve this requirement is given by

$$\lambda \in 2 + 4\mathbb{N} \quad \text{and} \quad \beta \in \mathbb{N} + \frac{1}{2}.$$

With this specific choice of parameters, a double pole appears, leading to a logarithmic term in the asymptotic behaviour. Given the particular interest in this case for quasi-

interpolation, we now derive the form of the asymptotic series up to the first logarithmic term.

To identify the location of the first double pole, we round the value $\frac{-n}{\lambda}$ to the nearest negative half-integer. This can be expressed as the formula $t = \left\lfloor -\frac{n}{\lambda} + \frac{1}{2} \right\rfloor - \frac{1}{2}$. This pole gives rise to a logarithmic singularity, and all poles of order one with real part larger than the double pole can be summed up, as shown below. The asymptotic series is given by

$$\begin{aligned}\hat{\varphi}(s) \sim & \sum_{j=0}^{\left\lceil \frac{n}{\lambda} - \frac{1}{2} \right\rceil + \lfloor \beta \rfloor} C_j(c, n, \lambda, \beta) s^{-n+\lambda(j-\beta)} + \sum_{j=0}^{\frac{1}{2}\left(-n+\lambda\left(\left\lceil \frac{n}{\lambda} - \frac{1}{2} \right\rceil + \frac{1}{2}\right)\right)} \tilde{C}_j(c, n, \lambda, \beta) s^{2j} \\ & + C(c, n, \lambda, \beta) s^{-n+\lambda\left(\left\lceil \frac{n}{\lambda} - \frac{1}{2} \right\rceil + \frac{1}{2}\right)} \log(cs) \qquad \text{as } s \to 0_+ \,, \end{aligned} \tag{3.4}$$

where $C_j, \tilde{C}_j$ and C are some constants depending on c, n, λ, β and j and can be computed by the residue theorem. The first sum collects the residues of all poles from $\Gamma(-\beta + t)$. The formula for the first constants C_j are given in equ. (3.3), but here we also include all poles of order one with negative real parts up to the first pole of order two. The second sum encompasses the residues of the poles of $\Gamma\left(\frac{n+\lambda t}{2}\right)$ up to and including the first pole of order two. The last term is the logarithmic part induced by the first pole of order two.

As λ or β increases, more even powers of s appear between the leading-order and the logarithmic part in the asymptotic series. In Section 4.1, we will show that this leads to improved decay rates for the quasi-Lagrange functions and enhanced polynomial reproduction. Consequently, this results in higher approximation orders. It is worth noting that the classical Hardy's multiquadric ($\lambda = 2, \beta = \frac{1}{2}$) corresponds to this specific choice, and we have demonstrated how this can be extended to other values of λ and β.

The analysis of the asymptotic behaviour as $s \to 0_+$ is now complete. As a next step, we investigate the behaviour of $\hat{\varphi}(s)$ for large arguments. To do so, we have to consider different values of λ and first assume that $\lambda \in 2\mathbb{N}$. In this case, all poles outside the contour will cancel out and the contour can be displaced arbitrarily far towards infinity. As shown in section 3.1, we use Cauchy's integral theorem and parametrize the contour as $s = R + \mathrm{i}T$, where $T \in (-\infty, \infty)$ and $R > 0$ is arbitrarily large. With this parametrization, equ. (3.2) transforms to

$$\hat{\varphi}(s) = \frac{2^n \pi^{\frac{n}{2}} c^{\lambda\beta}}{\Gamma(-\beta) s^n} \frac{1}{2\pi} \int_{-\infty}^{\infty} \frac{\Gamma(-R - \mathrm{i}T)\Gamma(-\beta + R + \mathrm{i}T)\Gamma\left(\frac{n+\lambda(R+\mathrm{i}T)}{2}\right)}{\Gamma\left(-\frac{\lambda(R+\mathrm{i}T)}{2}\right)} \left(\frac{2}{cs}\right)^{\lambda(R+\mathrm{i}T)} \mathrm{d}T$$

$$\leq Cs^{(-n-\lambda R)} \int_{-\infty}^{\infty} \left| \frac{\Gamma(-R-\mathrm{i}T)\Gamma(-\beta+R+\mathrm{i}T)\Gamma\left(\frac{n+\lambda(R+\mathrm{i}T)}{2}\right)}{\Gamma\left(-\frac{\lambda(R+\mathrm{i}T)}{2}\right)} \right| \mathrm{d}T.$$

Using the asymptotic expansion of the Gamma function

$$|\Gamma(x+iy)| \sim \sqrt{2\pi}|y|^{x-\frac{1}{2}}\mathrm{e}^{-\frac{\pi}{2}|y|} \qquad \text{as } y \to \pm\infty, \quad x \in \mathbb{R}, \tag{3.5}$$

we can deduce that the integral is absolutely convergent while R is finite. Therefore, the Fourier transform can be upper-bounded by

$$\hat{\varphi}(s) \leq C_R s^{-n-\lambda R},$$

where C_R is some constant depending on R. Since R is arbitrarily large, we showed that $\hat{\varphi}(s)$ decays faster than every polynomial can grow. In fact, we have not derived the exact asymptotic behaviour, but instead we got an upper bound on the decay rate of $\hat{\varphi}(s)$ for large arguments. Note that the same applies to all derivatives of $\hat{\varphi}(s)$

$$\begin{aligned}\frac{\partial^\rho}{\partial s^\rho}\hat{\varphi}(s) &= \frac{2^n\pi^{\frac{n}{2}}c^{\lambda\beta}}{\Gamma(-\beta)}\frac{1}{2\pi}\int_{-\infty}^{\infty} \frac{\Gamma(-R-\mathrm{i}T)\Gamma(-\beta+R+\mathrm{i}T)\Gamma\left(\frac{n+\lambda(R+\mathrm{i}T)}{2}\right)}{\Gamma\left(-\frac{\lambda(R+\mathrm{i}T)}{2}\right)} \frac{\partial^\rho}{\partial s^\rho} s^{-n}\left(\frac{2}{cs}\right)^{\lambda(R+\mathrm{i}T)} \mathrm{d}T \\ &\leq Cs^{(-n-\lambda R-\rho)} \int_{-\infty}^{\infty} \left| \frac{\Gamma(-R-\mathrm{i}T)\Gamma(-\beta+R+\mathrm{i}T)\Gamma\left(\frac{n+\lambda(R+\mathrm{i}T)}{2}\right)}{\Gamma\left(-\frac{\lambda(R+\mathrm{i}T)}{2}\right)} \right| \mathrm{d}T.\end{aligned}$$

The integrand decays exponentially and keeps the integral absolutely convergent. This also ensures that the change of the integral and the derivative is valid. As before, R is arbitrarily large, so the derivative of $\hat{\varphi}$ also decays faster than any polynomial grow.

For $\lambda \notin 2\mathbb{N}$, the first non-vanishing pole outside the contour is at $t = 1$. So the leading-order asymptotic behaviour is determined by the residue at $t = 1$. We get

$$\hat{\varphi}(s) \sim -\frac{2^{\lambda+n}\beta\pi^{n/2}c^{\lambda(\beta-1)}\Gamma\left(\frac{n+\lambda}{2}\right)}{\Gamma\left(-\frac{\lambda}{2}\right)} s^{-n-\lambda} \qquad \text{as } s \to \infty.$$

For the derivatives we get

$$\frac{\mathrm{d}^\rho}{\mathrm{d}s^\rho}\hat{\varphi}(s) \sim (-1)^{\rho+1}\frac{(n+\lambda+\rho)!}{(n+\lambda)!}\frac{2^{\lambda+n}\beta\pi^{n/2}c^{\lambda(\beta-1)}\Gamma\left(\frac{n+\lambda}{2}\right)}{\Gamma\left(-\frac{\lambda}{2}\right)} s^{-n-\lambda-\rho} \qquad \text{as } s \to \infty.$$

In summary, the derivatives decay even faster than the function itself. These results will be needed in the following section to apply the Strang and Fix conditions. Thus far, we have analyzed all possible asymptotic behaviours corresponding to various values of $\lambda > 0$ and $\beta > 0$.

3.2.1.2 Case 2: $\lambda > 0, \beta < 0$

Parameter configuration	RBF $\varphi(r) = \left(c^\lambda + r^\lambda\right)^\beta$	Contour integral of the Fourier transform $\hat{\varphi}(s)$
$\lambda > 0, \beta > 0$	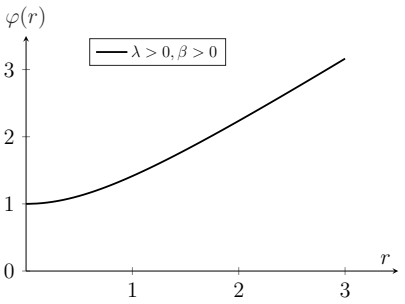	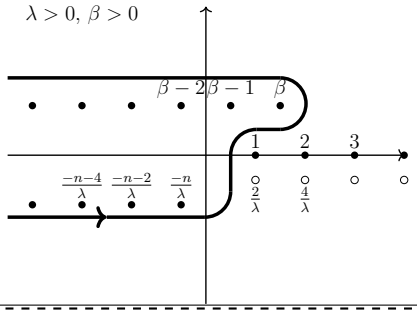
$\lambda > 0, \beta < 0$	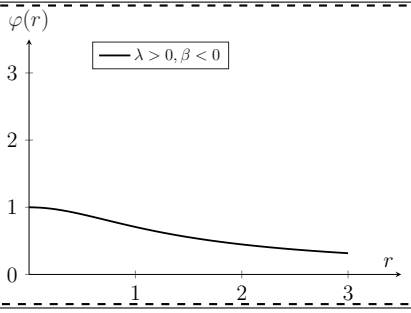	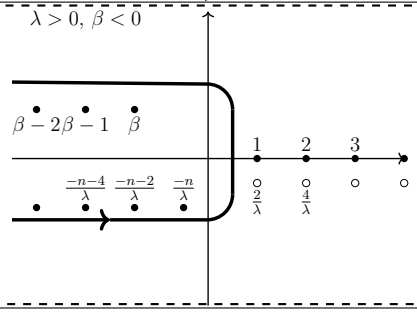
$\lambda < 0, \beta > 0$	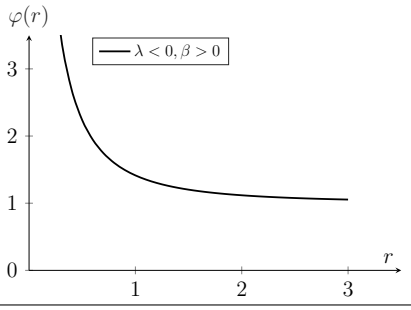	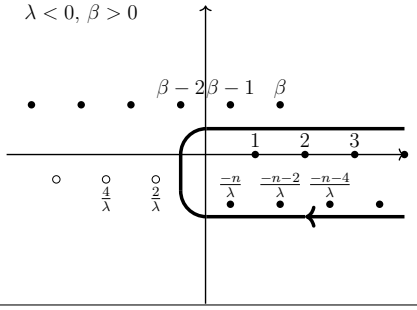
$\lambda < 0, \beta < 0$	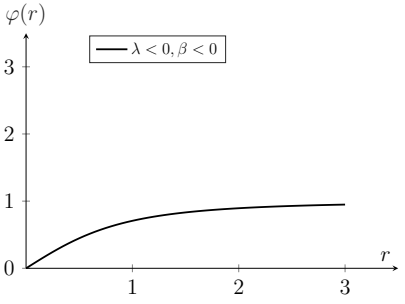	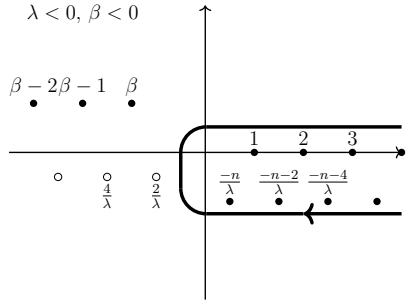

Table 3.2: Overview of the cases considered for the generalized multiquadric. The focus is on the framed case.

This case is a generalization of the classical inverse multiquadric ($\lambda = 2, \beta = -\frac{1}{2}$). For better comprehensibility, we define $\tilde{\beta} = -\beta$ and work with the positive variable $\tilde{\beta}$. The poles are visualized in figure 3.3. The only difference to the first case is that there

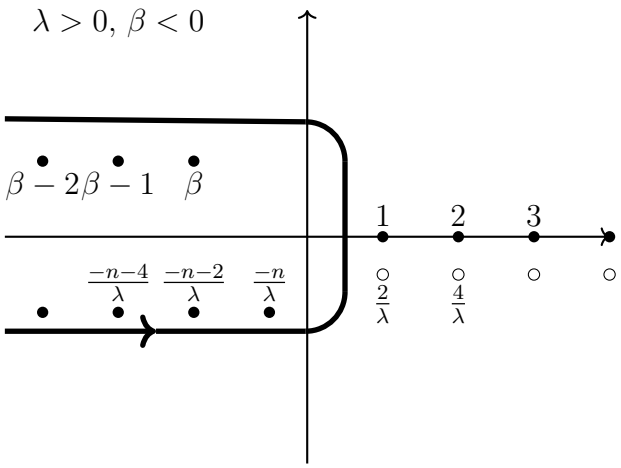

Figure 3.3: Visualization of the poles from equ. (3.2) for $\lambda > 0, \beta < 0$. The singularities of the Gamma functions in the numerator are depicted as dots, whereas the singularities of the Gamma function in the denominator are represented by circles, which may cancel poles. For the purpose of enhanced visualization, the poles are represented as if they had an imaginary component, although this is not the case. Every pole lies on the real axis. Additionally, the path of integration is depicted and indicates which poles have to be included. The example is provided for $|\lambda| = 2, |\beta| = \frac{3}{2}, n = 1$.

are no poles with positive real part inside the contour. Hence, we get analogous results to the first case and find the behaviour for $s \to 0_+$

$$\hat{\varphi}(s) = \begin{cases} \mathcal{O}\left(s^{-n+\lambda\tilde{\beta}}\right), & \tilde{\beta} < \frac{n}{\lambda} \\ \mathcal{O}\left(1\right), & \tilde{\beta} > \frac{n}{\lambda} \\ \mathcal{O}\left(\log(s)\right), & \tilde{\beta} = \frac{n}{\lambda}. \end{cases}$$

For the sake of clarity the big-$\mathcal{O}$ notation is used. The exact asymptotic behaviour was determined in the previously considered case. The utilization of classical quasi-interpolation is constrained by the dimension n, owing the assumption of a singularity at the origin. For a sufficiently large dimension n, this limitation can be advantageous for classical quasi-interpolation, as it enables the reduction of the singularity at the origin to a certain degree. The asymptotic behaviour as $s \to \infty$ is equivalent to the behaviour previously examined. For $\lambda \in 2\mathbb{N}$, the Fourier transform and all its derivatives decay faster than every polynomial and for $\lambda \notin 2\mathbb{N}$ we get

$$\frac{\partial^\rho}{\partial s^\rho}\hat{\varphi}(s) \leq C s^{-n-\lambda-\rho}, \qquad \rho \in \mathbb{N}.$$

3.2.1.3 Case 3: $\lambda < 0, \beta > 0$

Parameter configuration	RBF $\varphi(r) = \left(c^\lambda + r^\lambda\right)^\beta$	Contour integral of the Fourier transform $\hat{\varphi}(s)$
$\lambda > 0, \beta > 0$	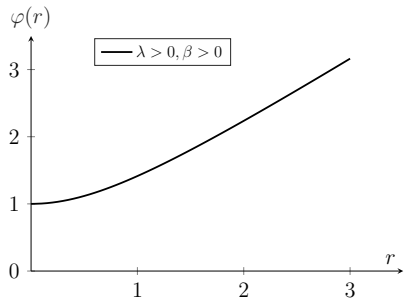	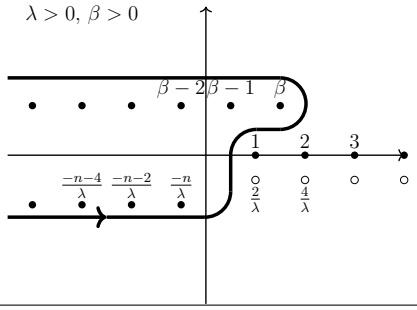
$\lambda > 0, \beta < 0$	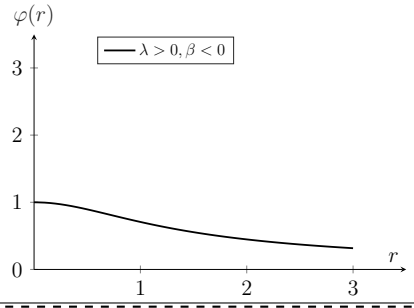	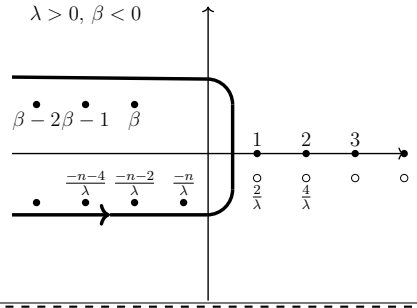
$\lambda < 0, \beta > 0$	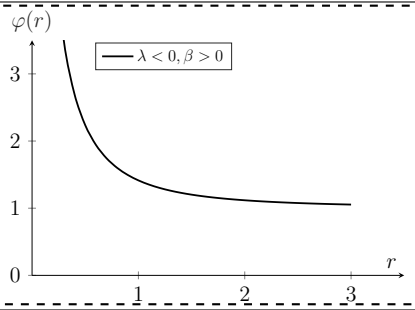	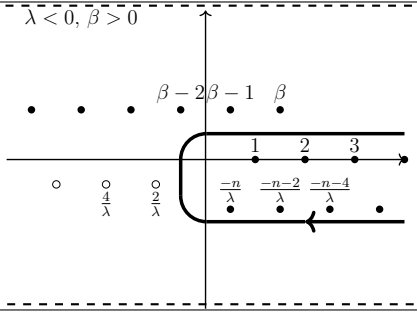
$\lambda < 0, \beta < 0$	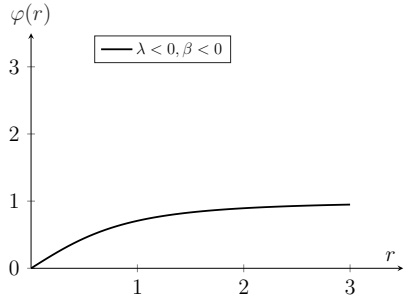	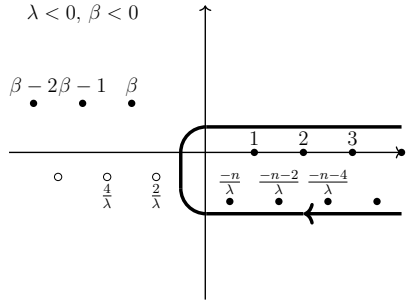

Table 3.3: Overview of the cases considered for the generalized multiquadric. The focus is on the framed case.

We define $\tilde{\lambda} = -\lambda$ to be positive. Under this assumption, the poles and the contour itself change due to the convergence properties of the Gamma functions. This is visualized in figure 3.4. The poles induced by $\Gamma(-\beta + t)$ lie outside of the contour. To distinguish

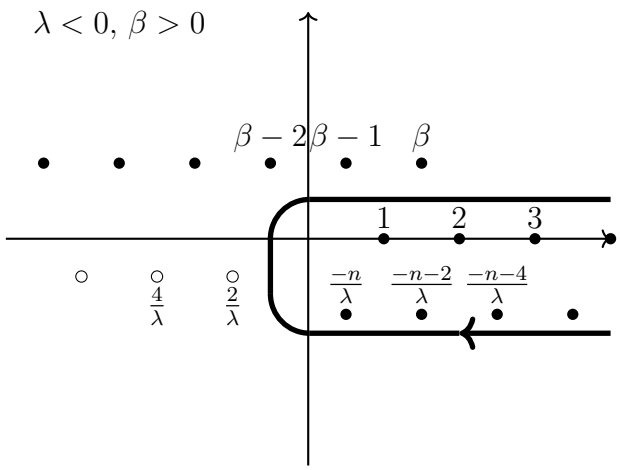

Figure 3.4: Visualization of the poles from equ. (3.2) for $\lambda < 0, \beta > 0$. The singularities of the Gamma functions in the numerator are depicted as dots, whereas the singularities of the Gamma function in the denominator are represented by circles, which may cancel poles. For the purpose of enhanced visualization, the poles are represented as if they had an imaginary component, although this is not the case. Every pole lies on the real axis. Additionally, the path of integration is depicted and indicates which poles have to be included. The example is provided for $|\lambda| = 2, |\beta| = \frac{3}{2}, n = 1$.

the poles outside and inside, they are now allowed to coincide. As a formula, this means that $\beta \notin \mathbb{N}$ and $(\beta - \mathbb{N}) \cap \frac{n+2\mathbb{N}}{\tilde{\lambda}} = \emptyset$. Given this, the asymptotic behaviour can be determined in the same manner as before. When calculating the residue, there appears one minus sign due to the direction of the contour integral. For $\frac{n}{\tilde{\lambda}} < 1$ we get

$$\hat{\varphi}(s) \sim \frac{2\pi^{\frac{n}{2}} c^{n-\tilde{\lambda}\beta}}{\Gamma(-\beta)\tilde{\lambda}} \frac{\Gamma(-\frac{n}{\tilde{\lambda}})\Gamma(-\beta + \frac{n}{\tilde{\lambda}})}{\Gamma\left(\frac{n}{2}\right)}, \qquad \text{as } s \to 0_+,$$

which is just a constant and has no singularity at the origin. The more suitable case is $\frac{n}{\tilde{\lambda}} > 1$, because the asymptotic behaviour is given by

$$\hat{\varphi}(s) \sim \frac{2^{n-\tilde{\lambda}} \pi^{\frac{n}{2}} c^{\tilde{\lambda}(1-\beta)} \beta}{s^{n-\tilde{\lambda}}} \frac{\Gamma\left(\frac{n-\tilde{\lambda}}{2}\right)}{\Gamma\left(\frac{\tilde{\lambda}}{2}\right)}, \qquad \text{as } s \to 0_+.$$

Therefore, there is a singularity if $\lambda < n$. In certain scenarios, this can be advantageous, for example, as reduction of the singularity for large dimensions. Finally, if $\frac{n}{\tilde{\lambda}} = 1$, we evaluate the residue of the double pole to obtain

$$\hat{\varphi}(s) \sim -\frac{\beta \pi^{n/2} c^{n(1-\beta)}}{n\Gamma\left(\frac{n}{2}\right)} \left(2n \log\left(\frac{cs}{2}\right) + 2H_{-\beta} + \gamma n - n\psi^{(0)}\left(\frac{n}{2}\right) - 2\right), \qquad \text{as } s \to 0_+.$$

In summary, we get for $\beta \notin \mathbb{N}$ and $\beta - \mathbb{N} \cap \frac{n+2\mathbb{N}}{\tilde{\lambda}} = \emptyset$,

$$\hat{\varphi}(s) = \begin{cases} \mathcal{O}(1), & n < \tilde{\lambda} \\ \mathcal{O}\left(s^{-n+\tilde{\lambda}}\right), & n > \tilde{\lambda} \\ \mathcal{O}(\log(s)), & n = \tilde{\lambda}. \end{cases}$$

A remarkable fact is that the order of the singularity does not depend on β. Hence, one could think that β can be chosen arbitrarily. However, the asymptotic behaviour for $s \to \infty$ is limited by β. In the next chapter, we will see its affect on the approximation order or the quasi-Lagrange operator.

For large arguments the asymptotic behaviour is given by the residue of the first non-vanishing pole outside the contour. This is for $t = \beta$ and the evaluation leads to

$$\hat{\varphi}(s) \sim \frac{\pi^{n/2} 2^{-\beta\tilde{\lambda}+n} \Gamma\left(\frac{1}{2}(n+\beta\tilde{\lambda})\right)}{\Gamma\left(-\frac{\beta\tilde{\lambda}}{2}\right)} s^{-n+\tilde{\lambda}\beta} \qquad \text{as } s \to \infty. \tag{3.6}$$

For the derivatives we get

$$\frac{\mathrm{d}^\rho}{\mathrm{d}s^\rho}\hat{\varphi}(s) \sim C s^{-n+\tilde{\beta}\lambda-\rho} \qquad \text{as } s \to \infty,$$

where C is some constant which can be derived by differentiating the leading asymptotic term of $\hat{\varphi}(s)$. The decay rate of the derivative is faster than that of the function itself.

Up to this point, all results seems to be applicable to quasi-interpolation. However, for this choice of parameters, the RBF itself becomes singular. This problem can be addressed in two ways. The first one is, that the quasi-Lagrange function is a linear combination of the RBFs and the coefficients μ_k have to ensure that the singularity cancels out. The second possibility is to use a linear combination of different parameters c within the RBF. Since the singularity of the Fourier transform depends on the constant c, this linear combination will not affect the order of the singularity. We will see in the next chapter that the decay rate of the Fourier transform of the RBF is not fast enough and therefore, this case is not usable in classical quasi-interpolation.

3.2.1.4 Case 4: $\lambda < 0, \beta < 0$

Parameter configuration	RBF $\varphi(r) = \left(c^\lambda + r^\lambda\right)^\beta$	Contour integral of the Fourier transform $\hat{\varphi}(s)$
$\lambda > 0, \beta > 0$	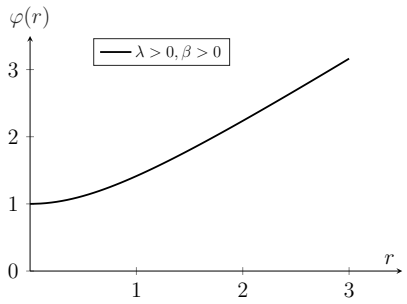	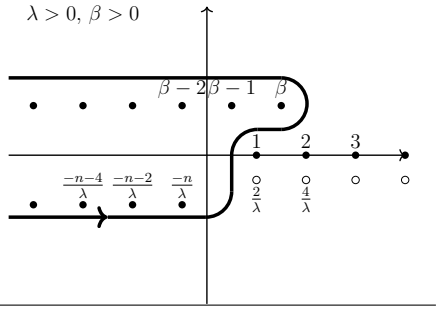
$\lambda > 0, \beta < 0$	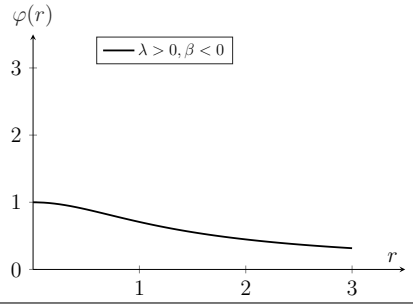	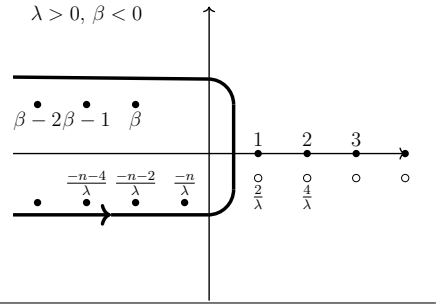
$\lambda < 0, \beta > 0$	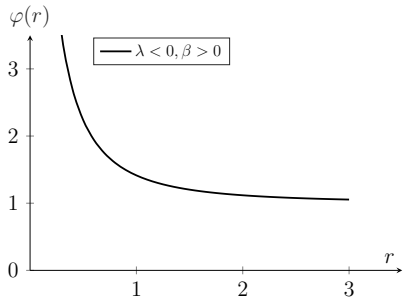	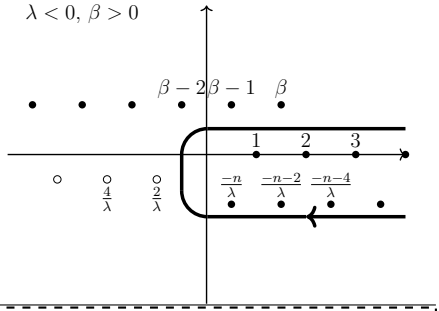
$\lambda < 0, \beta < 0$	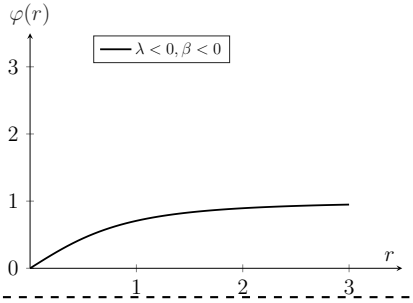	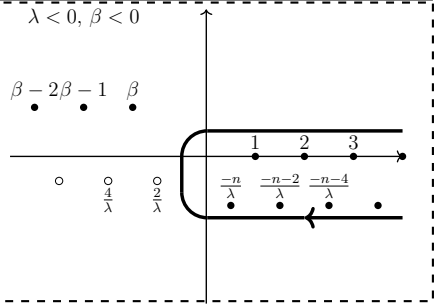

Table 3.4: Overview of the cases considered for the generalized multiquadric. The focus is on the framed case.

The last parameter configuration is $\lambda, \beta < 0$. Again, we define $\tilde{\lambda} = -\lambda$ and $\tilde{\beta} = -\beta$. The visualization of the poles is shown in figure 3.5. Analogous to the previous case but without the restriction on β, we find that the leading order pole can only be simple or

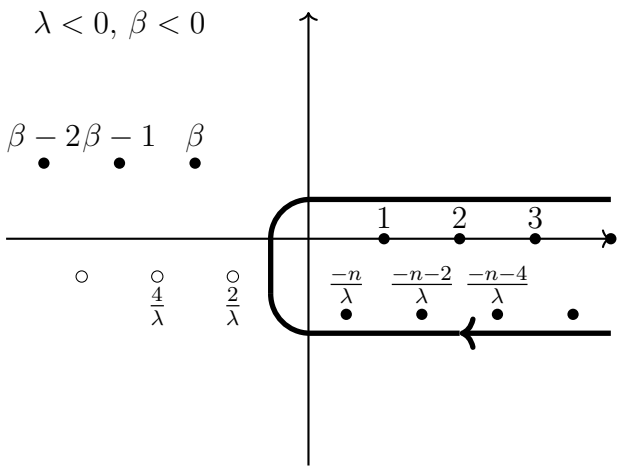

Figure 3.5: Visualization of the poles from equ. (3.2) for $\lambda < 0, \beta < 0$. The singularities of the Gamma functions in the numerator are depicted as dots, whereas the singularities of the Gamma function in the denominator are represented by circles, which may cancel poles. For the purpose of enhanced visualization, the poles are represented as if they had an imaginary component, although this is not the case. Every pole lies on the real axis. Additionally, the path of integration is depicted and indicates which poles have to be included. The example is provided for $|\lambda| = 2, |\beta| = \frac{3}{2}, n = 1$.

double. If $n < \tilde{\lambda}$, then the first pole is at $t = \frac{n}{\tilde{\lambda}}$ and the asymptotic behaviour for $s \to 0_+$ is evaluated as

$$\hat{\varphi}(s) \sim \frac{2\pi^{\frac{n}{2}} c^{n+\tilde{\lambda}\tilde{\beta}}}{\Gamma(\tilde{\beta})\tilde{\lambda}} \frac{\Gamma(-\frac{n}{\tilde{\lambda}})\Gamma(\tilde{\beta}+\frac{n}{\tilde{\lambda}})}{\Gamma\left(\frac{n}{2}\right)}, \qquad \text{as } s \to 0_+.$$

If $n > \tilde{\lambda}$, then the first pole is located at $t = 1$ and we obtain

$$\hat{\varphi}(s) \sim -\frac{2^{n-\tilde{\lambda}}\pi^{\frac{n}{2}} c^{\tilde{\lambda}(1+\tilde{\beta})}\tilde{\beta}}{s^{n-\tilde{\lambda}}} \frac{\Gamma\left(\frac{n-\tilde{\lambda}}{2}\right)}{\Gamma\left(\frac{\tilde{\lambda}}{2}\right)}, \qquad \text{as } s \to 0_+.$$

Finally, if $n = \lambda$, then the first pole double is located at $t = 1$ and we get

$$\hat{\varphi}(s) \sim \frac{\tilde{\beta}\pi^{n/2} c^{n(1+\tilde{\beta})}}{n\Gamma\left(\frac{n}{2}\right)} \left(2n \log\left(\frac{cs}{2}\right) + 2H_{\tilde{\beta}} + \gamma n - n\psi^{(0)}\left(\frac{n}{2}\right) - 2\right), \qquad \text{as } s \to 0_+.$$

In summary, for $s \to 0_+$, we have

$$\hat{\varphi}(s) = \begin{cases} \mathcal{O}(1), & n < \tilde{\lambda} \\ \mathcal{O}\left(s^{-n+\tilde{\lambda}}\right), & n > \tilde{\lambda} \\ \mathcal{O}(\log(s)), & n = \tilde{\lambda}. \end{cases}$$

These are the same results as in the previous case, just with a negative sign for β.

The noticeable difference is in the asymptotic behaviour as $s \to \infty$. As before, if all poles located outside the contour vanish, than $\hat{\varphi}(s)$ decays faster than any polynomial grows. Otherwise, the decay rate is limited by the first non-vanishing pole outside the contour. Suppose that the first non-vanishing pole is at $t = -\tilde{\beta} - a$ for $a \in \mathbb{N}$. Then, we get for large arguments

$$\hat{\varphi}(s) \sim \frac{(-1)^{a+1}}{\Gamma(a+1)} \frac{2^{n+\tilde{\lambda}(\tilde{\beta}+a)} \pi^{\frac{n}{2}}}{c^{\tilde{\lambda}a} s^{n+\tilde{\lambda}(\tilde{\beta}+a)}} \frac{\Gamma\left(\frac{n+\tilde{\lambda}\tilde{\beta}}{2}\right)}{\Gamma\left(-\frac{\tilde{\lambda}\tilde{\beta}}{2}\right)}, \qquad \text{as } s \to \infty.$$

The derivatives decay even faster.

So far, we have discussed all possible asymptotic behaviours for different parameters λ and β. We found that the most useful case for quasi-interpolation is given for

$$\lambda \in 2 + 4\mathbb{N} \text{ and } \beta \in \frac{1}{2} + \mathbb{N}.$$

Other cases are also suitable but not as good as this choice. Consequently, a comprehensive analysis of these parameters will be conducted in chapter 4.

Before proceeding with the analysis of the decay rate of the quasi-Lagrange function, we analyze the asymptotic behaviour of the generalized thin plate spline.

3.2.2 Generalized Thin Plate Spline

As a reminder, we defined the generalized thin plate spline as

$$\varphi(r) = \left(c^\lambda + r^\lambda\right) \log\left(c^\beta + r^\beta\right), \qquad r = ||x||,\ x \in \mathbb{R}^n,\ \lambda, \beta \in \mathbb{R}$$

and splitted this up into four functions $\varphi_1(r), \ldots, \varphi_4(r)$, see chapter 2. We derived the following expression for the Fourier transform of the generalized thin plate spline

$$\hat{\varphi}_4(s) = \frac{2^n \pi^{\frac{n}{2}} c^\lambda}{s^n} \frac{1}{2\pi \mathrm{i}} \int_L \frac{\Gamma\left(1 + \frac{\lambda}{\beta} - t\right) \Gamma\left(-\frac{\lambda}{\beta} + t\right)^2 \Gamma\left(\frac{n+\beta t}{2}\right)}{\Gamma\left(1 - \frac{\lambda}{\beta} + t\right) \Gamma\left(-\frac{\beta t}{2}\right)} \left(\frac{2}{cs}\right)^{\beta t} \mathrm{d}t \tag{3.7}$$

and analog

$$\hat{\varphi}_3(s) = \frac{2^n \pi^{\frac{n}{2}} c^\lambda}{s^n} \frac{1}{2\pi \mathrm{i}} \int_L \frac{\Gamma(1-t) \Gamma(t)^2 \Gamma\left(\frac{n+\beta t}{2}\right)}{\Gamma(1+t) \Gamma\left(-\frac{\beta t}{2}\right)} \left(\frac{2}{cs}\right)^{\beta t} \mathrm{d}t.$$

The Fourier transforms $\hat{\varphi}_1(s)$ and $\hat{\varphi}_2(s)$ are Dirac delta distributions or constants multiplied by some power of s, depending on the parameters λ and β. More precisely, we derived

$$\hat{\varphi}_2(s) = \begin{cases} \beta \log(c) \frac{\Gamma\left(\frac{n+\lambda}{2}\right)}{\Gamma\left(-\frac{\lambda}{2}\right)} 2^{\lambda+n} \pi^{n/2} s^{-n-\lambda}, & \frac{\lambda}{2} \notin \mathbb{N} \wedge \frac{\lambda}{2} \notin -\mathbb{N} - \frac{n}{2} \\ \beta \log(c) (2\pi)^n (-1)^{\frac{\lambda}{2}} \left(\partial_1^2 + \cdots + \partial_n^2\right)^{\frac{\lambda}{2}} \delta(s), & \frac{\lambda}{2} \in \mathbb{N} \end{cases}$$

$$\hat{\varphi}_1(s) = (2\pi)^n c^\lambda \log\left(c^\beta\right) \delta(s).$$

We concluded that $\hat{\varphi}_1(s)$ and $\hat{\varphi}_2(s)$ are identically zero for $s > 0$, or alternatively, that the asymptotic behaviour is already determined. This is why they are mostly neglected in this section. Furthermore, we only analyze $\hat{\varphi}_4(s)$ in detail because $\hat{\varphi}_3(s) = c^\lambda \left(\hat{\varphi}_4(s)\big|_{\lambda=0}\right)$ can be derived from $\hat{\varphi}_4(s)$.

As in preceding analyses, the RBF exhibits qualitatively distinct behaviour both near the origin and for large arguments, depending critically on the signs of the parameters λ and β, see figure 2.4. Consequently, a separate analysis of each of the four possible sign configurations is required. As before, every case starts with an overview table of the behaviours of the RBF and the visualization of the contour integral of the Fourier transform.

3.2.2.1 Case 1: $\lambda > 0, \beta > 0$

Parameter configuration	RBF $\varphi(r) = \left(c^\lambda + r^\lambda\right) \log\left(c^\beta + r^\beta\right)$	Contour integral of the Fourier transform $\hat{\varphi}_4(s)$
$\lambda > 0, \beta > 0$	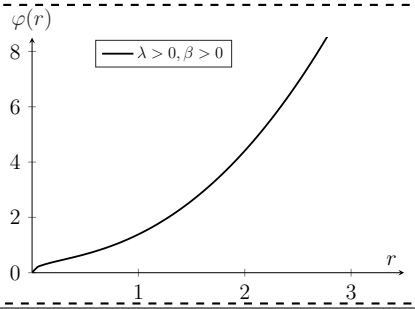	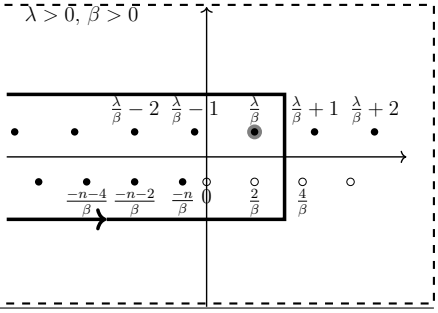
$\lambda < 0, \beta > 0$	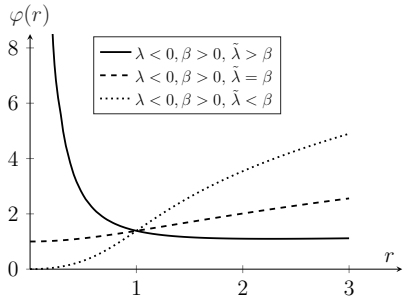	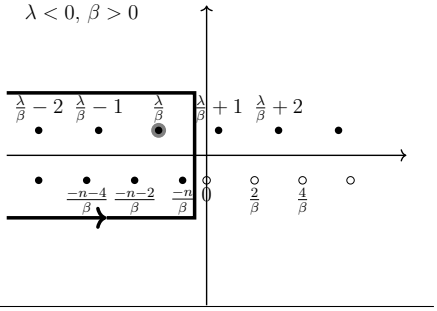
$\lambda > 0, \beta < 0$	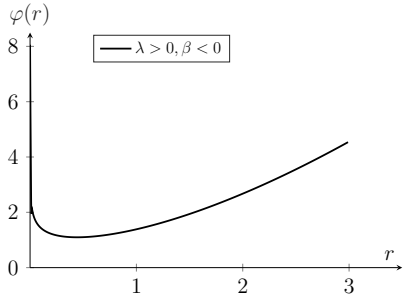	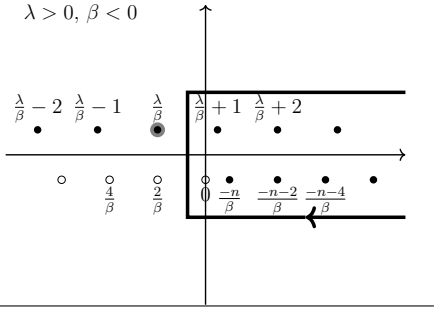
$\lambda < 0, \beta < 0$	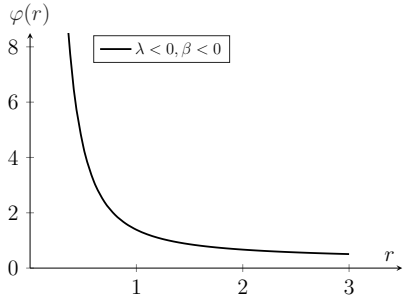	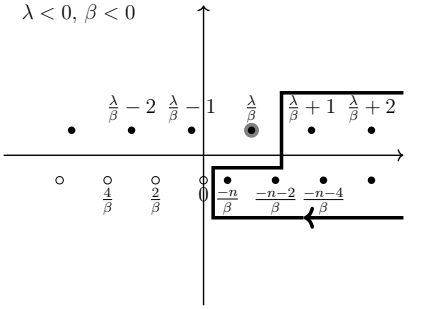

Table 3.5: Overview of the cases considered for the generalized thin plate spline. The focus is on the framed case.

First we assume that $\lambda, \beta > 0$. Figure 3.6 visualizes the poles of the Gamma functions and the path of integration. The first contributing pole is at $t = \frac{\lambda}{\beta}$. This pole is of order

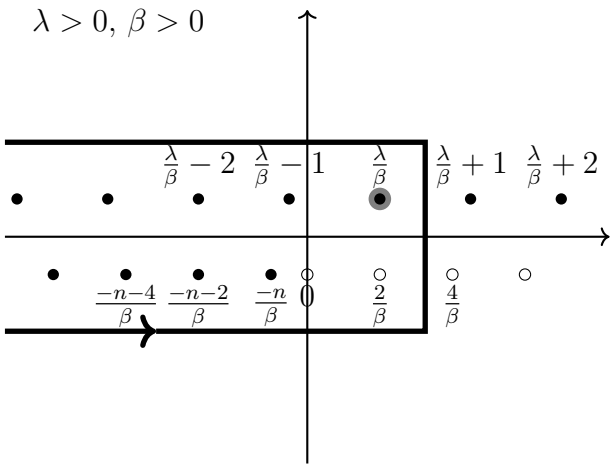

Figure 3.6: Visualization of the poles from equ. (3.7) for $\lambda > 0, \beta > 0$. The singularities of the Gamma functions in the numerator are depicted as dots, whereas the singularities of the Gamma function in the denominator are represented by circles, which may cancel poles. Dots with circles around represent double poles. For the purpose of enhanced visualization, the poles are represented as if they had an imaginary component, although this is not the case. Every pole lies on the real axis. Additionally, the path of integration is depicted and indicates which poles must be included. The example is provided for $|\lambda| = 2, |\beta| = \frac{5}{2}, n = 1$.

two if $\lambda \notin 2\mathbb{N}$, and a straightforward evaluation leads to

$$\hat{\varphi}_4(s) \sim \frac{\beta \pi^{n/2} 2^{\lambda+n-1} \Gamma\left(\frac{n+\lambda}{2}\right) \left(2\log(\frac{2}{cs}) + \psi^{(0)}\left(-\frac{\lambda}{2}\right) + \psi^{(0)}\left(\frac{n+\lambda}{2}\right)\right)}{s^{n+\lambda}\Gamma\left(-\frac{\lambda}{2}\right)} \qquad \text{as } s \to 0_+.$$

For $\lambda \in 2\mathbb{N}$, we evaluate the simple pole at $t = \frac{\lambda}{\beta}$ and get the asymptotic behaviour

$$\hat{\varphi}_4(s) \sim (-1)^{\frac{\lambda}{2}+1} 2^{n+\lambda-1} \pi^{n/2} \beta s^{-n-\lambda} \Gamma\left(\frac{n+\lambda}{2}\right) \Gamma\left(\frac{\lambda}{2}+1\right) \qquad \text{as } s \to 0_+.$$

Extracting the information from $\varphi_4(s)$ leads to the asymptotic behaviour of $\varphi_3(s)$

$$\hat{\varphi}_3(s) \sim -2^{n-1} \pi^{n/2} \beta c^{\lambda} s^{-n} \Gamma\left(\frac{n}{2}\right) \qquad \text{as } s \to 0_+.$$

In summary, as $s \to 0_+$, we have

$$\hat{\varphi}(s) = \begin{cases} \mathcal{O}\left(s^{-n-\lambda}\log(s)\right), & \lambda \notin 2\mathbb{N} \\ \mathcal{O}\left(s^{-n-\lambda}\right), & \lambda \in 2\mathbb{N}. \end{cases}$$

Of special interest for quasi-interpolation is the case where we have as many even

powers of s in our asymptotic expansion as possible. This is only achievable if $\lambda \in 2\mathbb{N}$ and hence, we conclude that in this case the dimension n should be even. This is in contrast to the case of the generalized multiquadric where this result was only achievable for odd dimensions.

We now assume that $n, \lambda \in 2\mathbb{N}$. The poles of $\Gamma\left(-\frac{\lambda}{\beta}+t\right)$ are located at $t = \frac{\lambda}{\beta} - d$, $d \in \mathbb{N}$ while the poles of $\Gamma\left(-\frac{n+\beta t}{2}\right)$ are located at $t = \frac{-n-2v}{\beta}, v \in \mathbb{N}$. A double pole appears if there exist some positive integer d and v so that $\lambda - d\beta = -n - 2v$. Hence, if $\beta \in \mathbb{Q}$, then there exist $d, v \in \mathbb{N}$ such that the equation holds and so a pole of order two will appear. This pole interrupts the series of even powers in s. On the other hand, if $\beta \in \mathbb{R}\backslash\mathbb{Q}$, then there will be no double pole, but the pole at $t = \frac{\lambda}{\beta} - 1$ will not result in an even power of s. The case, where $t = \frac{\lambda}{\beta} - 1$ does not results in an even power of s will be further analyzed in the next chapter.

The second case is for $\beta \in 2\mathbb{N}$. Then, all poles until the double pole will result in even powers of s. The first double pole is located at $t = \left\lfloor \frac{-\lambda-n}{\beta} \right\rfloor + \frac{\lambda}{\beta}$. So, the form of the asymptotic series is given by

$$\begin{aligned}\hat{\varphi}_4(s) \sim \sum_{j=0}^{\left\lceil \frac{\lambda+n}{\beta} \right\rceil} C_j(c,n,\lambda,\beta) s^{-n-\lambda+j\beta} + \sum_{j=0}^{\frac{-n-\lambda+\beta\left\lceil \frac{n+\lambda}{\beta} \right\rceil}{2}-1} \tilde{C}_j(c,n,\lambda,\beta) s^{2j} \\ + \hat{C}_1(c,n,\lambda,\beta) s^{-n-\lambda+\beta\left\lceil \frac{n+\lambda}{\beta} \right\rceil} \log\left(\frac{cs}{2}\right), \qquad \text{as } s \to 0_+, \end{aligned} \tag{3.8}$$

where $C_j, \tilde{C}_j$ and $\hat{C}_1$ are some constants depending on c, n, λ, β and j which can be evaluated using residue theorem for the corresponding poles. These results are also presented in [43] for the special case $\beta = \lambda = 2d, d \in \mathbb{N}$. Similarly, we get for $\hat{\varphi}_3(s)$ an asymptotic series of the same structure

$$\begin{aligned}\hat{\varphi}_3(s) \sim \sum_{j=0}^{\left\lceil \frac{n}{\beta} \right\rceil} C_j(c,n,\beta) s^{-n+j\beta} + \sum_{j=0}^{\frac{-n+\beta\left\lceil \frac{n}{\beta} \right\rceil}{2}-1} \tilde{C}_j(c,n,\beta) s^{2j} \\ + \hat{C}_1(c,n,\beta) s^{-n+\beta\left\lceil \frac{n}{\beta} \right\rceil} \log\left(\frac{cs}{2}\right), \qquad \text{as } s \to 0_+, \end{aligned} \tag{3.9}$$

for some other constants $C_j, \tilde{C}_j$ and $\hat{C}_1$ depending on c, n, β and j. Note that in both cases the power of s in the logarithmic term is always greater than or equal to zero. Hence, we have determined the asymptotic behaviour for small arguments and found that this RBF can only be used for quasi-interpolation if $\lambda \in 2\mathbb{N}$.

We continue to consider the case $\lambda \in 2\mathbb{N}$. The decay rate as $s \to \infty$ is given by

the first non-vanishing pole greater than $\frac{\lambda}{\beta}$. Let's assume that the first non-vanishing pole outside the path of integration is at $t = \frac{\lambda}{\beta} + 1$ which occurs for $\beta \notin 2\mathbb{N}$. With the parametrization $t = \mathrm{i}\tilde{t} + \frac{\lambda}{\beta} + 1 - \varepsilon$ we obtain

$$\begin{aligned}
\hat{\varphi}_4(s) &= \frac{2^n \pi^{\frac{n}{2}} c^\lambda}{s^n} \frac{1}{2\pi \mathrm{i}} \int_L \frac{\Gamma\left(1 + \frac{\lambda}{\beta} - t\right) \Gamma\left(-\frac{\lambda}{\beta} + t\right)^2 \Gamma\left(\frac{n+\beta t}{2}\right)}{\Gamma\left(1 - \frac{\lambda}{\beta} + t\right) \Gamma\left(-\frac{\beta t}{2}\right)} \left(\frac{2}{cs}\right)^{\beta t} \mathrm{d}t \\
&= \frac{2^n \pi^{\frac{n}{2}} c^\lambda}{s^n} \frac{1}{2\pi} \int_{-\infty}^{\infty} \frac{\Gamma\left(\varepsilon - \tilde{t}\right) \Gamma\left(1 - \varepsilon + \mathrm{i}\tilde{t}\right)^2 \Gamma\left(\frac{n}{2} + \frac{\lambda+\beta-\varepsilon\beta+\mathrm{i}\beta\tilde{t}}{2}\right)}{\Gamma\left(2 - \varepsilon + \mathrm{i}\tilde{t}\right) \Gamma\left(-\frac{\lambda+\beta-\varepsilon\beta+\mathrm{i}\beta\tilde{t}}{2}\right)} \left(\frac{2}{cs}\right)^{\lambda+\beta-\varepsilon\beta+\mathrm{i}\beta\tilde{t}} \mathrm{d}\tilde{t} \\
&\leq \frac{C}{c^{\beta(1-\varepsilon)} s^{n+\lambda+\beta(1-\varepsilon)}} \int_{-\infty}^{\infty} \left| \frac{\Gamma\left(\varepsilon - \mathrm{i}\tilde{t}\right) \Gamma\left(1 - \varepsilon + \mathrm{i}\tilde{t}\right)^2 \Gamma\left(\frac{n}{2} + \frac{\lambda+\beta-\varepsilon\beta+\mathrm{i}\beta\tilde{t}}{2}\right)}{\Gamma\left(2 - \varepsilon + \mathrm{i}\tilde{t}\right) \Gamma\left(-\frac{\lambda+\beta-\varepsilon\beta+\mathrm{i}\beta\tilde{t}}{2}\right)} \right| \mathrm{d}\tilde{t}.
\end{aligned}$$

The integral is independent of s and finite. This can be seen applying equ. (3.5) to the absolute values of the Gamma functions individually. Since $\varepsilon > 0$ is arbitrary we conclude that

$$\hat{\varphi}_4(s) = \mathcal{O}\left(s^{-n-\lambda-\beta}\right), \qquad \text{as } s \to \infty.$$

With the same logic we obtain

$$\hat{\varphi}_3(s) = \mathcal{O}\left(s^{-n-\beta}\right), \qquad \text{as } s \to \infty.$$

From the previous chapter, we also know that

$$\hat{\varphi}_2 = \begin{cases} \mathcal{O}\left(s^{-n-\lambda}\right), & \lambda \notin 2\mathbb{N} \qquad \text{as } s \to \infty \\ 0, & \lambda \in 2\mathbb{N} \qquad \text{as } s \to \infty. \end{cases}$$

Together we have

$$\hat{\varphi} = \mathcal{O}\left(s^{-n-\beta}\right), \qquad \text{as } s \to \infty, \quad \lambda \in 2\mathbb{N}, \beta \notin 2\mathbb{N}.$$

The decay rate of the derivatives of the Fourier transforms are even higher. This can be shown analogously to the cases of the generalized multiquadric. If there is no pole outside the contour due to pole cancellation for $\lambda, \beta \in 2\mathbb{N}$, then the decay rate of $\hat{\varphi}(s)$ and of all its derivatives is faster than any polynomial can grow. This is the optimal

setup for quasi-interpolation because of the high decay rate of the Fourier transform and the determinable even singularity at the origin.

3.2.2.2 Case 2: $\lambda < 0, \beta > 0$

Parameter configuration	RBF $\varphi(r) = \left(c^\lambda + r^\lambda\right) \log\left(c^\beta + r^\beta\right)$	Contour integral of the Fourier transform $\hat{\varphi}_4(s)$
$\lambda > 0, \beta > 0$	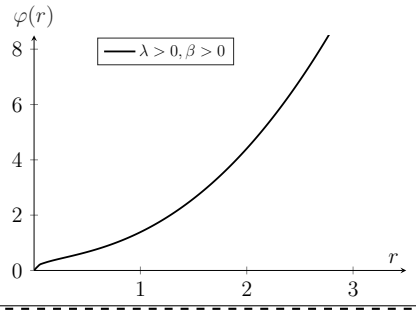	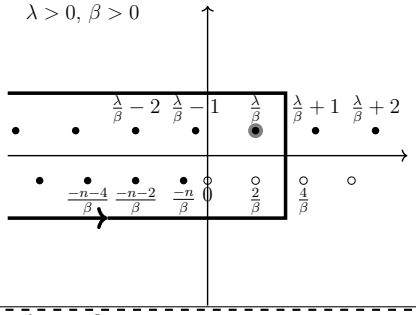
$\lambda < 0, \beta > 0$	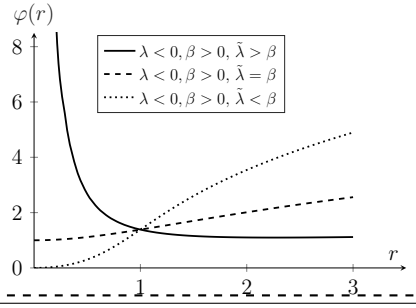	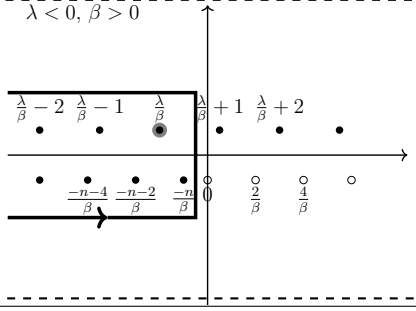
$\lambda > 0, \beta < 0$	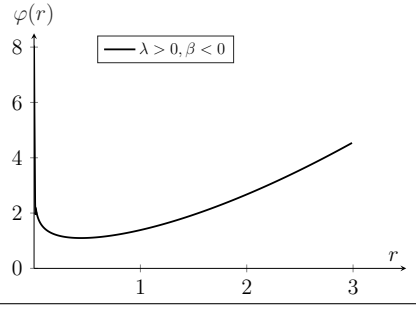	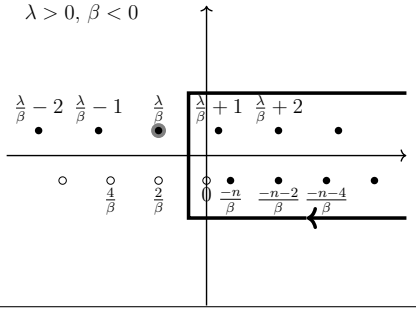
$\lambda < 0, \beta < 0$	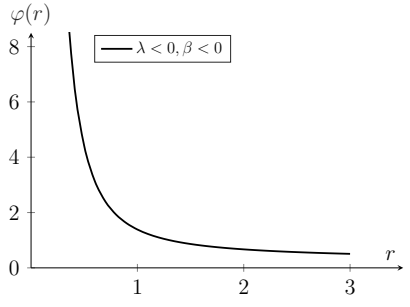	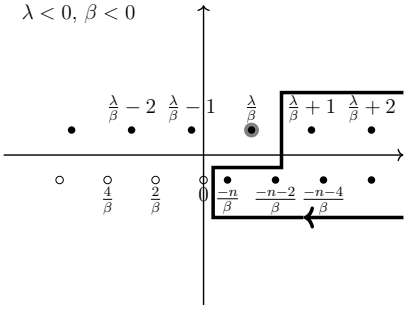

Table 3.6: Overview of the cases considered for the generalized thin plate spline. The focus is on the framed case.

As before, we define $\tilde{\lambda} = -\lambda$ to be positive. For this case, the RBF itself can be singular. To avoid this singularity, we can use the special constant value $c = 1$ and $\beta \geq \tilde{\lambda}$. Nevertheless, we analyze the RBF and will see if this case can be used for classical

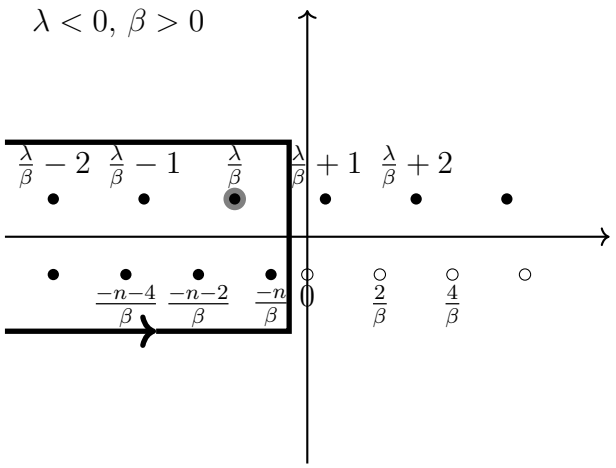

Figure 3.7: Visualization of the poles from equ. (3.7) for $\lambda < 0, \beta > 0$. The singularities of the Gamma functions in the numerator are depicted as dots, whereas the singularities of the Gamma function in the denominator are represented by circles, which may cancel poles. Dots with circles around represent double poles. For the purpose of enhanced visualization, the poles are represented as if they had an imaginary component, although this is not the case. Every pole lies on the real axis. Additionally, the path of integration is depicted and indicates which poles have to be included. The example is provided for $|\lambda| = 2, |\beta| = \frac{5}{2}, n = 1$.

quasi-interpolation. The poles of the Gamma functions and the path of integration are visualized in figure 3.7. There are two possible scenarios: If $\tilde{\lambda} > n$, then the leading order pole of $\hat{\varphi}_4(s)$ is at $t = -\frac{n}{\beta}$ which results in a constant leading behaviour as $s \to 0_+$. If $\tilde{\lambda} < n$, then the leading order pole is of order two at $t = \frac{-\tilde{\lambda}}{\beta}$, which results in a logarithmic term. Lastly, if $\tilde{\lambda} = n$, then the leading order pole is of order three resulting in a logarithmic squared term. In summary, we have

$$\hat{\varphi}_4(s) = \begin{cases} \mathcal{O}(1), & \tilde{\lambda} > n \\ \mathcal{O}(s^{-n+\tilde{\lambda}} \log(s)), & \tilde{\lambda} < n \\ \mathcal{O}(\log^2(s)), & \tilde{\lambda} = n. \end{cases}$$

None of these cases are suitable for classical quasi-interpolation because we can not achieve an even power of s for small arguments. Since $\lambda < 0$ the leading order singularity is not generated by $\hat{\varphi}_4(s)$ but rather by $\hat{\varphi}_3(s)$. The leading order is given by the pole of order one located at $t = 0$.

$$\hat{\varphi}_3(s) \sim c^{-\tilde{\lambda}} \beta \left(-2^{n-1}\right) \pi^{n/2} s^{-n} \Gamma\left(\frac{n}{2}\right), \qquad s \to 0_+.$$

Remember that

$$\hat{\varphi}_2(s) = \beta \log(c) \frac{\Gamma\left(\frac{n-\tilde{\lambda}}{2}\right)}{\Gamma(\frac{\tilde{\lambda}}{2})} 2^{-\tilde{\lambda}+n} \pi^{n/2} s^{-n+\tilde{\lambda}},$$

where the parameter configuration $\tilde{\lambda} \notin 2\mathbb{N} + n$ has to be satisfied.

For large arguments the decay rate is determined by the residue of the first non-vanishing pole outside the contour. For the different functions we get

$$\begin{aligned} \hat{\varphi}_4(s) &= \mathcal{O}(s^{-n+\tilde{\lambda}-\beta}), && s \to \infty, \\ \hat{\varphi}_3(s) &= \mathcal{O}(s^{-n-\beta}), && s \to \infty, \\ \hat{\varphi}_2(s) &= \mathcal{O}(s^{-n+\tilde{\lambda}}), && s \to \infty. \end{aligned}$$

The decay rate for large arguments is limited by $\hat{\varphi}_2(s)$ and is slower than s^{-n}. In the next chapter, we will see that this decay rate is not fast enough for quasi-interpolation. Therefore, this case will not be considered further.

3.2.2.3 Case 3: $\lambda > 0, \beta < 0$

Parameter configuration	RBF $\varphi(r) = \left(c^\lambda + r^\lambda\right) \log\left(c^\beta + r^\beta\right)$	Contour integral of the Fourier transform $\hat{\varphi}_4(s)$
$\lambda > 0, \beta > 0$	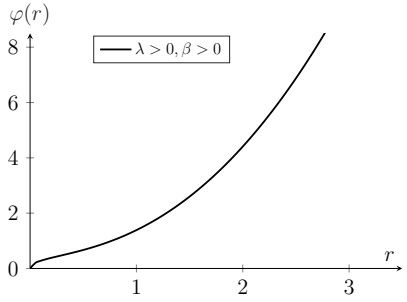	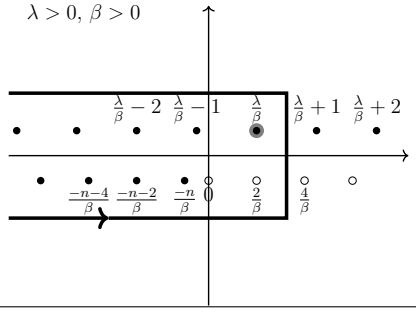
$\lambda < 0, \beta > 0$	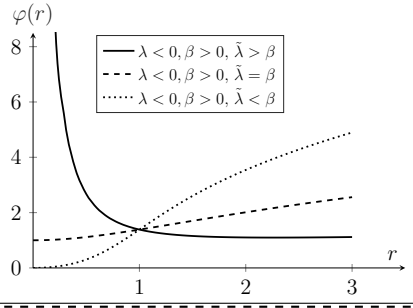	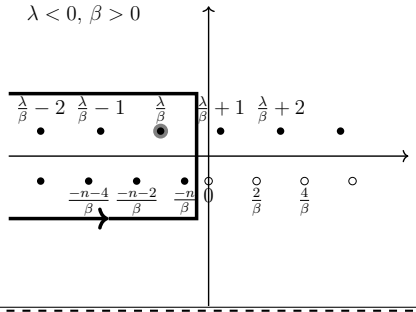
$\lambda > 0, \beta < 0$	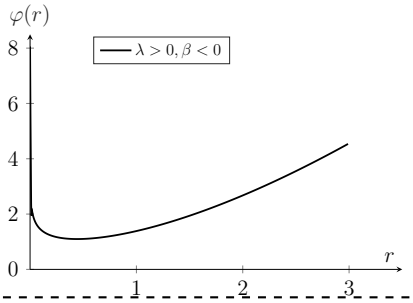	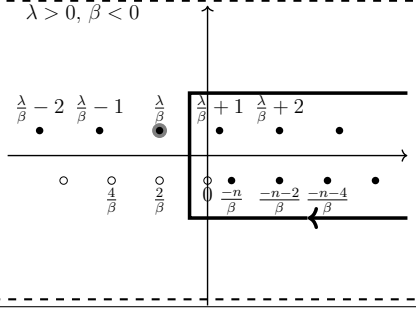
$\lambda < 0, \beta < 0$	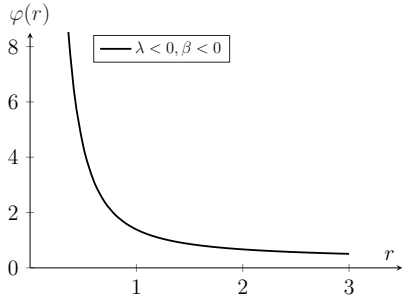	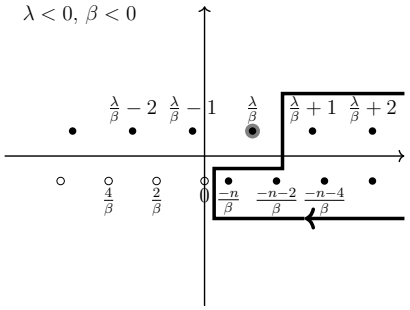

Table 3.7: Overview of the cases considered for the generalized thin plate spline. The focus is on the framed case.

Next, we analyze the case of positive λ and negative β. We define $\tilde{\beta} = -\beta$ to be positive. The RBF itself is singular for this choice of parameters. There is no special case to avoid this singularity directly. However, it can be addressed by using a linear

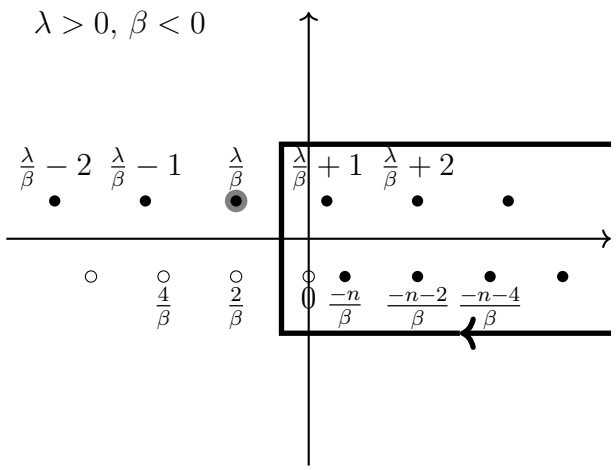

Figure 3.8: Visualization of the poles from equ. (3.7) for $\lambda > 0, \beta < 0$. The singularities of the Gamma functions in the numerator are depicted as dots, whereas the singularities of the Gamma function in the denominator are represented by circles, which may cancel poles. Dots with circles around represent double poles. For the purpose of enhanced visualization, the poles are represented as if they had an imaginary component, although this is not the case. Every pole lies on the real axis. Additionally, the path of integration is depicted and indicates which poles have to be included. The example is provided for $|\lambda| = 2, |\beta| = \frac{5}{2}, n = 1$.

combination of different values of λ and constants c, for example

$$\varphi(r) = (c_1^{\lambda_1} + r^{\lambda_1}) \log\left(\frac{1}{c_1^{\tilde{\beta}}} + \frac{1}{r^{\tilde{\beta}}}\right) - (c_2^{\lambda_2} + r^{\lambda_2}) \log\left(\frac{1}{c_2^{\tilde{\beta}}} + \frac{1}{r^{\tilde{\beta}}}\right),$$

provided that $c_1^{\lambda_1} = c_2^{\lambda_2}$ and $\lambda_1 \neq \lambda_2$. Then the linear combination is not singular and we can examine its applicability for quasi-interpolation. To do so, we still analyze the single RBF and not the linear combination directly. When β is negative, the contour and all poles compared to the previous case change their signs. This is shown in figure 3.8. If the first pole is at $t = -\frac{n}{\tilde{\beta}}$, then the asymptotic behaviour of the Fourier transform of the RBF at the origin is characterized by either a constant or a logarithmic term, depending on whether the pole is simple or of order two. Both cases are not useful for classical quasi-interpolation as they do not yield singularities with even powers of s. To achieve such behaviour, the leading-order term must be induced by a pole of the function $\Gamma\left(1 + \frac{\lambda}{\tilde{\beta}} + t\right)$. This means, for the values of λ and β there have to exist some $d \in \mathbb{N}$ such that $n + \lambda - d\tilde{\beta} > 0$ and $\lambda - d\tilde{\beta} \notin 2\mathbb{N}$. While the first condition ensures that we get a singularity at the origin, the second condition guarantees that this pole does not cancel out. Note that only finitely many values of d must be considered. Additionally, more than

one value of d may satisfy both conditions. The leading order is therefore determined by the smallest value of d satisfying both conditions. Consequently, we obtain

$$\hat{\varphi}_4(s) \sim \frac{(-1)^d \pi^{n/2} c^{d\tilde{\beta}} 2^{-d\tilde{\beta}+\lambda+n} \Gamma\left(\frac{1}{2}(n - d\tilde{\beta} + \lambda)\right)}{s^{n+\lambda-d\tilde{\beta}} d\Gamma\left(-\frac{\lambda-d\tilde{\beta}}{2}\right)} \qquad \text{as } s \to 0_+.$$

Since $\lambda - d\tilde{\beta} \notin 2\mathbb{N}$, we know that classical quasi-interpolation is only applicable in odd dimensions n provided that $\lambda - d\tilde{\beta}$ is odd. The most favorable scenario is for $d = 1$ because in this case, we achieve the highest order singularity at the origin. We now determine the asymptotic series for the most likely case $d = 1$, n odd, λ odd and $\tilde{\beta}$ even. For this special case the first double pole appears at $t = -\frac{\lambda}{\tilde{\beta}} + \left\lceil \frac{\lambda+n}{\tilde{\beta}} \right\rceil$ and thus, the asymptotic expansion is of the form

$$\begin{aligned}\hat{\varphi}_4(s) \sim \sum_{j=1}^{\left\lceil \frac{\lambda+n}{\tilde{\beta}} \right\rceil} C_j(c,n,\lambda,\tilde{\beta}) s^{-n-\lambda+j\tilde{\beta}} + \sum_{j=0}^{\frac{-n-\lambda+\beta\left\lceil \frac{n+\lambda}{\beta} \right\rceil}{2}-1} \tilde{C}_j(c,n,\lambda,\tilde{\beta}) s^{2j} \\ + \hat{C}_1(c,n,\lambda,\tilde{\beta}) s^{-n-\lambda+\beta\left\lceil \frac{n+\lambda}{\beta} \right\rceil} \log\left(\frac{cs}{2}\right), \qquad \text{as } s \to 0_+,\end{aligned}$$

where $C_j, \tilde{C}_j$ and $\hat{C}_1$ are some constants which can be evaluated using the residue theorem for the corresponding pole. The same series holds for $\hat{\varphi}_3$ with $\lambda = 0$. It is noteworthy that, aside from the logarithmic term present in both series, only even powers of s appear. The logarithmic part is multiplied by some power of s, which is greater than or equal to zero. For the combined Fourier transform, the sum of both series has to be taken into account.

Finally, assume that $\tilde{\beta}$ is not even. Then the pole at $t = \frac{\lambda}{\tilde{\beta}} + 2$ will not result in an even power of s. Assuming that the second pole is not a double pole, we obtain the asymptotic series

$$\hat{\varphi}_4(s) \sim \sum_{j=1}^{2} C_j(c,n,\lambda,\tilde{\beta}) s^{-n-\lambda+j\tilde{\beta}} + \sum_{j=0}^{\left\lfloor \frac{-n-\lambda+2\tilde{\beta}}{2} \right\rfloor} \tilde{C}_j(c,n,\lambda,\beta) s^{2j}, \qquad \text{as } s \to 0_+.$$

However, for $\hat{\varphi}_3$, the first non-even power of s appears at $t = 1$ which can reduce the capacity of the polynomial reproduction later on. The asymptotic behaviour for $s \to \infty$ is limited by the pole at $t = -\frac{\lambda}{\tilde{\beta}}$. If this pole is double (this is for $\lambda \notin 2\mathbb{N}$), we find that

$$\hat{\varphi}_4(s) = \mathcal{O}\left(s^{-n-\lambda}\log(s)\right) \qquad \text{as } s \to \infty,$$

and

$$\hat{\varphi}_3(s) = \mathcal{O}\left(s^{-n}\right) \qquad \text{as } s \to \infty.$$

If this pole is simple (this is for $\lambda \in 2\mathbb{N}$), we find that

$$\hat{\varphi}_4(s) = \mathcal{O}\left(s^{-n-\lambda}\right) \qquad \text{as } s \to \infty,$$

and

$$\hat{\varphi}_3(s) = \mathcal{O}\left(s^{-n}\right) \qquad \text{as } s \to \infty.$$

In this case the decay rate of the Fourier transform is entirely determined by the dimension n. In the next chapter we will see that this decay rate is too low to reproduce polynomials and therefore cannot be used. For this reason, this case will be excluded from further analysis.

3.2.2.4 Case 4: $\lambda < 0, \beta < 0$

Parameter configuration	RBF $\varphi(r) = \left(c^\lambda + r^\lambda\right) \log\left(c^\beta + r^\beta\right)$	Contour integral of the Fourier transform $\hat{\varphi}_4(s)$
$\lambda > 0, \beta > 0$	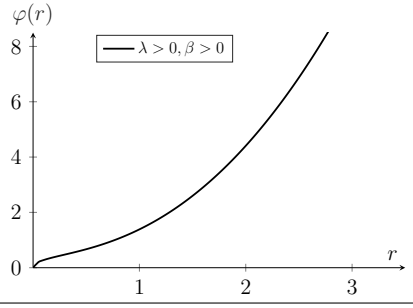	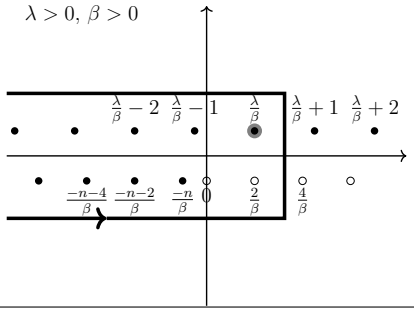
$\lambda < 0, \beta > 0$	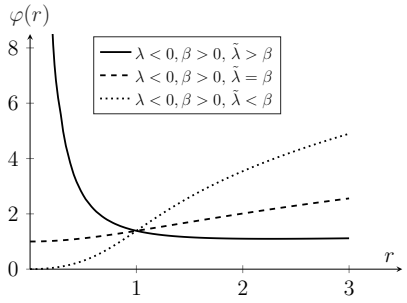	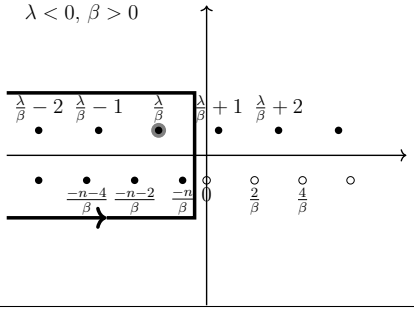
$\lambda > 0, \beta < 0$	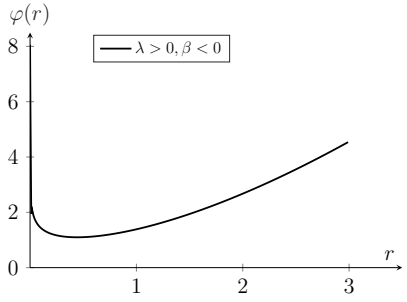	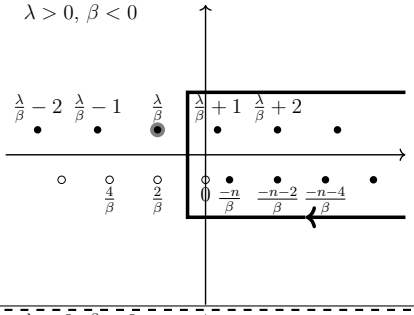
$\lambda < 0, \beta < 0$	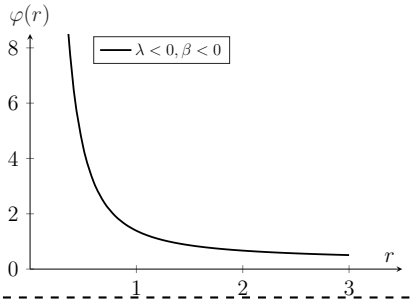	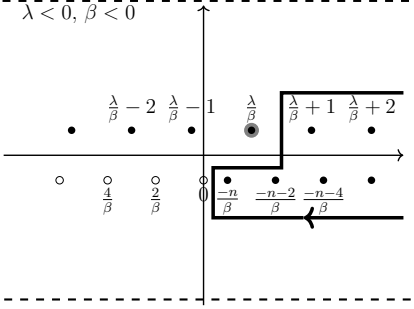

Table 3.8: Overview of the cases considered for the generalized thin plate spline. The focus is on the framed case.

For the last case, we define $\tilde{\lambda} = -\lambda > 0$ and $\tilde{\beta} = -\beta > 0$. The RBF is singular in this configuration. Therefore, it is necessary to consider a linear combination involving

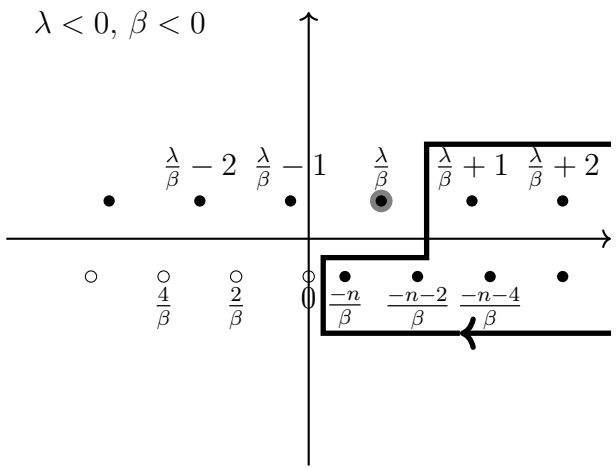

Figure 3.9: Visualization of the poles from equ. (3.7) for $\lambda < 0, \beta < 0$. The singularities of the Gamma functions in the numerator are depicted as dots, whereas the singularities of the Gamma function in the denominator are represented by circles, which may cancel poles. Dots with circles around represent double poles. For the purpose of enhanced visualization, the poles are represented as if they had an imaginary component, although this is not the case. Every pole lies on the real axis. Additionally, the path of integration is depicted and indicates which poles have to be included. The example is provided for $|\lambda| = 2, |\beta| = \frac{5}{2}, n = 1$.

different values of c, λ, and β, for example

$$\varphi(r) = \left(\frac{1}{c_1^{\tilde{\lambda}_1}} + \frac{1}{r^{\tilde{\lambda}_1}}\right) \log\left(\frac{1}{c_1^{\tilde{\beta}_1}} + \frac{1}{r^{\tilde{\beta}_1}}\right) - \left(\frac{1}{c_2^{\tilde{\lambda}_2}} + \frac{1}{r^{\tilde{\lambda}_2}}\right) \log\left(\frac{1}{c_2^{\tilde{\beta}_2}} + \frac{1}{r^{\tilde{\beta}_2}}\right),$$

where we assume that $c_1^{\tilde{\lambda}_1} = c_2^{\tilde{\lambda}_2}$ and $c_1^{\tilde{\beta}_1} \neq c_2^{\tilde{\beta}_2}$. A finite linear combination exists for the original RBF, and the following analysis will start with this fact. The poles of this last case are visualized in figure 3.9. The separation of the poles is only possible if $\tilde{\lambda} - d\tilde{\beta} \notin n + 2\mathbb{N}$ for all $d \in \mathbb{N}$. If $\tilde{\lambda} + \tilde{\beta} > n$, then the leading order pole is at $t = \frac{n}{\tilde{\beta}}$ which results in a constant behaviour of the Fourier transform of the RBF at the origin. If $\tilde{\lambda} + \tilde{\beta} = n$, then the leading-order term exhibits a logarithmic singularity at the origin and is therefore not feasible for quasi-interpolation. Hence, we assume that $\tilde{\lambda} + \tilde{\beta} < n$, and the leading order term is induced by the pole at $t = \frac{\tilde{\lambda}}{\tilde{\beta}} + 1$. This results in the asymptotic behaviour of

$$\hat{\varphi}_4(s) \sim -\frac{\pi^{n/2} c^{\tilde{\beta}} 2^{-\tilde{\beta}-\tilde{\lambda}+n} \Gamma\left(\frac{1}{2}(n-\tilde{\beta}-\tilde{\lambda})\right)}{s^{n-\tilde{\lambda}-\tilde{\beta}} \Gamma\left(\frac{\tilde{\lambda}+\tilde{\beta}}{2}\right)} \qquad \text{as } s \to 0_+.$$

Even more interesting is the function $\hat{\varphi}_3$, because the leading term for $\tilde{\beta} > n$ is given by

$$\hat{\varphi}_3(s) \sim -\frac{\pi^{n/2} c^{\tilde{\beta}} 2^{-\tilde{\beta}+n} \Gamma\left(\frac{1}{2}(n-\tilde{\beta})\right)}{s^{n-\tilde{\beta}} \Gamma\left(\frac{\tilde{\beta}}{2}\right)} \qquad \text{as } s \to 0_+,$$

which includes the higher singularity. Assume that $\tilde{\beta}$ is even. Then a double pole will appear at $t = -\tilde{\beta}\left\lceil \frac{n}{\tilde{\beta}} \right\rceil$ and the asymptotic series up to and including this double pole is given by

$$\begin{aligned}\hat{\varphi}_3(s) \sim \sum_{j=1}^{\left\lceil \frac{n}{\tilde{\beta}} \right\rceil} C_j(c,n,\tilde{\beta}) s^{-n+j\tilde{\beta}} + \sum_{j=0}^{\frac{-n+\tilde{\beta}\left\lceil \frac{n}{\tilde{\beta}} \right\rceil}{2}-1} \tilde{C}_j(c,n,\tilde{\beta}) s^{2j} \\ + \hat{C}_1(c,n,\tilde{\beta}) s^{-n+\tilde{\beta}\left\lceil \frac{n}{\tilde{\beta}} \right\rceil} \log\left(\frac{cs}{2}\right), \qquad \text{as } s \to 0.\end{aligned}$$

If $\tilde{\beta} \notin 2\mathbb{N}$, then the second pole does not result in an even power of s. To determine the polynomial reproduction and approximation order, the sum of $\hat{\varphi}_3$ and $\hat{\varphi}_4$ has to be taken into account.

Furthermore, as $s \to \infty$, the decay is governed by the first non-vanishing pole outside the contour, yielding

$$\hat{\varphi}_4(s) = \mathcal{O}\left(s^{-n+\tilde{\lambda}} \log(s)\right)$$

and

$$\hat{\varphi}_3(s) = \mathcal{O}\left(s^{-n}\right).$$

As in the previous case, the decay rate of the Fourier transform behaves like s^{-n} which is too slow for polynomial reproduction. Therefore, this case is also excluded from further analysis.

3.3 Summary

In this chapter, we determined the asymptotic behaviour of the Fourier transforms of the generalized multiquadric and the generalized thin plate spline for all possible parameter configurations λ and β. Understanding the asymptotic behaviour is essential for the subsequent determination of the coefficients μ_k of the quasi-Lagrange functions, in order

to ensure that the Strang and Fix conditions are satisfied. We identified a few interesting cases for classical quasi-interpolation, on which we will focus on in the following chapter.

1. For the generalized multiquadric we will further analyze the cases
   - $\lambda > 0, \beta > 0$ with $\lambda \in 2 + 4\mathbb{N}$, $\beta \in \frac{1}{2} + \mathbb{N}$ and n is odd
   - $\lambda > 0, \beta > 0$ with $\lambda\beta \in 1 + 2\mathbb{N}$ and n is odd
   - $\lambda > 0, \beta < 0$ with $\lambda\tilde{\beta} < n$
   - $\lambda < 0, \beta > 0$ with $n, \tilde{\lambda} \in 2\mathbb{N}$, $n > \tilde{\lambda}$ and $\tilde{\lambda}\beta < n + 1$
   - $\lambda < 0, \beta < 0$ with $n, \tilde{\lambda} \in 2\mathbb{N}$ and $n > \tilde{\lambda}$.
2. For the generalized thin plate spline we will focus on the cases
   - $\lambda > 0, \beta > 0$ with $\lambda, \beta \in 2\mathbb{N}$
   - $\lambda > 0, \beta > 0$ with $\lambda \in 2\mathbb{N}$ and $\beta \notin 2\mathbb{N}$.

Chapter 4

Quasi-Interpolation

In this section, we will employ the Strang and Fix conditions to determine the polynomial reproduction and the approximation order of the quasi-interpolant. The applicability of the Strang and Fix conditions requires the asymptotic decay rate of the quasi-Lagrange function for large arguments. To determine the decay rate of the quasi-Lagrange function, we utilize the following theorem.

Theorem 4.1 (Modified version of Theorem A from [14])**.** *Let $\varphi(||\cdot||) : \mathbb{R}^n \to \mathbb{R}$ be a continuous function with at most polynomial growth so that it can be viewed as a tempered distribution. Therefore it has a distributional Fourier transform $\hat{\varphi}$ which we specifically require to be of the form*

$$\hat{\varphi}(s) = \frac{F(s) + bG_0(s)\log(cs)}{G(s)} \tag{4.1}$$

for $s = ||\cdot||$ near the origin, say for $s \in B_1(0)$. Here b and c are constants, G_0 is a homogeneous polynomial of of degree n_0, n_0 is a nonnegative integer, and F and G are real-valued functions satisfying the following conditions:

(2A) G is a homogeneous polynomial of positive even degree $2m_1$ and $G(s) \neq 0$ for all $s > 0$.

(2B) $F \in C^{m_0}(B_1(0)) \cap C^{m_0+n+1}(B_1(0)\backslash\{0\})$ for some nonnegative integer m_0, $F(0) \neq 0$, and there exists $\theta \in (0, 1]$ such that for all $\gamma \in \mathbb{N}$ with $\gamma \leq m_0 + n + 1$,

$$|D^\gamma [F(s) - \tau_{m_0}(s)]| \leq Cs^{m_0+\theta-\gamma}, \qquad \text{as } s \to 0,$$

where τ_{m_0} denotes the Taylor polynomial of F of degree m_0 at the point $s = 0$.

(2C) The Fourier transform $\hat{\varphi}$ of φ is (m_0+n+1)-times continuously differentiable on the domain $\{s \in \mathbb{R}_+ : s > \frac{1}{4}\}$, and

$$\max_{\gamma \le m_0+n+1} \int_{||s|| \ge \frac{1}{4}} |D^\gamma \hat{\varphi}(s)| \, \mathrm{d}s \le C < \infty. \tag{4.2}$$

Under this assumptions, there exists coefficients μ_k such that the quasi-Lagrange function

$$\Psi(x) = \sum_{k \in \mathbb{Z}^n} \mu_k \varphi\left(||x-k||\right), \qquad x \in \mathbb{R}^n,$$

has the decaying property

$$|\Psi(x)| \le C\left(1+||x||\right)^{-n-m_2}, \qquad x \in \mathbb{R}^n,$$

where

$$m_2 = \begin{cases} m_0+\theta, & \text{if } b=0 \\ \min\{m_0+\theta, n_0\}, & \text{if } b \neq 0 \end{cases}$$

and furthermore, the operator defined by ("quasi-interpolation")

$$Q_h[f](x) = \sum_{j \in \mathbb{Z}^n} f(jh) \Psi\left(\frac{x-jh}{h}\right)$$

reproduces all polynomials of total degree at most $\ell_0 = \min\{m_0, 2m_1-1\}$ that is, $Q_h[p] = p$ for all $p \in \prod_{\ell_0}^n$.

Theorem 4.1 provides a framework for applying the Strang and Fix conditions by utilizing properties *(2A)*–*(2C)* to determine the decay rate of the quasi-Lagrange function. The condition *(2C)* is particularly crucial, as it ensures that the decay rate of the Fourier transform of the RBF, along with that of its derivatives, is sufficiently fast to guarantee the finiteness of the associated integral. This condition was employed in Section 3, where it was demonstrated that certain special cases are not suitable due to an insufficient rate of decay.

4.1 Polynomial Reproduction and Approximation Order

We start with Theorem 4.1 in conjunction with the Strang and Fix conditions to determine the polynomial reproduction and the approximation order for the identified cases stated in chapter 3. We choose the approximation order as an objective to measure effectiveness of the quasi-interpolation method for different RBFs. We begin with the cases of the generalized multiquadric.

4.1.1 Generalized Multiquadric

Case 1: $\lambda, \beta > 0$

For $\lambda, \beta > 0$ there are multiple applications for quasi-interpolation. In the following, we focus on the most practically relevant case. In the previous section we established that the highest singularity at the origin of $\hat{\varphi}(s)$ can be achieved if $\lambda \in 2 + 4\mathbb{N}$ and $\beta \in \frac{1}{2} + \mathbb{N}$. This case is especially interesting because in odd dimensions n all powers of s are even such that a finite trigonometric polynomial can handle them. On the other hand, there appears a double pole leading to a logarithmic term located at $t = \left\lfloor -\frac{n}{\lambda} + \frac{1}{2} \right\rfloor - \frac{1}{2}$. Comparing the asymptotic behaviour from equ. (3.4) with equ. (4.1), we get

$$\begin{aligned}\hat{\varphi}(s) \sim & \sum_{j=0}^{\left\lceil \frac{n}{\lambda} - \frac{1}{2} \right\rceil + \lfloor \beta \rfloor} C_j(c,n,\lambda,\beta) s^{-n+\lambda(j-\beta)} + \sum_{j=0}^{\frac{1}{2}\left(-n+\lambda\left(\left\lceil \frac{n}{\lambda} - \frac{1}{2} \right\rceil + \frac{1}{2}\right)\right)} \tilde{C}_j(c,n,\lambda,\beta) s^{2j} \\ & + C(c,n,\lambda,\beta) s^{-n+\lambda\left(\left\lceil \frac{n}{\lambda} - \frac{1}{2} \right\rceil + \frac{1}{2}\right)} \log(cs) \qquad \text{as } s \to 0_+ \\ & \overset{!}{=} \frac{F(s) + bG_0(s)\log(s)}{G(s)}\end{aligned}$$

from which we conclude that

$$\begin{aligned} G(s) &= s^{n+\lambda\beta}, \\ F(s) &= \sum_{j=0}^{\left\lceil \frac{n}{\lambda} - \frac{1}{2} \right\rceil + \lfloor \beta \rfloor} C_j(c,n,\lambda,\beta) s^{j\lambda} + \sum_{j=0}^{\frac{1}{2}\left(-n+\lambda\left(\left\lceil \frac{n}{\lambda} + \frac{1}{2} \right\rceil - \frac{1}{2}\right)\right)} \tilde{C}_j(c,n,\lambda,\beta) s^{2j+n+\lambda\beta}, \\ G_0(s) &= s^{\lambda\left(\left\lceil \frac{n}{\lambda} - \frac{1}{2} \right\rceil + \frac{1}{2} + \beta\right)}, \\ b &= C(c,n,\lambda,\beta). \end{aligned}$$

Checking the conditions of Theorem 4.1, we observe that $G_0(s)$ is a homogeneous polynomial of degree $n_0 = \lambda\left(\left\lceil \frac{n}{\lambda} - \frac{1}{2} \right\rceil + \frac{1}{2} + \beta\right)$ and that $b \neq 0$. Furthermore,

Parameter configuration	RBF $\varphi(r) = \left(c^\lambda + r^\lambda\right)^\beta$	Contour integral of the Fourier transform $\hat{\varphi}(s)$
$\lambda > 0, \beta > 0$	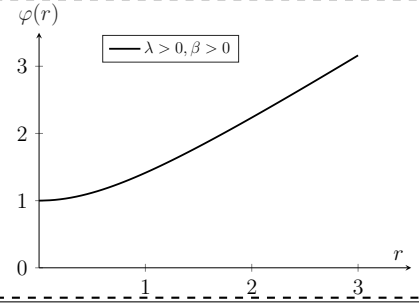	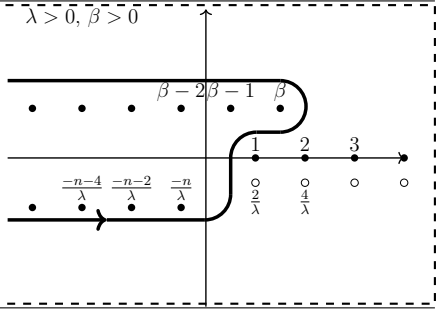
$\lambda > 0, \beta < 0$	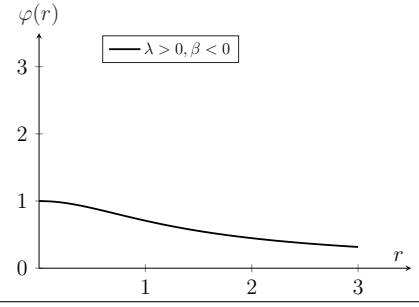	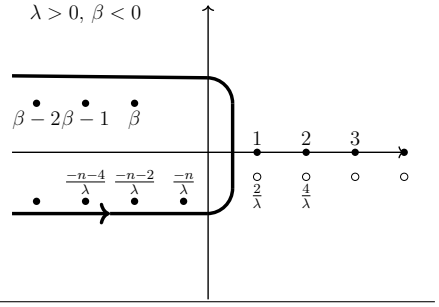
$\lambda < 0, \beta > 0$	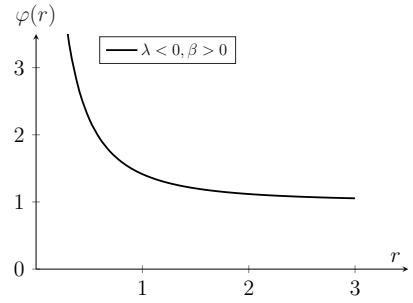	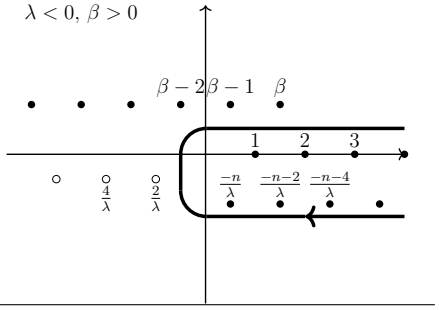
$\lambda < 0, \beta < 0$	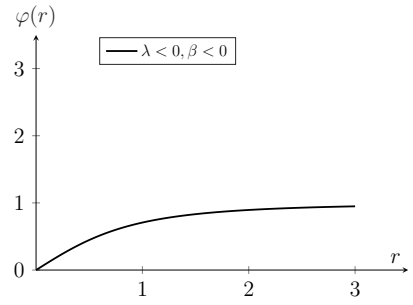	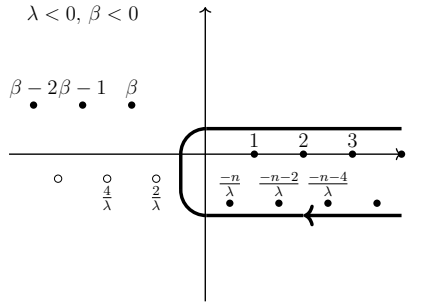

Table 4.1: Overview of the cases considered for the generalized multiquadric. The focus is on the framed case.

(2A) $G(s)$ is a homogeneous polynomial of positive even degree $2m_1 = n + \lambda\beta$, whose only zero is located at the origin.

(2B) $F(s)$ is a polynomial of degree n_0. Therefore, it is $C^\infty(\mathbb{R}_+)$ and the Taylor polynomial is exact with $m_0 = n_0$.

(2C) We showed that in this case the Fourier transform decays faster than any polynomial grows and the same holds for its derivatives. Hence, the integral in equ. (4.2) remains finite.

Applying Theorem 4.1, we conclude that there exist finitely many coefficients such that

$$|\Psi(x)| \leq C(1 + ||x||)^{-n-\lambda\left(\left\lceil \frac{n}{\lambda} - \frac{1}{2} \right\rceil + \frac{1}{2} + \beta\right)}.$$

Furthermore, the quasi-interpolation operator reproduces all polynomials of degree $n + \lambda\beta - 1$. With all necessary components now established, the Strang and Fix conditions can be applied, leading to the following uniform error estimate

$$||Q_h[f] - f||_\infty = \begin{cases} \mathcal{O}\left(h^{n+\lambda\beta} \log(1/h)\right) & \text{if } \frac{n}{\lambda} - \frac{1}{2} \in \mathbb{N}, \\ \mathcal{O}\left(h^{n+\lambda\beta}\right) & \text{if } \frac{n}{\lambda} - \frac{1}{2} \notin \mathbb{N}. \end{cases}$$

So far, we have the final results for the first special case of the generalized multiquadric. Other combinations of $\lambda\beta = 2d + 1, d \in \mathbb{N}$ are also suitable. Since double poles only appear for negative t, we conclude that

$$\begin{aligned} \hat{\varphi}(s) &\sim \sum_{j=0}^{1} C_j(c, n, \lambda, \beta) s^{-n+\lambda(j-\beta)} + \sum_{j=0}^{\left\lfloor \frac{1}{2}(-(\beta-1)\lambda - n) \right\rfloor} \tilde{C}_j(c, n, \lambda, \beta) s^{2j} \qquad \text{as } s \to 0_+ \\ &\stackrel{!}{=} \frac{F(s) + bG_0(s)\log(s)}{G(s)}. \end{aligned}$$

From this, it follows that

$$\begin{aligned} G(s) &= s^{n+\lambda\beta}, \\ F(s) &= \sum_{j=0}^{1} C_j(c, n, \lambda, \beta) s^{j\lambda} + \sum_{j=0}^{\left\lfloor \frac{1}{2}(-(\beta-1)\lambda - n) \right\rfloor} \tilde{C}_j(c, n, \lambda, \beta) s^{2j+n+\lambda\beta}, \\ G_0(s) &= 0, \\ b &= 0. \end{aligned}$$

(2A) G is a homogeneous polynomial of degree $2m_1 = n + \lambda\beta$.

(2B) F is a monomial of degree $n_0 = \lambda$. If $\lambda \notin \mathbb{N}$, then we choose $m_0 = \lfloor \lambda \rfloor$. The Taylor polynomial $\tau_{m_0}(s)$ is identically zero but the inequality holds with $\theta = \lambda - \lfloor \lambda \rfloor$. If

$\lambda \in \mathbb{N}$, then F is a polynomial and the Taylor polynomial is exact with $m_0 = \lambda$.

(2C) In general, we showed that $\hat{\varphi}(s)$ decays for large arguments like $s^{-n-\lambda}$, and the derivatives decay even faster. Therefore the integral in condition $(2C)$ remains finite.

For all suitable combinations ($\beta \notin \mathbb{N}$, $\lambda\beta$ odd, and odd dimension n), the decay rate of the quasi-Lagrange function is upper bounded by

$$|\Psi(x)| \leq C(1 + ||x||)^{-n-\lambda}$$

for some constant C and is capable of reproducing polynomials of degree $\lfloor \lambda \rfloor$. Furthermore, we achieve the error estimate via the Strang and Fix conditions

$$||Q_h[f] - f||_\infty = \begin{cases} \mathcal{O}\left(h^\lambda\right) & \text{if } \lambda \notin \mathbb{N} \\ \mathcal{O}\left(h^\lambda \log(1/h)\right) & \text{if } \lambda \in \mathbb{N}. \end{cases}$$

While multiple choices of the parameters λ and β are possible to use, classical quasi-interpolation is not achievable in even dimensions.

Case 2: $\lambda > 0, \beta < 0$

Parameter configuration	RBF $\varphi(r) = \left(c^\lambda + r^\lambda\right)^\beta$	Contour integral of the Fourier transform $\hat{\varphi}(s)$
$\lambda > 0, \beta > 0$	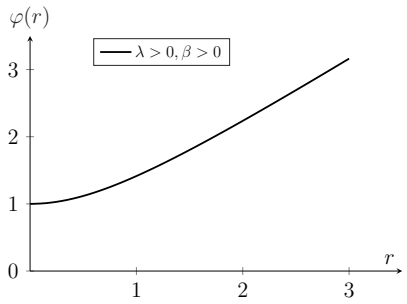	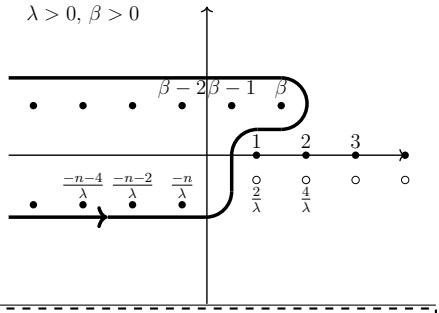
$\lambda > 0, \beta < 0$	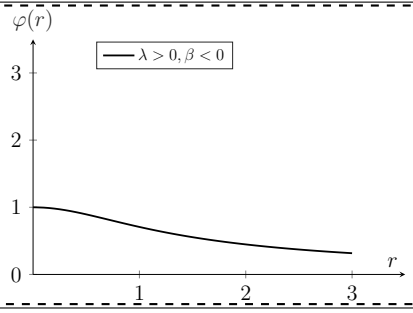	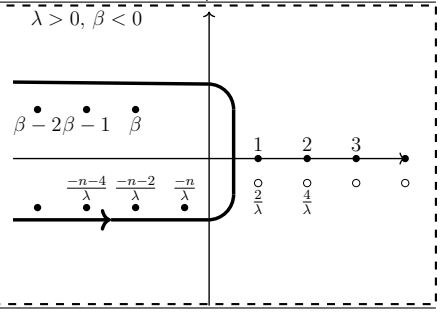
$\lambda < 0, \beta > 0$	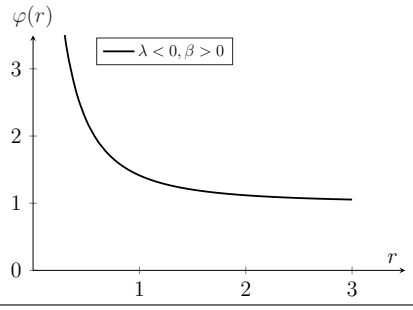	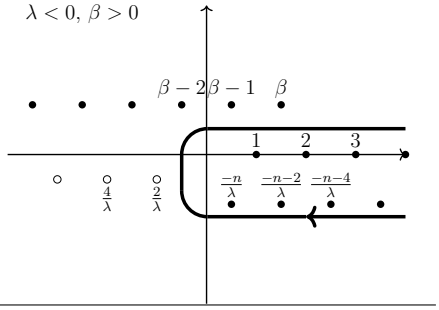
$\lambda < 0, \beta < 0$	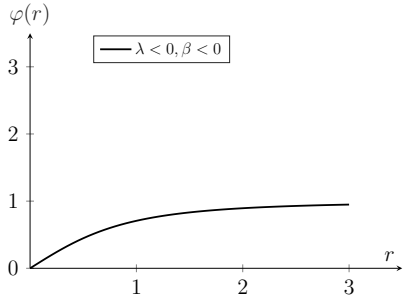	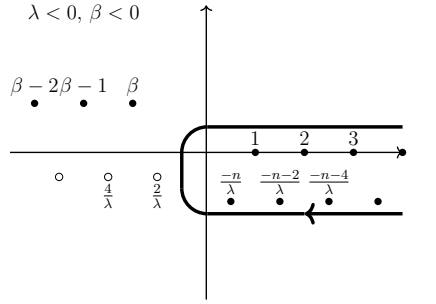

Table 4.2: Overview of the cases considered for the generalized multiquadric. The focus is on the framed case.

The asymptotic behaviour in this case is quite similar to the previous one. Since classical quasi-interpolation requires a singularity of the Fourier transform of the RBF at the origin, we have the requirement that $\tilde{\beta} < \frac{n}{\lambda}$, where $\tilde{\beta} = -\beta$. Furthermore, we assume

the leading-order singularity to be an even power of s, meaning that $n - \lambda\tilde{\beta} \in 2\mathbb{N}$. A direct consequence is that the dimension n has to be greater than or equal to three.

The best case occurs when $\lambda \in 2\mathbb{N}$ with $n - \lambda\tilde{\beta} \in 2\mathbb{N}$. In this situation, only even powers of s appear in the series until a logarithmic term arises. Note that there is no restriction on the parity of the dimension n. Comparing the asymptotic forms, we obtain

$$\begin{aligned}\hat{\varphi}(s) \sim & \sum_{j=0}^{\lceil \frac{n}{\lambda}-\frac{1}{2}\rceil+\lfloor -\tilde{\beta}\rfloor} C_j(c,n,\lambda,\tilde{\beta}) s^{-n+\lambda(j+\tilde{\beta})} + \sum_{j=0}^{\frac{1}{2}\left(-n+\lambda\left(\lceil \frac{n}{\lambda}-\frac{1}{2}\rceil+\frac{1}{2}\right)\right)} \tilde{C}_j(c,n,\lambda,\tilde{\beta}) s^{2j} \\ & + C(c,n,\lambda,\tilde{\beta}) s^{-n+\lambda\left(\lceil \frac{n}{\lambda}-\frac{1}{2}\rceil+\frac{1}{2}\right)} \log(cs) \qquad \text{as } s \to 0_+ \\ & \overset{!}{=} \frac{F(s) + bG_0(s)\log(s)}{G(s)}.\end{aligned}$$

From this, we conclude that

$$\begin{aligned} G(s) &= s^{n-\lambda\tilde{\beta}} \\ F(s) &= \sum_{j=0}^{\lceil \frac{n}{\lambda}-\frac{1}{2}\rceil+\lfloor -\tilde{\beta}\rfloor} C_j(c,n,\lambda,\tilde{\beta}) s^{j\lambda} + \sum_{j=0}^{\frac{1}{2}\left(-n+\lambda\left(\lceil \frac{n}{\lambda}+\frac{1}{2}\rceil-\frac{1}{2}\right)\right)} \tilde{C}_j(c,n,\lambda,\tilde{\beta}) s^{2j+n-\lambda\tilde{\beta}} \\ G_0(s) &= s^{\lambda\left(\lceil \frac{n}{\lambda}-\frac{1}{2}\rceil+\frac{1}{2}-\tilde{\beta}\right)} \\ b &= C(c,n,\lambda,\tilde{\beta}). \end{aligned}$$

To apply Theorem 4.1, we observe that $G_0(s)$ is a polynomial of degree $n_0 = \lambda\left(\lceil \frac{n}{\lambda} - \frac{1}{2}\rceil + \frac{1}{2} - \tilde{\beta}\right)$ and that $b \neq 0$. Furthermore,

(2A) $G(s)$ is a homogeneous polynomial of positive even degree $2m_1 = n - \lambda\tilde{\beta}$ and $G(s) \neq 0$ for all $s > 0$.

(2B) $F(s)$ is a polynomial of degree n_0. Therefore, the Taylor-polynomial is exact with $m_0 = n_0$.

(2C) $\hat{\varphi}(s)$ decays faster than any polynomial grows. Therefore, the integral is finite.

The application of Theorem 4.1 results in

$$|\Psi(x)| \leq C(1 + ||x||)^{-n-\left(\lambda\left(\lceil \frac{n}{\lambda}-\frac{1}{2}\rceil+\frac{1}{2}-\tilde{\beta}\right)\right)},$$

and the polynomial reproduction is limited to polynomials of degree $n - \lambda\tilde{\beta} - 1$, and the error estimate is given by

$$||Q_h[f] - f||_\infty = \begin{cases} \mathcal{O}\left(h^{n-\lambda\tilde{\beta}} \log(1/h)\right) & \text{if } \frac{n}{\lambda} - \frac{1}{2} \in \mathbb{N}, \\ \mathcal{O}\left(h^{n-\lambda\tilde{\beta}}\right) & \text{if } \frac{n}{\lambda} - \frac{1}{2} \notin \mathbb{N}. \end{cases}$$

Notice that this result does not depend on the parity of the dimension n.

A second case is for $\lambda \notin 2\mathbb{N}$. Then the pole located at $t = -\tilde{\beta} - 1$ results in a fractional or irrational power of s. Comparing the asymptotic behaviour with the form given in Theorem 4.1, we get

$$\begin{aligned} \hat{\varphi}(s) &\sim \sum_{j=0}^{1} C_j(c, n, \lambda, \tilde{\beta}) s^{-n+\lambda(j+\tilde{\beta})} + \sum_{j=0}^{\left\lfloor \frac{1}{2}((\tilde{\beta}+1)\lambda - n) \right\rfloor} \tilde{C}_j(c, n, \lambda, \tilde{\beta}) s^{2j} \qquad \text{as } s \to 0_+ \\ &\overset{!}{=} \frac{F(s) + bG_0(s)\log(s)}{G(s)} \end{aligned}$$

from which we conclude that

$$\begin{aligned} G(s) &= s^{n-\lambda\tilde{\beta}} \\ F(s) &= \sum_{j=0}^{1} C_j(c, n, \lambda, \tilde{\beta}) s^{j\lambda} + \sum_{j=0}^{\left\lfloor \frac{1}{2}((\tilde{\beta}+1)\lambda - n) \right\rfloor} \tilde{C}_j(c, n, \lambda, \tilde{\beta}) s^{2j+n-\lambda\tilde{\beta}} \\ G_0(s) &= 0 \\ b &= 0. \end{aligned}$$

Checking the conditions leads to

(2A) G is a homogeneous polynomial of degree $2m_1 = n - \lambda\tilde{\beta}$.

(2B) F is a monomial of degree $n_0 = \lambda$. If $\lambda \notin \mathbb{N}$, then we choose $m_0 = \lfloor \lambda \rfloor$. The Taylor polynomial $\tau_{m_0}(s)$ is identically zero, but the inequality holds with $\theta = \lambda - \lfloor \lambda \rfloor$. If $\lambda \in \mathbb{N}$, then F is a polynomial and the Taylor polynomial is exact with $m_0 = \lambda$.

(2C) In general, we showed that $\hat{\varphi}(s)$ decays for large arguments like $s^{-n-\lambda}$, and the derivatives decay even faster. Therefore the integral in condition remains finite.

With these conditions, we obtain the upper bound for the quasi-Lagrange function

$$|\Psi(x)| \leq C(1 + ||x||)^{-n-\lambda}$$

for some constant C and is capable of reproducing polynomials of degree $\lfloor \lambda \rfloor$. Furthermore, we achieve the error estimate via the Strang and Fix conditions

$$||Q_h[f] - f||_\infty = \begin{cases} \mathcal{O}\left(h^\lambda\right) & \text{if } \lambda \notin \mathbb{N} \\ \mathcal{O}\left(h^\lambda \log(1/h)\right) & \text{if } \lambda \in \mathbb{N}. \end{cases}$$

So far, we have investigated the most relevant cases of quasi-interpolation for this parameter configuration.

Case 3: $\lambda < 0, \beta > 0$

For this case, we notice that condition $(2C)$ from theorem 4.1 is not fulfillable because the decay rate of $\hat{\varphi}(s) \leq Cs^{-n+\tilde{\lambda}\beta}$ is not sufficient to keep the integral finite, see equ. 3.6. Therefore, this case can not be used for quasi-interpolation.

Case 4: $\lambda, \beta < 0$

Parameter configuration	RBF $\varphi(r) = \left(c^\lambda + r^\lambda\right)^\beta$	Contour integral of the Fourier transform $\hat{\varphi}(s)$
$\lambda > 0, \beta > 0$	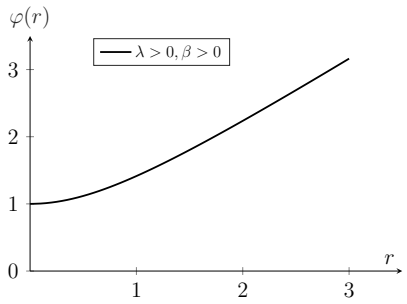	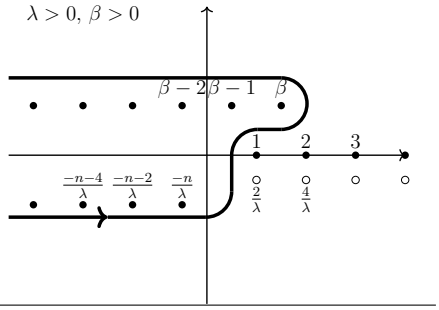
$\lambda > 0, \beta < 0$	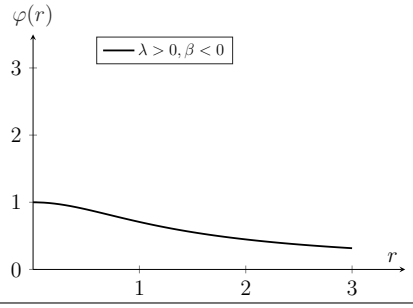	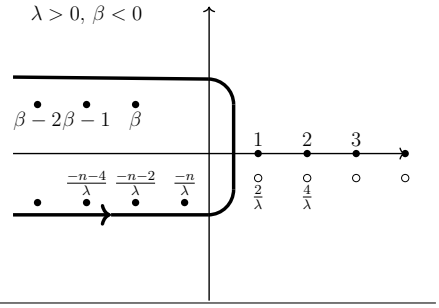
$\lambda < 0, \beta > 0$	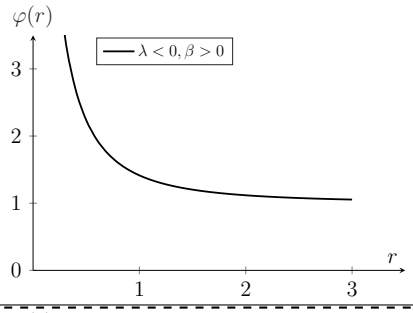	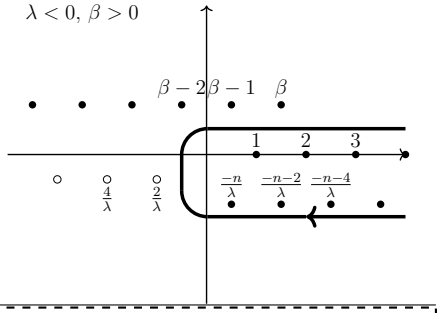
$\lambda < 0, \beta < 0$	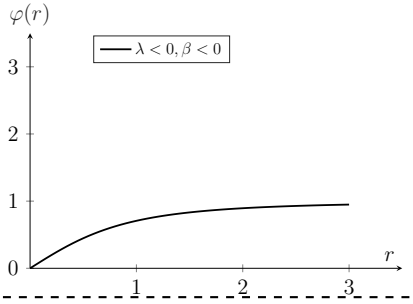	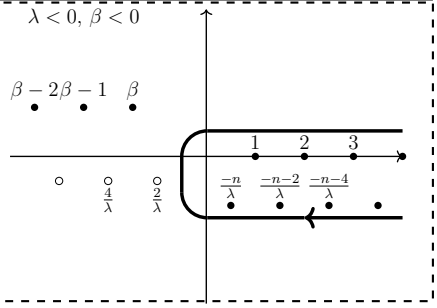

Table 4.3: Overview of the cases considered for the generalized multiquadric. The focus is on the framed case.

As before, we define $\tilde{\lambda} = -\lambda$ and $\tilde{\beta} = -\beta$ to be positive. In chapter 3 we found out that the only way to achieve a singular leading-order near the origin is for $n > \tilde{\lambda}$. Since we aim for an even power of s, we assume that $n - \tilde{\lambda} \in 2\mathbb{N}$. A direct consequence is

that the dimension $n \geq 3$ is required. In both cases (n odd or n even), there appears a double pole, leading to logarithmic terms in the asymptotic behaviour of our RBF near the origin. If n is even, then $\tilde{\lambda}$ is also even and the first double pole is at $t_0 = \left\lceil \frac{n}{\tilde{\lambda}} \right\rceil$. All poles less than t_0 lead to even powers of s such that a finite trigonometric polynomial can handle them. Comparing this with the conditions from theorem 4.1, we get

$$\begin{aligned}\hat{\varphi}(s) \sim & \sum_{j=1}^{\lceil \frac{n}{\tilde{\lambda}} \rceil - 1} C_j(c,n,\tilde{\lambda},\tilde{\beta}) s^{-n+j\tilde{\lambda}} + \sum_{j=0}^{\frac{\tilde{\lambda}}{2}\lceil \frac{n}{\tilde{\lambda}} \rceil} \tilde{C}_j(c,n,\tilde{\lambda},\tilde{\beta}) s^{2j} \\ & + C(c,n,\tilde{\lambda},\tilde{\beta}) s^{-n+\tilde{\lambda}\lceil \frac{n}{\tilde{\lambda}} \rceil} \log(cs) \qquad \text{as } s \to 0_+ \\ & \overset{!}{=} \frac{F(s) + bG_0(s)\log(s)}{G(s)}\end{aligned}$$

from which we conclude that

$$\begin{aligned} G(s) &= s^{n-\tilde{\lambda}}, \\ F(s) &= \sum_{j=0}^{\lceil \frac{n}{\tilde{\lambda}} \rceil} C_j(c,n,\tilde{\lambda},\tilde{\beta}) s^{j\tilde{\lambda}} + \sum_{j=0}^{\frac{\tilde{\lambda}}{2}\lceil \frac{n}{\tilde{\lambda}} \rceil} \tilde{C}_j(c,n,\tilde{\lambda},\tilde{\beta}) s^{2j+n-\tilde{\lambda}}, \\ G_0(s) &= s^{\tilde{\lambda}(\lceil \frac{n}{\tilde{\lambda}} \rceil - 1)}, \\ b &= C(c,n,\tilde{\lambda},\tilde{\beta}). \end{aligned}$$

We see that $G_0(s)$ is a polynomial of degree $n_0 = \tilde{\lambda}\left(\left\lceil \frac{n}{\tilde{\lambda}} \right\rceil - 1\right)$, with $b \neq 0$ and

(2A) $G(s)$ is a polynomial of degree of positive even degree $2m_1 = n - \tilde{\lambda}$.

(2B) F is a polynomial of degree n_0, and for $m_0 = n_0$ the Taylor polynomial is exact.

(2C) The integral of this condition is finite since $\hat{\varphi}(s) \leq Cs^{-n-\tilde{\lambda}\tilde{\beta}}$, and the derivatives decay even faster.

Applying Theorem 4.1 results in the decay rate of the quasi-Lagrange function is

$$|\Psi(x)| \leq C(1 + ||x||)^{-n-\tilde{\lambda}(\lceil \frac{n}{\tilde{\lambda}} \rceil - 1)}$$

and the polynomial reproduction holds for all polynomials of degree $n - \tilde{\lambda} - 1$. With this result, we can apply the Strang and Fix conditions to determine the uniform error

estimate of order $h^{n-\tilde{\lambda}}$ or $h^{n-\tilde{\lambda}}\log(1/h)$, respectively. This fact is mathematically given by

$$||Q_h[f]-f||_\infty = \begin{cases} \mathcal{O}\left(h^{n-\tilde{\lambda}}\log(1/h)\right) & \text{if } n,\tilde{\lambda}\in 2\mathbb{N}, n>\tilde{\lambda}, \left\lceil \frac{n}{\tilde{\lambda}} \right\rceil = \frac{n}{\tilde{\lambda}} \\ \mathcal{O}\left(h^{n-\tilde{\lambda}}\right) & \text{if } n,\tilde{\lambda}\in 2\mathbb{N}, n>\tilde{\lambda}, \left\lceil \frac{n}{\tilde{\lambda}} \right\rceil > \frac{n}{\tilde{\lambda}}. \end{cases}$$

Next, we analyze the case where n is odd. Then we also have to choose $\tilde{\lambda}$ odd. As a consequence, the residue evaluated at $t=2$ contains an odd power of s. Hence, for n odd, we obtain the asymptotic series

$$\begin{aligned} \hat{\varphi}(s) &\sim \sum_{j=0}^{1} C_j(c,n,\lambda,\tilde{\beta}) s^{-n+\lambda(j+1)} + \sum_{j=0}^{\frac{-n+2\tilde{\lambda}-1}{2}} \tilde{C}_j(c,n,\lambda,\tilde{\beta}) s^{2j} \qquad \text{as } s\to 0_+ \\ &\stackrel{!}{=} \frac{F(s)+bG_0(s)\log(s)}{G(s)} \end{aligned}$$

from which we conclude that

$$\begin{aligned} G(s) &= s^{n-\tilde{\lambda}} \\ F(s) &= \sum_{j=0}^{1} C_j(c,n,\tilde{\lambda},\tilde{\beta}) s^{j\lambda} + \sum_{j=0}^{\frac{-n+2\tilde{\lambda}-1}{2}} \tilde{C}_j(c,n,\lambda,\tilde{\beta}) s^{2j+n-\tilde{\lambda}} \\ G_0(s) &= 0 \\ b &= 0. \end{aligned}$$

(2A) $G(s)$ is a polynomial of positive even degree $2m_1 = n-\tilde{\lambda}$ and $G(s)\neq 0$ for all $s>0$

(2B) $F(s)$ is a polynomial of degree $\tilde{\lambda}$, and for $m_0=\tilde{\lambda}$ the Taylor polynomial is exact.

(2C) Again, the integral from this condition is finite for every choice of $\lambda,\beta<0$.

Therefore, we obtain

$$\Psi(x)| \leq C(1+||x||)^{-n-\tilde{\lambda}-1}.$$

The polynomial reproduction rate is given by $\ell_0 = \min\{\tilde{\lambda}, n-\tilde{\lambda}-1\}$. The highest possible order of polynomial reproduction is therefore given for $\tilde{\lambda}=\frac{n-1}{2}$. With these results, we apply the Strang and Fix conditions and end up with a uniform error estimate of order

$h^{\tilde{\lambda}}$ or $h^{\tilde{\lambda}}\log(1/h)$, respectively. This can be expressed as

$$||Q_h[f]-f||_\infty = \begin{cases} \mathcal{O}\left(h^{\tilde{\lambda}+1}\log(1/h)\right) & \text{if } \tilde{\lambda} \leq \frac{n-1}{2} \\ \mathcal{O}\left(h^{n-\tilde{\lambda}}\right) & \text{if } \tilde{\lambda} > \frac{n-1}{2}. \end{cases}$$

A comprehensive overview of the results achieved in this section for the generalized multiquadric is presented in table 4.4. These results are in complete agreement with examples found in the literature, for instance [16, p. 14]. They constitute a significant contribution of this thesis, presenting the findings for the first time in such a general form.

Conditions				Uniform error estimate
Case 1: $\lambda > 0, \beta > 0$				
$\lambda \in 2+4\mathbb{N}$	$\beta \in \frac{1}{2}+\mathbb{N}$	$n \in 1+2\mathbb{N}$	$\frac{n}{\lambda}-\frac{1}{2} \in \mathbb{N}$	$\mathcal{O}\left(h^{n+\lambda\beta}\log(1/h)\right)$
$\lambda \in 2+4\mathbb{N}$	$\beta \in \frac{1}{2}+\mathbb{N}$	$n \in 1+2\mathbb{N}$	$\frac{n}{\lambda}-\frac{1}{2} \notin \mathbb{N}$	$\mathcal{O}\left(h^{n+\lambda\beta}\right)$
$\lambda \in \mathbb{N}$	$\beta \notin \mathbb{N}, \beta > 0$	$n \in 1+2\mathbb{N}$	$\lambda\beta \in 1+2\mathbb{N}$	$\mathcal{O}\left(h^{\lambda}\log(1/h)\right)$
$\lambda \notin \mathbb{N}, \lambda > 0$	$\beta \notin \mathbb{N}, \beta > 0$	$n \in 1+2\mathbb{N}$	$\lambda\beta \in 1+2\mathbb{N}$	$\mathcal{O}\left(h^{\lambda}\right)$
Case 2: $\lambda > 0, \beta < 0$				
$\lambda \in 2\mathbb{N}$	$n > \lambda\tilde{\beta}$	$n-\lambda\tilde{\beta} \in 2\mathbb{N}$	$\frac{n}{\lambda}-\frac{1}{2} \in \mathbb{N}$	$\mathcal{O}\left(h^{n-\lambda\tilde{\beta}}\log(1/h)\right)$
$\lambda \in 2\mathbb{N}$	$n > \lambda\tilde{\beta}$	$n-\lambda\tilde{\beta} \in 2\mathbb{N}$	$\frac{n}{\lambda}-\frac{1}{2} \notin \mathbb{N}$	$\mathcal{O}\left(h^{n-\lambda\tilde{\beta}}\right)$
$\lambda \notin 2\mathbb{N}$	$n > \lambda\tilde{\beta}$	$n-\lambda\tilde{\beta} \in 2\mathbb{N}$	$\lambda \notin \mathbb{N}$	$\mathcal{O}\left(h^{\lambda}\right)$
$\lambda \notin 2\mathbb{N}$	$n > \lambda\tilde{\beta}$	$n-\lambda\tilde{\beta} \in 2\mathbb{N}$	$\lambda \in \mathbb{N}$	$\mathcal{O}\left(h^{\lambda}\log(1/h)\right)$
Case 4: $\lambda < 0, \beta < 0$				
$\tilde{\lambda} \in 2\mathbb{N}$	$n > \tilde{\lambda}$	$n \in 2\mathbb{N}$	$\frac{n}{\tilde{\lambda}} \in \mathbb{N}$	$\mathcal{O}\left(h^{n-\tilde{\lambda}}\log(1/h)\right)$
$\tilde{\lambda} \in 2\mathbb{N}$	$n > \tilde{\lambda}$	$n \in 2\mathbb{N}$	$\frac{n}{\tilde{\lambda}} \notin \mathbb{N}$	$\mathcal{O}\left(h^{n-\tilde{\lambda}}\right)$
$\tilde{\lambda} \in 1+2\mathbb{N}$	$n > \tilde{\lambda}$	$n \in 1+2\mathbb{N}$	$\tilde{\lambda} \leq \frac{n-1}{2}$	$\mathcal{O}\left(h^{\tilde{\lambda}+1}\log(1/h)\right)$
$\tilde{\lambda} \in 1+2\mathbb{N}$	$n > \tilde{\lambda}$	$n \in 1+2\mathbb{N}$	$\tilde{\lambda} > \frac{n-1}{2}$	$\mathcal{O}\left(h^{n-\tilde{\lambda}}\right)$

Table 4.4: A comprehensive overview of the results achieved for the generalized multiquadric.

4.1.2 Generalized Thin Plate Spline

In chapter 3.2.2 we showed that the only usable case for quasi-interpolation is the first one, when $\lambda, \beta > 0$. Hence, we will determine the approximation order for some possible choices of the parameters λ and β.

Case 1: $\lambda, \beta > 0$

Parameter configuration	RBF $\varphi(r) = \left(c^\lambda + r^\lambda\right) \log\left(c^\beta + r^\beta\right)$	Contour integral of the Fourier transform $\hat{\varphi}_4(s)$
$\lambda > 0, \beta > 0$	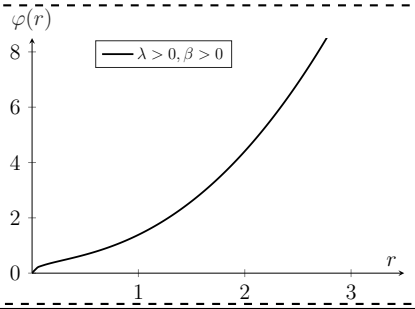	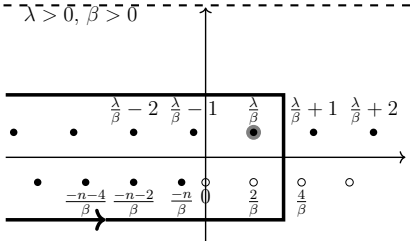
$\lambda < 0, \beta > 0$	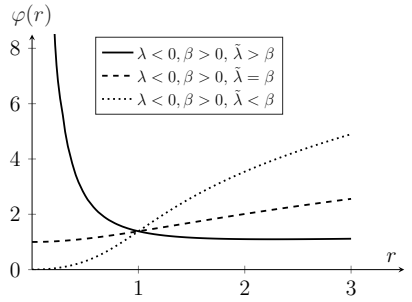	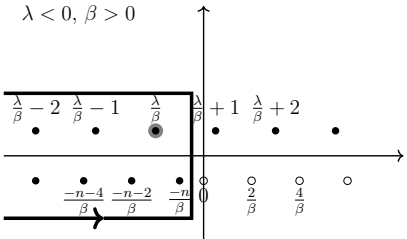
$\lambda > 0, \beta < 0$	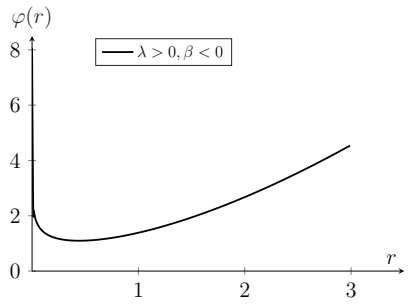	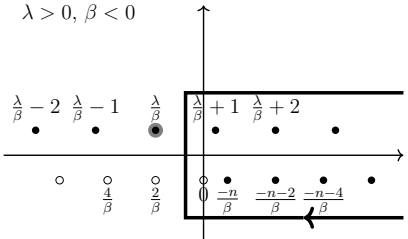
$\lambda < 0, \beta < 0$	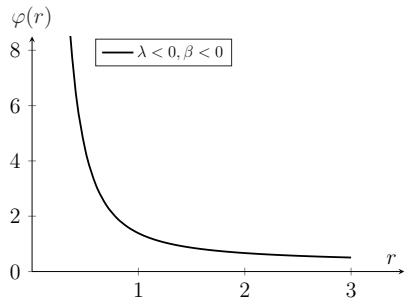	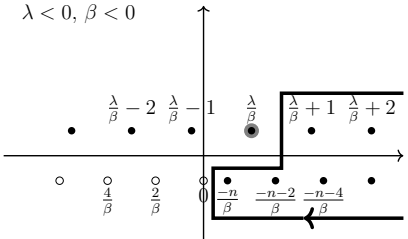

Table 4.5: Overview of the cases considered for the generalized thin plate spline. The focus is on the framed case.

This is the only case where the RBF itself is not singular and can be used directly. In the last chapter, we found out that classical quasi-interpolation is possible if $n, \lambda \in 2\mathbb{N}$. The best results are achievable if $\beta \in 2\mathbb{N}$. We found in equ. (3.8) and (3.9) that the asymptotic series contains only even powers of s until the first logarithmic term appears. This logarithmic term is multiplied by some positive power of s. The form of the asymptotic series is given by

$$\begin{aligned}\hat{\varphi}(s) &\sim \sum_{j=0}^{\frac{n+\lambda+d_0}{2}} C_j(c,n,\lambda,\beta)s^{-n-\lambda+2j} + \hat{C}_1(c,n,\lambda,\beta)s^{d_0}\log\left(\frac{cs}{2}\right), \qquad \text{as } s \to 0_+ \\ &\overset{!}{=} \frac{F(s) + bG_0(s)\log(s)}{G(s)},\end{aligned}$$

where $d_0 = \min\left\{-n+\beta\left\lceil\frac{n}{\beta}\right\rceil, -n-\lambda+\beta\left\lceil\frac{n+\lambda}{\beta}\right\rceil\right\} \geq 0$. Comparing this asymptotic behaviour with Theorem 4.1, we see that $G_0(s)$ is a polynomial of degree $n_0 = n+\lambda+d_0$ and $b \neq 0$. Furthermore, we get

(2A) G is a homogeneous polynomial of positive even degree $2m_1 = n+\lambda$, which has all zeros at the origin.

(2B) F is a polynomial of degree n_0. Therefore, it is $C^\infty(\mathbb{R}_+)$ and the Taylor-polynomial is exact with $m_0 = n_0$.

(2C) For this special case, the Fourier transform decays faster then any polynomial grows, and the same applies to the derivative. Hence, the integral stated above stays finite.

We conclude that there exist finitely many coefficients such that

$$|\Psi(x)| \leq C(1+||x||)^{-2n-\lambda-d_0}.$$

Furthermore, the quasi-interpolation operator reproduces all polynomials of degree $n+\lambda-1$. With all necessary components now established, the Strang and Fix conditions can be applied, leading to the following uniform error estimate

$$||Q_h[f]-f||_\infty = \begin{cases}\mathcal{O}\left(h^{n+\lambda}\log(1/h)\right) & \text{if } d_0 = 0, \\ \mathcal{O}\left(h^{n+\lambda}\right) & \text{if } d_0 > 0.\end{cases}$$

Next, we determine the approximation order if $\lambda \in 2\mathbb{N}$ but $\beta \notin 2\mathbb{N}$. In this case, the

asymptotic series is of the form

$$\hat{\varphi}(s) \sim \sum_{j=0}^{\frac{n+\lambda}{2}+\lfloor\frac{\beta}{2}\rfloor} C_j(c,n,\lambda,\beta)s^{-n-\lambda+2j} + \hat{C}_1(c,n,\lambda,\beta)s^{-n-\lambda+\beta} \qquad \text{as } s \to 0_+$$
$$\stackrel{!}{=} \frac{F(s) + bG_0(s)\log(s)}{G(s)}.$$

Comparing this with the requirements from Theorem 4.1, we see that $b = 0$, and therefore G_0 is irrelevant. Furthermore,

(2A) $G(s)$ is a homogeneous polynomial of positive even degree $2m_1 = n + \lambda$, which has all zeros at the origin.

(2B) $F(s)$ is not necessarily a polynomial but with $m_0 = \lfloor\beta\rfloor$ and $\theta = m_0 - \lfloor\beta\rfloor$, the required inequality holds.

(2C) The decay rate is given by $s^{-n-\beta}$ and all derivatives decay even faster. Therefore, the integral given above is finite.

Under these conditions, theorem 4.1 guarantees the existence of finitely many coefficients such that

$$|\Psi(x)| \leq C(1 + ||x||)^{-n-\beta}.$$

Furthermore, the quasi-interpolation operator reproduces all polynomials of degree $\min\{\lfloor\beta\rfloor, n + \lambda - 1\}$. With all necessary components now established, the Strang and Fix conditions can be applied, yielding to the following uniform error estimate

$$||Q_h[f] - f||_\infty = \begin{cases} \mathcal{O}\left(h^\beta\right) & \text{if } \lfloor\beta\rfloor < n + \lambda - 1, \\ \mathcal{O}\left(h^\beta \log(1/h)\right) & \text{if } \lfloor\beta\rfloor = n + \lambda - 1, \\ \mathcal{O}\left(h^{n+\lambda}\right) & \text{if } \lfloor\beta\rfloor > n + \lambda - 1. \end{cases}$$

The comprehensive overview of the results obtained in this section for the generalized thin plate spline are presented in table 4.6.

Conditions				Uniform error estimate
$\lambda \in 2\mathbb{N}$	$\beta \in 2\mathbb{N}$	$n \in 2\mathbb{N}$	$d_0 = 0$	$\mathcal{O}\left(h^{n+\lambda}\log(1/h)\right)$
$\lambda \in 2\mathbb{N}$	$\beta \in 2\mathbb{N}$	$n \in 2\mathbb{N}$	$d_0 > 0$	$\mathcal{O}\left(h^{n+\lambda}\right)$
$\lambda \in 2\mathbb{N}$	$\beta \notin 2\mathbb{N}$	$n \in 2\mathbb{N}$	$\beta < n+\lambda$	$\mathcal{O}\left(h^{\beta}\right)$
$\lambda \in 2\mathbb{N}$	$\beta \notin 2\mathbb{N}$	$n \in 2\mathbb{N}$	$\beta = n+\lambda$	$\mathcal{O}\left(h^{\beta}\log(1/h)\right)$
$\lambda \in 2\mathbb{N}$	$\beta \notin 2\mathbb{N}$	$n \in 2\mathbb{N}$	$\beta > n+\lambda$	$\mathcal{O}\left(h^{n+\lambda}\right)$

Table 4.6: A comprehensive overview of the results achieved for the generalized thin plate spline. Here, $d_0 = \min\left\{-n+\beta\left\lceil\frac{n}{\beta}\right\rceil, -n-\lambda+\beta\left\lceil\frac{n+\lambda}{\beta}\right\rceil\right\} \geq 0$.

4.2 Quasi-Interpolation of non-RBFs

Apart from quasi-interpolation using RBFs, which offers a constructive method for constructing the approximant, there exist other, more sophisticated approaches. Bessel functions offer numerous identities, including summation formulas that are structurally similar to those arising in the quasi-Lagrange operator. Bessel functions are also employed as kernels in classical RBF interpolation, even in cases where they are not positive definite [24]. Additionally, the von Neumann series plays a noteworthy role in function approximation.

Numerical experiments indicate that the Bessel function of the first kind is a suitable candidate as a quasi-Lagrange function. Summation over the index of the Bessel function reproduce polynomials of degree two. For $x \in \mathbb{R}$, we have found numerical evidence that

$$\begin{aligned}\sum_{j\in\mathbb{Z}} J_j(x) &= 1,\\ \sum_{j\in\mathbb{Z}} jJ_j(x) &= x,\\ \sum_{j\in\mathbb{Z}} j^2J_j(x) &= x^2.\end{aligned}$$

We will prove these claims later. While the first relation is widely known, the remaining two are less prominent. To the best of our knowledge, these relations have not been previously considered in the context of quasi-interpolation. For this reason, we propose using Bessel functions as our quasi-Lagrange functions, setting $\Psi_j(x) = J_j(x)$. For integer values of j the Bessel functions provide some useful symmetry properties

$$\begin{aligned}J_{-j}(x) &= (-1)^j J_j(x),\\ J_j(-x) &= J_{-j}(x).\end{aligned}$$

Consequently, many terms in the aforementioned sums cancel out. The behaviour of the Bessel function for large j and $x > 0$ is given by

$$J_j(x) \sim \frac{1}{\Gamma(j+1)} \left(\frac{x}{2}\right)^j \qquad \text{as } j \in \mathbb{Z}, j \to \infty$$
$$J_j(x) \sim \frac{(-1)^j}{\Gamma(-j+1)} \left(\frac{2}{x}\right)^j \qquad \text{as } j \in \mathbb{Z}, j \to -\infty.$$

The behaviour for $x < 0$ can be figured out using the above identities. For $x = 0$ we have

$$J_0(0) = 1, \tag{4.3}$$
$$J_j(0) = 0, \qquad \forall j \in \mathbb{Z}\backslash\{0\}. \tag{4.4}$$

In all cases, the above sums are absolutely convergent for polynomials of any degree. Note that the equ. (4.3) and (4.4) can also be written as $J_j(0) = \delta_{j,0}$ and therefore, the quasi-Lagrange operator will interpolate every function at $x = 0$. For an integer j the Bessel function has the integral representation

$$J_j(x) = \frac{1}{2\pi} \int_{-\pi}^{\pi} \mathrm{e}^{\mathrm{i}(j\tau - x\sin(\tau))} \mathrm{d}\tau.$$

With these identities, we now prove that the Bessel function, when used as a quasi-Lagrange function, reproduces polynomials of degree two. For $k \in \mathbb{N}$ we find

$$\begin{aligned}
\sum_{j\in\mathbb{Z}} j^k J_j(x) &= \sum_{j\in\mathbb{Z}} j^k \frac{1}{2\pi} \int_{-\pi}^{\pi} \mathrm{e}^{\mathrm{i}(j\tau - x\sin(\tau))} \mathrm{d}\tau \\
&= \frac{1}{2\pi} \int_{-\pi}^{\pi} \mathrm{e}^{-\mathrm{i}x\sin(\tau)} \sum_{j\in\mathbb{Z}} j^k \mathrm{e}^{\mathrm{i}j\tau} \mathrm{d}\tau \\
&= \frac{1}{2\pi} \int_{-\pi}^{\pi} \mathrm{e}^{-\mathrm{i}x\sin(\tau)} \sum_{j\in\mathbb{Z}} \frac{\mathrm{d}^k}{\mathrm{d}\tau^k} (-\mathrm{i})^k \mathrm{e}^{\mathrm{i}j\tau} \mathrm{d}\tau \\
&= \frac{(-\mathrm{i})^k}{2\pi} \int_{-\pi}^{\pi} \mathrm{e}^{-\mathrm{i}x\sin(\tau)} \frac{\mathrm{d}^k}{\mathrm{d}\tau^k} \underbrace{\sum_{j\in\mathbb{Z}} \mathrm{e}^{\mathrm{i}j\tau}}_{2\pi\Delta_{2\pi}(\tau)} \mathrm{d}\tau,
\end{aligned} \tag{4.5}$$

where $\Delta_{2\pi}(\tau)$ denotes the Dirac comp with period 2π. Since $\tau \in [-\pi, \pi]$, we can reduce the Dirac comp to the Dirac delta distribution. The sum $\sum_{j\in\mathbb{Z}} \mathrm{e}^{ij\tau}$ does not converge in a classical sense but can be interpreted as a functional in the sense that is explained in equation (4.7) and (4.8).

Integration by parts leads to

$$\begin{aligned}\sum_{j\in\mathbb{Z}} j^k J_j(x) &= \mathrm{i}^k \int_{-\pi}^{\pi} \delta(\tau) \frac{\mathrm{d}^k}{\mathrm{d}\tau^k} \mathrm{e}^{-\mathrm{i}x\sin(\tau)} \mathrm{d}\tau \\ &= \mathrm{i}^k \frac{\mathrm{d}^k}{\mathrm{d}\tau^k} \mathrm{e}^{-\mathrm{i}x\sin(\tau)} \Big|_{\tau=0}. \end{aligned} \tag{4.6}$$

The evaluation of the sum is now reduced to the calculation of the kth derivative of two chained functions. In equ. (4.5) we used a series representation of the Dirac delta distribution. This is justified by the relations

$$\lim_{n\to\infty} \int_{-\pi}^{\pi} \delta_n(x) f(x) \mathrm{d}x = f(0), \tag{4.7}$$

where

$$\delta_n(x) = \frac{1}{2\pi} \sum_{j=-n}^{n} \mathrm{e}^{\mathrm{i}jx}. \tag{4.8}$$

Further details and related identities concerning the representation of the Dirac delta distribution can be found in [1]. For the proof of the approximation order, we require equ. (4.6) in an explicit form. The kth derivative of a composition of two k-times differentiable functions f and g can be expressed using Faà di Bruno's formula

$$\frac{\mathrm{d}^k}{\mathrm{d}\tau^k} f\left(g(\tau)\right) = \sum \frac{k!}{m_1! m_2! \cdots m_k!} f^{(m_1+\cdots+m_k)}\left(g(\tau)\right) \cdot \prod_{\ell=1}^{k} \left(\frac{g^{(\ell)}(\tau)}{\ell!} \right)^{m_\ell},$$

where the sum is over all non-negative integer tuples $(m_1, \ldots, m_k)$ in conjunction with the constraint $1m_1 + 2m_2 + 3m_3 + \cdots + km_k = k$, [46, p. 85]. Applying this formula with $f(y) = \mathrm{e}^y$ and $g(\tau) = -\mathrm{i}x\sin(\tau)$, we obtain

$$\sum_{j\in\mathbb{Z}} j^k J_j(x) = \mathrm{i}^k \sum \frac{k!}{m_1! m_2! \cdots m_k!} (-\mathrm{i})^{m_1+\cdots+m_k} \mathrm{e}^{-\mathrm{i}x\sin(\tau)} \cdot \prod_{\ell=1}^{k} \left(\frac{x \frac{\partial^\ell}{\partial\tau^\ell} \sin(\tau)}{\ell!} \right)^{m_\ell} \Bigg|_{\tau=0}.$$

Next, we set τ to zero. If ℓ is even, then the ℓth derivative of $\sin(\tau)$ evaluated at zero is zero. Since any zero term causes the entire product to vanish, the only way for a summand to remain non-zero is if $m_\ell = 0$ for all $\ell \in 2\mathbb{N}$. We define $\tilde{k}$ to be the largest odd integer less than or equal to k and $\hat{k}$ be the largest even integer less than or equal to k. From this, it follows that

$$2m_2 + 4m_4 + \cdots + \hat{k}m_{\hat{k}} = 0,$$

which implies all $m_\ell = 0$ for even ℓ. Therefore, the sum runs only over non-negative integer tuples $(m_1, m_3 \ldots, m_{\tilde{k}})$ satisfying the constraint

$$1m_1 + 3m_3 + \cdots + \tilde{k}m_{\tilde{k}} = k.$$

With these results, we obtain

$$\sum_{j\in\mathbb{Z}} j^k J_j(x) = \sum \mathrm{i}^{k+3(m_1+m_3+\ldots m_{\tilde{k}})}(-1)^{m_3+m_7+\cdots+m_k} \frac{k!}{m_1!m_3!\cdots m_{\tilde{k}}!} \prod_{\ell=1}^{k} \left(\frac{x}{\ell!}\right)^{m_\ell}.$$

Next, we analyze the interaction between the imaginary unit and the minus signs. To do so, we write

$$\begin{aligned}\mathrm{i}^{k+3(m_1+m_3+\ldots m_{\tilde{k}})}(-1)^{m_3+m_7+\cdots+m_k} &= \mathrm{i}^{k+3(m_1+m_3+\ldots m_{\tilde{k}})+2(m_3+m_7+\cdots+m_k)} \\ &= \mathrm{i}^{k+3\left(m_1+\sum_{p=1}^{\frac{\tilde{k}-1}{2}} m_{2p+1}\right)+2\sum_{p=1}^{\left\lfloor\frac{k+1}{4}\right\rfloor} m_{4p-1}}\end{aligned}$$

and subsequently focus only on the exponent. Using the relation $m_1+3m_3+\cdots+\tilde{k}m_{\tilde{k}} = k$ for m_1, we get

$$\begin{aligned}&k + 3\left(m_1 + \sum_{p=1}^{\frac{\tilde{k}-1}{2}} m_{2p+1}\right) + 2\sum_{p=1}^{\left\lfloor\frac{k+1}{4}\right\rfloor} m_{4p-1} \\ =&4k + 3\left(-\sum_{p=1}^{\frac{\tilde{k}-1}{2}}(2p+1)m_{2p+1} + \sum_{p=1}^{\frac{\tilde{k}-1}{2}} m_{2p+1}\right) + 2\sum_{p=1}^{\left\lfloor\frac{k+1}{4}\right\rfloor} m_{4p-1} \\ =&4k - 3\sum_{p=1}^{\frac{\tilde{k}-1}{2}} 2p\, m_{2p+1} + 2\sum_{p=1}^{\left\lfloor\frac{k+1}{4}\right\rfloor} m_{4p-1}\end{aligned}$$

$$
\begin{aligned}
=&4k - 3 \sum_{p=1}^{\lfloor \frac{k+1}{4} \rfloor} 4p\, m_{4p+1} - 3 \sum_{p=1}^{\lfloor \frac{k+1}{4} \rfloor} (4p-2)\, m_{4p-1} + 2 \sum_{p=1}^{\lfloor \frac{k+1}{4} \rfloor} m_{4p-1} \\
=&4k - 3 \sum_{p=1}^{\lfloor \frac{k+1}{4} \rfloor} 4p\, m_{4p+1} - \sum_{p=1}^{\lfloor \frac{k+1}{4} \rfloor} (12p-4)\, m_{4p-1} \\
=&4 \left(k - 3 \sum_{p=1}^{\lfloor \frac{k+1}{4} \rfloor} p\, m_{4p+1} - \sum_{p=1}^{\lfloor \frac{k+1}{4} \rfloor} (3p-1)\, m_{4p-1} \right).
\end{aligned}
$$

Since all m_k and the index p are positive integers, we have shown that the exponent is an integer multiple of four. As $\mathrm{i}^4 = 1$, it follows that i raised to this exponent equals one. Consequently, all signs and powers of the imaginary unit cancel out, yielding

$$
\sum_{j\in\mathbb{Z}} j^k J_j(x) = \sum_{m_1, m_3, \ldots, m_{\tilde{k}}} \frac{k!}{m_1! m_3! \cdots m_{\tilde{k}}!} \prod_{\ell=1}^{k} \left(\frac{x}{\ell!} \right)^{m_\ell}, \tag{4.9}
$$

with the conditions

$$
\begin{aligned}
0 &= m_\ell, \qquad \ell \in 2\mathbb{N} \\
k &= m_1 + 3m_3 + \cdots + \tilde{k} m_{\tilde{k}}.
\end{aligned}
$$

The evaluations of equ. (4.9) for the first few values of k are given in table 4.7.

k	$\sum_{j\in\mathbb{Z}} j^k J_j(x)$
0	1
1	x
2	x^2
3	$x + x^3$
4	$4x^2 + x^4$
5	$x + 10x^3 + x^5$
6	$16x^2 + 20x^4 + x^6$

Table 4.7: Evaluation of the first six polynomials generated by equ. (4.9).

Note that for every $k \in \mathbb{N}$, the polynomial has only positive coefficients, and these polynomials are not orthogonal with respect to any inner product. This can be demonstrated using the recurrence relations that characterize orthogonal polynomials, [1].

Higher-degree monomials can be represented as linear combinations of the preceding polynomials. This is illustrated in Table 4.8

Monomial	$\sum_{j\in\mathbb{Z}} j^k J_j(x)$
1	$\sum_{j\in\mathbb{Z}} J_j(x)$
x	$\sum_{j\in\mathbb{Z}} jJ_j(x)$
x^2	$\sum_{j\in\mathbb{Z}} j^2 J_j(x)$
x^3	$\sum_{j\in\mathbb{Z}} (j^3 - j) J_j(x)$
x^4	$\sum_{j\in\mathbb{Z}} (j^4 - 4j^2) J_j(x)$
x^5	$\sum_{j\in\mathbb{Z}} (j^5 - 10j^3 + 9j) J_j(x)$
x^6	$\sum_{j\in\mathbb{Z}} (j^6 - 20j^4 + 64j^2) J_j(x)$

Table 4.8: Linear combinations for higher order monomials.

This enables the definition of more complex linear operators capable of reproducing higher-degree polynomials. We will not explore this topic further. Instead, we focus on modifying the quasi-Lagrange function to achieve higher polynomial reproduction.

Knowing the polynomial reproduction properties of the Bessel functions, we use them as our quasi-Lagrange functions and determine the approximation order of the quasi-Lagrange operator

$$Q_h[f] = \sum_{j\in\mathbb{Z}} f(jh) J_j\left(\frac{x}{h}\right).$$

To this end, we assume f is an analytic function with bounded derivatives. We define

$$p(y) = f(x) + f'(x)(y-x) + \frac{f''(x)}{2}(y-x)^2$$

as a polynomial of degree two. Note that the quasi-Lagrange operator will reproduce this special polynomial, hence

$$p(y) = \sum_{j\in\mathbb{Z}} p(jh) J_j\left(\frac{y}{h}\right).$$

For the special case $y = x$, we have

$$p(x) = \sum_{j\in\mathbb{Z}} p(jh) J_j\left(\frac{x}{h}\right) = f(x).$$

The function f is analytic and therefore, we can write f through the Taylor series evaluated at the point x and get

$$f(y) - p(y) = \sum_{k=3}^{\infty} \frac{f^{(k)}(x)}{k!}(y-x)^k.$$

With these identities we determine the approximation order

$$\begin{aligned} Q_h[f](x) - f(x) &= \sum_{j\in\mathbb{Z}} \left(f(jh) - p(jh)\right) J_j\left(\frac{x}{h}\right) \\ &= \sum_{j\in\mathbb{Z}} \sum_{k=3}^{\infty} \frac{f^{(k)}(x)}{k!} (jh-x)^k J_j\left(\frac{x}{h}\right), \end{aligned}$$

using the binomial theorem results in

$$= \sum_{j\in\mathbb{Z}} \sum_{k=3}^{\infty} \frac{f^{(k)}(x)}{k!} \sum_{\ell=0}^{k} \frac{k!}{\ell!(k-\ell)!} (-x)^{k-\ell} (jh)^{\ell} J_j\left(\frac{x}{h}\right).$$

Interchanging the order of summation and using the summation formula for the Bessel function results in

$$= \sum_{k=3}^{\infty} f^{(k)}(x) \sum_{\ell=0}^{k} \frac{(-x)^{k-\ell} h^{\ell}}{\ell!(k-\ell)!} \sum_{m_1, m_3, \ldots, m_{\tilde{\ell}}} \frac{\ell!}{m_1! m_3! \cdots m_{\tilde{\ell}}!} \cdot \prod_{j=1}^{\ell} \left(\frac{x}{j!h}\right)^{m_j},$$

where again $m_1 + 3m_3 + \cdots + \tilde{\ell} m_{\tilde{\ell}} = \ell$ and $m_2, m_4, \ldots, m_{\hat{\ell}} = 0$. Here, $\tilde{\ell}$ denotes the largest odd integer less than or equal to ℓ and $\hat{\ell}$ the largest even integer less than or equal to ℓ. The lowest order in h ($\mathcal{O}(h^0)$) appears if and only if $m_1 = \ell$. The summation condition ensures that only positive and even powers of h are obtained. The next order is then $\mathcal{O}(h^2)$, corresponding to $m_1 = \ell - 3, m_3 = 1$. This implies that $\ell \geq 3$. All subsequent terms appear at order $\mathcal{O}(h^4)$ or higher, occurring only for $\ell \geq 5$. Many terms arise only for sufficiently large ℓ. To handle these terms, we introduce the Heaviside step function as

$$\Theta(x) = \begin{cases} 1, & x \geq 0 \\ 0, & x < 0. \end{cases}$$

Evaluating the first terms of the sum results in

$$\begin{aligned} Q_h[f](x) - f(x) &= \sum_{k=3}^{\infty} f^{(k)}(x) \sum_{\ell=0}^{k} \frac{(-x)^{k-\ell} h^{\ell}}{(k-\ell)!} \left(\frac{x^{\ell}}{\ell! h^{\ell}} + \frac{x^{\ell-2}\Theta(\ell-3)}{(\ell-3)!3! h^{\ell-2}} + \Theta(\ell-5)\mathcal{O}(h^{4-\ell}) \right) \\ &= \sum_{k=3}^{\infty} f^{(k)}(x) \sum_{\ell=0}^{k} \frac{(-x)^{k-\ell}}{(k-\ell)!} \left(\frac{x^{\ell}}{\ell!} + \frac{x^{\ell-2} h^2 \Theta(\ell-3)}{(\ell-3)!3!} + \Theta(\ell-5)\mathcal{O}(h^4) \right). \end{aligned} \tag{4.10}$$

We now consider the first term

$$\sum_{\ell=0}^{k} \frac{(-x)^{k-\ell}}{(k-\ell)!}\frac{x^\ell}{\ell!} = \frac{(-x)^k}{k!}\sum_{\ell=0}^{k}\frac{(-1)^\ell k!}{\ell!(k-\ell)!}$$
$$= \frac{(-x)^k}{k!}\sum_{\ell=0}^{k}(-1)^\ell\binom{k}{\ell} = 0. \tag{4.11}$$

Since $k > 0$, the sum over alternating binomial coefficients is zero, and the first order $\mathcal{O}(h^0)$ cancels out. Next, we consider the second order:

$$\begin{aligned}\sum_{\ell=0}^{k} \frac{(-x)^{k-\ell}}{(k-\ell)!}\frac{x^{\ell-2}h^2\Theta(\ell-3)}{(\ell-3)!3!} &= \frac{(-x)^{k-2}h^2}{3!}\sum_{\ell=3}^{k}\frac{(-1)^\ell}{(k-\ell)!(\ell-3)!}\\ &= \frac{(-1)^{k-3}x^{k-2}h^2}{3!(k-3)!}\sum_{\ell=0}^{k-3}\frac{(-1)^\ell(k-3)!}{(k-\ell-3)!\ell!}\\ &= \frac{(-1)^{k-3}x^{k-2}h^2}{3!(k-3)!}\underbrace{\sum_{\ell=0}^{k-3}(-1)^\ell\binom{k-3}{\ell}}_{=\delta_{k,3}}\\ &= \frac{xh^2}{3!}\delta_{k,3}.\end{aligned}$$

Substituting the results back into equ. (4.10) results in the approximation order of $\mathcal{O}(h^2)$ or more precisely

$$Q_h[f](x) - f(x) = \frac{f^{(3)}(x)}{3!}xh^2 + \mathcal{O}(h^4). \tag{4.12}$$

Note that our quasi-Lagrange operator converges quadratically but not uniformly to the function f. At $x = 0$, the error is zero, meaning that we interpolate exactly there, but the error increases as $|x|$ grows.

This discovery gives rise to several natural questions:

1. Can we modify the Bessel function such that we achieve a higher polynomial reproduction and approximation order?

2. How can this be extended for scattered data?

3. Can uniform convergence be achieved in place of pointwise convergence?

4. Can this approach be extended to higher dimensions?

The answers to these questions are affirmative, and in the subsequent subsections, we will rigorously explore the procedures through which this can be achieved.

4.2.1 Enhanced Approximation Order

Instead of utilizing the Bessel function as the quasi-Lagrange function, we now modify the integral representation in the following manner

$$\Psi_j(x) = \frac{1}{2\pi}\int_{-\pi}^{\pi} \mathrm{e}^{\mathrm{i}(j\tau - x g(\tau))}\mathrm{d}\tau, \qquad j \in \mathbb{N},$$

for some function g which needs to be determined. For $g(\tau) = \sin(\tau)$, this corresponds to the definition of the Bessel function. With the assumption that Ψ_j decays sufficiently fast (a condition we will verify later), we obtain an expression analogous to equ. (4.6)

$$\sum_{j\in\mathbb{Z}} j^k \Psi_j(x) = \mathrm{i}^k \frac{\mathrm{d}^k}{\mathrm{d}\tau^k} \mathrm{e}^{-\mathrm{i}x g(\tau)}\Big|_{\tau=0}, \qquad k \in \mathbb{N}. \tag{4.13}$$

To determine the conditions on the function g for polynomial reproduction, we examine the first derivative ($k = 1$)

$$x \overset{!}{=} x\mathrm{e}^{-\mathrm{i}x g(\tau)} g^{(1)}(\tau).$$

From this, we can immediately deduce that $g(0) = 0$, and $g^{(1)}(0) = 1$. If we differentiate the right-hand side of this equation, we obtain only monomials, as every higher derivative of $g(\tau)$ vanishes at $\tau = 0$. This result is summarized in table 4.9.

Order of polynomial reproduction	Accumulated conditions
0	$g(0) = 0$
1	$g^{(1)}(0) = 1$
2	$g^{(2)}(0) = 0$
3	$g^{(3)}(0) = 0$
$\vdots$	$\vdots$
k	$g^{(k)}(0) = 0$

Table 4.9: Conditions the function $g(\tau)$ from equ. (4.13) must fulfill in order to achieve the desired polynomial reproduction, under the assumption that the sum converges.

The conditions are essential to ensure that the function $g(\tau)$ satisfies the required properties for polynomial reproduction. However, the convergence of the sum has to be

rigorously established to ensure that the series is well-defined and that the desired results hold consistently. This requirement, does not always hold. A clear illustration of this phenomenon is provided by the trivial solution $g(\tau) = \tau$. In this case the conditions are satisfied for polynomials of any degree. However, the quasi-Lagrange function can be evaluated exactly as $\Psi_j(x) = 2\pi \operatorname{sinc}(j - x) = \frac{2\sin(\pi(j-x))}{j-x}$, which decays so slowly that it is only capable of reproducing constants.

From this example, we observe that the function g influences the decay rate of the quasi-Lagrange function. Therefore, we aim to identify the specific properties of g that govern this decay behavior.

The integral representation of the quasi-Lagrange function can be interpreted as the j-th Fourier coefficient of a 2π-periodic function $\mathrm{e}^{ixg(\tau)}$. The decay rate is therefore closely linked to the Fourier series of $\mathrm{e}^{ixg(\tau)}$, where the decay rate is governed by the properties of $g(\tau)$. If $g(\tau)$ is not 2π-periodic, the periodic continuation of $g(\tau)$ will not be continuous. As a result, the decay rate of the Fourier coefficients will be in $\mathcal{O}(\frac{1}{j})$. This slow decay rate arises because the discontinuity in the periodic extension introduces additional high-frequency components, leading to a less rapid decay of the Fourier coefficients. For higher decay rates, the function $g(\tau)$ must be 2π-periodic. In this case, the smoothness of $g(\tau)$ directly influences the decay rate of the Fourier coefficients. Specifically, the smoother the function, the faster the decay of the Fourier coefficients. If the function $g(\tau)$ is in C^k, then the quasi-Lagrange function will decay at a rate of $\mathcal{O}(\frac{1}{j^{k+1}})$. This means that the smoother $g(\tau)$, the faster the decay of the corresponding quasi-Lagrange function. Finally, if $g(\tau)$ is smooth, the decay rate of the quasi-Lagrange function will exceed any polynomial rate, decaying faster than any polynomial function of j can grow. This represents the optimal decay rate achievable, which also holds true for the Bessel function.

To achieve the highest possible decay rate, we use the following approach

$$g(\tau) = \frac{1}{\mathrm{i}} \sum_{k=-\frac{N}{2}}^{\frac{N}{2}} a_k \mathrm{e}^{\mathrm{i}k\tau} = \sum_{k=0}^{\frac{N}{2}} b_k \sin(k\tau), \tag{4.14}$$

where we assume $N \in 2\mathbb{N}$ to be finite, and the coefficients $a_k \in \mathbb{R}$ respectively $b_k \in \mathbb{R}$ must be chosen such that the conditions summarized in table 4.9 are met. This approach guarantees the high decay rate as $g(\tau)$ is 2π-periodic and smooth. Using this approach, every second order of the derivatives evaluated at zero vanish automatically. Therefore, the degree of polynomial reproduction is even. For this approach, we can precisely

determine the decay rate of Ψ_j. We begin with the integral representation

$$\begin{aligned}
\Psi_j(x) &= \frac{1}{2\pi}\int_{-\pi}^{\pi} \mathrm{e}^{ij\tau}\mathrm{e}^{-ixg(\tau)}\mathrm{d}\tau = \frac{1}{2\pi}\int_{-\pi}^{\pi} \mathrm{e}^{ij\tau}\sum_{\ell=0}^{\infty}\frac{(-\mathrm{i}x)^\ell}{\ell!}g(\tau)^\ell\mathrm{d}\tau \\
&= \sum_{\ell=0}^{\infty}\frac{(-\mathrm{i}x)^\ell}{\ell!}\frac{1}{2\pi}\int_{-\pi}^{\pi}\mathrm{e}^{ij\tau}g(\tau)^\ell\mathrm{d}\tau \\
&= \sum_{\ell=0}^{\infty}\frac{(-x)^\ell}{\ell!}\frac{1}{2\pi}\int_{-\pi}^{\pi}\mathrm{e}^{ij\tau}\left(\sum_{k=-\frac{N}{2}}^{\frac{N}{2}} a_k\mathrm{e}^{\mathrm{i}k\tau}\right)^\ell\mathrm{d}\tau \\
&= \sum_{\ell=0}^{\infty}\frac{(-x)^\ell}{\ell!}\frac{1}{2\pi}\int_{-\pi}^{\pi}\mathrm{e}^{ij\tau}\sum_{|\alpha|=\ell}\binom{\ell}{\alpha}a^\alpha\mathrm{e}^{\mathrm{i}\tau\sum_{k=-\frac{N}{2}}^{\frac{N}{2}}k\alpha_k}\mathrm{d}\tau \\
&= \sum_{\ell=0}^{\infty}\frac{(-x)^\ell}{\ell!}\sum_{|\alpha|=\ell}\binom{\ell}{\alpha}a^\alpha\delta_{j,\sum_{k=-\frac{N}{2}}^{\frac{N}{2}}k\alpha_k} \\
&= \sum_{\ell=\lceil\frac{2j}{N}\rceil}^{\infty}\sum_{|\alpha|=\ell}\frac{(-x)^\ell a^\alpha}{\alpha!}\delta_{j,\sum_{k=-\frac{N}{2}}^{\frac{N}{2}}k\alpha_k},
\end{aligned}$$

where $\alpha = (\alpha_{-\frac{N}{2}}, \alpha_{-\frac{N}{2}+1}, \ldots, \alpha_{\frac{N}{2}})$ is the multi-index and $a = (a_{-\frac{N}{2}}, a_{-\frac{N}{2}+1}, \ldots, a_{\frac{N}{2}})$ is the vector containing the expansion coefficients of the sum. Non-vanishing terms in this sum occur only if $\ell \geq \frac{2j}{N}$, as only in this case the Kronecker delta condition is satisfied. From this expression, we observe that for large j, the function decays factorially, thereby ensuring that the quasi-Lagrange operator is well-defined for every polynomial. For a given N and coefficients a_k, this expression can be used to derive the series representation of the quasi-Lagrange function, which enables significantly faster evaluation compared to numerical integration.

With these results, we can now construct quasi-Lagrange functions that are capable of reproducing polynomials of arbitrary degree. For example, the quasi-Lagrange function using $g(\tau) = \frac{4}{3}\sin(\tau) - \frac{1}{6}\sin(2\tau)$ reproduces all polynomials of degree four. While these results are promising, our primary interest lies not in polynomial reproduction itself, but in the approximation order. The next step is therefore to determine the approximation order of our newly constructed quasi-Lagrange functions.

Analogously to equ. (4.9), we now have a slight modification

$$\sum_{j\in\mathbb{Z}} j^k\Psi_j(x) = \sum_{m_1,m_3,\ldots,m_{\tilde{k}}} \frac{k!}{m_1!m_3!\cdots m_{\tilde{k}}!}\prod_{\ell=1}^{k}\left(\frac{x\sum_{p=1}^{\frac{N}{2}}b_p p^\ell}{\ell!}\right)^{m_\ell}, \tag{4.15}$$

with the conditions

$$\begin{aligned} 0 &= m_\ell, \qquad \forall \ell \in 2\mathbb{N}, \\ k &= m_1 + 3m_3 + \cdots + \tilde{k} m_{\tilde{k}}, \end{aligned}$$

where b_p are the coefficients from equ. (4.14). As before, $\tilde{k}$ denotes the largest odd integer less than or equal to k. To derive the approximation order, we perform calculations similar to the previous case for the Bessel function. We assume that we have a quasi-Lagrange function that reproduces all polynomials of degree $n \in 2\mathbb{N}$. We define

$$p(y) = \sum_{k=0}^{n} \frac{f^{(k)}(x)}{k!}(y-x)^k$$

for the function f to be approximated and write

$$\begin{aligned} Q_h[f](x) - f(x) &= \sum_{j\in\mathbb{Z}} \left(f(jh) - p(jh)\right) \Psi_j\left(\frac{x}{h}\right) \\ &= \sum_{j\in\mathbb{Z}} \sum_{k=n+1}^{\infty} \frac{f^{(k)}(x)}{k!}(jh-x)^k \Psi_j\left(\frac{x}{h}\right). \end{aligned}$$

Applying the binomial theorem yields

$$= \sum_{j\in\mathbb{Z}} \sum_{k=n+1}^{\infty} \frac{f^{(k)}(x)}{k!} \sum_{\ell=0}^{k} \frac{k!}{\ell!(k-\ell)!}(-x)^{k-\ell}(jh)^\ell \Psi_j\left(\frac{x}{h}\right).$$

Interchanging the order of summation and using the summation formula for the new quasi-Lagrange function from equ. (4.15) leads to

$$= \sum_{k=n+1}^{\infty} \sum_{\ell=0}^{k} \frac{f^{(k)}(x)}{\ell!(k-\ell)!}(-x)^{k-\ell} h^\ell \sum_{m_1,m_3,\ldots,m_{\tilde{\ell}}} \frac{\ell!}{m_1! m_3! \cdots m_{\tilde{\ell}}!} \prod_{j=1}^{\ell} \left(\frac{x \sum_{p=1}^{\frac{N}{2}} b_p p^j}{hj!} \right)^{m_j},$$

where again $m_1 + 3m_3 + \cdots + \tilde{\ell} m_{\tilde{\ell}} = \ell$ and $m_2, m_4, \ldots, m_{\hat{\ell}} = 0$. The lowest order in h ($\mathcal{O}(h^0)$) appears if and only if $m_1 = \ell$. The next order is then given by $\mathcal{O}(h^n)$ for $m_1 = \ell - n - 1, m_{n+1} = 1$. Recall that, from the conditions for polynomial reproduction,

we know that

$$\begin{aligned}
g^{(1)}(\tau) &= \sum_k b_k k \cos(k\tau)\Big|_{\tau=0} &&= 1 \quad \Rightarrow \quad \sum_k b_k k &&= 1 \\
g^{(3)}(\tau) &= \sum_k b_k k^3 \cos(k\tau)\Big|_{\tau=0} &&= 0 \quad \Rightarrow \quad \sum_k b_k k^3 &&= 0 \\
&\vdots \\
g^{(n-1)}(\tau) &= \sum_k b_k k^{n-1} \cos(k\tau)\Big|_{\tau=0} &&= 0 \quad \Rightarrow \quad \sum_k b_k k^{n-1} &&= 0.
\end{aligned}$$

Therefore, all orders between 1 and n, vanish identically. The second non-vanishing term is for $\ell \geq n+1$. All following terms are of order h^{n+2} and appear for $\ell \geq n+3$. Taking these comments into consideration, the approximation error can be expressed as

$$\begin{aligned}
Q_h[f](x) - f(x) &= \sum_{k=n+1}^{\infty} \sum_{\ell=0}^{k} \frac{f^{(k)}(x)}{(k-\ell)!}(-x)^{k-\ell} h^\ell \left(\frac{x^\ell}{\ell! h^\ell} + \frac{x^{\ell-n}\Theta(\ell-n-1)\sum_{p=1}^{\frac{N}{2}} b_p p^{n+1}}{(\ell-n-1)!(n+1)! h^{\ell-n}} \right. \\
&\qquad \left. + \Theta(\ell-n-3)\mathcal{O}(h^{n+2-\ell}) \right) \\
&= \sum_{k=n+1}^{\infty} \sum_{\ell=0}^{k} \frac{f^{(k)}(x)(-x)^{k-\ell}}{(k-\ell)!} \left(\frac{x^\ell}{\ell!} + \frac{x^{\ell-n} h^n \Theta(\ell-n-1)\sum_{p=1}^{\frac{N}{2}} b_p p^{n+1}}{(\ell-n-1)!(n+1)!} \right. \\
&\qquad \left. + \Theta(\ell-n-3)\mathcal{O}(h^{n+2}) \right).
\end{aligned}$$

Analogous to the Bessel case, the sum over the first term cancels out. The calculation is shown in equ. (4.11). We will now focus on the second term

$$\begin{aligned}
\sum_{\ell=0}^{k} \frac{(-x)^{k-\ell}}{(k-\ell)!} \frac{x^{\ell-n} h^n \Theta(\ell-n-1)}{(\ell-n-1)!(n+1)!} &= \frac{(-x)^{k-n} h^n}{(n+1)!} \sum_{\ell=n+1}^{k} \frac{(-1)^\ell}{(k-\ell)!(\ell-n-1)!} \\
&= \frac{(-1)^{k+1} x^{k-n} h^n}{(n+1)!(k-n-1)!} \sum_{\ell=0}^{k-n-1} \frac{(-1)^\ell (k-n-1)!}{(k-n-1-\ell)!\ell!} \\
&= \frac{(-1)^{k-3} x^{k-n} h^n}{(n+1)!(k-n-1)!} \underbrace{\sum_{\ell=0}^{k-n-1} (-1)^\ell \binom{k-n-1}{\ell}}_{=\delta_{k,n+1}}
\end{aligned}$$

$$= \frac{xh^n}{(n+1)!}\delta_{k,n+1}.$$

Utilizing the results obtained, the final approximation order is derived as $O(h^n)$. The following formula expresses this result in more detail

$$Q_h[f](x) - f(x) = \frac{f^{(n+1)}(x)}{(n+1)!} xh^n \sum_{p=1}^{\frac{N}{2}} b_p p^{n+1} + \mathcal{O}(h^{n+2}),$$

where $\frac{N}{2}$ is the number of coefficients b_p used for the modification of the Bessel function as our new quasi-Lagrange function. To answer the initial question, we have developed an approach that enables the construction of a quasi-Lagrange function with polynomial reproduction and an approximation order of arbitrary degree.

4.2.2 Scattered Data

The majority of approximation tasks require approximating a function based on a set of scattered data. In the case of RBFs, the expansion of the trigonometric polynomial outlines the conditions necessary for handling scattered data. However, the application of our novel approach remains to be explored. In this subsection, we first derive an expression using the Bessel function and then generalize these results to achieve a higher approximation order.

Before we start, we define the set $\Xi = \{x_j, j \in \mathbb{Z}\}$ as the set of distinct scattered points with the associated function values f_j. Furthermore, we assume that Ξ is ordered and $x_j \to \pm\infty$ as $j \to \pm\infty$. In other words, Ξ is a quasi-uniform set.

Instead of directly using the Bessel function or the modified approach presented in the last subsection, we now use a linear combination of them as the quasi-Lagrange function

$$\Psi_j(x) = \sum_{k\in\mathbb{Z}} \mu_{j,k} J_{j+k}(x).$$

For better comprehension, we use the Bessel function. However, the modification is one to one interchangeable. We assume the coefficients $\mu_{j,k}$ to be finitely supported with respect to k. In the following, we will figure out how to determine these coefficients to make this approach applicable to scattered data.

We represent each scattered point as $x_j = jh + x_0 + \Delta_j$, where h is some grid spacing, x_0 is some translation, and Δ_j is the difference from the grid point to the actual data point. The translation x_0 is chosen such that $\Delta_0 = 0$. We then interpolate the function

f at x_0. The translation has no impact on the approximation order. Note that Δ_j is not necessarily small and depends on h. While the theoretical results are independent of h, in real world applications, the parameter h affects the summation convergence speed. This is due to the fact that both, the differences Δ_j and the coefficients $\mu_{j,k}$, change their values, and the argument of the Bessel function shrinks for larger values of h. Since the value of the Bessel function decays factorially, this effect has a greater impact and leads to practically faster convergence.

The decay rate of the quasi-Lagrange function is the same as that of the Bessel functions, and therefore, we know that the sum converges absolutely for every polynomial. Starting with the reproduction of constants, we obtain

$$\begin{aligned} 1 \overset{!}{=} \sum_{j\in\mathbb{Z}} \Psi_j \left(\frac{x-x_0}{h}\right) &= \sum_{j\in\mathbb{Z}}\sum_{k\in\mathbb{Z}} \mu_{j,k} J_{j+k}\left(\frac{x-x_0}{h}\right) \\ &= \sum_{j\in\mathbb{Z}}\sum_{k\in\mathbb{Z}} \mu_{j-k,k} J_{j}\left(\frac{x-x_0}{h}\right). \end{aligned}$$

With the condition $\sum_{k\in\mathbb{Z}} \mu_{j-k,k} = 1, \quad \forall j \in \mathbb{Z}$, we end up with

$$= \sum_{j\in\mathbb{Z}} J_j \left(\frac{x-x_0}{h}\right) = 1.$$

In the following step, we identify the conditions for linear polynomial reproduction

$$\begin{aligned} x \overset{!}{=} &\sum_{j\in\mathbb{Z}} x_j \Psi_j \left(\frac{x-x_0}{h}\right) = \sum_{j\in\mathbb{Z}} (jh + x_0 + \Delta_j) \sum_{k\in\mathbb{Z}} \mu_{j,k} J_{j+k}\left(\frac{x-x_0}{h}\right) \\ =&\sum_{j\in\mathbb{Z}}\sum_{k\in\mathbb{Z}} (jh + x_0 - kh + \Delta_{j-k}) \mu_{j-k,k} J_j \left(\frac{x-x_0}{h}\right) \\ =&\sum_{j\in\mathbb{Z}} (jh + x_0) \underbrace{\sum_{k\in\mathbb{Z}} \mu_{j-k,k}}_{=1} J_j \left(\frac{x-x_0}{h}\right) + \sum_{j\in\mathbb{Z}}\sum_{k\in\mathbb{Z}} (\Delta_{j-k} - kh) \mu_{j-k,k} J_j \left(\frac{x-x_0}{h}\right) \\ =&x + \sum_{j\in\mathbb{Z}}\sum_{k\in\mathbb{Z}} (\Delta_{j-k} - kh) \mu_{j-k,k} J_j \left(\frac{x-x_0}{h}\right). \end{aligned}$$

With the condition $\sum_{k\in\mathbb{Z}} (\Delta_{j-k} - kh) \mu_{j-k,k} = 0, \quad \forall j \in \mathbb{Z}$, we end up with

$$= x.$$

Finally, we check the required conditions for quadratic polynomial reproduction

$$
\begin{aligned}
x^2 \stackrel{!}{=} &\sum_{j\in\mathbb{Z}} x_j^2 \Psi_j\left(\frac{x-x_0}{h}\right) = \sum_{j\in\mathbb{Z}} (jh+x_0+\Delta_j)^2 \sum_{k\in\mathbb{Z}} \mu_{j,k} J_{j+k}\left(\frac{x-x_0}{h}\right) \\
=&\sum_{j\in\mathbb{Z}}\sum_{k\in\mathbb{Z}} (jh+x_0+\Delta_{j-k}-kh)^2 \mu_{j-k,k} J_j\left(\frac{x-x_0}{h}\right) \\
=&\sum_{j\in\mathbb{Z}}\sum_{k\in\mathbb{Z}} \left((jh+x_0)^2 + 2(jh+x_0)(\Delta_{j-k}-kh) + (\Delta_{j-k}-kh)^2\right) \mu_{j-k,k} J_j\left(\frac{x-x_0}{h}\right) \\
=&\sum_{j\in\mathbb{Z}} (jh+x_0)^2 J_j\left(\frac{x-x_0}{h}\right) \underbrace{\sum_{k\in\mathbb{Z}} \mu_{j-k,k}}_{=1} + \sum_{j\in\mathbb{Z}} 2(jh+x_0) \underbrace{\sum_{k\in\mathbb{Z}} (\Delta_{j-k}-kh)\mu_{j-k,k}}_{=0} J_j\left(\frac{x-x_0}{h}\right) \\
&+\sum_{j\in\mathbb{Z}}\sum_{k\in\mathbb{Z}} (\Delta_{j-k}-kh)^2 \mu_{j-k,k} J_j\left(\frac{x-x_0}{h}\right) \\
=&x^2 + \sum_{j\in\mathbb{Z}}\sum_{k\in\mathbb{Z}} (\Delta_{j-k}-kh)^2 \mu_{j-k,k} J_j\left(\frac{x-x_0}{h}\right).
\end{aligned}
$$

With the condition $\sum_{k\in\mathbb{Z}} (\Delta_{j-k}-kh)^2 \mu_{j-k,k} = 0, \quad \forall j \in \mathbb{Z}$, we end up with

$$= x^2.$$

In summary, we find that the quasi-Lagrange function $\Psi_j(x)$ reproduces all polynomials of degree two for scattered data, provided that the coefficients satisfy the conditions

- $\sum_{k\in\mathbb{Z}} \mu_{j-k,k} = 1, \qquad \forall j \in \mathbb{Z}$
- $\sum_{k\in\mathbb{Z}} (\Delta_{j-k}-kh)\mu_{j-k,k} = 0, \quad \forall j \in \mathbb{Z}$
- $\sum_{k\in\mathbb{Z}} (\Delta_{j-k}-kh)^2 \mu_{j-k,k} = 0, \quad \forall j \in \mathbb{Z}.$

The solution is not unique, as the number of coefficients is not fixed. In this specific example, we solve the system of equations using three non-zero coefficients, namely

$$
\begin{aligned}
\mu_{j+1,-1} &= \frac{\Delta_j\,(\Delta_{j-1}-h)}{(\Delta_j-\Delta_{j+1}-h)\,(-\Delta_{j-1}+\Delta_{j+1}+2h)} \\
\mu_{j,0} &= \frac{(h-\Delta_{j-1})\,(\Delta_{j+1}+h)}{(-\Delta_{j-1}+\Delta_j+h)\,(-\Delta_j+\Delta_{j+1}+h)} \\
\mu_{j-1,1} &= \frac{\Delta_j\,(\Delta_{j+1}+h)}{(-\Delta_{j-1}+\Delta_j+h)\,(-\Delta_{j-1}+\Delta_{j+1}+2h)}.
\end{aligned}
$$

In the final step, we shift back the index j and obtain the final scattered data representation for the Bessel function

$$\begin{aligned}\Psi_j(x) =& \frac{\Delta_{j-1}\left(\Delta_{j-2}-h\right)}{\left(\Delta_{j-1}-\Delta_j-h\right)\left(-\Delta_{j-2}+\Delta_j+2h\right)} J_{j-1}(x) \\ &+ \frac{\left(h-\Delta_{j-1}\right)\left(\Delta_{j+1}+h\right)}{\left(-\Delta_{j-1}+\Delta_j+h\right)\left(-\Delta_j+\Delta_{j+1}+h\right)} J_j(x) \\ &+ \frac{\Delta_{j+1}\left(\Delta_{j+2}+h\right)}{\left(-\Delta_j+\Delta_{j+1}+h\right)\left(-\Delta_j+\Delta_{j+2}+2h\right)} J_{j+1}(x),\end{aligned}$$

where $\Delta_j = jh + x_0 - x_j$ and h is the grid spacing which can be chosen arbitrarily. However, choosing h on the order of the distance between the data points is a reasonable approach. Up to this point, we showed for the explicit example of the Bessel function how we can derive a quasi-Lagrange operator which can also handle scattered data. Now, we will generalize this to the modified Bessel functions from section 4.2.1 and determine the conditions the coefficients have to satisfy.

Assume a quasi-Lagrange function $\tilde{\Psi}_j(x)$ is given, where the quasi-Lagrange operator, as shown in subsection 4.2.1, reproduces all polynomials of degree n on some grid with grid spacing h. Again we use the convention $x_j = jh + x_0 + \Delta_j$. For $0 \leq \ell \leq n$, we obtain

$$\begin{aligned}x^\ell \overset{!}{=} & \sum_{j\in\mathbb{Z}} x_j^\ell \Psi_j\left(\frac{x-x_0}{h}\right) = \sum_{j\in\mathbb{Z}} (jh+x_0+\Delta_j)^\ell \sum_{k\in\mathbb{Z}} \mu_{j,k}\tilde{\Psi}_{j+k}\left(\frac{x-x_0}{h}\right) \\ =& \sum_{j\in\mathbb{Z}}\sum_{k\in\mathbb{Z}} (jh+x_0+\Delta_{j-k}-kh)^\ell \mu_{j-k,k}\tilde{\Psi}_j\left(\frac{x-x_0}{h}\right) \\ =& \sum_{j\in\mathbb{Z}}\sum_{k\in\mathbb{Z}}\sum_{p=0}^{\ell} \binom{\ell}{p} (jh+x_0)^{\ell-p}(\Delta_{j-k}-kh)^p \mu_{j-k,k}\tilde{\Psi}_j\left(\frac{x-x_0}{h}\right) \\ =& \sum_{j\in\mathbb{Z}}\sum_{p=0}^{\ell} \binom{\ell}{p} (jh+x_0)^{\ell-p} \left(\sum_{k\in\mathbb{Z}} (\Delta_{j-k}-kh)^p \mu_{j-k,k}\right) \tilde{\Psi}_j\left(\frac{x-x_0}{h}\right).\end{aligned}$$

With the condition $\sum_{k\in\mathbb{Z}} (\Delta_{j-k}-kh)^p \mu_{j-k,k} = \delta_{p,0}, \quad \forall j \in \mathbb{Z}$ and $\forall\, 0 \leq p \leq \ell$, we continue with

$$\begin{aligned}=& \sum_{j\in\mathbb{Z}} (jh+x_0)^\ell \tilde{\Psi}_j\left(\frac{x-x_0}{h}\right) \\ =& x^\ell.\end{aligned}$$

To summarize this subsection, we conclude that if a quasi-Lagrange operator possesses a

specified polynomial reproduction ℓ and approximation order on an infinite grid, it can be extended to scattered data by introducing a new quasi-Lagrange function defined as a linear combination of the previously used functions. The coefficients $\mu_{j,k}$ are calculated by solving the linear system of equations

$$\sum_{k\in\mathbb{Z}}(\Delta_{j-k} - kh)^p \mu_{j-k,k} = \delta_{p,0}, \quad \forall j \in \mathbb{Z}, \forall\, 0 \leq p \leq \ell.$$

For the special case of the Bessel function, we have provided the explicit formulas for these coefficients. For practical computations, using a shifted version is recommended to avoid redundant evaluation of the same quasi-Lagrange function.

In conclusion, to address the initial question, the approach for the quasi-Lagrange function can indeed be used for quasi-interpolation of scattered data.

4.2.3 Uniform Convergence

For the Bessel function, we showed in equ. (4.12) that the approximation order is given by

$$Q_h[f](x) - f(x) = \frac{f^{(3)}(x)}{3!} x h^2 + \mathcal{O}(h^4).$$

There are some practical issues with the approach presented up to this section. Although we focus on the Bessel function, the same argument applies to the modified functions. The primary issue is that the convergence is only pointwise, not uniform. Consequently, for large arguments x, it is necessary to choose a sufficiently small grid size in order to achieve an adequate approximation. The second issue occurs also for large arguments x, because the sum $Q_h[f](x) = \sum_{j\in\mathbb{Z}} f(jh) J_j\left(\frac{x}{h}\right)$ converges slowly. The rapid decay of the Bessel function is only guaranteed when the order is significantly greater than the argument. Furthermore, evaluating the Bessel function for large arguments becomes more costly, as a larger number of terms in the series are required to converge.

To address the issues for large arguments, we propose introducing shifts such that the argument of the Bessel function always lies within the interval $(-\frac{h}{2}, \frac{h}{2}]$. This can be achieved by approximating each interval piecewise. Table 4.10 shows some examples of how the quasi-Lagrange operator changes for different intervals of x.

For the general definition, we need a function that determines in which interval the argument lies. We call this $\Lambda(x) = \left(\frac{x}{h} + \frac{1}{2}\right)/1$, where / is the quotient. In other words, the /1 operator takes only the integer part of the number. The quasi-Lagrange operator

$x \in$	$Q_h[f](x)$
$(-\frac{h}{2}, \frac{h}{2}]$	$\sum_{j\in\mathbb{Z}} f(jh) J_j\left(\frac{x}{h}\right)$
$(\frac{h}{2}, \frac{3h}{2}]$	$\sum_{j\in\mathbb{Z}} f((j+1)h) J_j\left(\frac{x-h}{h}\right)$
$(\frac{3h}{2}, \frac{5h}{2}]$	$\sum_{j\in\mathbb{Z}} f((j+2)h) J_j\left(\frac{x-2h}{h}\right)$
$(\frac{5h}{2}, \frac{7h}{2}]$	$\sum_{j\in\mathbb{Z}} f((j+3)h) J_j\left(\frac{x-3h}{h}\right)$
$\vdots$	$\vdots$
$(\frac{(2k-1)h}{2}, \frac{(2k+1)h}{2}]$	$\sum_{j\in\mathbb{Z}} f((j+k)h) J_j\left(\frac{x-kh}{h}\right)$

Table 4.10: Examples of shifts for piecewise approximation of each interval. Analogously, this can be done in the negative direction of x.

is then given by

$$Q_h[f](x) = \sum_{j\in\mathbb{Z}} f((j+\Lambda(x))h) J_j\left(\frac{x-\Lambda(x)h}{h}\right).$$

There are several things to note with this kind of approximation:

1. The function $\Lambda(x)$ is not continuous. Therefore, the entire quasi-Lagrange operator is not continuous on the interval boundaries.

2. Since the function $\Lambda(x)$ evaluates integer values, only the known values of f on the grid are utilized.

3. The argument of the Bessel function lies within the interval $(-\frac{h}{2}, \frac{h}{2}]$, which results in a rapidly converging quasi-Lagrange operator. Additionally, the evaluation of the Bessel function becomes more efficient.

4. Since the argument of the Bessel function is bounded by $\frac{h}{2}$, we get an approximation order of $\mathcal{O}(h^3)$, which is expressed as

$$Q_h[f](x) - f(x) = \frac{f^{(3)}(x)}{3!}\frac{h^3}{2} + \mathcal{O}(h^4).$$

   This proves not only uniform convergence, but also an improvement in the approximation order by one degree compared to previous results. This is a noteworthy outcome.

5. In fact, we are not merely interpolating the function at $x = 0$, but now for all given grid points. This is due to the property $J_j(0) = \delta_{j,0}$, which holds for the Bessel functions. This property also extends to the modified Bessel functions employed to

achieve enhanced approximation order. With these modifications, we have not only developed a quasi-interpolation method, but also an actual interpolation method, which represents a significant and remarkable result.

6. The concept can be similarly extended to scattered data in an analogous manner. If $x \in \left(\frac{x_{k-1}+x_k}{2}, \frac{x_k+x_{k+1}}{2}\right], k \in \mathbb{Z}$, then we can write

$$Q_h[f](x) = \sum_{j\in\mathbb{Z}} f(x_{j+k})\Psi_j\left(\frac{x-x_k}{h}\right).$$

In this particular example, the quasi-Lagrange function is denoted by Ψ, due to the necessity of a linear combination of Bessel functions when dealing with scattered data.

4.2.4 Higher Dimensions

We have achieved significant results for quasi-interpolation by utilizing modifications of the Bessel function as the quasi-Lagrange function. The only limitation is, that these results are restricted to one dimension. For the RBFs, we employed the Euclidean norm to reduce the problem to a univariate function, which allowed us to handle it effectively.

For the Bessel function approach, this is not feasible because it relies on specific terms canceling each other out. As such, the use of any absolute value is not applicable in this context. The simplest approach in higher dimensions is to use a tensor product for approximations. Let $x \in \mathbb{R}^n$ and $j \in \mathbb{Z}^n$, then we can define the quasi-Lagrange function as

$$\Psi_j(x) = J_{j_1}(x_1)J_{j_2}(x_2)\cdots J_{j_n}(x_n).$$

All properties and approximation orders will be consistent with the one-dimensional results. We have not identified a more elegant method to generalize these results to higher dimensions yet.

4.3 Summary

In this chapter, we presented the results for the new generalized multiquadric (see table 4.4) and the new generalized thin plate spline (see table 4.6) for the best parameter configurations usable in classical quasi-interpolation. To the best of our knowledge,

these results are shown for the first time in this level of generality. Furthermore, we achieved higher approximation orders than those of the classical multiquadric and thin plate spline. Beside the RBFs approach, we introduced a new non-RBF approach using Bessel or Bessel-like functions. We showed how the quasi-Lagrange function has to be modified to achieve sufficient approximation order. The extension to scattered data was presented, and the convergence properties and practical implementation were discussed.

In summary, while the RBF approach is well known, we presented new results for more general RBFs. The non-RBF approach is totally different in the results and the proof structure. There are two downsides to the non-RBF approach at the moment. On the one hand, the quasi-Lagrange operator is not continuous, and there is no elegant way for data in higher dimensions. On the other hand, the quasi-Lagrange operator has great convergence properties leading to efficient evaluation, and the approximation order compared to the classical quasi-interpolation in one dimension is quite high.

The non-RBF approach is presented here for the first time, and further research needs to be done for additional properties and applications.

Chapter 5

Numerical Examples

In this chapter, we present some numerical examples to illustrate the theoretical results achieved in chapter 4. For the sake of traceability, we consider examples in one and two dimensions, based on gridded data. We also present the exact coefficents used in the approximations. With these coefficients, one can directly evaluate the approximations and compare them to alternative methods of interest, without requiring a detailed understanding of the underlying theory developed in the preceding chapters.

5.1 Examples in 1D

To demonstrate the accuracy of our quasi-interpolation using the newly discovered functions, we employ three different test functions f_1, f_2, f_3 for approximation. These functions are also employed in [42].

$$
\begin{aligned}
f_1(x) &= (x+1)^3 \exp\left(-\frac{x^2}{10}\right) \cos(x-2), \\
f_2(x) &= 25 \exp\left(-\frac{x^2}{15}\right) |\sin(x)|^3, \\
f_3(x) &= 25 \exp\left(-\frac{x^2}{15}\right) |\sin(x)| \sin(x)^9,
\end{aligned}
$$

where $x \in \mathbb{R}$. While $f_1 \in C^\infty(\mathbb{R})$ is analytic, $f_2 \in C^2(\mathbb{R})$ is twice continuously differentiable, and $f_3 \in C^9(\mathbb{R})$ is nine times continuously differentiable. For comparison, a Gaussian function scaled by a factor of 25 is used to ensure that the test functions are approximately localized in the interval $[-10, 10]$ and have similar magnitudes. For

simplicity, we use gridded data with grid spacing h. The error is measured by

$$\mathrm{err}[f] = \left(\int_{-10}^{10} \left(f(x) - Q_h[f](x) \right)^2 \mathrm{d}x \right)^{\frac{1}{2}}.$$

The error integral is evaluated via `NIntegrate`, *Mathematica's* built-in function using a local adaptive integration strategy [32].

5.1.1 Generalized Multiquadric

In the previous chapter, we observed that the best results are achieved when $\lambda \in 2 + 4\mathbb{N}$ and $\beta \in \frac{1}{2} + \mathbb{N}$. To illustrate the method, we vary the parameter λ while fixing $\beta = \frac{1}{2}$, as in the classical multiquadric function. The RBFs are then given by

$$\begin{aligned} \varphi_1(r) &= \sqrt{c^2 + r^2}, \\ \varphi_2(r) &= \sqrt{c^6 + r^6}, \\ \varphi_3(r) &= \sqrt{c^{10} + r^{10}}. \end{aligned}$$

The first RBF is the classical multiquadric. The quasi-Lagrange function for the classical multiquadric is given by The quasi-Lagrange functions are given by

$$\Psi_1(x) = \frac{1}{2}\varphi_1(||x-1||) - \varphi_1(||x||) + \frac{1}{2}\varphi_1(||x+1||).$$

This quasi-Lagrange function exhibits the decay property $\Psi_1(x) \in \mathcal{O}\left((1+||x||)^{-3}\right)$ as $||x|| \to \infty$. Furthermore, the quasi-Lagrange operator reproduces all polynomials of degree one, and the approximation order is given by $\mathcal{O}\left(h^2 \log(1/h)\right)$.

The second quasi-Lagrange function is

$$\Psi_2(x) = \sum_{k=-4}^{4} \mu_k \varphi_2(||x-k||),$$

where the coefficients are

$$\begin{aligned} \mu_{-4} = \mu_4 &= \frac{14\sqrt{\pi} - 135c^4\Gamma\left(\frac{7}{6}\right)\Gamma\left(\frac{7}{3}\right)}{5760\sqrt{\pi}}, & \mu_{-3} = \mu_3 &= \frac{45c^4\Gamma\left(\frac{7}{6}\right)\Gamma\left(\frac{7}{3}\right) - 8\sqrt{\pi}}{240\sqrt{\pi}}, \\ \mu_{-2} = \mu_2 &= \frac{338\sqrt{\pi} - 945c^4\Gamma\left(\frac{7}{6}\right)\Gamma\left(\frac{7}{3}\right)}{1440\sqrt{\pi}}, & \mu_{-1} = \mu_1 &= \frac{945c^4\Gamma\left(\frac{7}{6}\right)\Gamma\left(\frac{7}{3}\right) - 488\sqrt{\pi}}{720\sqrt{\pi}}, \end{aligned}$$

$$\mu_0 = \frac{7\left(26\sqrt{\pi} - 45c^4\Gamma\left(\frac{7}{6}\right)\Gamma\left(\frac{7}{3}\right)\right)}{192\sqrt{\pi}}.$$

This quasi-Lagrange function exhibits the decay property $\Psi_2(x) \in \mathcal{O}\left((1+||x||)^{-7}\right)$ as $||x|| \to \infty$. Furthermore, the quasi-Lagrange operator reproduces all polynomials of degree three, and the approximation order is given by $\mathcal{O}\left(h^4\right)$.

The last quasi-Lagrange function is

$$\Psi_3(x) = \sum_{k=-7}^{7} \mu_k \varphi_3(||x-k||),$$

where the coefficients are given by

$$\begin{aligned}
\mu_{-7} &= \mu_7 = -\frac{c^8 q}{110592} + \frac{c^6 p}{82944} + \frac{37}{3628800}, & \mu_{-6} &= \mu_6 = \frac{7c^8 q}{55296} - \frac{c^6 p}{5184} - \frac{2767}{14515200},\\
\mu_{-5} &= \mu_5 = -\frac{91c^8 q}{110592} + \frac{115c^6 p}{82944} + \frac{6271}{3628800}, & \mu_{-4} &= \mu_4 = \frac{91c^8 q}{27648} - \frac{31c^6 p}{5184} - \frac{73811}{7257600},\\
\mu_{-3} &= \mu_3 = -\frac{1001c^8 q}{110592} + \frac{1441c^6 p}{82944} + \frac{157477}{3628800}, & \mu_{-2} &= \mu_2 = \frac{1001c^8 q}{55296} - \frac{187c^6 p}{5184} - \frac{1819681}{14515200},\\
\mu_{-1} &= \mu_1 = -\frac{1001c^8 q}{36864} + \frac{1529c^6 p}{27648} + \frac{286397}{1209600}, & \mu_0 &= \frac{143c^8 q}{4608} - \frac{55c^6 p}{864} - \frac{353639}{1209600},
\end{aligned}$$

where $q = \frac{5\sqrt{5}\pi^2}{2^{3/5}\Gamma\left(-\frac{8}{5}\right)\Gamma\left(-\frac{1}{5}\right)^2}$ and $p = \frac{5\sqrt{5}\pi^2}{\sqrt[5]{2}\Gamma\left(-\frac{6}{5}\right)\Gamma\left(-\frac{2}{5}\right)^2}$.
This quasi-Lagrange function exhibits the decay property $\Psi_3(x) \in \mathcal{O}\left((1+||x||)^{-11}\right)$ as $||x|| \to \infty$. Furthermore, the quasi-Lagrange operator reproduces all polynomials of degree five, and the approximation order is given by $\mathcal{O}\left(h^6\right)$.

Figure 5.1 shows the results of these approximants. The approximation order increases with higher values of the parameter λ, provided that the approximated function is sufficiently smooth. When aiming for an accurate approximation, the smoothness of the target function should be taken into consideration.

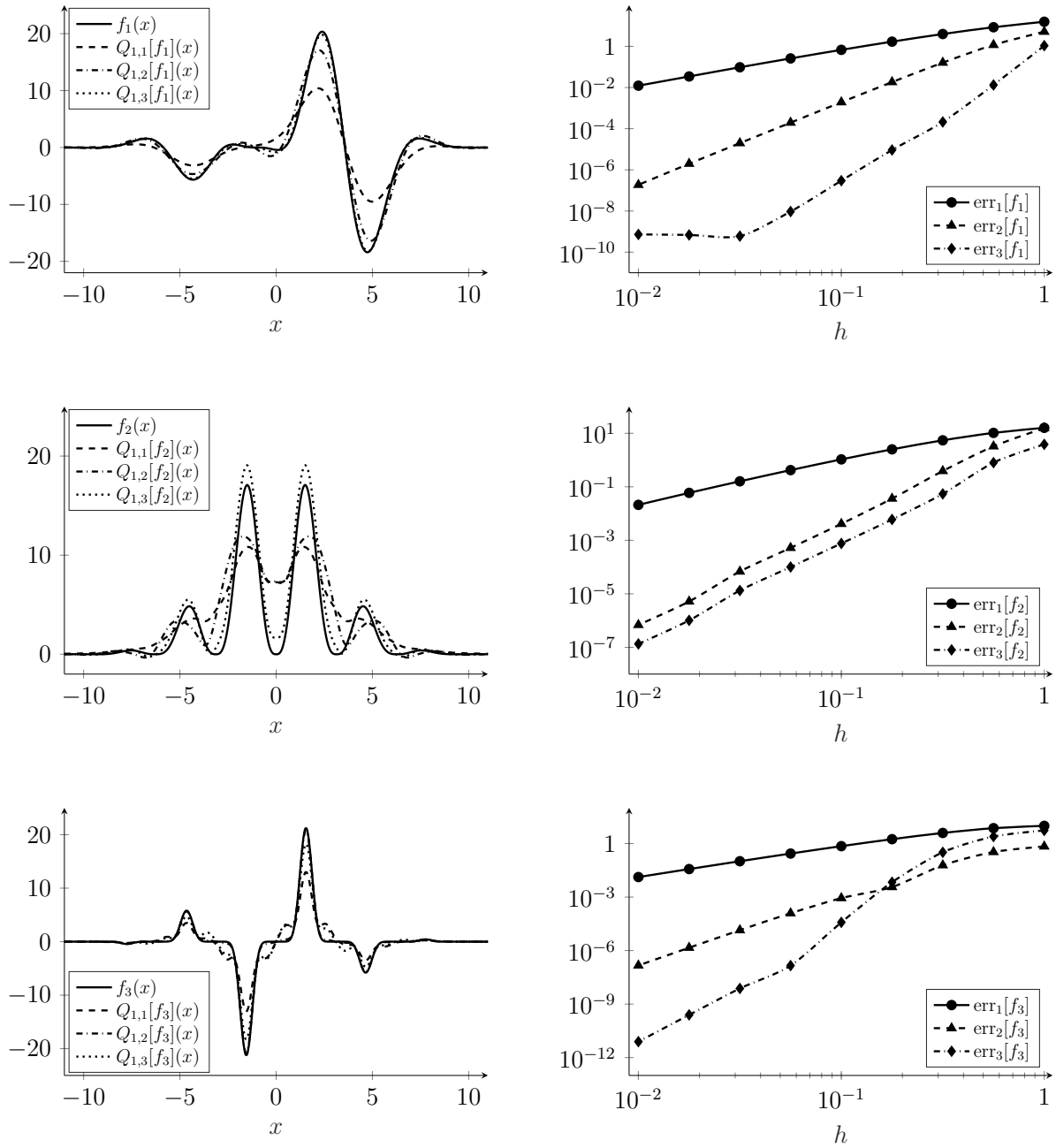

Figure 5.1: On the left side, the test functions f with their associated approximants is displayed. The first two approximants use an shape parameter $c = 1$ while the last one use $c = \frac{1}{2}$. On the right side, the error of the approximants to the test functions is visualized.

5.1.2 Non-Radial Basis Functions

As shown in Section 4.2.1, we present the first three approximants with increasing approximation order. Furthermore, we approximate each interval individually, as shown in section 4.2.3. This enables efficient computation of the modified Bessel function and facilitates fast convergence of the quasi-Lagrange operator. For demonstration purposes, we use gridded data. The quasi-Lagrange operator is given by

$$Q_{h,k}[f](x) = \sum_{j\in\mathbb{Z}} f((j+\Lambda(x))h)\Psi_{k,j}\left(\frac{x-\Lambda(x)h}{h}\right), \qquad k\in\{1,2,3\},$$

where k decides which quasi-Lagrange function is chosen and $\Lambda(x) = \left(\frac{x}{h}+\frac{1}{2}\right)/1$, where $/$ is the quotient, as shown in section 4.2.3. The first quasi-Lagrange function is the Bessel function itself, hence

$$\Psi_{1,j}(x) = J_j(x).$$

The Bessel function is well known and for small arguments the evaluation can be done efficiently using the series representation $J_j(x) = \sum_{k=0}^{\infty} \frac{(-1)^k}{k!\Gamma(j+k+1)}\left(\frac{x}{2}\right)^{2k+j}$. The quasi-Lagrange operator reproduces all polynomials of degree two and converges uniformly with $\mathcal{O}(h^3)$. The second approximant is built using the following quasi-Lagrange function

$$\Psi_{2,j}(x) = \frac{1}{2\pi}\int_{-\pi}^{\pi} \mathrm{e}^{ij\tau - ix\left(\frac{4}{3}\sin(\tau)-\frac{1}{6}\sin(2\tau)\right)}\mathrm{d}\tau.$$

Unfortunately, we were not able to derive a handy formula for the series representation, as we did for the Bessel function. However, for each j, the series representation can be determined using

$$\Psi_{2,j}(x) = \sum_{\ell=\left\lceil\frac{2j}{N}\right\rceil}^{\infty}\sum_{|\alpha|=\ell}\frac{(-x)^\ell a^\alpha}{\alpha!}\delta_{j,\sum_{k=-\frac{N}{2}}^{\frac{N}{2}} k\alpha_k},$$

where $a = \left(-\frac{1}{12}, \frac{4}{6}, 0, -\frac{4}{6}, \frac{1}{12}\right)$. All series representations up to order ten that are used for the approximation ($j\in[-15,15]$) are shown in the tables 5.1 and 5.2 .

They can be directly employed for approximation or to verify the previous formula. The quasi-Lagrange operator for this quasi-Lagrange function reproduces all polynomials of degree four, and the approximation order is given by $\mathcal{O}(h^5)$.

j	$\Psi_{2,j}(x)$
-15	$-\frac{56059x^{10}}{1560317578444800} - \frac{1789x^9}{78015878922240} - \frac{x^8}{270888468480}$
-14	$\frac{853x^{10}}{3715041853440} + \frac{56831x^9}{208042343792640} + \frac{x^8}{9674588160} + \frac{x^7}{180592312320}$
-13	$-\frac{291841x^{10}}{312063515688960} - \frac{6943x^9}{3250661621760} - \frac{149x^8}{90296156160} - \frac{x^7}{3224862720}$
-12	$\frac{9438209x^{10}}{4993016251023360} + \frac{12983x^9}{1218998108160} + \frac{11797x^8}{722369249280} + \frac{x^7}{134369280} + \frac{x^6}{2149908480}$
-11	$\frac{1177847x^{10}}{702142910300160} - \frac{95009x^9}{3250661621760} - \frac{1301x^8}{12899450880} - \frac{319x^7}{3224862720} - \frac{x^6}{44789760}$
-10	$-\frac{16965791x^{10}}{877678637875200} + \frac{539521x^9}{52010585948160} + \frac{3451x^8}{9674588160} + \frac{4019x^7}{5159780352} + \frac{x^6}{2239488} + \frac{x^5}{29859840}$
-9	$\frac{2578433x^{10}}{78015878922240} + \frac{11523713x^9}{58511909191680} - \frac{23579x^8}{54177693696} - \frac{629x^7}{179159040} - \frac{637x^6}{134369280} - \frac{x^5}{746496}$
-8	$\frac{227369021x^{10}}{5617143282401280} - \frac{67667x^9}{135444234240} - \frac{6667001x^8}{4334215495680} + \frac{701x^7}{100776960} + \frac{9919x^6}{358318080} + \frac{x^5}{46656} + \frac{x^4}{497664}$
-7	$-\frac{19268093x^{10}}{100306130042880} - \frac{309779x^9}{2167107747840} + \frac{232573x^8}{38698352640} + \frac{85067x^7}{11287019520} - \frac{3451x^6}{44789760} - \frac{127x^5}{746496} - \frac{x^4}{15552}$
-6	$\frac{461267x^{10}}{6501323243520} + \frac{7449853x^9}{3467372396544} - \frac{138049x^8}{67722117120} - \frac{503167x^7}{8599633920} + \frac{211x^6}{33592320} + \frac{3839x^5}{5971968} + \frac{x^4}{1296} + \frac{x^3}{10368}$
-5	$\frac{185696671x^{10}}{390079394611200} - \frac{361687x^9}{216710774784} - \frac{5383979x^8}{270888468480} + \frac{10687x^7}{214990848} + \frac{455x^6}{995328} - \frac{539x^5}{933120} - \frac{7x^4}{1728} - \frac{x^3}{432}$
-4	$-\frac{256393591x^{10}}{499301625102336} - \frac{113609x^9}{27088846848} + \frac{7252031x^8}{309586821120} + \frac{19973x^7}{134369280} - \frac{16289x^6}{26542080} - \frac{65x^5}{23328} + \frac{277x^4}{41472} + \frac{x^3}{54} + \frac{x^2}{288}$
-3	$-\frac{6351497x^{10}}{10402117189632} + \frac{4058693x^9}{650132324352} + \frac{1140293x^8}{38698352640} - \frac{261499x^7}{1074954240} - \frac{57871x^6}{67184640} + \frac{991x^5}{186624} + \frac{65x^4}{5184} - \frac{61x^3}{1296} - \frac{x^2}{18}$
-2	$\frac{9139867x^{10}}{7801587892224} + \frac{3787247x^9}{990677827584} - \frac{582917x^8}{9674588160} - \frac{3960581x^7}{25798901760} + \frac{2177x^6}{1119744} + \frac{10625x^5}{2985984} - \frac{131x^4}{3888} - \frac{43x^3}{1152} + \frac{2x^2}{9} + \frac{x}{12}$
-1	$\frac{9139867x^{10}}{31206351568896} - \frac{1338155x^9}{123834728448} - \frac{582917x^8}{38698352640} + \frac{371813x^7}{806215680} + \frac{2177x^6}{4478976} - \frac{491x^5}{41472} - \frac{131x^4}{15552} + \frac{11x^3}{72} + \frac{x^2}{18} - \frac{2x}{3}$
0	$-\frac{89429167x^{10}}{59440669655040} + \frac{99144709x^8}{1238347284480} - \frac{293441x^6}{107495424} + \frac{1451x^4}{27648} - \frac{65x^2}{144} + 1$

Table 5.1: Series representation up to order ten of the quasi-Lagrange function $\Psi_{2,j}(x)$ used for the approximations.

j	$\Psi_{2,j}(x)$
1	$\frac{9139867x^{10}}{31206351568896} + \frac{1338155x^9}{123834728448} - \frac{582917x^8}{38698352640} - \frac{371813x^7}{806215680} + \frac{2177x^6}{4478976} + \frac{491x^5}{41472} - \frac{131x^4}{15552} - \frac{11x^3}{72} + \frac{x^2}{18} + \frac{2x}{3}$
2	$\frac{9139867x^{10}}{7801587892224} - \frac{3787247x^9}{990677827584} - \frac{582917x^8}{9674588160} + \frac{3960581x^7}{25798901760} + \frac{2177x^6}{1119744} - \frac{10625x^5}{2985984} - \frac{131x^4}{3888} + \frac{43x^3}{1152} + \frac{2x^2}{9} - \frac{x}{12}$
3	$-\frac{6351497x^{10}}{10402117189632} - \frac{4058693x^9}{650132324352} + \frac{1140293x^8}{38698352640} + \frac{261499x^7}{1074954240} - \frac{57871x^6}{67184640} - \frac{991x^5}{186624} + \frac{65x^4}{5184} + \frac{61x^3}{1296} - \frac{x^2}{18}$
4	$-\frac{256393591x^{10}}{499301625102336} + \frac{113609x^9}{27088846848} + \frac{7252031x^8}{309586821120} - \frac{19973x^7}{134369280} - \frac{16289x^6}{26542080} + \frac{65x^5}{23328} + \frac{277x^4}{41472} - \frac{x^3}{54} + \frac{x^2}{288}$
5	$\frac{185696671x^{10}}{390079394611200} + \frac{361687x^9}{216710774784} - \frac{5383979x^8}{270888468480} - \frac{10687x^7}{214990848} + \frac{455x^6}{995328} + \frac{539x^5}{933120} - \frac{7x^4}{1728} + \frac{x^3}{432}$
6	$\frac{461267x^{10}}{6501323243520} - \frac{7449853x^9}{3467372396544} - \frac{138049x^8}{67722117120} + \frac{503167x^7}{8599633920} + \frac{211x^6}{33592320} - \frac{3839x^5}{5971968} + \frac{x^4}{1296} - \frac{x^3}{10368}$
7	$-\frac{19268093x^{10}}{100306130042880} + \frac{309779x^9}{2167107747840} + \frac{232573x^8}{38698352640} - \frac{85067x^7}{11287019520} - \frac{3451x^6}{44789760} + \frac{127x^5}{746496} - \frac{x^4}{15552}$
8	$\frac{227369021x^{10}}{5617143282401280} + \frac{67667x^9}{135444234240} - \frac{6667001x^8}{4334215495680} - \frac{701x^7}{100776960} + \frac{9919x^6}{358318080} - \frac{x^5}{46656} + \frac{x^4}{497664}$
9	$\frac{2578433x^{10}}{78015878922240} - \frac{11523713x^9}{58511909191680} - \frac{23579x^8}{54177693696} + \frac{629x^7}{179159040} - \frac{637x^6}{134369280} + \frac{x^5}{746496}$
10	$-\frac{16965791x^{10}}{877678637875200} - \frac{539521x^9}{52010585948160} + \frac{3451x^8}{9674588160} - \frac{4019x^7}{5159780352} + \frac{x^6}{2239488} - \frac{x^5}{29859840}$
11	$\frac{1177847x^{10}}{702142910300160} + \frac{95009x^9}{3250661621760} - \frac{1301x^8}{12899450880} + \frac{319x^7}{3224862720} - \frac{x^6}{44789760}$
12	$\frac{9438209x^{10}}{4993016251023360} - \frac{12983x^9}{1218998108160} + \frac{11797x^8}{722369249280} - \frac{x^7}{134369280} + \frac{x^6}{2149908480}$
13	$-\frac{291841x^{10}}{312063515688960} + \frac{6943x^9}{3250661621760} - \frac{149x^8}{90296156160} + \frac{x^7}{3224862720}$
14	$\frac{853x^{10}}{3715041853440} - \frac{56831x^9}{208042343792640} + \frac{x^8}{9674588160} - \frac{x^7}{180592312320}$
15	$-\frac{56059x^{10}}{1560317578444800} + \frac{1789x^9}{78015878922240} - \frac{x^8}{270888468480}$

Table 5.2: Series representation up to order ten of the quasi-Lagrange function $\Psi_{2,j}(x)$ used for the approximations.

The last approximant is built using the quasi-Lagrange function

$$\Psi_{3,j}(x) = \frac{1}{2\pi}\int_{-\pi}^{\pi} \mathrm{e}^{ij\tau - ix\left(\frac{3}{2}\sin(\tau) - \frac{3}{10}\sin(2\tau) + \frac{1}{30}\sin(3\tau)\right)}\mathrm{d}\tau.$$

Again, there is no handy series representation for all orders j, but for each j, the series representation can be determined using $\Psi_{3,j}(x) = \sum_{\ell=\left\lceil \frac{2j}{N}\right\rceil}^{\infty} \sum_{|\alpha|=\ell} \frac{(-x)^\ell a^\alpha}{\alpha!} \delta_{j,\sum_{k=-\frac{N}{2}}^{\frac{N}{2}} k\alpha_k}$, where $a = \left(\frac{1}{60}, -\frac{3}{20}, \frac{3}{4}, 0, -\frac{3}{4}, \frac{3}{20}, -\frac{1}{60}\right)$. The series representations up to order ten for the used approximations are shown in the tables 5.3 and 5.4. As before, they can be directly employed for approximation or to verify the previous formula. This quasi-Lagrange operator for the quasi-Lagrange function reproduces all polynomials of degree six, and the approximation order is given by $\mathcal{O}(h^7)$.

The results of the approximations are shown in figure 5.2. The left side reveals discontinuities in the approximations. The step size is chosen such that we can observe the discontinuity while also seeing that the approximation remains close to the function. The right side shows the corresponding error for different step sizes h. The error converges to zero, and, as expected, higher approximation orders result in faster convergence. Compared to the generalized multiquadrics in one dimension, the convergence is faster, and the evaluation is much quicker.

j	$\Psi_{3,j}(x)$
-20	$\frac{3836611631x^{10}}{1693052928000000000000} + \frac{1657351x^9}{1612431360000000000} + \frac{12533x^8}{75246796800000000} + \frac{x^7}{223948800000000}$
-19	$-\frac{1860401939x^{10}}{135444234240000000000} - \frac{401347913x^9}{45148078080000000000} - \frac{215711x^8}{94058496000000000} - \frac{x^7}{6998400000000}$
-18	$\frac{341518917727x^{10}}{4875992432640000000000} + \frac{107338279x^9}{1672151040000000000} + \frac{10675759x^8}{423263232000000000} + \frac{x^7}{331776000000} + \frac{x^6}{33592320000000}$
-17	$-\frac{16027329239x^{10}}{54177693696000000000} - \frac{17445806257x^9}{45148078080000000000} - \frac{21188063x^8}{94058496000000000} - \frac{1039x^7}{22394880000000} - \frac{x^6}{622080000000}$
-16	$\frac{108736622153x^{10}}{108355387392000000000} + \frac{5423804627x^9}{2821754880000000000} + \frac{1238233607x^8}{752467968000000000} + \frac{122687x^7}{223948800000000} + \frac{11x^6}{248832000000}$
-15	$-\frac{384286392863x^{10}}{150493593600000000000} - \frac{3147488469463x^9}{406332702720000000000} - \frac{20528299x^8}{2090188800000000} - \frac{10269179x^7}{2015539200000000} - \frac{11x^6}{13824000000} - \frac{x^5}{93312000000}$
-14	$\frac{76013405519x^{10}}{19349176320000000000} + \frac{156444480661x^9}{6449725440000000000} + \frac{15915077x^8}{335923200000000} + \frac{9864749x^7}{261273600000000} + \frac{643x^6}{62208000000} + \frac{x^5}{2073600000}$
-13	$\frac{345138200977x^{10}}{270888468480000000000} - \frac{2402256740567x^9}{45148078080000000000} - \frac{3385542767x^8}{18811699200000000} - \frac{3327919x^7}{14929920000000} - \frac{12607x^6}{124416000000} - \frac{23x^5}{2073600000}$
-12	$-\frac{397060054574903x^{10}}{14627977297920000000000} + \frac{64896621203x^9}{1254113280000000000} + \frac{343546509349x^8}{677221171200000000} + \frac{1715479x^7}{1658880000000} + \frac{1712777x^6}{2239488000000} + \frac{19x^5}{115200000} + \frac{x^4}{311040000}$
-11	$\frac{61137360457057x^{10}}{812665405440000000000} + \frac{6173374848827x^9}{45148078080000000000} - \frac{2793467743x^8}{3135283200000000} - \frac{135772133x^7}{37324800000000} - \frac{553751x^6}{124416000000} - \frac{901x^5}{518400000} - \frac{x^4}{8640000}$
-10	$-\frac{83737674221249x^{10}}{1160950579200000000000} - \frac{4510241722201x^9}{6449725440000000000} + \frac{1351409279x^8}{12541132800000000} + \frac{661205963x^7}{74649600000000} + \frac{4881563x^6}{248832000000} + \frac{69653x^5}{5184000000} + \frac{37x^4}{17280000}$
-9	$-\frac{445439239543x^{10}}{2^{25}3^85^97} + \frac{1486134651154789x^9}{2^{25}3^{12}5^{10}7} + \frac{5324833711x^8}{2^{20}3^45^97} - \frac{7031222659x^7}{2^{18}3^85^8} - \frac{71581x^6}{2^{13}9\ 5^6} - \frac{28627x^5}{2^{12}3^65^3} - \frac{x^4}{4\ 10^4} - \frac{x^3}{2^73^45^3}$
-8	$\frac{91806886293697x^{10}}{162533081088000000000} + \frac{1510073172067x^9}{11287019520000000000} - \frac{3240992618047x^8}{250822656000000000} - \frac{123372553x^7}{7464960000000} + \frac{75328891x^6}{622080000000} + \frac{653x^5}{2073600} + \frac{6919x^4}{34560000} + \frac{x^3}{48000}$
-7	$-\frac{14261621077639x^{10}}{2902376448000000000} - \frac{30610897102031x^9}{6449725440000000000} + \frac{22696245149x^8}{2239488000000000} + \frac{2032943807x^7}{20901888000000} - \frac{100709x^6}{2430000000} - \frac{88811x^5}{103680000} - \frac{599x^4}{540000} - \frac{7x^3}{24000}$
-6	$-\frac{259434565423927 01x^{10}}{29255954595840000000000} + \frac{37189247746393x^9}{5016453120000000000} + \frac{23460351116879x^8}{846526464000000000} - \frac{1241280001x^7}{8294400000000} - \frac{225287179x^6}{447897600000} + \frac{6389x^5}{5760000} + \frac{639817x^4}{155520000} + \frac{39x^3}{16000} + \frac{x^2}{7200}$
-5	$\frac{31735617344698079x^{10}}{13544423424000000000000} + \frac{120823627586903x^9}{45148078080000000000} - \frac{349844338553x^8}{4702924800000000} - \frac{5646357713x^7}{74649600000000} + \frac{32403803x^6}{24883200000} + \frac{1412243x^5}{1036800000} - \frac{24983x^4}{2880000} - \frac{5x^3}{384} - \frac{x^2}{400}$
-4	$-\frac{3612193491757729x^{10}}{5417769369600000000000} - \frac{114815386001531x^9}{5643509760000000000} + \frac{4447319038579x^8}{188116992000000000} + \frac{5117004797x^7}{9331200000000} - \frac{4649689x^6}{9953280000} - \frac{1629941x^5}{207360000} + \frac{34657x^4}{11520000} + \frac{967x^3}{24000} + \frac{19x^2}{800}$
-3	$-\frac{1105667190259501x^{10}}{3009871872\ 10^{11}} + \frac{30428765549810 21x^9}{20316635136\ 10^{10}} + \frac{99978348311x^8}{746496\ 10^9} - \frac{36152889829x^7}{80621568\ 10^6} - \frac{41026441x^6}{13824\ 10^6} + \frac{28289039x^5}{3732480000} + \frac{5269x^4}{160000} - \frac{22517x^3}{432000} - \frac{9x^2}{80} - \frac{x}{60}$
-2	$\frac{22364874466615237x^{10}}{54177693696\ 10^{11}} + \frac{94422952852243x^9}{4514807808\ 10^9} - \frac{1079186409451x^8}{6718464\ 10^9} - \frac{5665425893x^7}{8957952\ 10^6} + \frac{980282977x^6}{248832\ 10^6} + \frac{1529689x^5}{138240000} - \frac{150673x^4}{2880000} - \frac{4223x^3}{48000} + \frac{43x^2}{160} + \frac{3x}{20}$
-1	$\frac{1284093801869687x^{10}}{6772211712\ 10^{11}} - \frac{165927444008111x^9}{4514807808\ 10^9} - \frac{491661572767x^8}{6718464\ 10^9} + \frac{10568781103x^7}{8957952\ 10^6} + \frac{11033623x^6}{62208\ 10^5} - \frac{3157733x^5}{138240000} - \frac{2081x^4}{90000} + \frac{10729x^3}{48000} + \frac{23x^2}{200} - \frac{3x}{4}$
0	$-\frac{530287847809431 67x^{10}}{8707129344000000000000} + \frac{4703102954219x^8}{19349176320000000} - \frac{4180070983x^6}{671846400000} + \frac{4664791x^4}{51840000} - \frac{2107x^2}{3600} + 1$

Table 5.3: Series representation up to order ten of the quasi-Lagrange function $\Psi_{3,j}(x)$ used for the approximations.

j	$\Psi_{3,j}(x)$
1	$\frac{1284093801869687x^{10}}{677221171200000000000} + \frac{165927444008111x^9}{4514807808000000000} - \frac{491661572767x^8}{6718464000000000} - \frac{10568781103x^7}{8957952000000} + \frac{11033623x^6}{6220800000} + \frac{3157733x^5}{138240000} - \frac{2081x^4}{90000} - \frac{10729x^3}{48000} + \frac{23x^2}{200} + \frac{3x}{4}$
2	$\frac{223648744666615237x^{10}}{5417769369600000000000} - \frac{94422952852243x^9}{4514807808000000000} - \frac{1079186409451x^8}{6718464000000000} + \frac{5665425893x^7}{8957952000000} + \frac{980282977x^6}{248832000000} - \frac{1529689x^5}{138240000} - \frac{150673x^4}{2880000} + \frac{4223x^3}{48000} + \frac{43x^2}{160} - \frac{3x}{20}$
3	$-\frac{1105667190259501x^{10}}{2^{27}3^85^{11}7} - \frac{3042876554981021x^9}{2^{24}3^{11}5^{10}7} + \frac{99978348311x^8}{2^{19}3^65^9} + \frac{36152889829x^7}{2^{18}3^95^6} - \frac{41026441x^6}{2^{15}3^35^6} - \frac{28289039x^5}{2^{13}3^65^4} + \frac{5269x^4}{2^85^4} + \frac{22517x^3}{2^73^35^3} - \frac{9x^2}{80} + \frac{x}{60}$
4	$-\frac{3612193491757729x^{10}}{5417769369600000000000} + \frac{114815386001531x^9}{5643509760000000000} + \frac{4447319038579x^8}{188116992000000000} - \frac{5117004797x^7}{9331200000000} - \frac{4649689x^6}{9953280000} + \frac{1629941x^5}{207360000} + \frac{34657x^4}{11520000} - \frac{967x^3}{24000} + \frac{19x^2}{800}$
5	$\frac{31735617344698079x^{10}}{13544423424000000000000} - \frac{120823627586903x^9}{45148078080000000000} - \frac{349844338553x^8}{4702924800000000} + \frac{5646357713x^7}{74649600000000} + \frac{32403803x^6}{24883200000} - \frac{1412243x^5}{1036800000} - \frac{24983x^4}{2880000} + \frac{5x^3}{384} - \frac{x^2}{400}$
6	$-\frac{25943456542392701x^{10}}{29255954595840000000000} - \frac{37189247746393x^9}{5016453120000000000} + \frac{23460351116879x^8}{846526464000000000} + \frac{1241280001x^7}{8294400000000} - \frac{225287179x^6}{447897600000} - \frac{6389x^5}{5760000} + \frac{639817x^4}{155520000} - \frac{39x^3}{16000} + \frac{x^2}{7200}$
7	$-\frac{14261621077639x^{10}}{29023764480000000000} + \frac{30610897102031x^9}{6449725440000000000} + \frac{22696245149x^8}{2239488000000000} - \frac{2032943807x^7}{20901888000000} - \frac{100709x^6}{2430000000} + \frac{88811x^5}{103680000} - \frac{599x^4}{540000} + \frac{7x^3}{24000}$
8	$\frac{91806886293697x^{10}}{162533081088000000000} - \frac{1510073172067x^9}{11287019520000000000} - \frac{3240992618047x^8}{250822656000000000} + \frac{123372553x^7}{7464960000000} + \frac{75328891x^6}{622080000000} - \frac{653x^5}{2073600} + \frac{6919x^4}{34560000} - \frac{x^3}{48000}$
9	$-\frac{445439239543x^{10}}{3009871872000000000} - \frac{1486134651154789x^9}{1218998108160000000000} + \frac{5324833711x^8}{1161216000000000} + \frac{7031222659x^7}{671846400000000} - \frac{71581x^6}{1152000000} + \frac{28627x^5}{373248000} - \frac{x^4}{40000} + \frac{x^3}{1296000}$
10	$-\frac{83737674221249x^{10}}{1160950579200000000000} + \frac{4510241722201x^9}{6449725440000000000} + \frac{1351409279x^8}{12541132800000000} - \frac{661205963x^7}{74649600000000} + \frac{4881563x^6}{248832000000} - \frac{69653x^5}{5184000000} + \frac{37x^4}{17280000}$
11	$\frac{61137360457057x^{10}}{812665405440000000000} - \frac{6173374848827x^9}{45148078080000000000} - \frac{2793467743x^8}{3135283200000000} + \frac{135772133x^7}{37324800000000} - \frac{553751x^6}{124416000000} + \frac{901x^5}{518400000} - \frac{x^4}{8640000}$
12	$-\frac{397060054574903x^{10}}{14627977297920000000000} - \frac{64896621203x^9}{1254113280000000000} + \frac{343546509349x^8}{677221171200000000} - \frac{1715479x^7}{16588800000000} + \frac{1712777x^6}{2239488000000} - \frac{19x^5}{115200000} + \frac{x^4}{311040000}$
13	$\frac{345138200977x^{10}}{270888468480000000000} + \frac{2402256740567x^9}{45148078080000000000} - \frac{3385542767x^8}{18811699200000000} + \frac{3327919x^7}{14929920000000} - \frac{12607x^6}{124416000000} + \frac{23x^5}{2073600000}$
14	$\frac{76013405519x^{10}}{19349176320000000000} - \frac{156444480661x^9}{6449725440000000000} + \frac{15915077x^8}{335923200000000} - \frac{9864749x^7}{261273600000000} + \frac{643x^6}{62208000000} - \frac{x^5}{2073600000}$
15	$-\frac{384286392863x^{10}}{150493593600000000000} + \frac{3147488469463x^9}{406332702720000000000} - \frac{20528299x^8}{2090188800000000} + \frac{10269179x^7}{2015539200000000} - \frac{11x^6}{13824000000} + \frac{x^5}{93312000000}$
16	$\frac{108736622153x^{10}}{108355387392000000000} - \frac{5423804627x^9}{282175488000000000} + \frac{1238233607x^8}{752467968000000000} - \frac{122687x^7}{223948800000000} + \frac{11x^6}{248832000000}$
17	$-\frac{16027329239x^{10}}{541776936960000000000} + \frac{17445806257x^9}{45148078080000000000} - \frac{21188063x^8}{940584960000000000} + \frac{1039x^7}{22394880000000} - \frac{x^6}{622080000000}$
18	$\frac{341518917727x^{10}}{4875992432640000000000} - \frac{107338279x^9}{1672151040000000000} + \frac{10675759x^8}{423263232000000000} - \frac{x^7}{331776000000} + \frac{x^6}{33592320000000}$
19	$-\frac{1860401939x^{10}}{135444234240000000000} + \frac{401347913x^9}{45148078080000000000} - \frac{215711x^8}{94058496000000000} + \frac{x^7}{6998400000000}$
20	$\frac{3836611631x^{10}}{1693052928000000000000} - \frac{1657351x^9}{1612431360000000000} + \frac{12533x^8}{752467968000000000} - \frac{x^7}{223948800000000}$

Table 5.4: Series representation up to order ten of the quasi-Lagrange function $\Psi_{3,j}(x)$ used for the approximations.

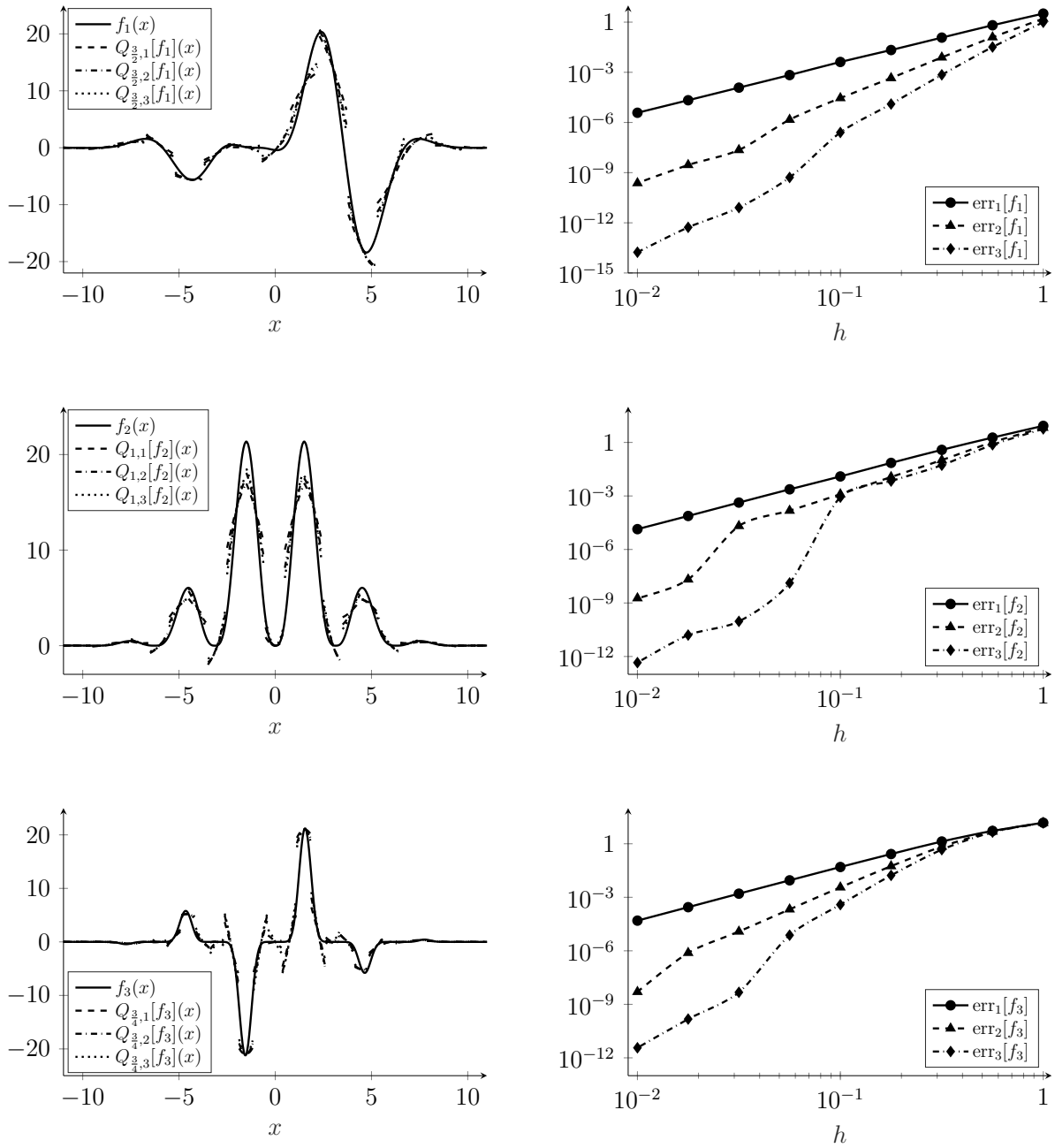

Figure 5.2: The left side shows the test functions $f(x)$ together with their associated approximants. The right side displays the error of the approxmants with respect to the test functions.

5.2 Examples in 2D: Generalized Thin Plate Spline

As in the one-dimensional case, we use three similar test functions. For $x \in \mathbb{R}^2$, we have

$$\begin{aligned} f_1(x) &= \mathrm{e}^{-\frac{\|x\|^2}{10}} \cos\left(\left\|x - \begin{pmatrix}2\\2\end{pmatrix}\right\|\right) \cdot \left\|x - \begin{pmatrix}1\\1\end{pmatrix}\right\|^3, \\ f_2(x) &= 25\,\mathrm{e}^{-\frac{\|x\|^2}{15}} \left|\sin\left(\|x\|\right)\right|^3, \\ f_3(x) &= 25\,\mathrm{e}^{-\frac{\|x\|^2}{15}} \left|\sin\left(\|x\|\right)\right| \sin\left(\|x\|\right)^9. \end{aligned}$$

The error between the test functions and the approximants is measured by

$$\mathrm{err}[f] = \left(\int_{[-10,10]^2} \left(f(x) - Q_h[f](x)\right)^2 \mathrm{d}x\right)^{\frac{1}{2}}.$$

The most promising case for quasi-interpolation is for $\lambda, \beta \in 2\mathbb{N}$. To be more specific, we use the following three RBFs

$$\begin{aligned} \varphi_1(r) &= \left(c^2 + r^2\right) \log\left(c^2 + r^2\right), \\ \varphi_2(r) &= \left(c^4 + r^4\right) \log\left(c^4 + r^4\right), \\ \varphi_3(r) &= \left(c^6 + r^6\right) \log\left(c^6 + r^6\right). \end{aligned}$$

The first RBF is the classical thin plate spline, which represents the classical results, while the others are our new generalizations to test for practical purposes. For simplicity and to provide explicit coefficients, we use gridded data. The quasi-Lagrange function for the classical thin plate spline is given by

$$\Psi_1(x) = \sum_{\|k\|_1 \le 3} \mu_k \varphi_1(||x - k||), \qquad x \in \mathbb{R}^2, c \in \mathbb{R}, k \in \mathbb{Z}^2.$$

The used coefficients are

$$\begin{aligned} \frac{-3c^2 - 2}{192\pi} &= \mu_{\binom{3}{0}} = \mu_{\binom{-3}{0}} = \mu_{\binom{0}{3}} = \mu_{\binom{0}{-3}}, \\ \frac{-9c^2 - 2}{192\pi} &= \mu_{\binom{2}{1}} = \mu_{\binom{-2}{1}} = \mu_{\binom{2}{-1}} = \mu_{\binom{-2}{-1}} = \mu_{\binom{1}{2}} = \mu_{\binom{-1}{2}} = \mu_{\binom{1}{-2}} = \mu_{\binom{-1}{-2}}, \\ \frac{9c^2 + 7}{48\pi} &= \mu_{\binom{2}{0}} = \mu_{\binom{-2}{0}} = \mu_{\binom{0}{2}} = \mu_{\binom{0}{-2}}, \\ \frac{9c^2 + 5}{24\pi} &= \mu_{\binom{1}{1}} = \mu_{\binom{-1}{1}} = \mu_{\binom{1}{-1}} = \mu_{\binom{-1}{-1}}, \end{aligned}$$

$$\begin{aligned}\frac{-171c^2-154}{192\pi} &= \mu_{\binom{1}{0}} = \mu_{\binom{-1}{0}} = \mu_{\binom{0}{1}} = \mu_{\binom{0}{-1}},\\ \frac{21c^2+23}{12\pi} &= \mu_{\binom{0}{0}}.\end{aligned}$$

With these coefficients, we find that $\Psi_1(x) \in \mathcal{O}\left((1+||x||)^{-6}\right)$ as $||x|| \to \infty$. Furthermore, the polynomial reproduction is exact for all polynomials of degree three, and the approximation order is given by $||Q_h f - f||_\infty = \mathcal{O}\left(h^4 \log(1/h)\right)$ as $h \to 0$.

The second quasi-Lagrange function is given by

$$\Psi_2(x) = \sum_{\|k\|_1 \leq 6} \mu_k \varphi_2(||x-k||), \qquad x \in \mathbb{R}^2, c \in \mathbb{R}, k \in \mathbb{Z}^2,$$

with the coefficients

$$\begin{aligned}\frac{-63\pi c^6+315c^4-556}{24772608\pi} &= \mu_{\binom{6}{0}} = \mu_{\binom{-6}{0}} = \mu_{\binom{0}{6}} = \mu_{\binom{0}{-6}},\\ \frac{-315\pi c^6+1050c^4-656}{20643840\pi} &= \mu_{\binom{5}{1}} = \mu_{\binom{-5}{1}} = \mu_{\binom{5}{-1}} = \mu_{\binom{-5}{-1}},\\ &= \mu_{\binom{1}{5}} = \mu_{\binom{-1}{5}} = \mu_{\binom{1}{-5}} = \mu_{\binom{-1}{-5}},\\ \frac{315\pi c^6-1470c^4+2264}{5160960\pi} &= \mu_{\binom{5}{0}} = \mu_{\binom{-5}{0}} = \mu_{\binom{0}{5}} = \mu_{\binom{0}{-5}},\\ \frac{-105\pi c^6+245c^4-68}{2752512\pi} &= \mu_{\binom{4}{2}} = \mu_{\binom{-4}{2}} = \mu_{\binom{4}{-2}} = \mu_{\binom{-4}{-2}},\\ &= \mu_{\binom{2}{4}} = \mu_{\binom{-2}{4}} = \mu_{\binom{2}{-4}} = \mu_{\binom{-2}{-4}},\\ \frac{1575\pi c^6-5250c^4+3032}{5160960\pi} &= \mu_{\binom{4}{1}} = \mu_{\binom{-4}{1}} = \mu_{\binom{4}{-1}} = \mu_{\binom{-4}{-1}},\\ &= \mu_{\binom{1}{4}} = \mu_{\binom{-1}{4}} = \mu_{\binom{1}{-4}} = \mu_{\binom{-1}{-4}},\\ \frac{-1035\pi c^6+4425c^4-6124}{1474560\pi} &= \mu_{\binom{4}{0}} = \mu_{\binom{-4}{0}} = \mu_{\binom{0}{4}} = \mu_{\binom{0}{-4}},\\ \frac{-75\pi c^6+150c^4-32}{1474560\pi} &= \mu_{\binom{3}{3}} = \mu_{\binom{-3}{3}} = \mu_{\binom{3}{-3}} = \mu_{\binom{-3}{-3}},\\ \frac{525\pi c^6-1400c^4+408}{860160\pi} &= \mu_{\binom{3}{2}} = \mu_{\binom{-3}{2}} = \mu_{\binom{3}{-2}} = \mu_{\binom{-3}{-2}},\\ &= \mu_{\binom{2}{3}} = \mu_{\binom{-2}{3}} = \mu_{\binom{2}{-3}} = \mu_{\binom{-2}{-3}},\\ \frac{-3675\pi c^6+12530c^4-7536}{1376256\pi} &= \mu_{\binom{3}{1}} = \mu_{\binom{-3}{1}} = \mu_{\binom{3}{-1}} = \mu_{\binom{-3}{-1}},\\ &= \mu_{\binom{1}{3}} = \mu_{\binom{-1}{3}} = \mu_{\binom{1}{-3}} = \mu_{\binom{-1}{-3}},\\ \frac{10575\pi c^6-42750c^4+56632}{2211840\pi} &= \mu_{\binom{3}{0}} = \mu_{\binom{-3}{0}} = \mu_{\binom{0}{3}} = \mu_{\binom{0}{-3}},\end{aligned}$$

$$
\begin{aligned}
\frac{-975\pi c^6+3025c^4-1204}{245760\pi} &= \mu_{\binom{2}{2}} = \mu_{\binom{-2}{2}} = \mu_{\binom{2}{-2}} = \mu_{\binom{-2}{-2}},\\
\frac{5\left(441\pi c^6-1596c^4+1240\right)}{172032\pi} &= \mu_{\binom{2}{1}} = \mu_{\binom{-2}{1}} = \mu_{\binom{2}{-1}} = \mu_{\binom{-2}{-1}},\\
&= \mu_{\binom{1}{2}} = \mu_{\binom{-1}{2}} = \mu_{\binom{1}{-2}} = \mu_{\binom{-1}{-2}},\\
\frac{-276675\pi c^6+1117375c^4-1546588}{13762560\pi} &= \mu_{\binom{2}{0}} = \mu_{\binom{-2}{0}} = \mu_{\binom{0}{2}} = \mu_{\binom{0}{-2}},\\
\frac{-17175\pi c^6+67750c^4-77568}{491520\pi} &= \mu_{\binom{1}{1}} = \mu_{\binom{-1}{1}} = \mu_{\binom{1}{-1}} = \mu_{\binom{-1}{-1}},\\
\frac{21945\pi c^6-92750c^4+150536}{430080\pi} &= \mu_{\binom{1}{0}} = \mu_{\binom{-1}{0}} = \mu_{\binom{0}{1}} = \mu_{\binom{0}{-1}},\\
\frac{-26715\pi c^6+118545c^4-235804}{368640\pi} &= \mu_{\binom{0}{0}}.
\end{aligned}
$$

With these coefficients, we find that $\Psi_2(x) \in \mathcal{O}\left((1+||x||)^{-10}\right)$ as $||x|| \to \infty$. Furthermore, the polynomial reproduction is given for all polynomials of degree five and the approximation order is determined by $||Q_h f - f||_\infty = \mathcal{O}\left(h^6\right)$ for $h \to 0$.

The last example of a quasi-Lagrange function is given by

$$
\Psi_3(x) = \sum_{\|k\|_1 \le 9} \mu_k \varphi_3(||x-k||), \qquad x \in \mathbb{R}^2, c \in \mathbb{R}, k \in \mathbb{Z}^2,
$$

with the coefficients

$$
\begin{aligned}
-\frac{c^{10}}{2^{22}3^5 5\sqrt{3}} + \frac{c^8}{2^{20}3^6\sqrt{3}} - \frac{161c^6}{2^{22}3^7 5\pi} - \frac{4679}{2^{16}3^8 5^2 11\pi} &= \mu_{\binom{9}{0}} = \mu_{\binom{-9}{0}} = \mu_{\binom{0}{9}} = \mu_{\binom{0}{-9}},\\
-\frac{c^{10}}{2^{22}3^3 5\sqrt{3}} + \frac{7c^8}{2^{20}3^6\sqrt{3}} - \frac{287c^6}{2^{22}3^6 5\pi} - \frac{4201}{2^{16}3^7 385\pi} &= \mu_{\binom{8}{1}} = \mu_{\binom{-8}{1}} = \mu_{\binom{8}{-1}} = \mu_{\binom{-8}{-1}}\\
&= \mu_{\binom{1}{8}} = \mu_{\binom{-1}{8}} = \mu_{\binom{1}{-8}} = \mu_{\binom{-1}{-8}},\\
\frac{c^{10}}{2^{20}3^3 5\sqrt{3}} - \frac{67c^8}{2^{21}3^6\sqrt{3}} + \frac{7c^6}{2^{18}3^5\pi} + \frac{381511}{2^{18}3^6 5^2 77\pi} &= \mu_{\binom{8}{0}} = \mu_{\binom{-8}{0}} = \mu_{\binom{0}{8}} = \mu_{\binom{0}{-8}},\\
-\frac{c^{10}}{2^{20}3^3 5\sqrt{3}} + \frac{11c^8}{2^{19}3^6\sqrt{3}} - \frac{35c^6}{2^{20}3^6\pi} - \frac{5221}{2^{14}3^7 5^2 77\pi} &= \mu_{\binom{7}{2}} = \mu_{\binom{-7}{2}} = \mu_{\binom{7}{-2}} = \mu_{\binom{-7}{-2}}\\
&= \mu_{\binom{2}{7}} = \mu_{\binom{-2}{7}} = \mu_{\binom{2}{-7}} = \mu_{\binom{-2}{-7}},\\
\frac{c^{10}}{2^{17}3^3 5\sqrt{3}} - \frac{53c^8}{2^{18}3^6\sqrt{3}} + \frac{343c^6}{2^{19}3^5 5\pi} + \frac{10777}{2^{12}3^6 5^2 77\pi} &= \mu_{\binom{7}{1}} = \mu_{\binom{-7}{1}} = \mu_{\binom{7}{-1}} = \mu_{\binom{-7}{-1}}\\
&= \mu_{\binom{1}{7}} = \mu_{\binom{-1}{7}} = \mu_{\binom{1}{-7}} = \mu_{\binom{-1}{-7}},\\
-\frac{73c^{10}}{2^{22}3^3 5\sqrt{3}} + \frac{557c^8}{2^{20}3^6\sqrt{3}} - \frac{1717c^6}{2^{22}3^5\pi} - \frac{1210057}{2^{16}3^6 5^2 77\pi} &= \mu_{\binom{7}{0}} = \mu_{\binom{-7}{0}} = \mu_{\binom{0}{7}} = \mu_{\binom{0}{-7}},
\end{aligned}
$$

$$-\frac{7c^{10}}{2^{20}3^4 5\sqrt{3}}+\frac{7c^8}{2^{19}3^5\sqrt{3}}-\frac{91c^6}{2^{20}3^5 5\pi}-\frac{6763}{2^{13}3^8 5^2 77\pi}=\mu_{\binom{6}{3}}=\mu_{\binom{-6}{3}}=\mu_{\binom{6}{-3}}=\mu_{\binom{-6}{-3}}$$
$$=\mu_{\binom{3}{6}}=\mu_{\binom{-3}{6}}=\mu_{\binom{3}{-6}}=\mu_{\binom{-3}{-6}},$$
$$\frac{7c^{10}}{2^{18}3^3 5\sqrt{3}}-\frac{301c^8}{2^{19}3^6\sqrt{3}}+\frac{581c^6}{2^{17}3^6 5\pi}+\frac{502037}{2^{16}3^7 5^2 77\pi}=\mu_{\binom{6}{2}}=\mu_{\binom{-6}{2}}=\mu_{\binom{6}{-2}}=\mu_{\binom{-6}{-2}}$$
$$=\mu_{\binom{2}{6}}=\mu_{\binom{-2}{6}}=\mu_{\binom{2}{-6}}=\mu_{\binom{-2}{-6}},$$
$$-\frac{121c^{10}}{2^{20}3^3 5\sqrt{3}}+\frac{1519c^8}{2^{19}3^6\sqrt{3}}-\frac{5621c^6}{2^{20}3^6\pi}-\frac{387041}{2^{12}3^7 5^2 77\pi}=\mu_{\binom{6}{1}}=\mu_{\binom{-6}{1}}=\mu_{\binom{6}{-1}}=\mu_{\binom{-6}{-1}}$$
$$=\mu_{\binom{1}{6}}=\mu_{\binom{-1}{6}}=\mu_{\binom{1}{-6}}=\mu_{\binom{-1}{-6}},$$
$$\frac{c^{10}}{2^{13}3^4\sqrt{3}}-\frac{31c^8}{2^{14}3^5\sqrt{3}}+\frac{7931c^6}{2^{17}3^6 5\pi}+\frac{4465757}{2^{14}3^8 385\pi}=\mu_{\binom{6}{0}}=\mu_{\binom{-6}{0}}=\mu_{\binom{0}{6}}=\mu_{\binom{0}{-6}},$$
$$-\frac{7c^{10}}{2^{21}3^3 5\sqrt{3}}+\frac{7c^8}{2^{17}3^6\sqrt{3}}-\frac{217c^6}{2^{21}3^5 5\pi}-\frac{5}{2^{14}3^6 7\pi}=\mu_{\binom{5}{4}}=\mu_{\binom{-5}{4}}=\mu_{\binom{5}{-4}}=\mu_{\binom{-5}{-4}}$$
$$=\mu_{\binom{4}{5}}=\mu_{\binom{-4}{5}}=\mu_{\binom{4}{-5}}=\mu_{\binom{-4}{-5}},$$
$$\frac{7c^{10}}{2^{17}3^3 5\sqrt{3}}-\frac{259c^8}{2^{18}3^6\sqrt{3}}+\frac{679c^6}{2^{19}3^6\pi}+\frac{6863}{2^{10}3^7 5^2 77\pi}=\mu_{\binom{5}{3}}=\mu_{\binom{-5}{3}}=\mu_{\binom{5}{-3}}=\mu_{\binom{-5}{-3}}$$
$$=\mu_{\binom{3}{5}}=\mu_{\binom{-3}{5}}=\mu_{\binom{3}{-5}}=\mu_{\binom{-3}{-5}},$$
$$-\frac{119c^{10}}{2^{20}3^2 5\sqrt{3}}+\frac{1267c^8}{2^{19}3^5\sqrt{3}}-\frac{11627c^6}{2^{20}3^6\pi}-\frac{1482043}{2^{14}3^7 5^2 77\pi}=\mu_{\binom{5}{2}}=\mu_{\binom{-5}{2}}=\mu_{\binom{5}{-2}}=\mu_{\binom{-5}{-2}}$$
$$=\mu_{\binom{2}{5}}=\mu_{\binom{-2}{5}}=\mu_{\binom{2}{-5}}=\mu_{\binom{-2}{-5}},$$
$$\frac{7c^{10}}{2^{15}3^3\sqrt{3}}-\frac{1687c^8}{2^{16}3^6\sqrt{3}}+\frac{30121c^6}{2^{17}3^6 5\pi}+\frac{604273}{2^{12}3^7 385\pi}=\mu_{\binom{5}{1}}=\mu_{\binom{-5}{1}}=\mu_{\binom{5}{-1}}=\mu_{\binom{-5}{-1}}$$
$$=\mu_{\binom{1}{5}}=\mu_{\binom{-1}{5}}=\mu_{\binom{1}{-5}}=\mu_{\binom{-1}{-5}},$$
$$-\frac{143c^{10}}{2^{18}3^2 5\sqrt{3}}+\frac{155c^8}{2^{15}3^4\sqrt{3}}-\frac{44471c^6}{2^{19}3^6\pi}-\frac{1780567}{2^{14}3^7 77\pi}=\mu_{\binom{5}{0}}=\mu_{\binom{-5}{0}}=\mu_{\binom{0}{5}}=\mu_{\binom{0}{-5}},$$
$$\frac{7c^{10}}{2^{19}3^3\sqrt{3}}-\frac{1225c^8}{2^{20}3^6\sqrt{3}}+\frac{7c^6}{2^{17}3^3\pi}+\frac{25247}{2^{17}3^6 5^2 7\pi}=\mu_{\binom{4}{4}}=\mu_{\binom{-4}{4}}=\mu_{\binom{4}{-4}}=\mu_{\binom{-4}{-4}},$$
$$-\frac{1183c^{10}}{2^{21}3^3 5\sqrt{3}}+\frac{2863c^8}{2^{18}3^6\sqrt{3}}-\frac{156611c^6}{2^{21}3^6 5\pi}-\frac{121063}{2^{14}3^7 5^2 7\pi}=\mu_{\binom{4}{3}}=\mu_{\binom{-4}{3}}=\mu_{\binom{4}{-3}}=\mu_{\binom{-4}{-3}}$$
$$=\mu_{\binom{3}{4}}=\mu_{\binom{-3}{4}}=\mu_{\binom{3}{-4}}=\mu_{\binom{-3}{-4}},$$
$$\frac{7c^{10}}{2^{13}3^2 5\sqrt{3}}-\frac{301c^8}{2^{14}3^5\sqrt{3}}+\frac{56021c^6}{2^{17}3^6 5\pi}+\frac{11594689}{2^{14}3^7 5^2 77\pi}=\mu_{\binom{4}{2}}=\mu_{\binom{-4}{2}}=\mu_{\binom{4}{-2}}=\mu_{\binom{-4}{-2}}$$
$$=\mu_{\binom{2}{4}}=\mu_{\binom{-2}{4}}=\mu_{\binom{2}{-4}}=\mu_{\binom{-2}{-4}},$$
$$-\frac{1729c^{10}}{2^{18}3^3 5\sqrt{3}}+\frac{10213c^8}{2^{16}3^6\sqrt{3}}-\frac{143549c^6}{2^{19}3^6\pi}-\frac{69871601}{2^{14}3^7 5^2 77\pi}=\mu_{\binom{4}{1}}=\mu_{\binom{-4}{1}}=\mu_{\binom{4}{-1}}=\mu_{\binom{-4}{-1}}$$

$$
\begin{aligned}
&= \mu_{\binom{1}{4}} = \mu_{\binom{-1}{4}} = \mu_{\binom{1}{-4}} = \mu_{\binom{-1}{-4}},\\
\frac{203c^{10}}{2^{16}3^2 5\sqrt{3}} - \frac{10129c^8}{2^{17}3^5\sqrt{3}} + \frac{14483c^6}{2^{15}3^6\pi} + \frac{207731443}{2^{14}3^7 5^2 77\pi} &= \mu_{\binom{4}{0}} = \mu_{\binom{-4}{0}} = \mu_{\binom{0}{4}} = \mu_{\binom{0}{-4}},\\
\frac{133c^{10}}{2^{16}3^4\sqrt{3}} - \frac{1015c^8}{2^{17}3^4\sqrt{3}} + \frac{8953c^6}{2^{18}3^5\pi} + \frac{93007}{2^9 3^8 5^2 7\pi} &= \mu_{\binom{3}{3}} = \mu_{\binom{-3}{3}} = \mu_{\binom{3}{-3}} = \mu_{\binom{-3}{-3}},\\
-\frac{6503c^{10}}{2^{19}3^3 5\sqrt{3}} + \frac{72023c^8}{2^{18}3^6\sqrt{3}} - \frac{7259c^6}{2^{14}3^6\pi} - \frac{6257149}{2^{14}3^7 5^2 7\pi} &= \mu_{\binom{3}{2}} = \mu_{\binom{-3}{2}} = \mu_{\binom{3}{-2}} = \mu_{\binom{-3}{-2}}\\
&= \mu_{\binom{2}{3}} = \mu_{\binom{-2}{3}} = \mu_{\binom{2}{-3}} = \mu_{\binom{-2}{-3}},\\
\frac{917c^{10}}{2^{15}3^3 5\sqrt{3}} - \frac{43505c^8}{2^{16}3^6\sqrt{3}} + \frac{154147c^6}{2^{17}3^6\pi} + \frac{80673911}{2^{12}3^7 5^2 77\pi} &= \mu_{\binom{3}{1}} = \mu_{\binom{-3}{1}} = \mu_{\binom{3}{-1}} = \mu_{\binom{-3}{-1}}\\
&= \mu_{\binom{1}{3}} = \mu_{\binom{-1}{3}} = \mu_{\binom{1}{-3}} = \mu_{\binom{-1}{-3}},\\
-\frac{29407c^{10}}{2^{18}3^4 5\sqrt{3}} + \frac{5033c^8}{2^{14}3^5\sqrt{3}} - \frac{907879c^6}{2^{19}3^6\pi} - \frac{2357310013}{2^{14}3^8 5^2 77\pi} &= \mu_{\binom{3}{0}} = \mu_{\binom{-3}{0}} = \mu_{\binom{0}{3}} = \mu_{\binom{0}{-3}},\\
\frac{5173c^{10}}{2^{17}3^3 5\sqrt{3}} - \frac{239687c^8}{2^{18}3^6\sqrt{3}} + \frac{102571c^6}{2^{16}3^6\pi} + \frac{60754949}{2^{15}3^7 5^2 7\pi} &= \mu_{\binom{2}{2}} = \mu_{\binom{-2}{2}} = \mu_{\binom{2}{-2}} = \mu_{\binom{-2}{-2}},\\
-\frac{42763c^{10}}{2^{19}3^3 5\sqrt{3}} + \frac{519365c^8}{2^{18}3^6\sqrt{3}} - \frac{26383c^6}{2^{16}3^4\pi} - \frac{7346527}{2^{14}3^6 35\pi} &= \mu_{\binom{2}{1}} = \mu_{\binom{-2}{1}} = \mu_{\binom{2}{-1}} = \mu_{\binom{-2}{-1}}\\
&= \mu_{\binom{1}{2}} = \mu_{\binom{-1}{2}} = \mu_{\binom{1}{-2}} = \mu_{\binom{-1}{-2}},\\
\frac{863c^{10}}{2^{13}3^3 5\sqrt{3}} - \frac{43061c^8}{2^{14}3^6\sqrt{3}} + \frac{218869c^6}{2^{17}3^5\pi} + \frac{270458603}{2^{14}3^5 5^2 77\pi} &= \mu_{\binom{2}{0}} = \mu_{\binom{-2}{0}} = \mu_{\binom{0}{2}} = \mu_{\binom{0}{-2}},\\
\frac{10469c^{10}}{2^{16}3^3 5\sqrt{3}} - \frac{525049c^8}{2^{17}3^6\sqrt{3}} + \frac{2006669c^6}{2^{18}3^6\pi} + \frac{39058291}{2^{11}3^7 5^2 7\pi} &= \mu_{\binom{1}{1}} = \mu_{\binom{-1}{1}} = \mu_{\binom{1}{-1}} = \mu_{\binom{-1}{-1}},\\
-\frac{212041c^{10}}{2^{20}3^3 5\sqrt{3}} + \frac{1355111c^8}{2^{18}3^6\sqrt{3}} - \frac{3555559c^6}{2^{20}3^5\pi} - \frac{3706471}{2^{10}3^5 5^2 7\pi} &= \mu_{\binom{1}{0}} = \mu_{\binom{-1}{0}} = \mu_{\binom{0}{1}} = \mu_{\binom{0}{-1}},\\
\frac{599569c^{10}}{2^{18}3^5 5\sqrt{3}} - \frac{3460955c^8}{2^{19}3^6\sqrt{3}} + \frac{2615419c^6}{2^{16}3^7\pi} + \frac{399291565}{2^{16}3^8 7\pi} &= \mu_{\binom{0}{0}}.
\end{aligned}
$$

With these coefficients, we find that $\Psi_3(x) \in \mathcal{O}\left((1+||x||)^{-14}\right)$ as $x \to \infty$. Furthermore, the polynomial reproduction is given for all polynomials of degree seven and the approximation order is determined by $||Q_h f - f||_\infty = \mathcal{O}\left(h^8\right)$ for $h \to 0$.

The results with these approximants are shown in Figure 5.3. The results support the theory. For small h, numerical errors lead to issues in the evaluation of the quasi-Lagrange function, as each summand grows larger while the sum itself decays to zero. This effect becomes more pronounced for higher values of λ. For small grid sizes h, the effect becomes dominant so that the error no longer decreases significantly. As in the 1D case, the decay rate of the errors $\mathrm{err}_2[f_2]$ and $\mathrm{err}_3[f_2]$ are the same. This occurs

because the function $f_2 \in C^2(\mathbb{R}^2)$ is not smooth enough and therefore does not meet the conditions required by the Strang and Fix conditions.

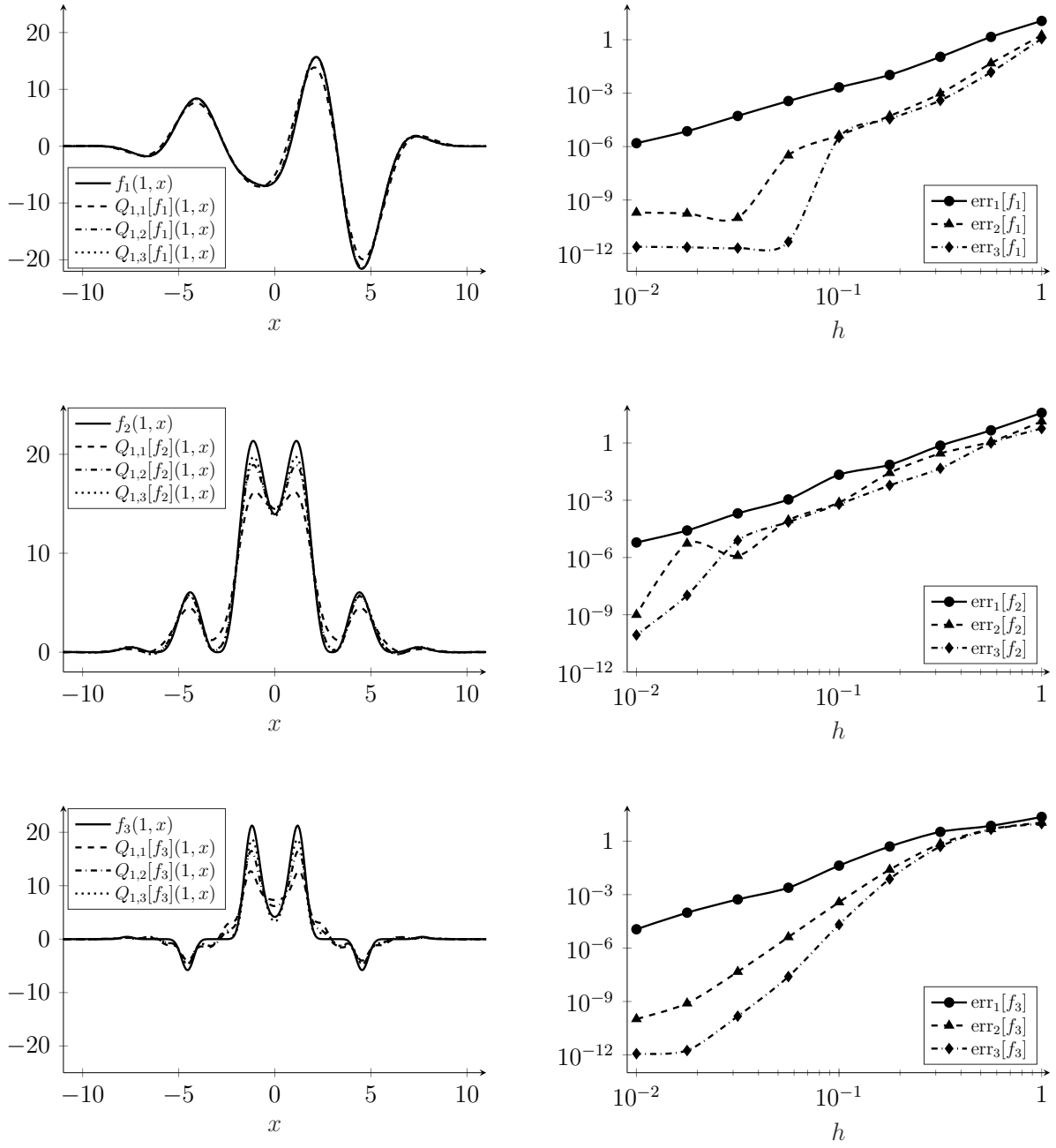

Figure 5.3:
The left side shows a slice of the test functions $f(1,x)$, along with their corresponding approximants. For all approximants, the parameters $c = 1$ and $h = 1$ were used. The right side displays the approximation error with respect to the test functions, integrated over the entire two-dimensional domain.

5.3 Summary

In this chapter, we presented three numerical examples. Each example was tested using three different test functions, representing various classes of differentiability. Furthermore, we provided the exact coeffiencts, such that the results can be verified and tested against other approximations methods.

In the one-dimensional case we demonstrated that the class of generalized multiquadrics outperformed the classical multiquadric for all test functions. As expected, the numerical results confirmed that higher approximation orders led to faster error decay.

The second one-dimensional example focused on the Bessel approach. The results confirmed the expected behavior of approximation orders again. Compared to the generalized multiquadrics, the Bessel method yielded even better accuracy while requiring less computational effort. These results make the approach even more interesting for further analysis.

Finally, we examined a two-dimensional example using the class of generalized thin plate splines. As anticipated, higher approximation orders generally improved the results. However, the error did not decrease significantly for larger values of λ, due to numerical instabilities. Additionally, the differentiability of the test function influenced the outcome. Higher approximation orders did not always lead to improved accuracy in cases where the test function lacked sufficient smoothness.

In conclusion, the theoretical introduced generalizations were validated by the numerical experiments, consistently yielding superior practical performance over the classical methods.

Chapter 6

Summary and Future Work

In this thesis, we introduced two new classes of RBFs for quasi-interpolation. Our approach led to significant results, including improved approximation orders and uniform convergence. In particular, we carried out the following steps, which are also of interest for other applications.

- We derived an integral representation of the generalized Fourier transform for a broad class of RBFs. The results were verified against several special cases from the literature. Additionally, we introduced a new generalized multiquadric and a new generalized thin plate spline and calculated their Fourier transforms.

- With the explicit integral representation of the generalized Fourier transform, we were able to determine its asymptotic behavior for both, small and large arguments. We demonstrated how to extract this information in general and proceeded to analyze the asymptotic behavior of the Fourier transform for the newly introduced generalized multiquadric and generalized thin plate spline. We distinguished between several cases, ultimately excluding some because they were not suitable for quasi-interpolation.

- For the usable cases, we applied the Strang and Fix conditions to determine the approximation order. We demonstrated how different parameters of our newly introduced generalizations impact the approximation order and explored how to adjust these parameters to improve it. The generality of these steps enabled the efficient determination of the approximation order for other RBF classes as well.

- We further introduced a new class of non-RBFs for quasi-interpolation with the Bessel function $J_\nu(x)$ serving as a representative of this class. To the best of

our knowledge, we demonstrated that the Bessel function can be used for quasi-interpolation for the first time. Additionally, we derived the approximation order and demonstrated an improvement through the modification of the Bessel function. Using these functions, we also demonstrated how to handle scattered data and efficiently evaluate the approximant.

- Finally, we verified the achieved results through numerical examples in one and two dimensions. For this purpose, we explicitly provided the coefficients used for the quasi-Lagrange function, enabling others to verify the results or compare them to other approximation methods.

We summarized the development of a methodology that enables the efficient determination of the approximation order for quasi-interpolation. Additionally, we enhanced the understanding of how different parameters impact the approximation order. Based on these results, the question arises whether there are other, potentially better RBFs that offer superior approximation properties compared to the examples we used for our demonstration. There exist many other functions, like the Dagum-function $\varphi(r) = 1 - \left(\frac{r^\beta}{1+r^\beta}\right)^\gamma, r \geq 0$ which can be used for quasi-interpolation [13]. Further generalizations of these functions may lead to improved or more efficient quasi-interpolation approximations.

The use of the Bessel function as a non-RBF quasi-Lagrange function was entirely novel. This work demonstrated, that the approach is not only possible, but also efficient. However, several open questions remain in this area. Can we further extend the class of Bessel functions, along with their modifications, to achieve better approximation orders? The efficient evaluation was only possible with the trade-off that the approximant was not continuous. Can we overcome this issue? Finally, is there a more elegant method for extending the results to higher dimensions than the tensor product? These represent some of the open questions we intend to explore in future work.

List of Figures

List of Tables

List of Symbols

Number Sets

$2\mathbb{N}$	The even natural numbers including zero
$2\mathbb{N}+1$	The odd natural numbers
$\mathbb{C}$	The complex numbers
$\emptyset$	The empty set
$\mathbb{N}$	The natural numbers including zero
$\mathbb{R}$	The real numbers
$\mathbb{R}^n$	The real vectors of dimension n
$\mathbb{R}_+$	The positive real numbers excluding zero
Ξ	Quasi-uniform set
$\mathbb{Z}$	The integers
$\mathbb{Z}^n$	The integer vectors of dimension n

Functions

$\delta(\cdot)$	Dirac Delta-distribution
$\Delta_{2\pi}(\cdot)$	Dirac comb with period 2π
$\delta_{i,j}$	Kronecker delta
Γ	Gamma function
$\hat{f}$	Fourier transform of the function f

$\Lambda(\cdot)$	Sorting function
$\lceil\cdot\rceil$	Ceiling function
$\lfloor\cdot\rfloor$	Floor function
$\lvert\cdot\rvert$	Absolute value
ϕ	Multivariate RBF
$\psi^{(0)}$	Digamma function
Ψ	Quasi-Lagrange function
Θ	Heaviside step function
φ	Univariate RBF
$\lVert\cdot\rVert$	Euclidean norm
f	Some function
f^*	Mellin transform of the function f
$G_{p,q}^{m,n}$	Meijer G-function
H_q	Harmonic numbers
$H_{p,q}^{m,n}$	Fox H-function
J_ν	Bessel function of the first kind
K_ν	Modified Bessel function of the second kind
$P(\cdot)$	Trigonometric polynomial
$p(\cdot)$	Some polynomial
$Q_h[f]$	Quasi-Lagrange operator
$s(\cdot)$	Interpolation function

Constants

Δ_j	Difference of jth grid and scattered point

e	Euler's number
γ	Euler-Mascheroni constant
λ, β	Parameters varying the RBFs of interest
i	Imaginary unit
π	Pi
C	Arbitrary constant
c	The constant shift of the RBF
h	Fill distance
n	Dimension

Other Symbols

$\mathbf{A}$	Interpolation matrix
$\mathbf{v}$	Vector
$\mathcal{O}$	Landau big-O symbol
μ_k	Coefficients for the quasi-Lagrange function
Ind	Winding number
Res	Residue operator
$\prod_{\ell_0}^{n}$	Set of all polynomials of degree ℓ_0 in n dimensions
$\sim$	Asymptotic equivalence symbol
ε	Shape parameter
C^k	Set of k-times differentiable functions
$L, \tilde{L}$	Path of integration
$r = \|\cdot\|$	Radial part of some vector

Bibliography

[1] *NIST Digital Library of Mathematical Functions*. `https://dlmf.nist.gov/`, Release 1.2.1 of 2024-06-15. F. W. J. Olver, A. B. Olde Daalhuis, D. W. Lozier, B. I. Schneider, R. F. Boisvert, C. W. Clark, B. R. Miller, B. V. Saunders, H. S. Cohl, and M. A. McClain, eds.

[2] G. E. Andrews, R. Askey, and R. Roy. *Special Functions*, volume 71 of *Encyclopedia of Mathematics and its Applications*. Cambridge University Press, Cambridge, 1999.

[3] G. Arora, KiranBala, H. Emadifar, and M. Khademi. A review of radial basis function with applications explored. *Journal of the Egyptian Mathematical Society*, 31(1), 2023.

[4] R. Beals. *Special Functions and Orthogonal Polynomials*. Cambridge University Press, Cambridge, 2016.

[5] C. M. Bender and S. A. Orszag. *Advanced Mathematical Methods for Scientists and Engineers I: Asymptotic Methods and Perturbation Theory*. Springer, New York, 1999.

[6] A. Bors. Introduction of the Radial Basis Function (RBF) Networks. *Online symposium for electronics engineers*, pages 1–7, 2001.

[7] M. A. Bouhlel and J. R. R. A. Martins. Gradient-enhanced kriging for high-dimensional problems. *Engineering with Computers*, 35(1):157–173, 2019.

[8] D. S. Broomhead and D. Lowe. Multivariable Functional Interpolation and Adaptive Networks. *Complex Systems*, 2, 1988.

[9] J. Bruna and J. Cufí. *Complex Analysis*. European Mathematical Society, Zürich, 2013.

[10] Y. A. Brychkov, O. Marichev, and A. Prudnikov. Integrals and Series, vol 3: More Special Functions. *Gordon and Breach Science Publishers*, 1990.

[11] M. D. Buhmann. On Quasi-interpolation with Radial Basis Functions. *Journal of Approximation Theory*, 72(1):103–130, 1993.

[12] M. D. Buhmann. *Radial Basis Functions: Theory and Implementations*, volume 12. Cambridge University Press, Cambridge, 2003.

[13] M. D. Buhmann and F. Dai. Compression using Quasi-Interpolation. *Jaen Journal on Approximation*, 7(2):203–230, 2015.

[14] M. D. Buhmann and F. Dai. Pointwise approximation with quasi-interpolation by radial basis functions. *Journal of Approximation Theory*, 192:156–192, 2015.

[15] M. D. Buhmann and J. Jäger. *Quasi-Interpolation*. Cambridge University Press, Cambridge, 2022.

[16] M. D. Buhmann, J. Jäger, J. Jódar, and M. L. Rodríguez. New methods for quasi-interpolation approximations: Resolution of odd-degree singularities. *Mathematics and Computers in Simulation*, 223:50–64, 2024.

[17] C.-S. Chen, A. Noorizadegan, D. L. Young, and C. S. Chen. On the selection of a better radial basis function and its shape parameter in interpolation problems. *Applied Mathematics and Computation*, 442, 2023.

[18] R. Chen and Z. Wu. Solving partial differential equation by using multiquadric quasi-interpolation. *Applied Mathematics and Computation*, 186(2):1502–1510, 2007.

[19] G. Dijk. *Distribution Theory: Convolution, Fourier Transform, and Laplace Transform*. De Gruyter, Berlin, 2013.

[20] D. Dominici and R. S. Maier, editors. *Special functions and orthogonal polynomials: AMS Special Session on Special Functions and Orthogonal Polynomials, April 21 - 22, 2007, Tucson, Arizona*, volume 471. American Mathematical Society, Providence, Rhode Island, 2008.

[21] A. Durán, R. Estrada, and R. Kanwal. Extensions of the Poisson Summation Formula. *Journal of Mathematical Analysis and Applications*, 218(2):581–606, 1998.

[22] R. Dwivedi. *Gauss Hypergeometric Function: Special Matrix Functions, q-Special Functions*. De Gruyter, Berlin and Boston, 2025.

[23] G. E. Fasshauer and J. G. Zhang. On choosing "optimal" shape parameters for RBF approximation. *Numerical Algorithms*, 45(1-4):345–368, 2007.

[24] B. Fornberg, E. Larsson, and G. Wright. A new class of oscillatory radial basis functions. *Computers & Mathematics with Applications*, 51(8):1209–1222, 2006.

[25] M. Gasca and T. Sauer. On the history of multivariate polynomial interpolation. *Journal of Computational and Applied Mathematics*, 122(1):23–35, 2000. Numerical Analysis in the 20th Century Vol. II: Interpolation and Extrapolation.

[26] I. M. Gel'fand and G. E. Schilow. Verallgemeinerte Funktionen (Distributionen). I: Verallgemeinerte Funktionen und das Rechnen mit ihnen. *Biometrische Zeitschrift*, 5:56–57, 1960.

[27] I. M. Gel'fand and G. E. Šilov. *Generalized Functions: Volume 1: Properties and Operations*. Academic Press, New York, 1964.

[28] S. S. S. Ghalichi, M. Amirfakhrian, and T. Allahviranloo. An algorithm for choosing a good shape parameter for radial basis functions method with a case study in image processing. *Results in Applied Mathematics*, 16, 2022.

[29] R. Gorenflo, A. A. Kilbas, F. Mainardi, and S. Rogosin. *Mittag-Leffler Functions, Related Topics and Applications*. Springer Monographs in Mathematics. Springer Berlin Heidelberg and Imprint Springer, Berlin, Heidelberg, 2020.

[30] J. L. Griffith. On fourier transforms of radial functions. *Journal of the Australian Mathematical Society*, 5(3):289–298, 1965.

[31] F. Haslinger. *Complex Analysis: A Functional Analytic Approach*. De Gruyter, Berlin, Germany and Boston, Massachusetts, 2018.

[32] W. R. Inc. Mathematica, Version 13.3. Champaign, Illinois, 2023.

[33] A. Iske. Scattered data approximation by positive definite kernel functions. *Rendiconti del Seminario Matematico. Universitá e Politecnico di Torino*, 3, 2011.

[34] D. S. Jones. *The Theory of Generalised Functions*. Cambridge University Press, Cambridge, 1982.

[35] K. Kodaira. *Complex Analysis*, volume 107. Cambridge University Press, Cambridge, 2007.

[36] S. Liu and C. C. L. Wang. Quasi-interpolation for surface reconstruction from scattered data with radial basis function. *Computer Aided Geometric Design*, 29(7):435–447, 2012.

[37] Y. L. Luke. *Mathematical Functions and their Approximations*. Academic Press rapid manuscript reproduction. Academic Press, New York, 1975.

[38] S. Mallat. *A Wavelet Tour of Signal Processing*. Academic Press, Boston, 1999.

[39] D. E. Marshall. *Complex Analysis*. Cambridge University Press, Cambridge, 2019.

[40] M. Mongillo. Choosing Basis Functions and Shape Parameters for Radial Basis Function Methods. *SIAM Undergraduate Research Online*, 4, 2011.

[41] J. Ortmann and M. Ortmann. A Measurement based Predictive Maintenance Algorithm for Rigid-Body Dynamical Systems using Radial Basis Function Approximation and Information Theory. In *2023 27th International Conference on System Theory, Control and Computing (ICSTCC)*, pages 461–466, 2023.

[42] M. Ortmann and M. Buhmann. High accuracy quasi-interpolation using a new class of generalized multiquadrics. *Journal of Mathematical Analysis and Applications*, 538(1), 2024.

[43] M. Ortmann and M. Buhmann. On Quasi-Interpolation and Their Associated Shift-Invariant Space Using a New Class of Generalized Thin Plate Splines and Inverse Multiquadrics. *Journal of Fourier Analysis and Applications*, 31(3):42, 2025.

[44] R. Paris and D. Kaminski. *Asymptotics and Mellin-Barnes Integrals*, volume 85 of *Encyclopedia of Mathematics and its Applications*. Cambridge University Press, Cambridge, 2001.

[45] L. Piegl. *The NURBS Book*. Monographs in Visual Communication. Springer Berlin and Springer Heidelberg, Berlin, Heidelberg, 1997.

[46] I. R. Porteous. *Geometric Differentiation: For the Intelligence of Curves and Surfaces*. Cambridge University Press, Cambridge, v 3.02 edition, 1994.

[47] R. Schaback. Creating Surfaces from Scattered Data Using Radial Basis Functions. *Mathematical Methods for Curves and Surfaces*, pages 477–496, 1995.

[48] B. Schölkopf and A. J. Smola. *Learning with Kernels: Support Vector Machines, Regularization, Optimization, and Beyond*. MIT Press, Cambridge, Massachusetts, 2002.

[49] E. Stade. *Fourier Analysis*. Pure and Applied Mathematics. Wiley, Hoboken, New Jersey, 2005.

[50] P. Strumiłło and W. Kamiński. Radial Basis Function Neural Networks: Theory and Applications. In L. Rutkowski and J. Kacprzyk, editors, *Neural Networks and Soft Computing*, pages 107–119. Physica-Verlag HD, Heidelberg, 2003.

[51] P. P. Teodorescu. *Distribution Theory: With Applications in Engineering and Physics*. Wiley-VCH Verlag GmbH & Co. KGaA, Weinheim, 2013.

[52] H. Wendland. *Scattered Data Approximation*. Cambridge Monographs on Applied and Computational Mathematics. Cambridge University Press, Cambridge, 2004.

[53] William H. Press, Saul A. Teukolsky, William T. Vetterling, and Brian P. Flannery. *Numerical Recipes: The Art of Scientific Computing*. Cambridge University Press, Cambridge, v 3.02 edition, 2007.

[54] O. Zienkiewicz, R. Taylor, and D. Fox. Galerkin Method of Approximation: Irreducible and Mixed Forms. In *The Finite Element Method for Solid and Structural Mechanics*, pages 21–55. Butterworth-Heinemann, Oxford, 2014.

Selbstständigkeitserklärung

Ich erkläre: Ich habe die vorgelegte Dissertation selbstständig und ohne unerlaubte fremde Hilfe und nur mit den Hilfen angefertigt, die ich in der Dissertation angegeben habe. Alle Textstellen, die wörtlich oder sinngemäß aus veröffentlichten Schriften entnommen sind, und alle Angaben, die auf mündlichen Auskünften beruhen, sind als solche kenntlich gemacht. Ich stimme einer evtl. Überprüfung meiner Dissertation durch eine Antiplagiat-Software zu. Bei den von mir durchgeführten und in der Dissertation erwähnten Untersuchungen habe ich die Grundsätze guter wissenschaftlicher Praxis, wie sie in der „Satzung der Justus-Liebig-Universität Gießen zur Sicherung guter wissenschaftlicher Praxis“ niedergelegt sind, eingehalten.

Angaben zu auf künstlicher Intelligenz (KI) basierender Hilfen wie ChatGPT oder SchulKI von OpenAI oder Gemini von Google zur Erstellung meiner Dissertation (Zutreffendes angekreuzt):

- ☐ Ich habe bei der Erstellung dieses Textes kein KI-Tool verwendet.
- ☐ Ich habe ein KI-Tool in den folgenden Bereichen eingesetzt (Mehrfachnennungen möglich):
  - ☐ Ideen finden, meine Kreativität anregen
  - ☐ Verstehen von Konzepten, Recherche von Fakten und Definitionen
  - ☐ Optimierung eines von mir verfassten Textes
  - ☐ Erstellen ganzer Textpassagen nach meinen Vorgaben

Folgende KI-Tools habe ich verwendet, damit aufgeführte Teile meines Textes von dem Tool wie folgt profitiert haben:

Datum: _____ Unterschrift: _____